Molecular Characterization of *Chlamydia* – Host Interactions During the Early Stages of Infection

Inaugural dissertation

for the attainment of the title of doctor
in the Faculty of Mathematics and Natural Sciences
at the Heinrich Heine University Düsseldorf

presented by

Fabienne Kocher (née Büchler)

from Rorschach (Switzerland)

Düsseldorf, October 2024

from the Institute for Functional Microbial Genomics
at the Heinrich Heine University Düsseldorf
Published by permission of the
Faculty of Mathematics and Natural Sciences at
Heinrich Heine University Düsseldorf

Supervisor: Prof. Dr. Johannes H. Hegemann
Co-supervisor: Prof. Dr. Dieter Willbold

Date of the oral examination: 7 July 2025

Contents

Contents I

Abbreviations IV

Summary VII

1 Introduction 1

1.1 Chlamydia 1

1.1.1 Chlamydial taxonomy 1

1.1.2 Genome and genomics 2

1.1.3 Pathogeny and relevance for public health 4

1.1.4 Chlamydial infection cycle 6

1.1.5 Adhesion 7

1.2 Polymorphic membrane proteins (Pmps) 8

1.2.1 Pmp expression 11

1.2.2 Pmp function 12

1.2.3 Pmp processing 13

1.2.4 Oligomerisation 15

1.2.5 Vaccination 17

1.3 Endocytosis 19

1.3.1 Clathrin-meditated endocytosis 20

1.3.2 Key processes for endocytosis 22

1.3.3 SNX9 and N-WASP as mediators for endocytosis 24

1.3.4 Endocytosis as entry point for obligate intracellular pathogens 26

1.4 The *Cpn* entry-related effector SemD 29

2 Objectives of this work 32

3 Part I: Manuscript I 33

4 Part II: Manuscript II 68

5 Part III: Further Results 106

5.1 Introduction and Summary of previous results 106

5.2 Objectives 106

5.3 Material 107

5.3.1 Chemicals and reagents 107
5.3.2 Material, machines and devices 109
5.3.3 Solutions and buffers 111
5.3.4 Enzymes 113
5.3.5 Antibodies 113
5.3.6 Kits 114
5.3.7 Plasmids and oligonucleotides 114
5.3.8 Cells and cell lines 116
5.3.9 DNA and Protein size standards 116
5.3.10 Media 117
5.4 Methods 118
5.4.1 Cultivation of different organisms 118
5.4.2 Biomolecular methods 121
5.4.3 Biochemical methods 127
5.4.4 Cell biological methods 134
5.4.5 Bioinformatic programs 135
5.5 Further Results 136
5.5.1 Adhesion of *Ctr* PmpG to epithelial cells 136
5.5.2 Identification of *Ctr* PmpD binding partners using APEX2 proximity labelling 139
5.6 Discussion 150
5.6.1 Soluble recombinant PmpG mediates adhesion to epithelial cells 150
5.6.2 Preliminary data suggest the interaction of *Ctr* PmpD with IGF2R 151
6 Part IV: Final Discussion and Outlook 156
6.1 *Ctr* PmpD directly binds to secreted clusterin for facilitated host cell entry and likely uses IGF2R as co-receptor 156
6.2 PmpG is a weak adhesin on epithelial host cells 159
6.3 SemD modulates the host actin cytoskeleton by structurally and functionally mimicking host cell Cdc42 160
7 Supplementary material 163
8 References 165
9 List of Figures 181
10 Scientific record 182
10.1 Publications 182

10.1.1 Published 182
10.1.2 Submitted / under review 182
10.2 Presentations 182
10.3 Poster 183
11 Acknowledgments 185
12 Statutory declaration 188

Abbreviations

°C	Celsius degree
%	Percentage
aa	Amino acid
Aβ	Amyloid β
AP	Alkaline phosphatase
APEX2	Ascorbate peroxidase 2
APH	Amphipathic helix
Arp2/3	Actin-related proteins 2 and 3
ATP	Adenosine triphosphate
BAR	Bin-Amphiphysin-Rvs
BN	Blue native
bp	Base pair
BSA	Bovine serum albumin
C.	*Chlamydia*
CME	Clathrin-mediated endocytosis
CIE	Clathrin-independent endocytosis
COMC	*Chlamydia* outer membrane complex
COPD	Chronic obstructive pulmonary disease
CPAF	Chlamydia protease-like activity factor
Cpn	*Chlamydia pneumoniae*
Cps	*Chlamydia psittaci*
Ctr	*Chlamydia trachomatis*
DAPI	4′,6-diamidino-2-phenylindole
DNA	Deoxyribonucleic acid
dNTP	Deoxy nucleoside-5'-Triphosphate
E.	*Escherichia*
e.g.	*„exempli gratia“*, for example
EB	Elementary body
EGF	Epidermal growth factor
EGFR	Epidermal growth factor receptor
et al.	*„et alii“,* and others
Fig.	Figure
FITC	Fluorescein isothiocyanate (NHS-Fluorescein)
FCS	Fetal calf serum
FLAG	Foreign lymphocyte antigen
FT	Flow through
g	Gram
h	Hour
hpi	hours post infection

HBSS	Hank‘s balanced salt solution
His	Histidine tag
hMW	High molecular weight
IGF2R	Insulin like growth factor 2 receptor
kDa	Kilo Dalton
L	Litre
LGV	Lymphogranuloma venereum
M	Molarity
Mbp	Mega-base-pair
mg	Milligram
min	Minute
ml	Milliliter
mM	Millimolar
MOI	Multiplicity of infection
MOMP	Major outer membrane protein
MW	Molecular weight
nM	Nanomolar
nm	Nanometer
nt	Nucleotide
OD	Optical density
OmcA	Outer membrane protein A
OmcB	Outer membrane protein B
ON	Over night
PAGE	Polyacrylamide gel electrophoresis
PBS	Phosphate buffered saline
PCR	Polymerase chain reaction
PD	Passenger domain
PFA	Paraformaldehyde
PG	Peptidoglycan
Pgp	Plasmid glycoprotein
pH	*„pondus hydrogenii“,* power of hydrogen
$PI(4,5)P_2$	Phosphatidylinositol 4,5-biphosphate
PID	pelvic inflammatory disease
PIP	Phosphatidylinositol phosphate
PM	Plasma membrane
Pmp	Polymorphic membrane protein
POCP	Percentage of conserved proteins
PRD	Proline-rich domain
PS	Phosphatidylserine
PX	Phox-homology

PZ	Plasticity zone
r	Recombinant
RB	Reticulate body
RNA	Ribonucleic acid
Rpm	Revolutions per minute
RT	Room temperature
S.	*Saccharomyces*
SDS	Sodium dodecyl sulphate
sec	Seconds
SEC	Size exclusion chromatography
SH3	Src homology 3
SNX9	Sorting-nexin 9
SS	Signal sequence
T3SS	Type-III-secretion system
T5SS	Type-V-secretion system
Tarp	translocated actin recruiting phosphoprotein
µg	Microgram
µl	Microliter
µm	Micrometer
UV	Ultraviolet
WASP	Wiskott-Aldrich-Syndrome-Protein
WB	Western blot
WHO	World health organisation
x g	times gravity

Summary

Chlamydia trachomatis (*Ctr*) and *Chlamydia pneumoniae* (*Cpn)* are human pathogenic bacteria of the genus *Chlamydia*. They target epithelial cells, with *Ctr* causing infections of the eyes and the urogenital tract, and *Cpn* causing respiratory tract infections. Owing to their obligate intracellular lifestyle, adhesion to and internalization into host cells are crucial steps for establishing infection.

Chlamydial adhesion is mediated by several components, including polymorphic membrane proteins (Pmps), a protein family found in all chlamydial species. In *Ctr*, all nine Pmps (PmpA-PmpI) act as adhesins on epithelial cells, but for none of them have the host cell binding partners been identified. After adhesion, internalization is triggered through host endocytic processes, engulfing the bacteria in a membrane-enclosed vesicle, termed inclusion. To facilitate internalization, *Chlamydia* injects entry-related early effector proteins into the host cell cytosol via its Type-III-secretion system (T3SS), thereby manipulating the host endocytic machinery. After secretion, the *Cpn* effector SemD binds via its amphipathic helix to the inner leaflet of the plasma membrane (PM), underneath the attached chlamydial cell. There, it recruits key components of the host endocytic machinery, such as SNX9 and N-WASP via its proline-rich domain and its N-WASP binding domain, respectively. While SNX9 functions as a membrane bender and enhances scission of the matured vesicle from the PM, activated N-WASP is an actin modulator, mediating F-actin polymerization and branching via the Arp2/3 complex. Intriguingly, SemD recruiting N-WASP simultaneously leads to the activation of the latter in a yet unknown manner, independently of its endogenous activator $Cdc42_{GTP}$.

In the first part of this work, focusing on *Ctr* adhesion, two parallel approaches were used to identify a potential host cell binding partner for *Ctr* PmpD. In approach (I), a proteolytically processed PmpD fragment found during infection *in vivo* was recombinantly produced (rD72) and used as bait in pulldown assays on epithelial cells. Clusterin, a host cell protein with a secreted isoform (sCLU), was identified as a binding partner. sCLU is responsible for the clearance of misfolded proteins from the extracellular space by endocytosis and is an inhibitor of the terminal complement pathway. *In vitro* assays verified the direct interaction of rD72 and sCLU. Additionally, *in vivo* infection experiments showed significantly reduced *Ctr* infectivity in the absence of sCLU in the cell culture medium overlaying epithelial cells during the early infection

stages, suggesting that sCLU facilitates *Ctr* infectivity by binding the *Ctr* adhesin PmpD. In approach (II), the adhesive domain of PmpD, shown to be chlamydial cell surface-localized, was genetically fused to APEX2, a peroxidase which biotinylates nearby proteins (1-10 nm). Transformed *Ctr* EBs, producing the fusion protein, were used for infecting epithelial cells. Biotinylated proteins were identified and showed significant enrichment of the host insulin-like growth factor 2 receptor (IGF2R) and future experiments are needed to confirm the direct interaction.

In the second part of this work, *Cpn* internalization via SemD was investigated. Structural analysis of SemD demonstrated that by combining flexible and structured domains, steric hindrance between individual host cell binding sites of SemD is minimized, allowing the simultaneous interaction with the host cell PM, SNX9 and N-WASP. Co-crystallization of SemD and N-WASP revealed that SemD structurally mimics $Cdc42_{GTP}$ for N-WASP activation. In biochemical assays, it was further revealed that SemD binds N-WASP much more strongly than $Cdc42_{GTP}$ does, allowing SemD to displace $Cdc42_{GTP}$ from an already formed N-WASP – $Cdc42_{GTP}$ complex, making $Cdc42_{GTP}$ redundant during the early infection.

Identification of PmpD host cell binding partners and an understanding of the activation mechanism of SemD on N-WASP may in future allow for the development of small inhibitors that block a chlamydial infection.

1 Introduction

1.1 Chlamydia

Bacteria belonging to the family of *Chlamydiaceae* are Gram-negative, coccoid-shaped pathogens that cause a wide variety of acute and chronic diseases in humans and animals [1, 2]. Regardless of the host and tissue tropism, all species belonging to the genus *Chlamydia* are obligate intracellular bacteria and share a unique biphasic developmental cycle, switching between two distinct morphological forms [3]. Outside the host cell, *Chlamydia* exist as metabolically inactive, infectious elementary bodies (EBs), which are adapted to resist unfavourable extracellular conditions. Inside the host cell, they differentiate into metabolically active reticulate bodies (RBs), focused on division and replication [4, 5]. *Chlamydia* are optimally adapted to their obligate intracellular developmental cycle and hijack nutrients from their host. Hence, *Chlamydia* have eliminated many genes from functional pathways, mainly anabolic, and therefore have a highly reduced genome [3].

1.1.1 Chlamydial taxonomy

Chlamydial diseases can be traced back to ancient China in the 27th century BC, where the first reference to trachoma as well as potential methods for its treatment were described. Since then, repeated records were found in which similar diseases were described, until research in the early 20th century led to the development of methods that allowed the isolation of the causative pathogen. Its ability to form intracellular vacuoles led to the name "*Chlamydia*", derived from "khlamus", a Greek word which means mantle [6]. Soon after, in experiments using antibiotics, the sensitivity of *Chlamydia* to sulphanilamide was shown, leading to the suggestion that *Chlamydia* are not viral pathogens, as it was previously assumed, but rather bacterial pathogens [6].
Since then, advances in microbiology, genetics and molecular biology led to ongoing discussions about the chlamydial taxonomy, resulting in several changes over the past decades. It was originally proposed that the genus *Chlamydia* includes two species, *Chlamydia trachomatis (Ctr)* and *Chlamydia psittaci (Cps)*, which was then expanded by two further species, namely *Chlamydia pneumoniae* (*Cpn*) and *C. pecorum* [7-9].

Later, through comparative analysis of the 16S and 23S ribosomal RNA (rRNA), Everett, Bush and Andersen proposed to divide the order *Chlamydiales* into four families (*Chlamydiaceae*, *Parachlamydiaceae*, *Waddliaceae* and *Simkaniaceae*) and the family of *Chlamydiaceae* into two genera; *Chlamydia* (including *Ctr, C. suis* and *C. muridarum)* and *Chlamydiophila (Cpn, Cps, C. pecorum, C. caviae, C. abortus* and *C. felis)* [10, 11]. Based on extensive characterization of complete genomes, Stephens et al. successfully argued for the recombination of the genera *Chlamydia* and *Chlamydophila* into a single genus, named *Chlamydia* [12, 13]. Pannekoek et al. [14] later validated the taxonomy by conducting a "percentage of conserved proteins" (POCP) analysis, in which they compared all species currently classified within the *Chlamydiaceae* family. Pillonel et al. [15] yielded the same result via the identification and comparison of so-called "core proteins" (Fig. 1).

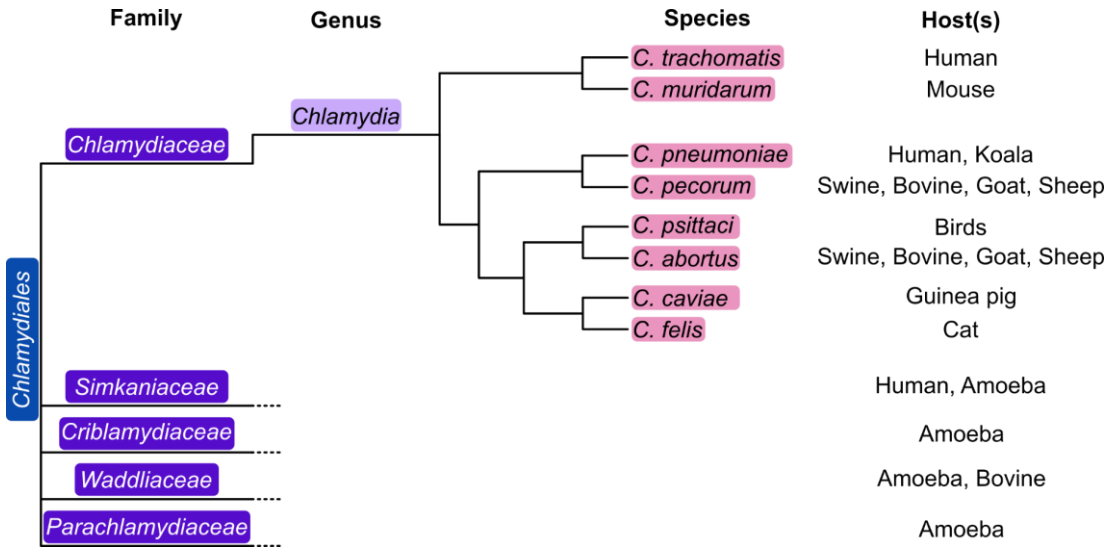

Figure 1: Chlamydial taxonomy

Overview of the order *Chlamydiales*, including the family of *Chlamydiaceae* with the genus *Chlamydia*. The lengths of the lines are not representative for phylogenetic distances. On the right are the host organisms listed, infected by the individual species. The phylogenetic tree is modified after Pillonel et al. [15] and Pannekoek et al. [14].

1.1.2 Genome and genomics

In 1998, Stephens et al. [3] sequenced the first chlamydial genome, which was from *Ctr* serovar D. Since then, due to decreasing costs and ongoing developments in sequencing methods, an increasing number of fully sequenced chlamydial genomes have been published [16].

Chlamydia have a significantly reduced genome with a single, circular chromosome of approximately 1-1.2 Mbp, which is highly conserved and syntenic [16, 17]. It is suggested that the genome reduction is a result of their evolutionary transition to an intracellular life cycle and their co-evolution with a eukaryotic host [18-21]. As *Chlamydia* hijack nutrients from the host cell, genes that are otherwise metabolically relevant have been eliminated [3, 22]. The residual genome is a mix of highly conserved genes and polymorphic genes, which are assumed to be involved in host and tissue tropism, as well as virulence [16]. Examples of genomic regions with high variability include genes in the plasticity zone (PZ), genes encoding membrane proteins (e.g. the major outer membrane proteins (MOMP) or polymorphic membrane proteins (Pmps)) and genes encoding distinct metabolic pathways [18, 22, 23]. Additionally, members of the genus *Chlamydia* (except *C. abortus* strains and most *Cpn* strains) possess an additional plasmid that is approximately 7.5 kbp in size and contributes to infectivity [24]. The conserved plasmid carries eight open reading frames, encoding plasmid glycoprotein 1-8 (Pgp1-8), probably implicated in plasmid replication and bacterial virulence [24, 25]. Due to their reduced genome, chlamydial proteins typically contain multiple functional domains, thus allowing a single protein to perform several different functions.

For decades, gene manipulation and transformation of *Chlamydia* were not possible. This changed with the observation that separate *Ctr* inclusions within a single host cell can fuse, leading to lateral gene transfer between different serotypes [26-28]. In 2011, Wang et al. [29] reported the first success in genetic manipulation of *Ctr* by transforming a plasmid shuttle vector using $CaCl_2$ treatment. The vector used for transformation was based on the plasmid inherently carried by *Ctr*, into which genes for antibiotic resistance and a protein of interest were inserted, under the control of a standard *E. coli* promoter, also functioning in *Ctr* [29]. EBs were treated with $CaCl_2$ and heat to induce uptake of the foreign DNA and transformed EBs were selected using antibiotics [29, 30]. Since then, the toolbox for genetic manipulation of *Chlamydia* has been expanded [31-36]. However, most methods are primarily used for genetic manipulation of *Ctr,* while the toolbox to manipulate the *Cpn* genome remains limited. To date, the only success in genetic manipulation of *Cpn* has been the transformation with a plasmid encoding a red-shifted green fluorescent protein (RSGFP) fused to chloramphenicol acetyltransferase [37].

1.1.3 Pathogeny and relevance for public health

Individual chlamydial species have successfully adapted to their respective hosts. In particular, *Ctr* has specialized in infecting humans, while *Cpn* infects both humans and koalas. Moreover, other species, such as *Cps* and *C. abortus*, have evolved zoonotic potential and can be transmitted to humans [38].

1.1.3.1 Chlamydia trachomatis

Worldwide, *Ctr* is the major cause of infection-related blindness and the major contributor to sexually transmitted diseases (STDs) [39]. According to the latest WHO estimates (as of 2020), among adults aged between 15 – 49 years, 128.5 million new infections with *Ctr* occurred worldwide. In the same age category, WHO estimates a total prevalence of 4 % in women and 2.5 % men [40].

The species of *Ctr* can be further subdivided into 19 different serovars, grouped into three biovars (Fig. 2). Serovars belonging to the trachoma biovar cause infections of the eyes and are the primary cause of acquired blindness, especially in developing countries [39]. Serovars D-K, belonging to the genital tract biovar, infect the urogenital tract and are the most prevalent sexually transmitted bacterial pathogens. However, approximately 70 % of infected women exhibit no or very mild symptoms. From these, 15 – 40 % ascend to the upper genital tract and can result in severe diseases, including cervicitis, urethritis or pelvic inflammatory disease (PID). If left untreated, these diseases have a high prevalence of resulting in infertility or ectopic pregnancies. In men, infections most commonly lead to inflammation of the urethra [39, 41]. The lymphogranuloma venereum (LGV) biovar consists of four serovars that also infect the urogenital tract, similar to serovars D-K. However, these serovars can then spread to the lymphatic system and lead to systemic infections known as lymphogranuloma

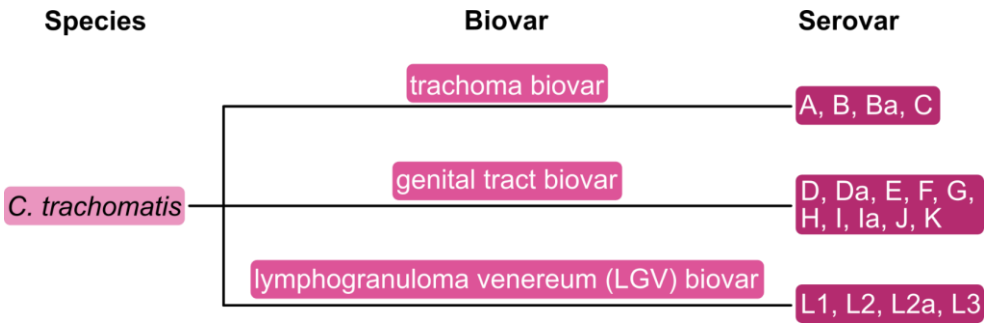

Figure 2: *Ctr* biovars and serovars

Overview of the species of *Ctr*, divided in three biovars. Each biovar can further be subdivided in specific serovars.

venereum (LGV). This disease is characterized by enlarged lymph nodes and inflammation of the lining of the rectum and colon [39, 41, 42]. If LGV is left untreated, it can lead to chronic lesions of internal tissues [43].

1.1.3.2 Chlamydia pneumoniae

Cpn infects the upper and lower respiratory tract and is transmitted from human to human via respiratory droplets [44, 45]. Similar to *Ctr*, most *Cpn* infections (~70 %) are asymptomatic or have very mild symptoms, while the residual 30 % result in severe, community-acquired pneumonia with symptoms such as bronchitis, upper respiratory tract infections, or other atypical symptoms [46]. Additionally, *Cpn* is associated with further inflammatory conditions, including chronic obstructive pulmonary disease (COPD), lung cancer, Alzheimer's disease, asthma, or atherosclerosis [47]. The antibody prevalence is around 50 % by the age of 20 and rises up to 80 % by the age of 70 [44]. This indicates that most individuals have been infected with *Cpn* at least once in a lifetime, highlighting the relevance of this bacterial pathogen.

1.1.3.3 Management and Treatment

The clearance of a diagnosed chlamydial infection is relatively straightforward with antibiotics like azithromycin or doxycycline, achieving a 95 % effectiveness rate, typically without complications [48]. Yet, several factors hamper the management of chlamydial infections. First, reinfection is common, especially for the sexually transmitted species, due to the nontreatment of infected sexual partners [48]. Second, even if antibiotics are promising for bacterial clearance, there are no cost-effective drugs available for the treatment in developing countries. Third, as there is no preventive vaccine available at the moment and most infections remain asymptomatic, untreated cases are common and thus connected with unknowingly spreading within the community [49]. Last but not least, chlamydial persistence is a critical yet not fully understood aspect. Under stressing conditions, evoked by for example penicillin, IFN-γ or nutrient deprivation, RBs transform into long-lasting, metabolically inactive forms called aberrant bodies (ABs) [50]. ABs are resilient against these stresses and can go back to RBs and resume their developmental cycle when conditions improve [50]. Considering these complications, the primary goal of treatment is not clearing an existing infection but rather preventing a new one, potentially through an effective vaccine, discussed in detail in section 1.2.5.

1.1.4 Chlamydial infection cycle

Chlamydia have a distinct biphasic developmental cycle and infect eukaryotic cell for successful division and replication. Further, in the course of their developmental cycle, *Chlamydia* adopt two distinct morphological forms [4]. The small (0,3 µm), metabolically inactive elementary body (EB) is the infectious form, specialised on extracellular resistance and on the attachment to and internalization into the host cell [51]. Chlamydial EBs have an inner and outer membrane, which ensures stability and resistance to osmotic pressure [41]. Further, the outer membrane is abundant in cysteine-rich proteins that are crosslinked by disulfide bonds and establish a protein network known as the chlamydial outer membrane complex (COMC). The most dominant protein in this network is the major outer membrane protein (MOMP), which accounts for up to 60 %. The remaining 40 % consists of a mix of other surface proteins, including the outer membrane proteins A and B (OmcA and OmcB), Ctad1

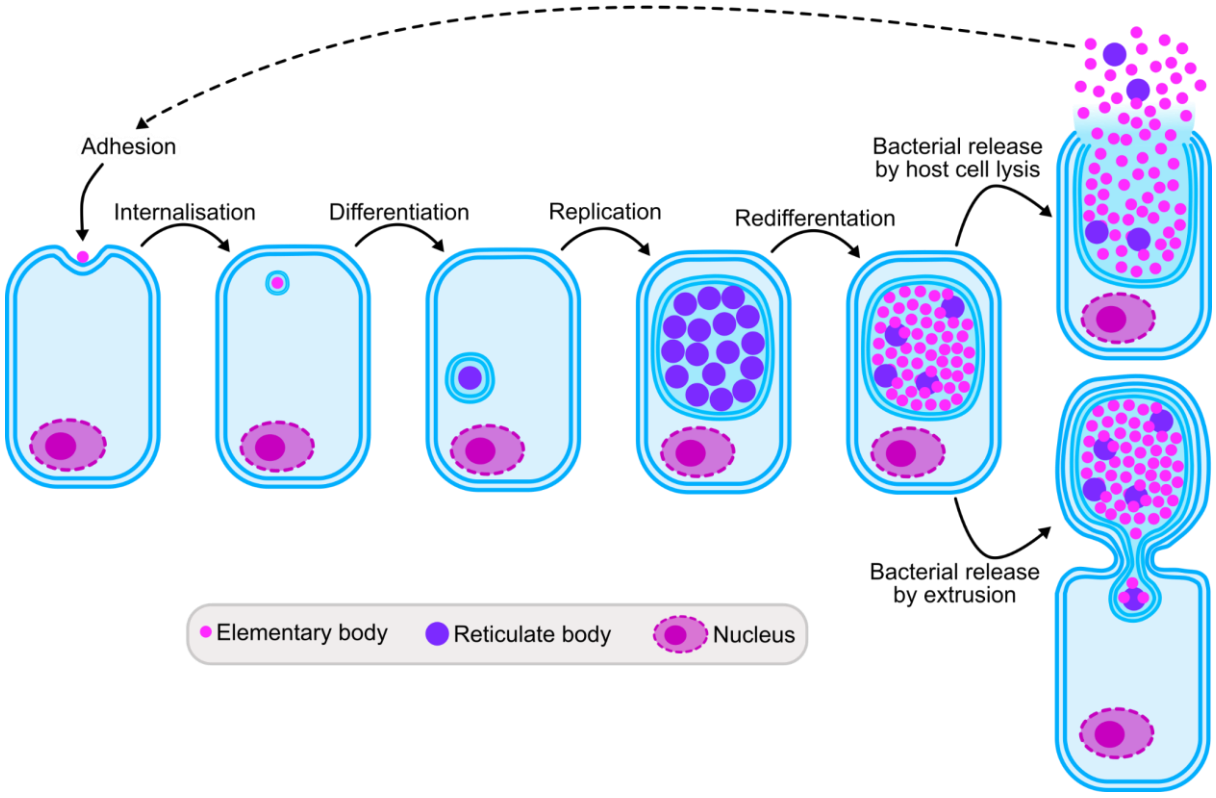

Figure 3: Schematic representation of the chlamydial developmental cycle

The chlamydial life cycle starts with an elementary body (EB) that adheres to a host cell. Upon interaction of chlamydial surface proteins with host cell receptors, internalization is triggered, and the EB is taken up by the non-phagocytic host cell. Inside, the EB stays in a membrane-enclosed compartment (inclusion) and differentiates into a reticulate body (RB), which divides and replicates in 9 - 11 cycles. The pool of RBs transitions back to EBs, which exit the cell by either extrusion of the intact inclusion or by host cell lysis. The released EBs are ready to start a new infection cycle.

and polymorphic membrane proteins (Pmps) [52-54]. Besides membrane stability and EB protection, this protein network also mediates the first steps of a chlamydial infection, which are the adhesion to and internalization into the target host cell (Fig. 3). Additionally, to enhance chlamydial uptake, the EB secretes entry-related early effector proteins into the host cell cytosol via its type-III-secretion system (described in detail in section 1.3.4.3). These modulate and manipulate the host endocytic machinery, mediating the successful uptake of the EB into a membrane-enclosed compartment termed inclusion (Fig. 3). There, the EB differentiates into the second morphological form, the reticulate body (RB). The non-infectious RB is characterized by a size of approximately 1 µm in diameter and is metabolically active. It is specialised in driving chlamydial replication and hijacking ATP and nutrients from the host cell. Furthermore, it is responsible for preparing components that are needed in the metabolically inactive EB [4, 55]. After 9-11 division cycles, the pool of RBs asynchronously transitions back to EBs, which then leave the cell by either extrusion of the intact inclusion or by cell lysis (Fig. 3) [56]. Released EBs then infect a neighbouring cell, restarting the infection cycle. While the stages of the developmental cycle are the same for all chlamydia, *Ctr* needs ~ 48 h while *Cpn* needs ~ 72 h [57, 58].

1.1.5 Adhesion

In particular for obligate intracellular pathogens like *Chlamydia*, adhesion – the first direct contact with the host cell – is crucial for establishing infection. Typically, adhesion is a multifactorial process involving numerous microbial and host cell proteins [59]. In *Chlamydia*, adhesion is still not fully elucidated and varies across species, which exhibit different tissue tropisms and hence utilize individual components for adhesion [60]. However, the overall mechanism involves two main steps. The initial contact is mediated by reversible, unspecific interactions between EB and host cell [61]. Most chlamydial species use the highly abundant OmcB for low-affinity binding to heparan sulfate-like glycosaminoglycans (HS-GAGs), long polysaccharides bound to PM or matrix proteins (proteoglycans) of almost all human cell types [62-66]. This first contact is thought to influence tissue tropism across different chlamydial species [61]. The second step involves the stable, irreversible interaction with the host cell, mediated via both general and species-specific chlamydial adhesins [59, 61]. A prominent general adhesin is MOMP, and in *Cpn*, its interaction with the host insulin-like growth factor 2 receptor (IGF2R) is proposed [59, 67]. Species-specific examples include *Ctr* Ctad1,

which binds the β1-integrin receptor, and *Cpn* GroEL1, whose receptor is not yet identified [68, 69]. Additionally, *Cpn* LipP, which was initially identified as adhesin, binds negatively charged phospholipids and promotes EB internalization [70].
Finally, polymorphic membrane proteins (Pmps), present in all chlamydial species, play a significant role in EB adhesion and internalization and will be introduced in detail in the next chapter.

1.2 Polymorphic membrane proteins (Pmps)

The first polymorphic membrane protein (Pmp) was identified in *C. abortus* as a 90 kDa major immunogenic protein [71]. In the following years, through genome sequencing and comparative genome analysis, Pmps could be identified in all chlamydial species [72]. Even in the family of *Waddliaceae*, which belongs to the order *Chlamydiales*, a Pmp-like protein was identified [73]. With the current state of research, the Pmp family represents the largest protein family in *Chlamydia*, comprising 13.6 % and 17.5 % of the chlamydia-specific coding capacity in *Ctr* and *Cpn*, respectively [3, 74]. This highlights their crucial role in chlamydial pathogenesis. Based on genomic comparisons and bioinformatic analyses, Pmps have been classified into six phylogenetic subgroups (Fig. 4a) [75-77]. *Ctr* possesses nine Pmps, with one to two representatives per subgroup, *Cpn* possesses 21 Pmps, which are unevenly distributed among the subgroups (Fig. 4a) [72, 75]. Thereby, subgroup G is particularly expanded, with thirteen representatives (Fig. 4a) [72, 75].
The genetic arrangement of *pmps* reveals an organisation in gene clusters, located in different chromosomal regions. In *Ctr*, two such clusters were identified with *pmpA-B-C* in one cluster and *pmpE-F-G-H-I* in the second cluster. *pmpD* is found as stand-alone gene [75]. Based on RT-PCR, it has been suggested that *pmpABC*, *pmpFE,* and *pmpGH* are organized into operons, as they are co-transcribed [78]. For *Cpn*, *pmps* are organized in three clusters and, similarly to *Ctr pmpD*, *Cpn pmp21* is found as stand-alone gene [75]. Interestingly, in *pmps* a particularly high mutation rate can be observed, suggesting that they are under evolutionary pressure [75]. For both *Ctr* and *Cpn* all *pmps* are transcribed and for *Ctr* all of them are also translated. For *Cpn*, *pmp3, 4, 5, 10, 12* and *17* possess a frameshift mutation or a premature stop codon, preventing their translation [79-81].

When comparing the amino acid sequence identity of Pmps of different species and subgroups, variable similarities become apparent. Within the same species, Pmps from the same subgroup typically show higher sequence identities than Pmps from different subgroups (PmpB and PmpC from *Ctr*: 50.7 % identity, PmpB and PmpD from

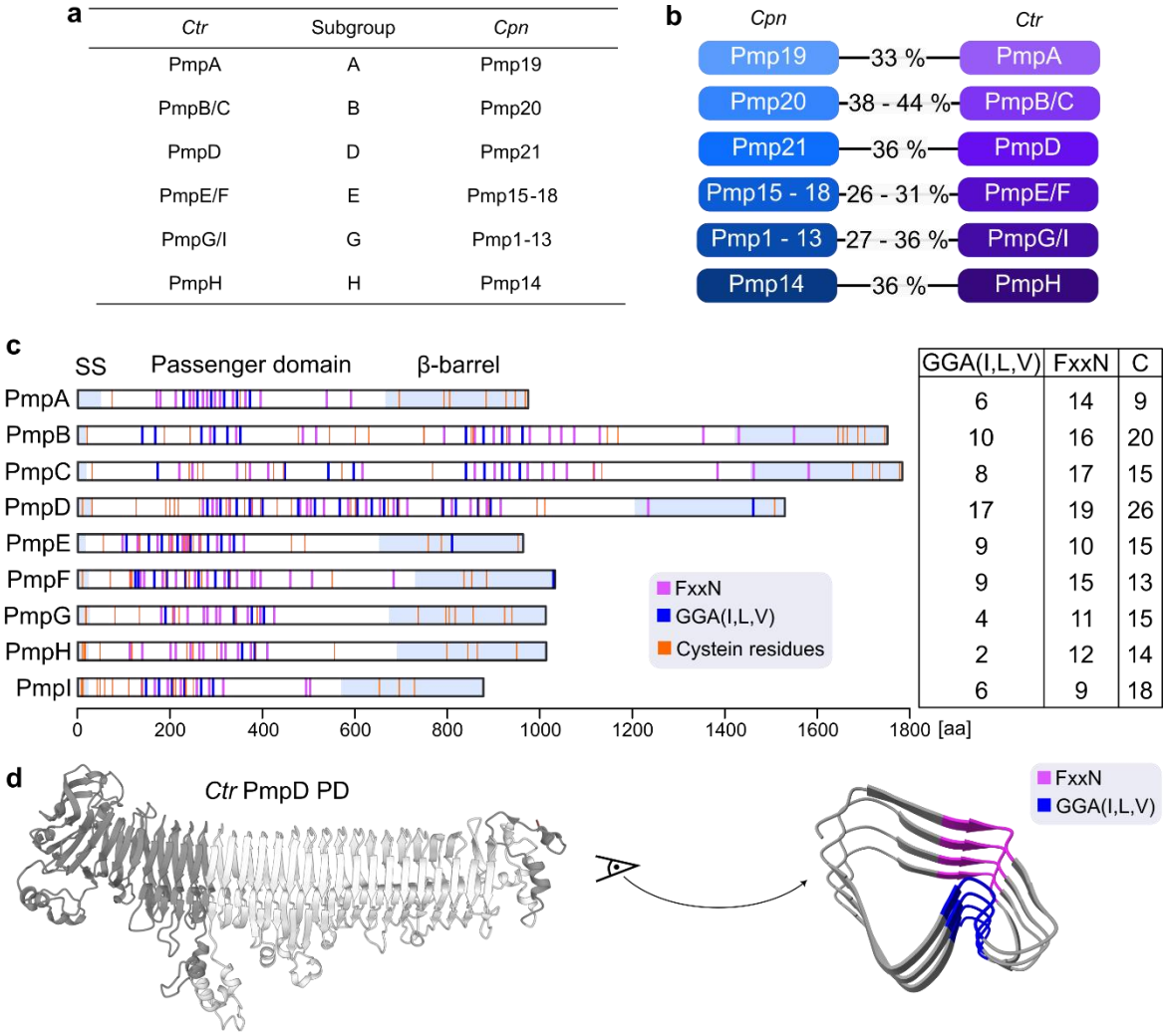

Figure 4: Properties and domain architecture of Pmps

a Classification of *Chlamydia trachomatis (Ctr)* and *Chlamydia pneumoniae (Cpn)* Pmps in the according subgroups. **b** Sequence identity between *Cpn* and *Ctr* Pmps belonging to the same subgroups. Sequence alignments were performed using EMBL-EBI [82]. **c** Schematic representation of all nine *Ctr* Pmps. The N-terminal signal sequence (SS) and the C-terminal β-barrel are indicated by blue boxes, the location of the characteristic GGA(I,L,V) (blue) and FxxN (magenta) repeats are indicated and the total number of each motif type is given on the right. Cysteine (C) residues are marked in orange and the total number is given on the right. Pmps with the marked motifs and Cysteine residues were created using a self-written code in RStudio [83]. **d** Predicted 3D structure of the *Ctr* PmpD PD performed by RoseTTAFold [84]. (*left*) dark grey and light grey colouring refers to the fragments p30 and p73 introduced in section 1.2.3. (*right*) View into the tube formed by β-sheets with the stacked GGA(I,LV) and FxxN repeats, coloured in blue and magenta, respectively.

Ctr: 21 % identity). Similarly, across different species, Pmps from the same subgroup provide higher sequence identities than from different subgroups (*Ctr* PmpD and *Cpn* Pmp21: 36 % identity, *Ctr* PmpD and *Cpn* Pmp20: 25.7 %) (Fig. 4b) [75, 82, 85, 86]. Among different *Ctr* serovars, PmpA, PmpD and PmpI are the most conserved Pmps with sequence similarities of 99.9 %, 99.1 % and 99.2 %, respectively [78]. Concludingly, based on the high heterogeneity of Pmps, it is proposed that they are involved in tissue tropism and that the large variation in the number of Pmps is suggested to have resulted from gene duplication [78, 85, 87].

Based on their domain organisation, Pmps are believed to belong to type-V-autotransporters, characterized by an N-terminal secretory sequence (SS) for Sec-dependent transport across the inner chlamydial membrane, a C-terminal domain with β-barrel characteristics that spans the chlamydial outer membrane, and a central passenger domain (PD) (Fig. 4c) [75, 81, 88-92]. The SS and the β-barrel primary function for correct localization of the functional PD. The latter is characterized by FxxN (where the first x can be any amino acid except proline and the second x can be any amino acid except methionine, tryptophan or cysteine) and GGA(I,L,V) motifs, which are thought to play a particular role in chlamydial adhesion and infectivity [75, 85, 93-97]. The FxxN and GGA(I,L,V) repeats are found on average 11.3 and 5 times in *Cpn* Pmps and 13.6 and 6.5 times in *Ctr* Pmps, respectively [74, 75]. These tetrapeptide motifs are rather untypical and rarely found in other organisms than *Chlamydia*. However, there are some examples, including OmpA from *Rickettsia conorii* (7 FxxN and 7 GGA(I,L,V) motifs, binds to the host α2β1 integrin receptor), Zonadhesin from *Mus musculus* (5 FxxN and 1 GGA(I,L,V) motifs) or Mucin 5B from *Homo sapiens* (12 FxxN and 4 GGA(I,L,V)) [98-100]. All of these non-chlamydial proteins are characterized as adhesins or invasins, similar to the chlamydial Pmp family. Beside these tetrapeptide motifs, Pmps are rich in cysteine residues, which are mainly found in the PD and in the β-barrel and are thought to form disulfide bridges with the COMC, contributing to its stability [75, 94, 101].

Structure predictions of Pmp PDs suggest that they are prone to form triangular β-helical structures, with the FxxN and GGA(I,L,V) motifs stacked on top of each other (Fig. 4d) [102, 103]. However, there are no structural data available yet, that could confirm this. The only evidence supporting this prediction comes from circular

dichroism data, which indicate that certain Pmp PD fragments have a high propensity in β-sheet secondary structure, interspersed with random coil elements [95, 101].

1.2.1 Pmp expression

Based on their large number, Pmps are suspected to be involved in essential functions during the chlamydial infection cycle. Therefore, it is not surprising that different Pmps are up- and down-regulated at various stages of the infection cycle.

In the case of *Ctr*, Nunes et al. [104] investigated the expression profiles of the nine *pmp* genes throughout the developmental cycle. Across all serovars examined, they found that *pmpA*, which peaks at 12 hours post infection (hpi), is the least expressed gene, measured by mRNA levels [104]. Further, proteomic analysis of purified EBs and RBs indicated that PmpA is present only in RBs and thus is thought to have a critical function during EB to RB conversion [105]. Contrary, *pmpF* showed the highest relative mRNA expression, peaking between 18 - 36 hpi [104]. Additionally, proteomic analysis revealed that PmpF is only detected in EBs [105]. Intriguingly, *pmpE*, which is localised in the same genomic cluster as *pmpF,* has a significantly lower overall mRNA level [104]. The remaining *pmps* from *Ctr* are upregulated after 24 hpi, aligning with the mid-cycle where replicated RBs begin transitioning back to EBs. This pattern coincides with proteomic studies, where PmpC, D, E, G and I were found in both RBs and EBs [105]. Although the overall expression levels across different *Ctr* serovars are similar, there are some minor differences in time points at which specific *pmps* reach their maximal mRNA levels. For example, while the *pmpD* mRNA level peaks at 36 hpi in all tested serovars, *pmpG* peaks at 18 hpi in serovar L2 but at 24 hpi in serovar E [104]. Interestingly, *pmp* transcript levels are partially altered during the infection cycle in the presence of stress conditions, induced by penicillin treatment [78]. While *pmpE, F, G* and *H* transcription levels are significantly reduced, *pmpA*, *D* and *I* transcription levels are not significantly affected. Hence, this suggests that the latter might have a crucial role in aberrant bodies and for the chlamydial persistence [78].

For *Cps*, a similar but not identical expression pattern compared to *Ctr* was observed. While *pmpA* is upregulated early in infection too (~ 6 hpi), the other *pmps* were upregulated later at approximately 24 hpi [106]. The main difference between *Cps* and *Ctr* is seen in the expression pattern of *pmpH*. In *Cps, pmpH* transcript level increases at 2 hpi, drops at 6 hpi, and increases again at 24 hpi. In *Ctr*, the *pmpH* transcript level remains low until 24 hpi, after which it increases sharply [104, 106].

This large variation in *pmp* expression levels across different serovars and species, along with the Pmp localization on the chlamydial surface, indicates that Pmps have a critical role in the chlamydial infection cycle and are thus tightly regulated both temporally and spatially.

1.2.2 Pmp function

One of the first indications that Pmps function as adhesins and invasins on epithelial cells came from a study by Crane et al. [107]. They aimed to find potential target proteins (other than MOMP) for a protein-based vaccine. Thereby, they demonstrated that antibodies specific to PmpD were pan-neutralizing, suggesting that PmpD, localized on the bacterial surface, plays a functional role in attachment to host cells. Subsequent studies further confirmed the adhesive properties of Pmps in both *Cpn* and *Ctr* [93, 94].

Mölleken et al. [94] demonstrated, that Pmp6, Pmp20 and Pmp21 from *Cpn* mediate adhesion to epithelial cells and further, by testing individual fragments of Pmp21, they found that at least two tetrapeptide motifs are required for effective binding (either 2x FxxN or a combination of one FxxN and one GGA(I,L,V) motif). Additionally, they showed that upon preincubation of epithelial cells with recombinant Pmp protein fragments, a subsequent chlamydial infection can be significantly reduced. For Pmp21, they tested individual PD fragments and concluded that especially fragments resembling the naturally processed Pmp21 variants were most effective in inhibiting a subsequent chlamydial infection. Thus, they concluded that these fragments adopt favourable conformations for receptor binding [89, 90, 94].

For *Ctr*, Becker et al [93] demonstrated that all nine Pmps adhere to epithelial cells. Additionally, preincubation of cells with recombinant protein fragments from each of the nine Pmps resulted in a significant decrease of a following *Ctr* infection, albeit to varying degrees. By combining different Pmps and preincubating them with HEp-2 cells, they found that a following chlamydial infection is additively reduced. This led them to the suggestion, that each Pmp interacts with a different surface structure on the host cell [93].

Based on these data, *Cpn* Pmp21 was further investigated with the goal of identifying the host cell receptor it binds to, which was found to be the epidermal growth factor receptor (EGFR) [108]. Fluorescent latex beads coated with recombinant Pmp21 were incubated with epithelial cells and microscopic analysis showed that EGFR at the cell

surface colocalizes with the beads, which are then internalized into the host cells. These findings suggest that Pmp21 functions as an adhesin and invasin by binding to and activating the EGFR, which triggers intracellular signal transduction and initiates endocytic uptake processes [108, 109]. Given that *Ctr* PmpD is the homologue of *Cpn* Pmp21, it was speculated that PmpD might also bind to EGFR. However, preliminary data could not support this hypothesis [86]. Interestingly, Li et al. [110], working on *Cps*, suggested through biochemical assays that Pmp17G, a member of subgroup G, binds to and activates the EGFR in a way similar to *Cpn* Pmp21 [110].

Despite the lack of evidence for EGFR binding, interest in *Ctr* PmpD remained high. Kari et al. [111] used a *Ctr pmpD* null mutant, which showed significantly reduced adhesion and infectivity in the eyes of macaques (non-human primates) and cultured human cell lines, but had no effect on infection efficiency or chlamydial growth when infecting murine cells *in vitro* or in an *in vivo* murine mucosal infection model. Based on these results, PmpD was suggested to play a particular role in tissue and host specificity. Another study from Tan et al. [81] has shown that in some *Ctr* inclusions, the expression of specific *pmps* is uniformly shut off. However, especially for *pmpD* (and p*mpI*) these “off” frequencies were significantly lower than for other *pmps*, further suggesting a crucial role of PmpD during infection. Consistently, PmpD is highly conserved across different serovars, and evidence was provided by a combination of electron microscopy and biochemistry that PmpD may form relatively large, flower-like oligomeric structures on the EB surface [112, 113]. Additionally, an antibody specific against *Ctr* PmpD was able to neutralize a *Ctr* infection, but not infections caused by *Cpn*, *C. muridarum* or *C. caviae* [107]. This correlates with genomic studies of *Ctr pmps*, where phylogenetic reconstructions, based on all *pmp* genes, clustered *Ctr* serovars according to their tissue tropism [87]. In conclusion, it is suggested that PmpD plays a critical role in chlamydial adhesion to host cells, as well as in tissue and host tropism and immune evasion. Identifying host cell binding partner(s) for PmpD could reveal important mechanisms during the initial stages of a chlamydial infection and may provide a potential approach for developing therapeutic strategies.

1.2.3 Pmp processing

During the characterisation of Pmps, it became evident that beside their full-length forms, Pmps are also proteolytically processed *in vivo*, typically resulting in soluble fragments of the PD [81, 89, 90, 94, 107, 113-115]. *Cpn* Pmp21 and its *Ctr* homologue

PmpD are the most extensively studied Pmps in terms of proteolytic processing but also for other species processed Pmps were demonstrated, such as for example for Pmp18D from *C. abortus* [116].

For *Cpn* Pmp21, in addition to the cleavage of the N-terminal secretion signal, two further processing sites have been identified [90]. One cleavage site is located centrally within the PD, after residue 660, while the second site is located in the C-terminal part of the PD, just before the β-barrel (Fig. 5a). This results in two soluble Pmp21 fragments: one approximately 70 kDa (N-PmpD) and the other around 55 kDa (M-PmpD) [90]. During a chlamydial infection, both full-length Pmp21 and its processed fragments were detected on the chlamydial surface [89, 90]. Hence, through the presence of different Pmp21 fragments (and potentially other Pmp fragments), the heterogeneity on the chlamydial surface is suggested to be increased. This might help the pathogen evade the host immune response and is thought to also increase its

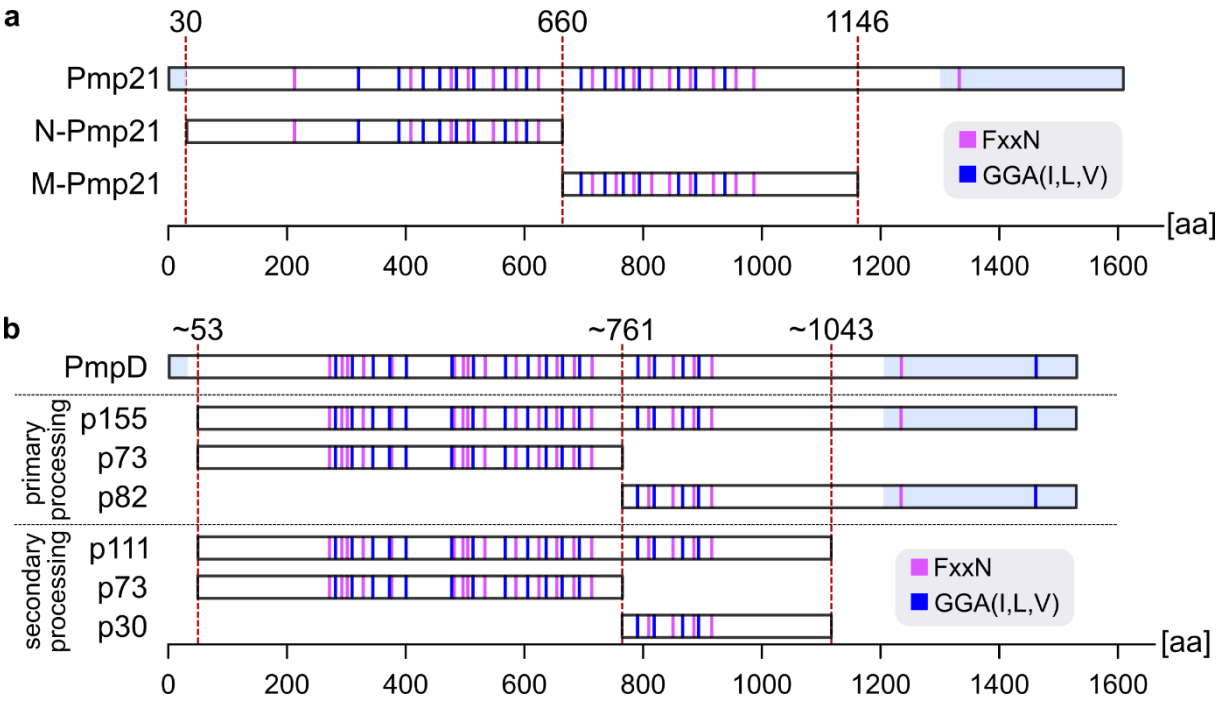

Figure 5: Suggested processing of *Cpn* Pmp21 and *Ctr* PmpD

a Schematic representation of Cpn Pmp21 with FxxN and GGA(I,L,V) motifs in magenta and blue, respectively, and the signal sequence and β-barrel in bright blue. Proposed processing sites are marked with dashed red lines and the resulting Pmp21 fragments are shown below (N-Pmp21 and M-Pmp21) [2, 3]. **b** Schematic representation of Ctr PmpD with FxxN and GGA(I,L,V) motives in magenta and blue, respectively, and the signal sequence and β-barrel in bright blue. Proposed processing sites are marked with dashed red lines. Primary processing is suggested to create membrane-bound, insoluble fragments while secondary processing is suspected to create soluble PmpD fragments [8].

adhesion to and internalization into the host cell, since all Pmp21 fragments were shown to adhere to epithelial cells [94].

In *Ctr,* processing sites were identified for all Pmps except PmpA and PmpC [92]. By using antibodies against *Ctr* PmpD, Crane et al. [107] identified smaller protein fragments with molecular weights of approximately 80 kDa and 42 kDa. Further studies, utilizing specific antibodies against individual domains of *Ctr* PmpD, revealed that at 24 – 48 hpi, not only full-length PmpD (~155 kDa) but also two fragments (p73 and p82) with molecular weights of 73 and 82 kDa, respectively, were detected by immunoblotting [91, 113]. The cleavage sites were located within the PmpD PD, with the first site just after the SS at residue 53, and the second site in the middle of the PmpD PD at residue 761 (Fig. 5b) [113]. Additionally, Swanson et al. [113] used anti-PmpD antibodies to immunoprecipitate complexes from the EB surface. Analysis of the samples by blue native-PAGE showed three distinct oligomeric complexes with molecular weights of 850 kDa, 530 kDa, and 100 kDa. Full-length PmpD (~155 kDa) and p82, both possessing the membrane-anchoring β-barrel, were detected in the 850 kDa and 530 kDa complexes. Interestingly, the p73 fragment, lacking the membrane-anchored β-barrel, was also found in both complexes [113]. Thus, they concluded that soluble p73 forms oligomeric complexes with other Pmps on the chlamydial surface, similar to what has been demonstrated for *Cpn* Pmp21 fragments. Analysis of infected cells at 30 hpi showed the presence of an additional PmpD fragment, p111, which is suggested to be further cleaved into two fragments; p73 and p30 (Fig. 5b) [92, 113]. However, localization of these fragments on the chlamydial surface has not yet been shown [113].

Despite the identification of proteolytic cleavage sites in several Pmps, it is still unknown, whether Pmps have autoproteolytic activity or if they are cleaved by host or chlamydial proteases. Hence, further research is needed to resolve the mechanism behind Pmp processing and to reveal the role of the processed fragments in chlamydial pathogenesis.

1.2.4 Oligomerisation

As mentioned in section 1.2.3, Pmps are proteolytically processed, which sometimes results in soluble fragments, lacking the membrane-anchoring β-barrel. However, using Blue native-PAGE and immunoblotting, some of these fragments were identified on the chlamydial surface [113]. Additionally, analysis of the *Ctr* L2 surface indicated

the presence of high molecular weight oligomeric structures, involving Pmps [90, 113]. These data strongly indicate, that Pmps participate in forming homo- and heterooligomeric structures on the chlamydial surface. *In vitro* studies on *Cpn* Pmp21 focused on one hand on the potential formation of oligomeric structures in solution and on the other hand on the characteristics that may drive this self-adhesion. Therefore, Luczak et al. [95], working on *Cpn* Pmps, used soluble fragments of Pmp21 and showed, that these fragments are prone to form oligomeric structures in solution, resembling elongated protofibrils, as they are typically formed by the protein fragment amyloid β42 (Aβ42) [117]. Further, they demonstrated that a *Cpn* Pmp21 fragment, containing two FxxN motifs, had a much higher capacity to form oligomeric structures compared to point-mutated versions in which the FxxN motifs were replaced by SxxV motifs [95]. Ultimately, Luczak et al. [95] performed adhesion assays on human HEp-2 cells, testing the binding of monomeric and oligomeric Pmp21 fragments with either FxxN or SxxV repeats. Their results showed that the characteristic tetrapeptide motifs are crucial for forming high molecular weight oligomers, which in turn enhance binding to the host cell surface [95]. These findings were further supported by Paes et al. [101], who showed that covalent disulfide bridges, formed by cysteine residues of the *Ctr* PmpD PD, contribute to the formation of stable, high molecular weight oligomers. In a further study on *Ctr* Pmps, Favaroni and Hegemann [96] investigated the role of FxxN and GGA(I,L,V) repeats in the oligomerization process. They used motif-rich and motif-poor recombinant protein fragments from different *Ctr* Pmps and demonstrated *in vitro* that the number of motifs is not important for oligomeric structure formation, as long as at least two motifs are present in the corresponding Pmp fragment [96]. Additionally, they showed that homooligomers were prone to form significantly shorter filaments than heterooligomers, which formed filaments of up to 2 µm in length [96]. Regarding adhesion to epithelial cells, data from Favaroni and Hegemann [96] suggest that a higher number of motifs correlates with stronger affinity to host cells, as fragments with fewer motifs exhibited comparably weak adhesion.

Currently, there is no *in vivo* data available regarding the presence of these filamentous structures on the chlamydial surface. Nevertheless, it is conceivable that these oligomers form *in vivo*, supported by the fact that soluble (β-barrel deficient) Pmp fragments have been found attached to the chlamydial surface, as extensively discussed in previous chapters. Moreover, it is hypothesized that through the

combination of different Pmp subtypes, not only increased host cell affinity is achieved but also enhanced antigenic epitope presentation. This would provide a potential mechanism for decoying and evading the host immune response [96].

1.2.5 Vaccination

As a human pathogen, *Ctr* is the major agent of preventable blindness and the leading bacterial cause for sexually transmitted diseases (STDs) [118]. Even though a chlamydial infection can be treated with antibiotics, therapy is often started too late or not at all because chlamydial infections rarely come with any symptoms. Furthermore, even if treated, chlamydial persistence can occur and reactivation of the infection is likely after treatment has ended. Untreated chlamydial infections of the urogenital tract in women can result in severe outcomes, including infertility and ectopic pregnancies [41, 119]. *Chlamydia* has been in focus for more than two decades but despite stringent public health control programs, infection rates for *Ctr* infections have not decreased [120, 121]. To effectively control chlamydial infections, a protective vaccine needs to be administered before sexual maturity. Initial approaches for developing a chlamydial vaccine were based on inactivated or live-attenuated EBs. However, due to relatively high costs of a whole cell vaccine as well as safety concerns, as later studies indicated the potential for a worsened secondary infection, research diverged from this idea and converged on a subunit- (protein-) based vaccine [122, 123]. The development of a subunit-based vaccine can either be based on using crude outer membrane protein preparations from infectious EBs, purified recombinant outer membrane proteins or a mix of recombinant peptides. However, for the development of a protein-based vaccine, which is effective against several chlamydial serovars or even species, a protein needs to be used which is present universally in several serovars or species and contains conserved domains which function as antibody epitopes.

One such protein is MOMP, encoded by *ompA*. MOMP is highly abundant in the chlamydial outer membrane, accounting for ~ 60% of the total outer membrane protein mass, and the protein encounters variable and conserved domains (VD and CD), both encompassing T- and B-cell epitopes [52, 124, 125]. In a preclinical study, mice were immunized with native MOMP prior to a chlamydial infection, leading to significant protection, displayed by a decreased time the mice shed viable organisms and generally less mice with positive cultures [126]. Succeeding preclinical studies using purified MOMP and adjuvants further indicated robust immune responses and a

significant protection against chlamydial infections [127-134]. Further, Sun et al. [132] prepared vaccines based on either native or recombinantly prepared MOMP and compared their ability to protect against a chlamydial infection. Even though both vaccines indicated a significant protection compared to the control group receiving no vaccination, they could show that vaccines based on native MOMP elicit even better protection than if prepared with recombinantly expressed MOMP [132]. Hence, for strong protection, the MOMP structure is suggested to be critical. This, however, is a limiting factor since the upscaling of MOMP production in its native form from infectious EBs is challenging, and the recombinantly expressed protein could not be obtained in a correctly folded form, in which it retains its epitopes, so far [52]. Hence, the best alternative so far is CTH522, a recombinant fusion protein consisting of the MOMP VD4 from *Ctr* serovars D, E, F and G [135]. A vaccine based on CTH522, combined with the liposomal adjuvant CAF01, was shown to provide protection against a subsequent *Ctr* challenge in mice [135]. Following these results, the vaccine was tested in a phase-1 clinical trial in humans, where it demonstrated a highly immunogenic effect [136].

Another protein family whose members are present in all chlamydial species, predicted to be located on the chlamydial surface, and critical for chlamydial infections are Pmps [93, 94]. Previous studies support a potential usage of Pmps for protein-based vaccines, as for example Pmp6 from *Cpn*, which has been shown to be clearly immunodominant [137]. Also, Tan et al. [138] could show that patients infected with *Ctr* elicit high titres against individual or multiple Pmp subtypes. Since Pmps are prone to form high molecular weight homo- and heterooligomers *in vitro*, it is conceivable that such oligomers also form on the chlamydial surface *in vivo* (see section 1.2.4). This could result in a high number of different heteromeric complexes which lead to a significant increase in antigen variation on the chlamydial surface and in turn helps the chlamydia to escape the immune system [96]. Pmp-based vaccines could elicit antibodies against specific Pmp subunits and/or Pmp complexes thus reduce the chlamydial advantage of presenting a large variety of antigens. This was already proven by various studies on Pmp-based vaccines. Paes et al. [139] demonstrated, that a vaccine based on recombinant *Ctr* PmpD, in combination with adjuvants, elicits significant protection against a *Ctr* infection in mice. Müller et al. [140] used a vaccine based on PmpA in combination with adjuvants, which led to a significantly decreased

severity of genital tract lesions in mice challenged with *C. muridarum*. More recently, Pal et al. [141] even tested the ability of Pmps to elicit cross species protection. Therefore, they used recombinant fragments of all nine Pmps from *Ctr*, in combination with adjuvants, as a vaccine in mice and then challenged them with *C. muridarum*. Results showed, that especially PmpC, G and H elicited the best protection, which was measured by the body weight changes and the number of IFU recovered from the mice's lungs. Additionally, Lanfermann et al. [142] used a protein-based vaccine containing fragments of *Ctr* PmpA, D, G, H and Ctad1, combined with cyclic-di-adenosine monophosphate as adjuvant, and demonstrated cross-serovar protection against both urogenital and ocular strains of *Ctr* [142].

A third protein which was tested as antigenic target was the chlamydial protease-like activity factor (CPAF), which is secreted into the host cell cytosol. Interestingly, patients that encounter a chlamydial infection demonstrated a higher antibody titre against CPAF than against other, surface-exposed proteins, including MOMP [143, 144]. In vaccine studies, recombinant CPAF together with interleukin-12 was used for immunizing mice and subsequent challenging with *C. muridarum* showed significantly reduced bacterial shedding and accelerated infection clearance [145]. Hence, the first milestones in developing a vaccine against chlamydia is set. However, future research is required to establish a highly effective vaccine, for which it is possible to upscale the production of the needed peptides and adjuvants to a sufficient amount.

1.3 Endocytosis

Endocytosis is a cellular process which occurs in all eukaryotic cells for internalizing components of the PM and the extracellular space by engulfing them within a plasma membrane vesicle [146, 147]. Via endocytosis, cells regulate various processes such as communication and response to extracellular stimuli, homeostasis, signalling, and nutrient uptake [148, 149]. Based on the size of the cargo and the uptake mechanism, different types of endocytosis are distinguished. The uptake of large particles (> 500 nm) is referred to as phagocytosis, while the ingestion of large extracellular bulk-phase volumes is termed pinocytosis [148]. Smaller particles are typically taken up via receptor-mediated endocytosis, where a ligand binds to a cell surface receptor, which triggers intracellular signalling, leading to the internalization of the

receptor-bound ligand. Typically, the formed vesicle has a diameter of roughly 100-200 nm [150]. Depending on the mechanism, the vesicle is either cytosolically coated with or without clathrin and the process is hence referred to as clathrin-mediated endocytosis (CME) or clathrin-independent endocytosis (CIE) [151]. Vesicles formed through CIE lack a distinct cytosolic coat and do not have a specific cargo selection mechanism [151]. Contrary, vesicles formed through CME involve specific cargo recognition and are coated with clathrin, as well as clathrin adaptor proteins [148, 150]. Following, CME will be introduced in more detail.

1.3.1 Clathrin-meditated endocytosis

CME, a common form of receptor-mediated endocytosis is responsible for the internalization of hormones, antibodies and nutrients, such as iron or cholesterol [152]. CME involves more than 40 proteins which are tightly regulated during several, partly overlapping, phases (Fig. 6) [152, 153]. The first phase of CME, known as receptor activation, begins when ligand molecules in the extracellular space bind to and activate specific cell surface receptors, which leads to intracellular signal transduction, initiating endocytotic processes (Fig. 6). For example, the epidermal growth factor (EGF), which binds to the EGF receptor, leads to the dimerization of the latter, resulting in its activation through autophosphorylation of the intracellular receptor domains [154]. This ligand-based receptor activation allows the recruitment of intracellular endocytic key proteins and with that to the transition to phase two; membrane bending. Two main proteins in this process are the adaptor protein AP2 and clathrin. AP2 binds to motifs located on the cytoplasmic side of the activated receptors as well as to phosphatidylinositol 4,5-biphosphate ($PI(4,5)P_2$) [152]. Following, enriched AP2 at the site of endocytosis recruits clathrin and other accessory proteins, leading to membrane invagination and stabilization of the clathrin-coated pit (Fig. 6) [155]. This pit rapidly grows by further membrane invagination, transitioning into phase three; vesicle budding and scission. Vesicle budding is supported by a tight network of polymerized and branched F-actin, located at the coat and at the base of the growing vesicle [150, 156, 157]. To establish such an F-actin network around the budding vesicle, BAR (Bin-Amphiphysin-Rvs) domain proteins, which sense specific degrees of membrane bending, bind to the invaginating membrane and recruit via their SH3 domains further proteins, such as for example members of the Wiskott-Aldrich-Syndrome-Protein (WASP) family [158]. WASP, in its active state, engages with the Arp2/3 complex which

initiates F-actin polymerization and branching, providing mechanical forces which are needed for further invagination of the PM and the growth of the endocytic pit [150]. A typical endocytic vesicle of a mammalian cell grows to a diameter of approximately 100-200 nm before it is released into the cytosol [159, 160]. The scission of the vesicle from the donor membrane is catalysed mainly by sorting nexin 9 (SNX9), a BAR-domain protein, which recruits dynamin, a large GTPase [161, 162]. The interplay of SNX9 and dynamin leads to a helical collar which arranges around the neck of the forming vesicle and eventually breaks it, releasing the matured vesicle from the donor membrane to the cytosol (Fig. 6) [150, 162]. The entire endocytic process is thought to be self-regulatory, as an expanding pit has a progressively changing membrane curvature, leading to the binding of different BAR domain proteins [150, 163]. At an early stage of endocytosis, proteins with an F-BAR domain, such as FCHO1/2, are

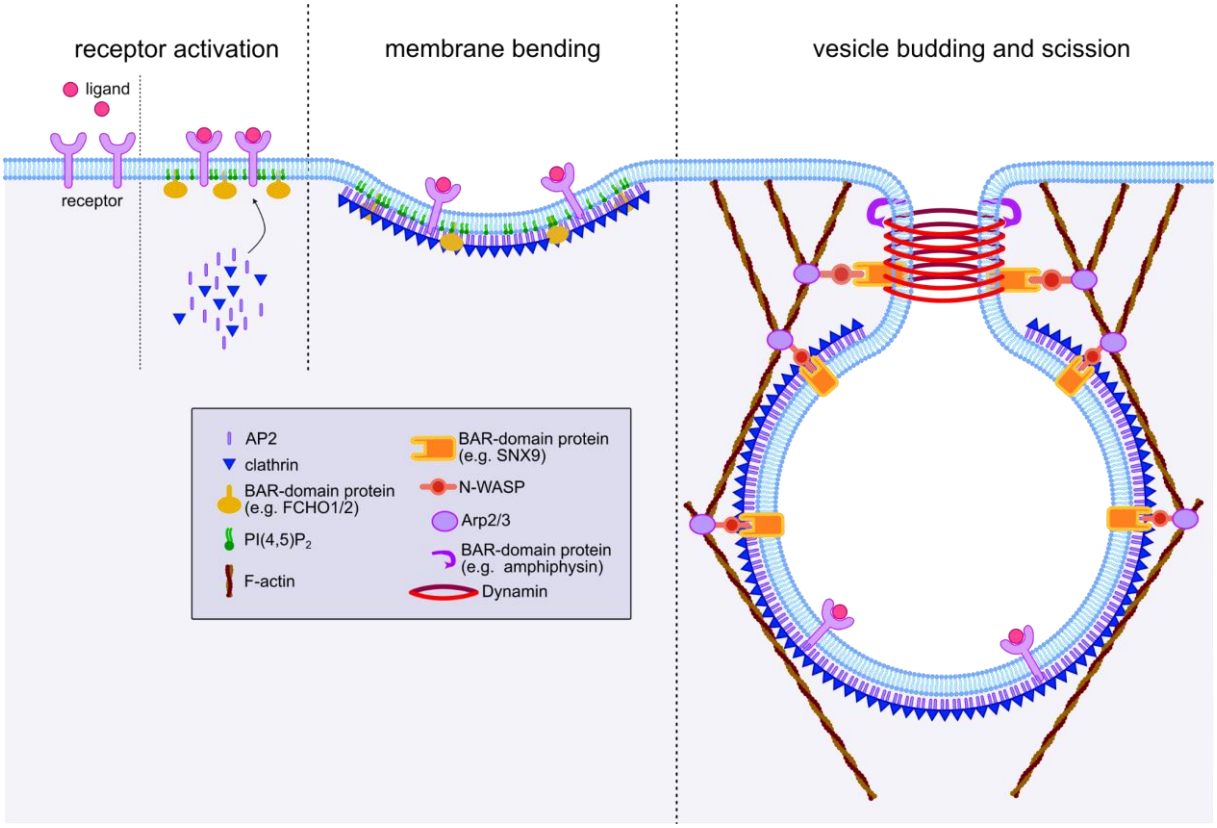

Figure 6: Schematic representation of the initial steps of clathrin-mediated endocytosis

Binding of a ligand to its receptor leads to the activation of the latter and hence to downstream signalling. BAR-domain proteins are recruited to the side of endocytosis and $PI(4,5)P_2$ lipids are accumulated in the inner leaflet of the membrane. The adaptor protein AP2 and clathrin are recruited, leading to the formation of a clathrin coated pit. This pit then grows by the acquisition of further BAR-domain proteins, WASP protein family members and the actin cytoskeleton and is finally pinched of from the donor membrane via the recruitment of dynamin.

recruited and promote the clustering of $PI(4,5)P_2$ at the site of endocytosis, facilitating AP2 and clathrin assembly [164]. During the intermediate stage, BAR domain proteins, such as SNX9, are recruited, which are involved in significant membrane remodelling and the recruitment of other factors, including members of the WASP family. Also, late in endocytosis, SNX9, together with N-BAR domain proteins like amphiphysin and endophilin, assists in scission of the matured vesicle from the donor membrane by recruiting other factors, like dynamin (Fig. 6) [165-168]. Eventually, the clathrin coat is disassembled from the released vesicle by Hsp70 and auxilin and proceeds to fuse with the early endosome [169, 170].

1.3.2 Key processes for endocytosis

In CME, two critical structures must be modulated: the PM, which has a tightly controlled lipid composition and undergoes significant deformation, and the actin cytoskeleton, which provides the mechanical forces required for reshaping the membrane, expanding the endocytic pit and scission the matured vesicle.

1.3.2.1 The role of the plasma membrane during endocytosis

The PM establishes a semipermeable barrier that separates the extracellular space from the cytosol. It basically consists of a lipid bilayer with a hydrophobic core and is equipped with further components such as cholesterol, glycolipids, carbohydrates, and proteins. The overall structure of the PM is rather dynamic, with a fluid-like characteristic, allowing the membrane to bend, fuse and undergo fission, in order to fulfil various biological tasks such as the formation of an endocytic vesicle [171].

During CME, the membrane needs to extensively bend inwards, forming an endocytic pit, which is mediated via several mechanisms. First, membrane deformation can be achieved by changes in lipid composition. Individual phospholipids exhibit distinct architectures depending on the size of their head group and on the length and saturation of their acyl chain [172]. For example, $PI(4,5)P_2$ has a rather large head group and is accumulated early in CME at the cytosolic side of the PM, leading to its invagination through steric pressure [173]. Secondly, membrane deformation is facilitated by the reversible insertion of integral membrane proteins, protein domains or hydrophobic protein motifs [172]. Throughout CME, BAR domain proteins tightly regulate membrane invagination and fission [164, 166, 174]. As already mentioned in 1.3.1, individual BAR domain proteins detect specific membrane curvatures and bind

to them as dimers, stabilizing and enhancing the membrane curvature and further recruiting key endocytic components for example elements of the actin cytoskeleton [167]. Thirdly, membrane deformation is induced by mechanical forces generated through the cytoskeleton and molecular motor proteins [172]. Thereby, especially the actin cytoskeleton adopts a crucial function for CME, introduced in section 1.3.2.2.

1.3.2.2 The role of the actin-cytoskeleton during endocytosis

The cytoskeleton is a dynamic network of different protein filaments, responsible for cell shape and its resistance against deformation. In eukaryotes, the four main components of the cytoskeleton are the actin filaments, microtubules, intermediate filaments and septins [175, 176]. For endocytic processes, especially the actin filaments and the microtubule network play a crucial role. While the actin cytoskeleton is associated with vesicular growth and maturation, the microtubule network helps to transport the matured vesicle away from the cell cortex to its designated destination within the cell [160, 177, 178]. Despite their different functions, their polymerisation mechanism is related. Under physiological conditions, spontaneous polymerisation is possible but unfavourable. Therefore, regulatory proteins in the cell, such as the Arp2/3 complex, help form a nucleation centre consisting of monomer subunits (globular actin or α/β-tubulin) from where the actin filaments and microtubules then polymerize [179]. The Arp2/3 complex consists of seven subunits from which two (Arp2 and Arp3) closely resemble monomeric actin and thus serve as an actin nucleation centre [180, 181]. To establish a branched actin network, the Arp2/3 complex assembles at the side of a pre-existing actin filament and anchors a new filament in a 70 ° angle to the mother filament [182]. In the context of CME, the growing vesicle and the associated membrane curvature lead to the recruitment of the BAR domain protein SNX9 which in turn recruits proteins from the WASP family, such as for example N-WASP [183, 184]. The C-terminus of active N-WASP, the VCA domain, recruits the Arp2/3 complex, which anchors to a pre-existing filament and initiates F-actin polymerisation and branching [185]. Even though the exact role of the actin network around the growing vesicle is not fully understood, it is suggested that the branched actin filaments provide the mechanical forces needed for supporting the invagination of the membrane during vesicular growth. The newly branched actin filaments are linked with proteins bound to the endocytic coat which allows an efficient transmission of force on the budding vesicle [186].

1.3.3 SNX9 and N-WASP as mediators for endocytosis

For CME, over 40 proteins are involved to enhance the endocytic vesicle formation. Two of them, SNX9 and N-WASP, are introduced in more detail.

1.3.3.1 SNX9 is involved in membrane invagination and connects the PM with the actin cytoskeleton

SNX9 belongs to the SNX protein family, which was initially identified in the context of endosomal sorting [187]. Members of the SNX family are very diverse in architecture and in function but all of them possess a phox-homology (PX) domain that enables binding to phosphatidylinositol (PIP) containing membranes [188]. Beside the PX-domain, SNX9 possesses an N-terminal SH3 domain, an adjacent low complexity (LC) domain, and a C-terminal BAR domain (Fig. 7). With its PX and BAR domain, SNX9 provides a relatively large lipid-binding pocket, enabling it to mediate a wide range of interactions [168]. This differs from other SNX family members, which typically exhibit a high affinity for a specific PIP [189]. The SNX9 SH3 domain functions as a protein-binding platform for proline-rich domains (PRD) found in eukaryotic, prokaryotic, or viral proteins. As a result, it often serves as a target for pathogens to manipulate host cell mechanisms, as for example for the *E. coli* protein EspF or the *Cpn* SemD [168, 190-192].

During CME, SNX9 primarily functions as membrane curvature sensor and as anchor point for recruiting key components of the endocytic machinery, that are involved in later stages of CME [168]. With its BAR domain, SNX9 binds to specific curved endocytic membranes [167, 189]. Further, via the LC domain, it stabilizes the position of clathrin and AP2 at the invaginating pit and recruits the Arp2/3 complex [166, 193].

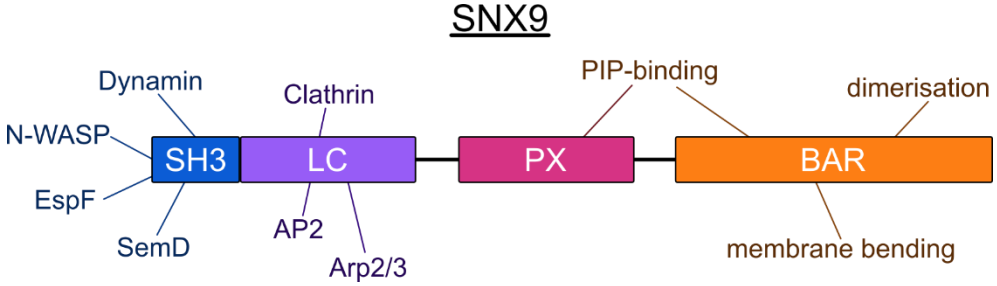

Figure 7: Schematic representation of SNX9 domains and their functions
SNX9 contains distinct domains, each with specific functions. Here, the focus was set on the roles related to endocytosis. SH3: Src-homology 3, LC: low complexity region, PX: Phox-homology domain, BAR: Bin-Amphiphysin-rvs domain. Modified form Bendris et al. [168]

Through its SH3-domain, membrane-bound SNX9 interacts with PRDs, as found in family members of the actin modulator WASP [194]. Additionally, via the SH3-domain, SNX9 mediates recruitment of dynamin to the vesicular neck, facilitating scission of the vesicle from the donor membrane. Thus, during endocytosis, SNX9 is an important membrane bender and adaptor protein, directing processes involved in membrane modulation and actin cytoskeleton remodelling.

1.3.3.2 N-WASP binds and stabilizes the Arp2/3 complex for establishing an actin network around the budding vesicle

N-WASP is one out of nine WASP-family members and ubiquitously expressed in mammalian cells [195]. The C-terminus of WASP proteins is conserved and can be seen as “output” region, as it is responsible for signal transduction and protein recruitment. It includes both the VCA domain (verprolin homology, cofilin homology and acidic domain), responsible for binding the Arp2/3 complex and globular actin, and the PRD, binding to the SH3-domain of proteins, like SNX9 [196]. The N-terminus of individual WASP proteins is unique and acts as regulator of the “output” domain. The N-terminus of N-WASP consists of a WASP-homology 1 (WH1) domain, also known as Ena/VASP-homology 1 (EVH1), a basic region (BR), and a GTPase binding domain (GBD) (Fig. 8) [197]. The GBD domain can be further subdivided into a Cdc42- and Rac-interactive binding domain (CRIB) and a C-sub domain [198]. Most of the BR-domain is responsible for binding anionic phospholipids, with a preference for $PI(4,5)P_2$, but the BR-domains final C-terminal residues are also involved in Cdc42 binding [198, 199].

In a resting cell, N-WASP is present in an autoinhibited state, in which the GBD domain binds the VCA domain and masks it from binding to actin or the Arp2/3 complex (Fig. 8) [195]. During CME, N-WASP activation is achieved by various mechanisms, which function synergistically. The main activation mechanism involves active Cdc42 ($Cdc42_{GTP}$), which engages with the CRIB domain and the C-terminal residues of the BR-domain [199]. This interaction transforms N-WASP into an open state where the internal blockage is abrogated and the VCA domain is freely accessible. Further, N-WASP activation is enhanced by the interaction of the PRD with an SH3-domain (section 1.3.3.1), or by phosphorylation of specific serine or tyrosine residues in the CRIB domain, by for example Src family Kinases [200, 201].

In conclusion, N-WASP activation is mediated via various synergistic and additive mechanisms. This allows it to act as signalling molecule to modulate the F-actin network around the growing endocytic pit by recruiting the Arp2/3 complex.

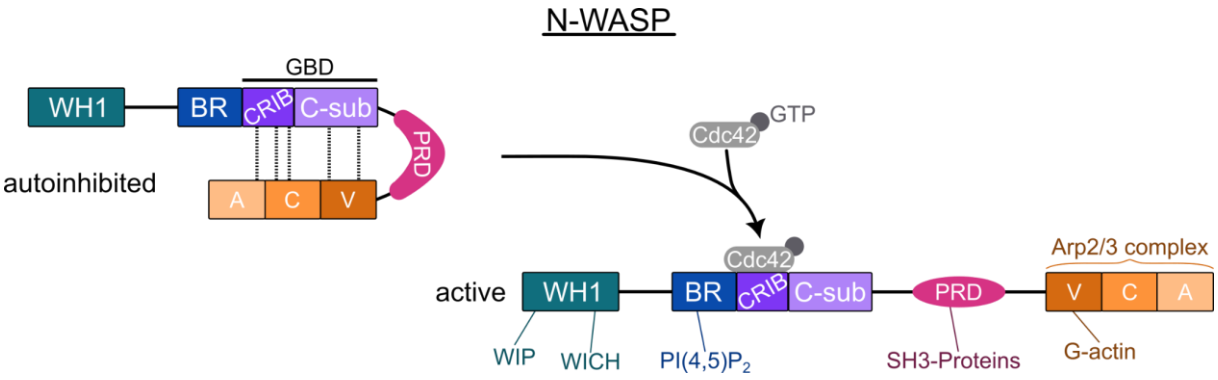

Figure 8: Schematic representation of N-WASP domains and their functions

In a resting cell, N-WASP function is blocked through autoinhibition. During endocytosis, the small Rho GTPase Cdc42, activated by the replacement of its GDP with a GTP, binds to autoinhibited N-WASP, thus activating it. The individual N-WASP domains are then freely accessible and perform their designated function for proceeding endocytotic processes. WH1: WASP-homology 1, BR: basic region, CRIB: Cdc42- and Rac-interactive binding, PRD: proline-rich domain, VCA: verprolin homology, cofilin homology and acidic domain. Modified from Thrasher et al. [202].

1.3.4 Endocytosis as entry point for obligate intracellular pathogens

The extracellular space presents harsh conditions for pathogens, since it is abundant in harmful components, such as immune cells and antibodies. To survive, pathogens must either protect themselves from this hostile environment or escape it [203]. One effective strategy is, to invade a host cell, in which the pathogen divides and replicates in a protective vacuole. While viruses must invade host cells to replicate as they have no own metabolism, bacterial and eukaryotic parasites are often, but not always, self-replicative and exploit the protective environment of vacuoles for their division and replication [204]. Regardless of their need to invade host cells, pathogens typically hijack the endocytic machinery to facilitate uptake [205, 206].

Viruses often utilize the CME pathway as an entry mechanism, as the size of a typical clathrin-coated vesicle (100-200 nm in diameter) is suitable for most viruses [160, 207]. However, there are also examples of viruses utilizing the CIE pathway and larger viruses that hijack macropinocytosis for their uptake [208-210].

Bacterial pathogens are more complex than viruses and are generally larger with a typical length/diameter of 1-5 µm [204]. To enter non-phagocytic host cells, which normally do not engulf larger particles, bacteria use a mechanism that, in its later

stages, closely resembles phagocytosis but the induction of the primary stages is induced by the bacterium itself [211]. Thereby, two mechanisms can be defined: the zipper mechanism and the trigger mechanism [212].

1.3.4.1 Zipper mechanism

The zipper mechanism is based on bacterial surface proteins that function as adhesins and induce receptor-mediated uptake. First, the bacterium adheres to the host cell by binding to and activating specific host cell receptors. Following receptor activation, which leads to intracellular signalling cascades, the actin cytoskeleton and PM are reorganised for the formation of a phagocytic cup. Once the membrane has fully engulfed the bacterium, the cup seals, enclosing the bacterium in a large vesicle inside the host cell [212]. A bacterial prime example utilizing the zipper mechanism is the food-borne, Gram-positive pathogen *Listeria monocytogenes* [213]. For receptor activation, *Listeria monocytogenes* relies on two surface proteins. The first, Internalin A (InlA) is covalently anchored to the bacterial cell wall and binds to E-cadherin on the host cell. E-cadherin is a transmembrane protein located only at the adherens junctions of polarized epithelial cells [212, 214]. Binding initiates intracellular signal transduction, leading to actin remodelling and, ultimately, uptake of *L. monocytogenes*. The second surface protein, Internalin B (InlB) is loosely attached to the bacterial surface via its C-terminal tail and binds to three different host cell receptors [215]. The most significant one is the receptor tyrosine kinase Met, which is expressed on all epithelial cells and typically interacts with hepatocyte growth factor (HGF) [216]. When InlB binds to Met, a signalling cascade similar to that of HGF binding is induced: Met dimerises and its intracellular domains are autophosphorylated. As such, they serve as protein binding sites for adaptor molecules that promote phagocytic processes [215].

1.3.4.2 Trigger mechanism

For the trigger mechanism, bacterial pathogens use the needle-like type-III-secretion system (T3SS) to secrete entry-related effector proteins, which are stored in the bacterial cytoplasm, into the host cell cytosol, where they manipulate key components of the host endocytic machinery and elements of the cytoskeleton [212]. This manipulation induces membrane protrusions that engulf the bacterium, ultimately enclosing it completely [217]. A well-known pathogen that uses, among others, the trigger mechanism is the Gram-negative bacterium *Salmonella*. After establishing

initial contact, *Salmonella* releases various effector proteins into the host cytosol. Most of these effectors target small host G-proteins, through which they control the actin polymerization and branching machinery. Others, such as for example SopB, modify the composition of the PM beneath the attached bacteria, further facilitating bacterial engulfment and entry [217].

1.3.4.3 Chlamydial uptake into a non-professional phagocytic host cell

The categorisation of *Chlamydia* into one of these mechanisms is challenging, as they use a combination of both. However, the extent to which CME supports chlamydial uptake is still debated. For *Ctr*, microscopic analyses have shown that clathrin is associated with the vesicle engulfing the EB, while other studies have indicated that chlamydial uptake is not impaired when CME is inhibited [218-223]. Additionally, there is evidence, suggesting the involvement of both, phagocytosis and pinocytosis in the uptake process [224, 225].

The probably most prominent chlamydial entry process associated with the zipper mechanism involves the *Cpn* specific outer membrane protein Pmp21. By binding to and activating the host EGFR, it initiates EB uptake through endocytotic processes (described in previous chapters) [108]. Similarly, the *Cps* specific Pmp17G is believed to bind to and activate the EGFR as well, mediating EB uptake via the zipper mechanism [110]. For other chlamydial species, the activation of specific host cell receptors, and consequently the use of the zipper mechanism, has been suggested as well. For instance, the host cell receptor Ephrin A2 was indicated to facilitate *Ctr* uptake [226]. However, the exact processes and the involved chlamydial and host proteins remain largely unknown and require further investigation [226, 227].

Chlamydia also possess a T3SS and secrete entry-related effector proteins into the host cytosol, modulating the actin cytoskeleton and mediate internalization via the trigger mechanism [228]. For example, the *Ctr* translocated actin recruiting phosphoprotein (TarP) is a soluble secreted early effector that nucleates actin filaments beneath the EB entry site [229]. Further, the *Ctr* translocated membrane-associated effector A (TmeA) synergistically promotes the EB entry by binding to the inner leaflet of the PM and recruiting N-WASP, which promotes F-actin polymerization and branching via the Arp2/3 complex [230]. For *Cpn*, such early secreted effector proteins were identified as well, such as for example CPn0572, the ortholog to *Ctr* TarP. In the host cytosol beneath the EB entry side, CPn0572 binds

and polymerises actin. However, differing to TarP, CPn0572 has also been demonstrated to stabilize F-actin filaments by displacing and blocking cofilin (an endogenous actin-severing protein) from binding and to affect the microtubule cytoskeleton dynamics [231-233]. In addition to CPn0572, other *Cpn* effectors have been identified, such as the membrane-bound effectors SemC and SemD, which will be introduced in chapter 1.4 [191, 234].
Summarized, it is suggested that *Chlamydia* may have evolved an internalization process that involves both the zipper- and trigger-mechanism, to facilitate a highly efficient uptake into a protective vacuole.

1.4 The *Cpn* entry-related effector SemD

Since chlamydial elementary bodies (EBs) are metabolically inert, the proteins necessary for adhesion and internalization processes must be produced in the reticulate body (RB) during the preceding infection cycle. Therefore, to identify potential proteins crucial for the initial steps of infection, it is important to determine which genes are upregulated during the late stages of a preceding infection. A genome wide transcriptional analysis identified 88 *Cpn* genes that were significantly upregulated during the later stages of a chlamydial infection [234]. Among these genes, an operon was identified, consisting of *cpn0676*, *cpn0677 (semD)* and *cpn0678 (semC),* all of which showed increased transcript levels after 36 hpi [234]. Comparison with other chlamydial species revealed that the genes in this cluster are part of a syntenic locus (Fig. 9a). While CPn0676 is conserved among all chlamydial species (39-44 % identity), *Cpn* SemD and SemC are more complex. Other chlamydial species have a single gene at this locus, such as *Cps* with *sinC* and *Ctr* with *tmeA*. The amino acid identity of SemD and SemC with these proteins is relatively low, with homology to SINC at 21 % and 14 %, respectively, and less than 5 % to TmeA (Fig. 9a). Functional analysis of the proteins encoded by this syntenic locus revealed a high variety in function. *Cps* SINC functions during the late stages of infection, associating with the nuclear membrane [235]. *Ctr* TmeA is an early secreted effector that recruits and activates the host N-WASP to regulate actin polymerization and branching via the Arp2/3 complex [230]. *Cpn* SemC and SemD are substrates of the T3SS and bind via an N-terminal amphipathic helix (APH) to the cytosolic leaflet of the PM at the site of

EB entry. Besides the APH, SemC possesses three PRDs, of which the first was demonstrated to bind to the SNX9-SH3 domain [234]. SemD has a more complex structure (Fig. 9b). In addition to the APH, which has a high affinity for phosphatidylserine (PS), a specific phospholipid found in the inner leaflet of the PM, SemD has two PRDs, two Wiskott-Aldrich homology 2 (WH2) domains and one C-terminal N-WASP binding domain. *In vitro* experiments using giant unilamellar vesicles (GUVs), a synthetic model membrane, demonstrated that over time, SemD can deform the membrane by inducing an inwardly directed force [191]. Additionally, membrane-bound SemD serves as a binding platform for additional host key endocytic proteins. Spona et al. [191] showed that the PRD1 is responsible for binding to the SH3 domains of the BAR-domain-containing proteins Pacsin2/3 and SNX9, which are crucial during endocytic processes for remodelling the PM (section 1.3). With the WH2 domain, SemD recruits G-actin, however it remains unclear whether both WH2 domains are involved in G-actin binding [191]. It has been suggested that by binding G-actin, SemD significantly increases its local concentration, thus providing the necessary subunits for rapid polymerisation and branching of F-actin around the

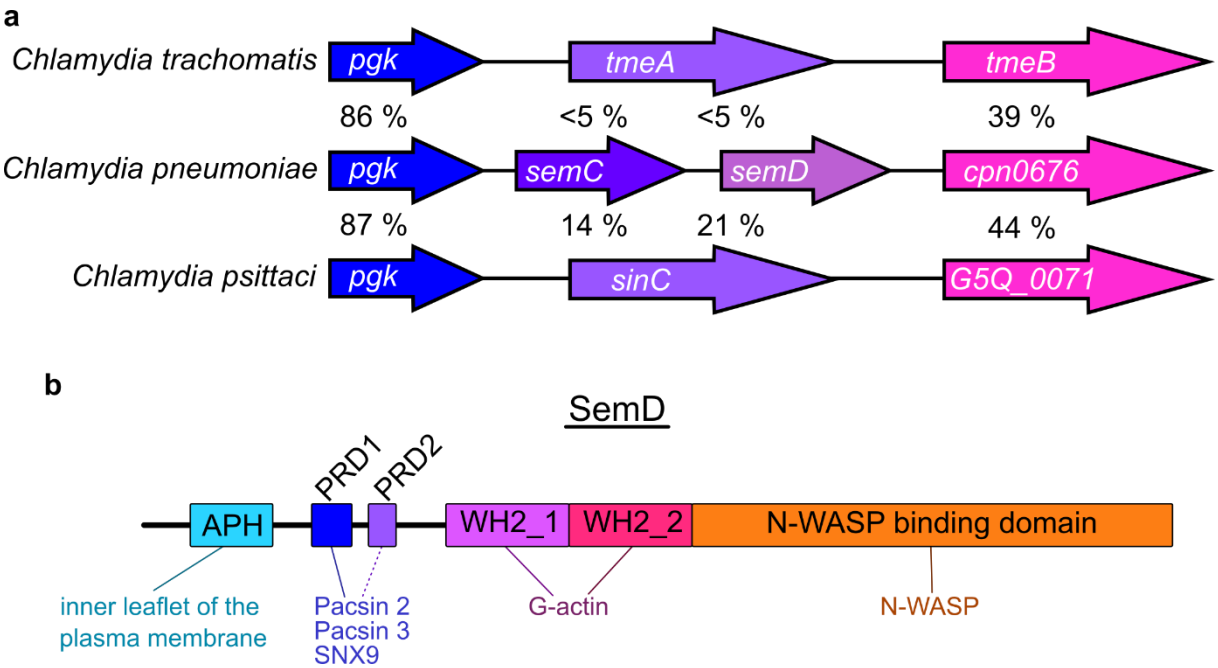

Figure 9: Schematic representation of the operon containing *semC*, *semD* and *cpn0676* and the domain organisation of SemD

a Schematic representation of the gene clusters encoding for chlamydial effector proteins. Percentages indicate the amino acid identity between homologues [234]. **b** SemD protein architecture with the according interaction partners are indicated. APH: amphipathic helix, PRD: proline-rich domain, WH2: Wiskott-Aldrich homology 2 domain

growing vesicle. The C-terminal N-WASP binding domain is responsible for binding to N-WASP and Spona et al. [191] further showed that the C-terminal part of SemD is sufficient for N-WASP activation, leading to Arp2/3-mediated F-actin branching and polymerization (section 1.3.3.2). For doing so, they incubated G-actin, N-WASP and Arp2/3 with GUV-bound SemD and demonstrated rapid F-actin polymerization at the perimeter of the GUV. In the negative control, where SemD was excluded, F-actin was not detected [191].

Summarized, membrane-bound SemD centralizes components for membrane deformation (via Pacsin2/3 and SNX9) and provides the mechanical forces needed for vesicular growth (via the branched actin cytoskeleton) at the site of EB entry [191]. However, the mechanistic details of how N-WASP activation is mediated by SemD in the absence of N-WASP's endogenous activator, $Cdc42_{GTP}$, remain unknown. Additionally, the question of how this multivalent interaction is spatially (and/or temporally) coordinated has yet to be answered.

2 Objectives of this work

As obligate intracellular pathogens, *Chlamydia* rely on adhesion to and internalization into host cells. Yet, many mechanisms are still not fully understood.

While for all nine *Ctr* Pmps adhesion to epithelial cells was shown, the first part of this work focuses on two of them; PmpD and PmpG. PmpD, which is surface-exposed on EBs, was shown to be crucial early in infection (section 1.2), however, its host cell binding partner(s) remain unknown. The aim is to identify host cell binding partner(s) for *Ctr* PmpD, using two approaches in parallel. In approach (I), soluble recombinant PmpD is used as bait in pulldown experiments on epithelial cells, followed by mass spectrometry to identify enriched proteins. In approach (II), PmpD is genetically fused to APEX2 and transformed *Ctr* expressing the fusion construct are used to infect epithelial cells. During early infection, when EBs adhere to the host cell surface, APEX2 activity is initiated, biotinylating proteins proximal to APEX2-PmpD, which are then identified by mass spectrometry analysis.

For PmpG, which has an unusual species-specific subgroup expansion (section 1.2), adhesion to epithelial cells has been shown, but its adhesion capacity remains controversial across different adhesion assays. The aim is to investigate adhesion of PmpG on epithelial cells and develop a standardized method assessing its binding capacity.

The second part of this work focuses on SemD, a *Cpn* entry-related early effector that is secreted into the host cell cytosol and required for *Cpn* internalization. Previous research has shown, that after its secretion, SemD binds to the inner leaflet of the plasma membrane at the site of EB entry and acts as binding platform for key components of the host endocytic machinery, such as SNX9 and N-WASP, an actin cytoskeleton modulator. Further, it was shown that SemD also activates N-WASP, bypassing the activation by its endogenous activator, $Cdc42_{GTP}$. The aim of this work is, to structurally characterize SemD, helping to identify how the multiple interactions with host cell proteins and the membrane are spatially regulated. Further, structural analysis of SemD and N-WASP should clarify how N-WASP activation in the absence of $Cdc42_{GTP}$ is mediated.

3 Part I: Manuscript I

Title:

Secreted host cell clusterin binds *Chlamydia trachomatis* PmpD and is essential for infection

Authors:

Fabienne Kocher, Johannes H. Hegemann

Contribution:

Fabienne Kocher (F.K.): 90 %, Johannes H. Hegemann (J.H.H.): 10 %

F.K. and J.H.H. jointly planned the experiments. F.K. provided the experimental data for all figures (except Fig. 2B,C), analysed the data, wrote the manuscript and prepared the figures. F.K. and J.H.H discussed the data. J.H.H revised the manuscript. Gereon Poschmann (G.P.) generated the mass spectrometry data, shown in Fig. 2B,C.

Submitted to:

Frontiers in Cellular and Infection Microbiology, October 2024

2023 Impact Factor: 4.6

I hereby confirm that this information is correct.

Düsseldorf, 22 October 2024

Fabienne Kocher

Secreted host cell clusterin binds *Chlamydia trachomatis* PmpD and is essential for infection

Fabienne Kocher[1], Johannes H. Hegemann[1*]

1 Heinrich Heine University Düsseldorf, Faculty of Mathematics and Natural Sciences, Institute for Functional Microbial Genomics, Düsseldorf, Germany

* Corresponding author: johannes.hegemann@hhu.de

Abstract

For the obligate intracellular pathogen *Chlamydia*, especially the adhesion to and internalization into the host cell are pivotal steps to establish an infection. *Chlamydia trachomatis (Ctr)* possesses a family of polymorphic membrane proteins (Pmps) which were shown to be crucial during the adhesion and internalization step, however, the involved host cell molecules were unknown. Here, we show that a recombinant fragment of *Ctr* PmpD, which forms high molecular weight oligomers in solution and shows adhesion to epithelial cells, directly binds to secreted clusterin (sCLU), a chaperone-like protein secreted into the extracellular space by the host cell and part of the chaperone- and receptor-mediated extracellular protein degradation (CRED) pathway. Using *in vitro* assays, we show the direct interaction of sCLU and soluble rPmpD. In infection experiments, depletion of sCLU from the cell culture medium leads to a significant decrease in *Ctr* infection efficiency. Thus, sCLU is the first host cell interaction partner identified for a *Ctr* Pmp, and moreover the first example for sCLU as host cell receptor for host cell internalization by a pathogen.

Introduction

Chlamydia trachomatis (*Ctr*) is the most common bacterial cause of sexually transmitted infections worldwide. If untreated, it can lead to infertility or ectopic pregnancies [1]. Additionally, *Ctr* is the leading cause of trachoma, the world's primary cause of infectious blindness, targeted for elimination by the end of the decade [2]. *Ctr* belongs to the genus *Chlamydia*, which are obligate intracellular, Gram-negative bacterial pathogens, infecting epithelial cells [3]. Most chlamydial species are pathogenic to animals. However, two species, *Ctr* and *Chlamydia pneumoniae* (*Cpn*), from which the latter infects the upper and lower respiratory tract, are human pathogenic species [4]. *Ctr* can be subdivided into 19 serovars, grouped into three biovars, each responsible for specific pathological conditions [5]. Serovars A-C lead to trachoma and blindness [5]. Serovars D-K cause infections of the genital tract and can lead to pelvic inflammatory disease (PID), ectopic pregnancy and infertility in women and to urethritis and epididymitis in men [5]. Serovars A-K typically cause local infections only. Serovars L1-L3, also known as the lymphogranuloma venereum biovar, lead to invasive infections of the urogenital and anorectal tract and cause systemic infections [6].

All chlamydial species, including *Ctr*, possess a unique developmental cycle, altering between two morphological forms; the infectious but metabolically inactive elementary body (EB) and the metabolically active but non-infectious reticulate body (RB) [7]. The initial step of a chlamydial infection is the EB adherence to and internalization of the host cell. Inside the host cell, the EB stays in a membrane-enclosed compartment termed inclusion, in which it differentiates into an RB. By hijacking nutrients from the host cell, the RB undergoes repeated replication cycles, before the pool of RBs asynchronously transitions back into EBs which are released into the extracellular space via cell lysis or extrusion of the inclusion [3, 7-9].

For obligate intracellular pathogens, adhesion to and internalization of the host cell is of utmost importance. For the successful implementation of these processes, *Chlamydia* have evolved different adhesins such as GroEL1, MOMP, OmcB, Ctad1 and the family of polymorphic membrane proteins (Pmps) [10-16].

Pmps are found in all chlamydial species and can be subdivided in six phylogenetic subtypes (A to H), with 21 members in *Cpn* and 9 members in *Ctr* [17]. Pmps share between 19 % and 40 % sequence identity across species and are thought to belong to type V autotransporters, based on their domain architecture [18]. They possess an

N-terminal secretion signal, a C-terminal β-barrel and a central passenger domain (PD) [18]. The signal sequence allows the Sec-dependent transportation across the inner membrane into the periplasmic space, where the Sec sequence is typically split off and the protein folds. The β-barrel is inserted into the outer membrane, supported by the BAM-complex, forming a channel for the PD to be exported to the cell surface [19]. There is evidence, that the extracellular Pmp PDs exists as both, membrane-anchored and soluble forms, for which proteolytical processing sites were identified [20-22]. Further, the Pmp PD is exceptionally rich in FxxN and GGA(I,L,V) motifs, which were shown to be crucial for adhesion to epithelial cells [23].

Among the nine *Ctr* Pmps, which were all shown to possess adhesive functions on epithelial cells and are essential for infection [13], PmpD and its *Cpn* homologue Pmp21 are the best studied ones today. Proteomic studies suggest that PmpD undergoes proteolytic processing, resulting in several fragments with or without the β-barrel [20, 24]. Interestingly, immunoaffinity-purified PmpD from the EB surface is organised into high-molecular weight complexes, consisting of four to six PmpD fragments [20]. *In vitro*, the formation of such high molecular weight oligomers was shown for *Ctr* PmpA, PmpD, PmpG and PmpI and their importance for the adhesion to epithelial cells was suggested [25]. Biochemical studies showed that the monomeric PmpD PD has a high β-sheet content and likely folds into a triangular β-helical structure [26, 27]. Oligomeric PmpD PD however, were suggested to form fibril-like structures, resembling the amyloid fibrils formed by the amyloid protein fragment β42 [25, 27, 28]. Functional studies have shown that PmpD makes a critical contribution to the infection process. Anti-PmpD antibodies exhibit significant pan-neutralizing activity against a number of different *Ctr* serovars in cell culture and a PmpD-based vaccine has shown protective effects in mice [29, 30]. Additionally, a *pmpD* null mutant of *Ctr* serovar D showed significantly reduced adhesion and internalization capacities in human cell lines and non-human primate models, but not in murine cells [31]. Interestingly, in *C. muridarum* transposon-mediated inactivation of PmpD, PmpA or PmpI led to growth attenuation and reduced infectious progeny suggesting functional aspects in addition to adhesion [32]. For the *Ctr* PmpD homologue in *Cpn*, Pmp21, similar structural and functional characteristics have been shown [23, 33, 34]. However, the role of PmpD and Pmp21 in infection are thought to be species-specific, as recombinant Pmp21 reduces *Cpn* but not *Ctr* infection and vice versa [13]. Pmp21 binds to and activates the epidermal growth factor receptor (EGFR), which facilitates chlamydial uptake via

endocytosis, showing that Pmp21 functions as both, adhesin and invasin [33]. Similarly, *C. psittaci* Pmp17G, belonging to a different subtype than *Ctr* PmpD or *Cpn* Pmp21, is suggested to bind the EGFR, too [35]. Importantly, while several human cell surface receptors such as heparan sulfate proteoglycans, CFTR, β1-integrin, ephrin A2, and protein disulphide isomerase have been associated with adhesion and/or internalization of *Ctr*, no receptor has been identified for *Ctr* Pmps to date [36].

Here, we used a proteolytically processed form of *Ctr* PmpD, found in both soluble and membrane-bound complexes during infection, to identify its host cell binding partners [20]. Biochemical characterization of the recombinant PmpD fragment, rD72, indicated the formation of high molecular weight oligomers, and adhesion to epithelial cells in a concentration-dependent manner. Incubation of rD72 with human epithelial HEp-2 cells followed by immune precipitation and affinity enrichment and mass spectrometry analysis revealed clusterin (CLU) as rD72 host binding partner. Clusterin is a human protein, part of which is secreted into the extracellular space, where it facilitates *in vivo* clearance of extracellular misfolded proteins with a high preference for amyloid β-like structures. Secreted CLU (sCLU) binds to its cargo protein, induces uptake of the complex into the target cell, which eventually results in protein degradation inside the cell. Although sCLU is known for its chaperone-like function, its exact mechanism for cargo recognition and transport remains unclear. Additionally, CLU acts as human terminal pathway inhibitor by interacting with the membrane attacking complex (MAC) which is formed as a result of the activation of the host's complement system [37]. Using biochemical and biological approaches we confirmed the direct interaction of PmpD with sCLU. Importantly, we further demonstrate that the absence of sCLU in the cell culture medium significantly reduces *Ctr* infection in epithelial cells. Summarized, we show that *Ctr* PmpD binds secreted clusterin and that the presence of extracellular sCLU is essential for a *Ctr* infection.

Results

D72, a proteolytically processed fragment of PmpD, forms high molecular weight homooligomers and shows binding to epithelial cells

In previous studies, it was shown that all nine Pmps from *Ctr* bind to epithelial cells and block a subsequent *Ctr* infection, which is why Pmps were defined as adhesins [13]. Pmp fragments used in these studies were designed with focus on regions with high GGA(I,L,V) and FxxN motif density, since these characteristic tetrapeptide motifs had been shown to be essential for adhesion [23]. Here, we focus on D72, a *Ctr* PmpD fragment that was found in *in vivo* studies (Fig. 1A) [20, 24]. D72 spans the N-terminal half of the PmpD PD, spanning the amino acid residues 68 – 761, thus comprising 12 GGA(I,L,V) and 14 FxxN motifs, as well as the RGD motif [38, 39]. Structure prediction tools suggest that recombinant D72 (rD72) forms a lengthy β-helical structure as already suggested for fragments of other Pmp PDs (Fig. S1) [40].

In order to characterize the biochemical and functional properties of rD72, the adhesive capacity of rD72 to epithelial cells was investigated as well as its ability to form high molecular weight oligomers. To this end, D72 was expressed in and purified from *E. coli* with an N-terminal 10x His-Tag (rD72, Fig. 1A). Adhesion to epithelial cells was tested by incubating human HEp-2 cells with different concentrations of soluble rD72 in the cell culture medium (ccm). The binding of rD72 to HEp-2 cells was detectable even at the lowest concentration of 0.25 µM. With increasing concentration of rD72 in the ccm, binding of rD72 also increased (Fig. 1B).

Pmp protein fragments have been shown to form homo- and heterooligomers *in vitro* [20, 25, 27, 34]. The oligomerisation of rD72 was investigated by size exclusion chromatography (SEC), Blue Native-PAGE (BN) and SDS-PAGE (Fig. 1C). Soluble rD72 was separated by SEC on a Superose 6 column and eluted in a broad peak, which started after the column void volume and covered one third of the total column bed volume (Fig. 1C). SDS-PAGE verified the presence of full length rD72 (Fig. 1C, *bottom*). The BN analysis of the SEC elution fraction at 1.4 ml revealed a high molecular weight oligomer of a size of 720 – 1048 kDa corresponding to a calculated 10-mer to 15-mer (Fig. 1C, *right*).

Taken together, these data indicate that rD72 is a biologically functional PmpD fragment, adhering to epithelial cells. Further, rD72 shows comparable biochemical characteristics to other Pmp PD fragments, including a high degree of oligomerisation

in solution [25, 27, 34]. Based on this, rD72 was used in further experiments with the goal to identify host cell binding partner(s).

Secreted clusterin is a host cell binding partner for rD72

We applied immune precipitation experiments to identify potential rD72 host cell binding partner(s). For this, the cell culture medium (ccm) of confluent HEp-2 cells was supplemented with soluble rD72 and incubated for 1 h at 4 °C. As negative control, ccm was supplemented with fresh PBS. Following, cell lysis was performed to solubilize both soluble and membrane-anchored protein complexes, and rD72-containing complexes were isolated by affinity purification (AP) using Ni-NTA agarose. The individual purification steps were monitored via Western Blot analysis, with anti-His antibodies used to detect rD72 (Fig. 2A). The protein composition in the elution fraction, containing enriched rD72, was analysed using mass spectrometry, to identify enriched proteins co-eluting with rD72.

Intriguingly, mass spectrometry analysis revealed only six significantly enriched host cell proteins in the AP elution fraction (Fig. 2B, Fig. S2, Table S2). From these six proteins, five proteins are suggested to be localized intracellular and thus are not accessible for extracellular rD72. Interestingly, four out of these five intracellular proteins are predicted to be mitochondrial components (Table S2). Only one significantly enriched protein, clusterin (CLU), which possesses a secreted isoform, secreted clusterin (sCLU), resides in the extracellular space and therefore was a potential candidate as rD72 host cell binding partner [41]. Detailed analysis of the CLU peptide intensities in each sample derived from mass spectrometry revealed, that CLU was not found in the negative control replicates while it was evidently enriched in all five replicates of the test samples (Fig. 2C).

CLU is an ATP-independent chaperone whose main function is to stabilise misfolded proteins and inhibit protein aggregation which form amorphous or amyloid aggregates, particularly in the extracellular space [42, 43]. sCLU derives from a precursor peptide of ~50 kDa, which undergoes extensive posttranslational modifications, such as heavy glycosylation [44]. Further, sCLU possesses five intramolecular disulphide bonds which keep the α- and β-chains in an antiparallel arrangement after cleavage of the precursor molecule (Fig. 2D) [45]. The fully glycosylated α- and β-chains have a molecular weight of 34-36 kDa and 36-39 kDa, respectively [46].

In vitro pulldown assays verify the rD72 – sCLU interaction

Mass spectrometry analysis of pulldown experiments revealed an interaction between rD72 and the host cell protein clusterin, which possesses a secreted isoform. To investigate the levels of intra- and extracellular CLU, HEp-2 cells were seeded at sub-confluency and grown for two days at 37 °C in ccm. Afterward, the used ccm and the cultured cells were separately analysed by Western blot using an anti-clusterin α-chain antibody, directed against the clusterin α-chain (Fig. 3A). For fresh ccm, which was used as negative control, no unspecific signals were observed. In contrast, in used ccm from HEp-2 cells grown for two days, a broad protein band was identified ranging from approximately 40 kDa to 45 kDa, which corresponds to the secreted CLU α-chain (Fig. 3A). In the cell lysate, multiple bands were observed, representing the cleaved and uncleaved clusterin precursor, which show different degrees of posttranslational modifications (Fig. 3A). Thus, during growth HEp-2 cells secrete mature clusterin into the ccm supernatant.

To verify the direct interaction between sCLU and rD72, a biochemical *in vitro* pulldown assay was performed, using rD72 as bait (Fig. 3B). For this, ccm from HEp-2 cells grown for two days was collected and incubated with soluble rD72. rD72 was then affinity-purified using Ni-NTA agarose and the elution fractions were tested for their protein composition by Western blot. As negative control, collected ccm was incubated with Ni-NTA agarose in the absence of rD72 (Fig. 3C). While the negative control showed no unspecific binding of sCLU to the agarose, the test samples consisting of ccm plus His-tagged rD72 as bait clearly demonstrated co-elution of both proteins in the elution fraction. These findings confirm a direct interaction of sCLU with rD72.

Depletion of secreted clusterin from the cell culture medium reduces the chlamydial infection

After verifying the direct interaction of sCLU and *Ctr* PmpD, the role of sCLU during the initial stages of a chlamydial infection was investigated. To this end, HEp-2 cells were grown in ccm for two days and prior to infection the amount of clusterin in the ccm was manipulated using four different experimental approaches (Fig. 4A). Approach (i) was a regular infection experiment, serving as control, in which *Ctr* EBs were added to HEp-2 cells in two-days-old supernatant ccm (rich in sCLU) (“old medium”, Fig. 4A, B). In approach (ii), the ccm in which cells were grown for two days

was removed and replaced by fresh ccm, thus without sCLU (“new medium”, Fig. 4A, B). The fresh ccm was then supplemented with *Ctr* EBs to initiate infection. In the third approach (iii), after two days of cell growth, soluble rD72 was added to sCLU-rich “old medium” and incubated for 1 h before *Ctr* EBs were added (“rD72 treatment”, Fig. 4A). Western blot analysis showed no significant change in sCLU abundance after 1 h incubation with rD72, compared to the sCLU abundance in approach (i) (Fig. 4B). In the fourth approach, the “old medium” in which cells were grown for two days was isolated from the cells and sCLU was depleted by affinity purification (AP). The flow through, depleted in sCLU, was transferred back to the cell monolayer, which was then challenged with *Ctr* EBs (Fig. 4A, B).

For all approaches, adhesion of EBs to epithelial cells was allowed for 2h before unbound EBs were removed and infection was continued for 24 hours (Fig. 4C). Interestingly, the infection of cells in the presence of “fresh medium” without detectable sClu (approach (ii)) revealed a significantly reduced infection rate of 0.7 compared to the control experiment (i) with an infection rate of 1 (Fig. 4D). The same reduction in the infection rate (0.72) was observed in approach (iv), where the “old medium” was depleted of sClu (Fig. 4D). In contrast, preincubation of the “old medium”, abundant in sClu, with rD72 in approach (iii) led to a small increase in infection rate (1.1) compared to the control (i) (Fig. 4D). Previously it was published that preincubation with soluble rPmpD (and all other rPmps) blocks the subsequent infection. However, in these experiments the used ccm (rich in sCLU) was replaced with fresh ccm (no sCLU) prior to the *Ctr* infection [13]. Moreover, this very slight increase obtained in approach (iii) confirms published data indicating that incubation of infectious EBs with adhesion-competent D72 can functionally replace the naturally exposed adhesive structures probably by rD72 binding to the EB cell surface [25].

In conclusion, the results obtained from approaches (i) to (iv) clearly indicate the relevance of secreted clusterin for a successful *Ctr* infection.

Discussion

A critical step in the *Ctr* developmental cycle is the initial adhesion to and subsequent internalization into epithelial host cells. The first contact between pathogen and host is mediated by chlamydial adhesins including GroEL1, MOMP, OmcB, Ctad1 and Pmps, binding to specific host cell proteins [11, 12, 16, 23, 36]. The family of Pmps plays a crucial but complex role in the adhesion and internalization processes [36, 47]. All nine *Ctr* Pmps have demonstrated adhesion to epithelial cells, and infection-blocking assays using soluble recombinant Pmp fragments indicated that each protein contributes to *Ctr* infectivity; however their host cell binding partners remained unknown [13]. Here, we show that PmpD, which forms high molecular weight (hMW) oligomers in solution and shows adhesion to epithelial cells, interacts with the secreted host cell chaperone clusterin (sCLU). The absence of sCLU in the cell culture medium (ccm) during the early *Ctr* infection leads to a significantly reduced infectivity.

Biochemical characterisation of rD72, a recombinantly expressed PmpD PD fragment which can be found *in vivo* during infection [20], has shown that it forms hMW oligomers in solution, as indicated by SEC analysis and Blue Native-PAGE (Fig. 1). The SEC elution profile for rD72 resembles that of the 65 kDa PmpD PD fragment investigated by Paes et al. [27]. Similarly, Favaroni et al., using yet another motif-rich 66 kDa PmpD PD fragment, obtained similar results and further suggested, based on transmission electron microscopy, that these hMW oligomers may form protofibril-like structures [25]. Additionally, Luczak et al. working on Pmp21, the *Cpn* homologue to *Ctr* PmpD, showed that these hMW oligomers formed by Pmp21 possess an amyloid-like character [34], highly similar to the amyloid-fibrils formed by $A\beta_{42}$, a protein which is an expedient component of Alzheimer's disease [28]. Thus, these converging data, in combination with data from structure prediction tools, that suggest the same structural architecture for all Pmp PDs, support the hypothesis that the hMW oligomers formed by rD72 also exhibit protofibril structures with amyloid-like properties.

Using rD72 bound to HEp-2 cells as bait in pulldown assays, we identified CLU as a direct interaction partner via mass spectrometry (Fig. 2 and 3). CLU is a ubiquitously expressed protein, present in nearly all human tissues, and exists in multiple isoforms, including a secreted isoform found in the extracellular space [44]. sCLU is secreted via secretory vesicles or by non-regulated pathways, bypassing secretion or exocytosis compartments [48]. Outside the cell, sCLU has chaperone-like activity and clears the extracellular space of misfolded proteins, which might otherwise lead to unstructured

amorphous or amyloid aggregates [42, 49, 50]. Thus, sCLU is associated with several proteinopathic diseases, including Alzheimer´s disease [51]. During Alzheimer's disease, Aβ peptides accumulate in the extracellular space of brain cells and eventually oligomerize and aggregate, forming amyloid fibrils. sCLU binds to Aβ oligomers in the brain, preventing aggregation and inducing the clearance of Aβ via transportation across the blood-brain-barrier [52, 53]. The endocytic mechanism triggered by sCLU for cargo uptake and eventually leading to lysosomal degradation are not fully identified yet. Recently it was demonstrated that sCLU is part of the chaperone- and receptor-mediated extracellular protein degradation (CRED) pathway for aberrant extracellular proteins, and that, among others, sCLU – cargo complexes bind to heparan sulfate (HS) receptors on the cell via electrostatic interactions [54].

Our data indicate that sCLU directly binds to soluble rD72, which has been shown to form hMW oligomers, likely with amyloid-like characteristics. Hence, it is suggested that the sCLU - rD72 interaction is based on rD72's capacity to form amyloid-like aggregates, which are natural cargo targets of sCLU. Importantly, manipulating sCLU abundance in the ccm by two different means, complete change of ccm or immunodepletion of sCLU from the 2-day-old ccm, prior to the chlamydial infection demonstrates that the infection rate reduced by approximately 30 % in the absence of sCLU (Fig. 4). Thus, sCLU is an essential component of *Ctr* infectivity. Thus, we would like to propose that sCLU may not only bind soluble recombinant PmpD, but also binds to EB surface-localized PmpD and possibly all other Pmp proteins which have been shown to form fibrillary homo- and heterooligomers *in vitro* [25]. Thus, EBs may be treated as cargo by sCLU, facilitating their host cell internalization, similar to the mechanism of Aβ clearance from the extracellular space, using the CRED pathway. The uptake mechanism into the host cell may be mediated by heparan sulfate receptors. Additionally, the potential involvement of a co-receptor in facilitating endocytic uptake of the EB by CRED is likely. Previous studies on different bacterial and viral pathogens using heparan sulfate for host cell entry have shown that they also rely on co-receptors, for enhancing internalization into the host cell through endocytic processes [55-57]. Heparan sulfate is also the host receptor for the *Ctr* adhesin OmcB [12]. Interestingly, blocking adhesion of *Ctr* EBs to HEp-2 cells by heparin (a heparan sulfate analogue) reduced binding down to approximately 5 %, while addition of rOmcB reduced adhesion of EBs down to approximately 30 %. The differences in adhesion inhibition could be explained by the fact that blocking by heparin blocks the binding of

both OmcB and sCLU, while blocking by OmcB only blocks its binding sites on heparan sulfate [12].

After sCLU-triggered internalization, the endocytic vesicle is typically designated for lysosomal degradation [54, 58]. Nevertheless, chlamydia bypasses this degradation step, expectedly through the tight regulation of Rab GTPase recruitment to the early inclusion membrane, mediating the transition from an early endosome to a slowly recycling endosome, providing a protective environment termed inclusion for the further progression through the chlamydial development cycle [59].

Simultaneously, while EB uptake may be facilitated by sCLU recruitment and the CRED pathway, a possible inhibitory effect of CLU on the terminal complement pathway needs to be considered, too. Among others, *Pseudomonas aeruginosa* and *Staphylococcus aureus* recruit sCLU, which inhibits the MAC, to their cell surface, helping them in evading the host immune response, thereby enhancing the pathogen's survival and infectivity [60-62]. A similar mechanism may be conceivable for *Ctr*, where recruitment of sCLU to the EB cell surface may not only facilitate endocytic uptake via CRED, but also may help to escape the host immune response through MAC inhibition until the infectious EB is internalized and thus protected against further immune attacks. However, this hypothesis needs experimental validation.

In conclusion, our data support a unique adhesion and invasion strategy driven by the interaction of *Ctr* PmpD (and very likely all other Pmps) and sCLU. By binding to sCLU, *Ctr* may not only hijack a host component for initiating uptake into the cell, but also strategically evade the host immune response by inhibiting the MAC from the terminal complement pathway via sCLU. Like this, sCLU would be essential for the early *Ctr* infection process and simultaneously evokes the immune escape.

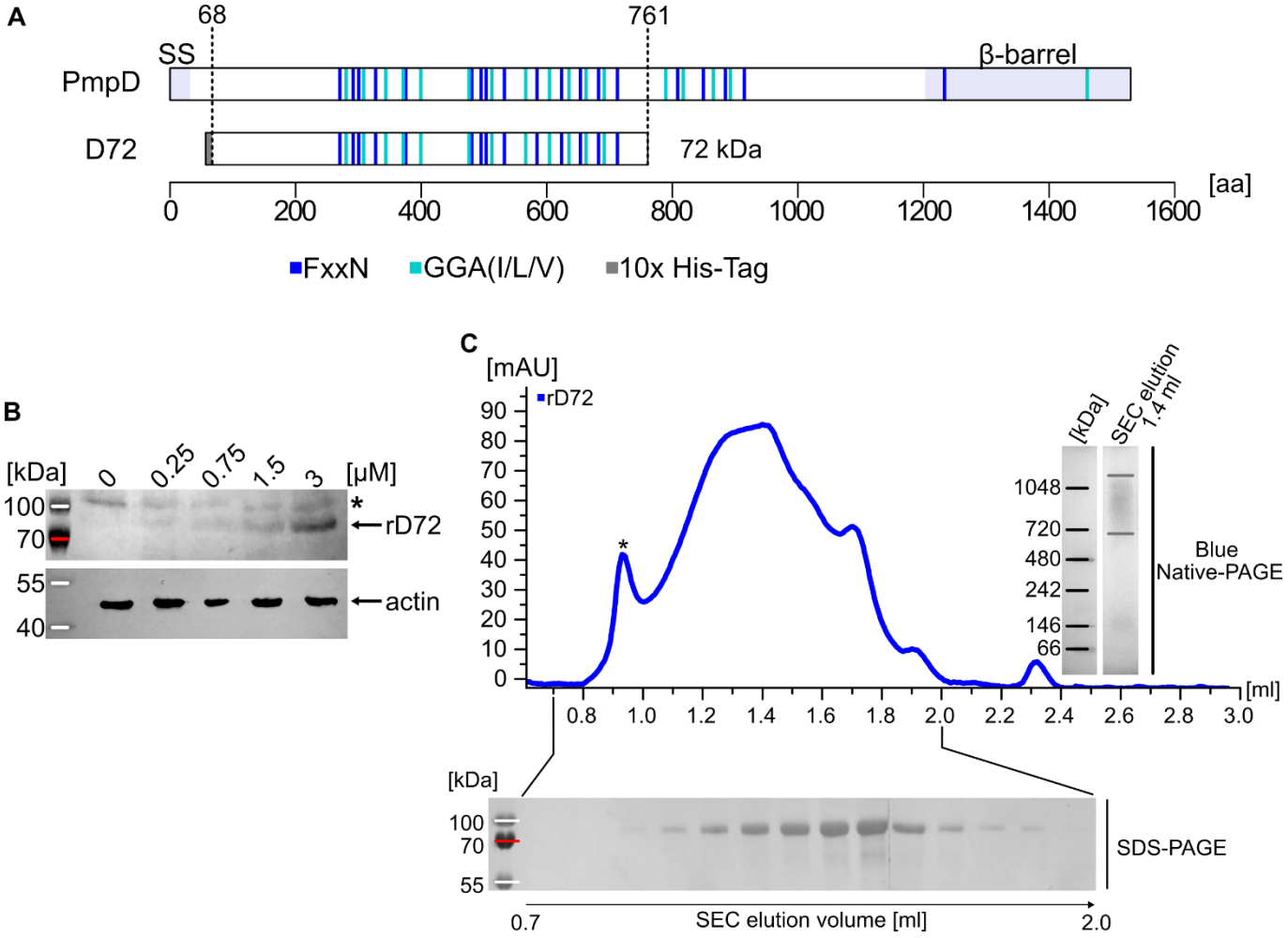

Figure 1: Recombinant D72 is a biologically functional fragment of *Ctr* PmpD. **(A)** Schematic representation of *Ctr* PmpD and the proteolytically processed fragment D72, spanning aa residues 68 – 761. The N-terminal signal sequence (SS), the passenger domain (PD) and the C-terminal β-barrel are indicated. The positions of the FxxN and GGA(I,L,V) motifs are marked in dark and light blue, respectively. The grey box indicates the genetically fused 10x His-Tag. The processed fragment includes 14 FxxN and 12 GGA(I,L,V) motifs. Image generated in R Studio with a customized code [63, 64]. **(B)** Increasing concentrations of His-tagged soluble recombinant D72 (rD72) in cell culture medium (ccm) was incubated with HEp-2 cells. Bound protein was visualized by Western blot using an anti-His antibody. Unspecific bands are indicated with an asterisk. Actin was used as an internal loading control. **(C)** Size exclusion chromatography (SEC) was used for analysing the oligomeric state of rD72 in solution. The void volume is indicated by an asterisk. Samples from the individual elution fractions were taken and analysed by SDS-PAGE (bottom). From the elution fraction at 1.4 ml, a sample was taken and analysed by Blue Native-PAGE (right).

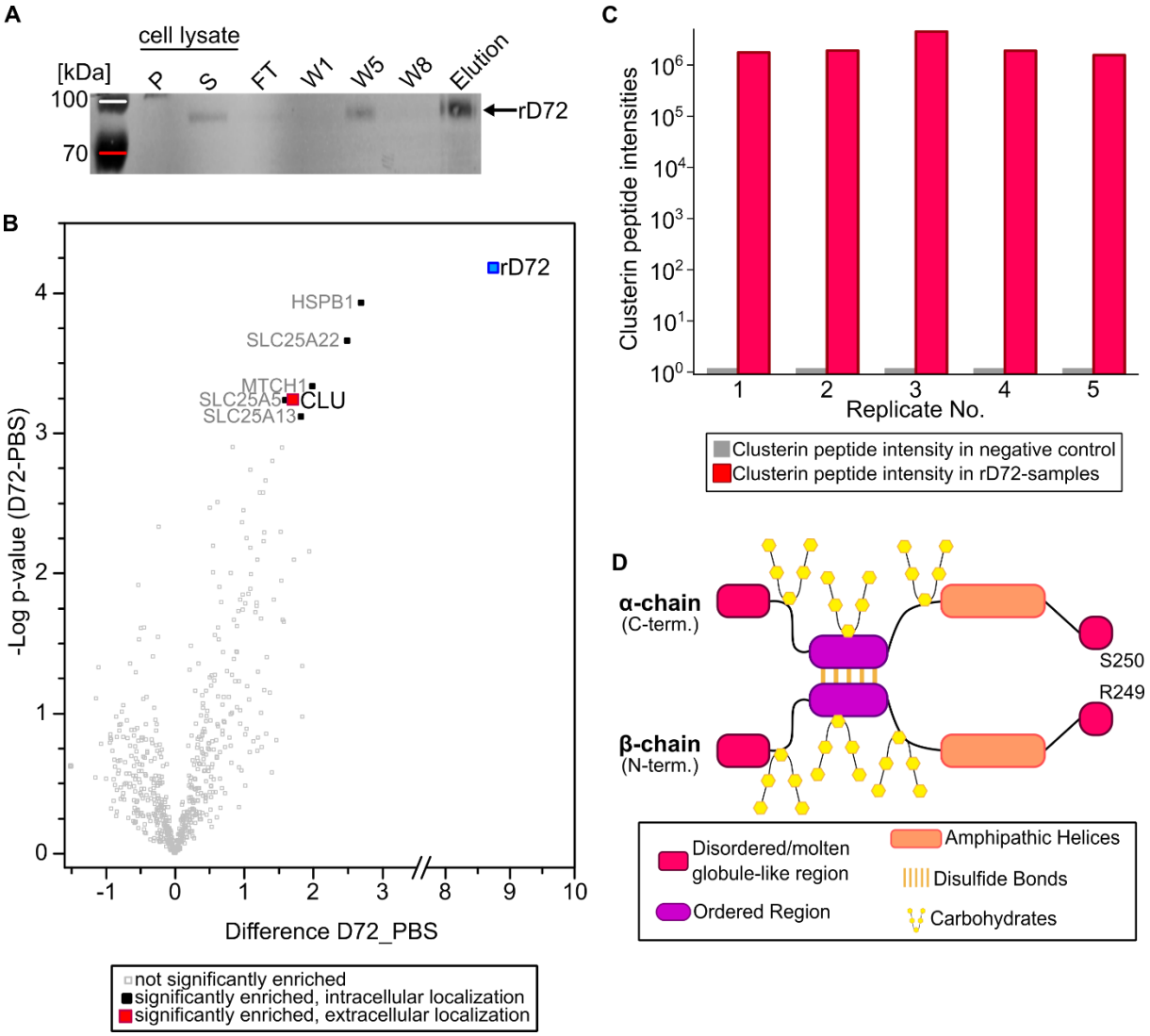

Figure 2: rD72 binds to the secreted host cell chaperone clusterin.

(A) Pulldown experiment in which rD72 was incubated on HEp-2 cells grown for two days in cell culture medium (ccm), allowing the binding to its host interaction partner. Cells were lysed to bring protein complexes into the soluble fraction and the lysate was cleared by centrifugation (P = pellet, S = supernatant). rD72 and the bound host cell interaction partner were co-purified using Ni-NTA agarose. Fractions of the individual Ni-NTA-purification steps were analysed by Western Blot and probed with anti-His antibody. (FT = flow through, W1 = wash 1, W5 = wash 5, W8 = wash 8) **(B)** Volcano plot of human proteins identified by mass spectrometry after affinity purification (n=5). Significantly enriched proteins, compared to the PBS negative control, are labelled (Uniprot nomenclature). The fold change (rD72 minus PBS) is plotted against the difference in mean values of log2 label-free quantitation (LFQ) intensities (rD72 minus PBS). **(C)** The peptide intensities of clusterin of each replicate are compared between the test sample containing rD72 (red columns) and the corresponding PBS negative

control (grey columns). **(D)** Schematic representation of secreted human clusterin (sCLU). Intracellularly, precursor clusterin is N-glycosylated and possesses five intramolecular disulfide bonds. Precursor clusterin is cleaved between R249 and S250, generating the secreted isoform (sCLU) which has antiparallel arranged α- and β-chains. Mature sCLU has a molecular weight of ~70 kDa and is secreted into the extracellular space.

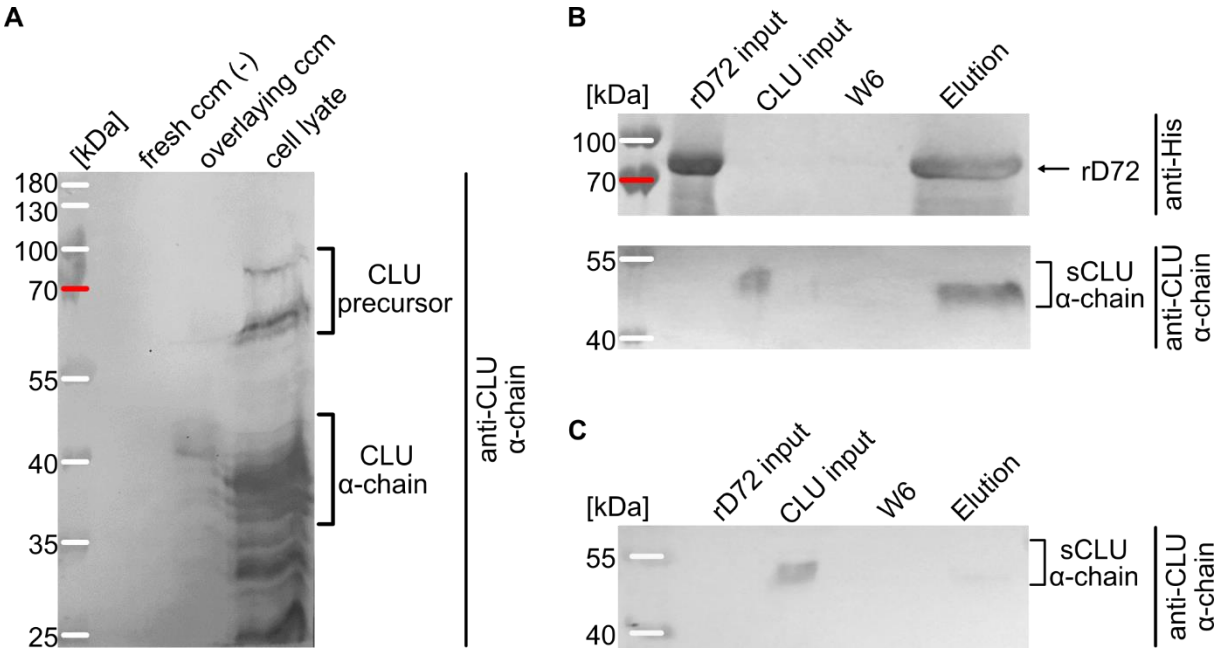

Figure 3: *In vitro* interaction of rD72 and clusterin.

(A) Analysis of clusterin abundance in HEp-2 cells by Western Blot analysis, using an antibody against the clusterin α-chain. As negative control, fresh cell culture medium (ccm) was used (-). In the isolated ccm of cells grown for 2 days (overlaying ccm), the posttranslational modified clusterin α-chain is detected at ~40-45 kDa (theoretical MW: 36-39 kDa). In the cell lysate, bands at 60-80 kDa appear corresponding to the precursor clusterin and bands at ~40-45 kDa for the fully processed α-chain of secreted clusterin (sCLU). **(B)** Ni-NTA pulldown assays where rD72 was used as bait and incubated with isolated ccm from epithelial cells grown for two days. The protein composition of the individual fractions from the pulldown assay were tested by Western blot, using anti-His and anti-clusterin α-chain antibodies. (W6 = wash 6). **(C)** Negative control of the Ni-NTA pulldown assay, with used ccm from HEp-2 cells grown for two days in the absence of rD72. Fractions were separated by SDS/PAGE and analysed via Western blot, using an anti-clusterin α-chain antibody.

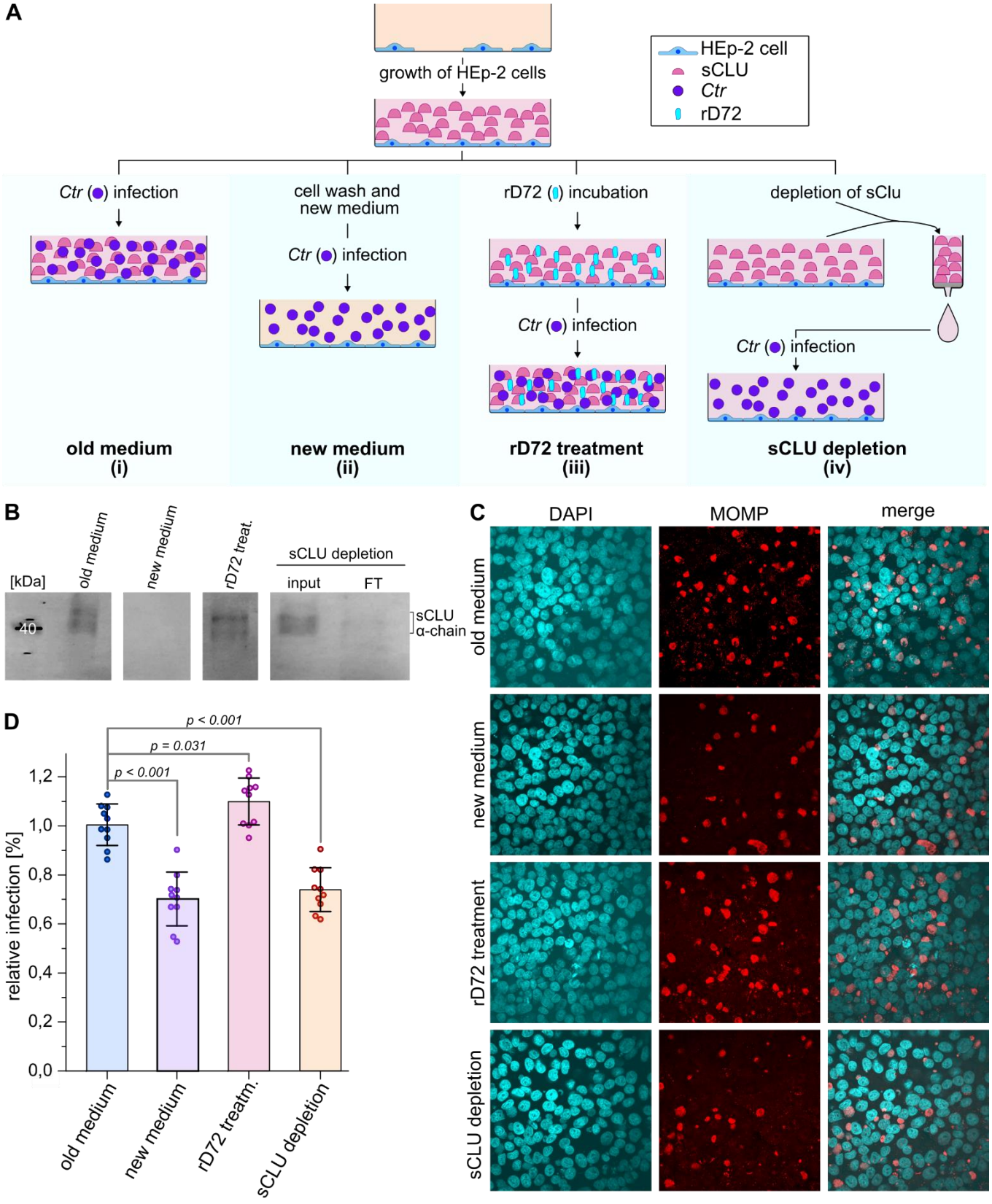

Figure 4: sCLU facilitates uptake of *Ctr* into the host cell.

(A) Schematic representation of the different experimental setups to test the effect of sCLU during the initial steps of a chlamydial infection. For all four approaches (i-iv), confluent cells were grown for two days in ccm. For approach (i), the ccm of confluently

grown cells was supplemented with *Ctr* EBs. For approach (ii), the cells were washed and fresh ccm supplemented with *Ctr* EBs was added, containing no sCLU. For approach (iii), the ccm was supplemented with soluble rD72 and incubated with HEp-2 cells for one hour before *Ctr* EBs were added to the ccm. For approach (iv), the used ccm used for cell growth was isolated and sCLU was extracted via affinity purification (AP) and the flow-through, depleted of sCLU, was returned to the HEp-2 cells, supplemented with *Ctr* EBs. For all four approaches, EBs were incubated with HEp-2 cells for 2 h at 37 °C before the unbound EBs were removed. After 24 h, the infection was stopped by fixing and permeabilizing the cells with PFA and methanol. **(B)** Western blot analysis of ccm, using an anti-clusterin α-chain antibody. For approaches i-iii, samples were taken from the ccm immediately before the supplementation with *Ctr* EBs. For approach iv, the AP input (input) and the AP flow-through (FT) were analysed. **(C)** Sections of immunofluorescence microscopy pictures of the individual infection approaches as depicted in (A). DNA is visualized with DAPI (cyan) and inclusions are visualized with an anti-MOMP antibody (red). Images are representative of three biologically independent replicates (n=3). **(D)** Infection rates of the individual approaches (i-iv) were determined by calculating the ratio of inclusions to the number of HEp-2 cells. The infection rate of approach (i) was set to 1 and approaches (ii-iv) were normalized to it. Three biologically independent experiments (n=3) were performed, and for each replicate, 3-4 images on different sections were taken. The means are indicated by the height of the individual bars (± SD) and the *P*-values are indicated.

Material and Methods

Antibodies and reagents

The following primary antibodies were used: anti-clusterin α-chain (Santa Cruz, sc-5289), anti-penta-His (Qiagen, #34660), anti-β-actin (Thermo Scientific, MA5-15739) and anti-MOMP (Bio-Rad, #1990-0804). The secondary antibodies anti-mouse, coupled to alkaline phosphatase, and anti-goat, coupled to Alexa Fluor™ 594, were purchased from Thermo Scientific.

Bacterial strains and cell lines

The *Saccharomyces cerevisiae* strain CEN.PK2 was used for cloning steps. *E. coli* XL1 blue (Stratagene) and Origami (Novagen) were used for plasmid amplification and protein expression, respectively.

HEp-2 cells (ATCC: CCL-23) were cultured in cell culture medium (ccm), composed of DMEM medium (Thermo Scientific, Waltham, MA, USA) supplemented with 10 % FCS, MEM vitamins and nonessential amino acids (Thermo Scientific, Waltham, MA, USA), Amphotericin B and Gentamycin (Life technologies).

Ctr serovar E (DK-20) (London) (NCBI accession number: CP015304.1) was propagated in HEp-2 cells in cell culture medium supplemented with 1.2 µl/ml cycloheximide (Sigma), purified by centrifugation and stored in SPG buffer (220 mM sucrose, 3.8 mM KH_2PO_4, 10.8 mM Na_2HPO_4, 4.9 mM L-glutamine), as previously described.[65]

Cloning, protein expression and purification

Cloning steps were carried out by *in vivo* homologous recombination in *S. cerevisiae*. The DNA fragment of *pmpD* encoding the D72 protein variant (residues D68-A761) was amplified via PCR from *Ctr* serovar E (DK20) genomic DNA and cloned into the expression vector pKM32 (generating an N-terminal 10xHis-fusion) [23]. Plasmids were amplified in *E. coli* XL1 blue and the sequence was verified prior to use.

Expression of the His-tagged protein was carried out in the *E. coli* Origami strain. Proteins were purified using Ni-NTA Agarose (Thermo Scientific) and dialysed in phosphate-buffered saline (PBS) (10 mM Na_2HPO 4, 1.8 mM KH_2PO_4, 137 mM NaCl, 2.7 mM KCl, pH 7.4).

Immunoblotting and Coomassie-Staining

SDS-PAGE and immunoblotting were performed according to the standard protocol described by Sambrook and Maniatis et al.[66] His-tagged recombinant proteins were detected with monoclonal anti-His antibodies and clusterin was detected with anti-clusterin α-chain antibodies. Both were visualized with AP-conjugated antibodies. SDS Gels were stained with Coomassie Brilliant Blue G250 (Serva).

Blue-Native PAGE

Blue-Native PAGE analysis was performed using Native PAGE Novex 3-12 % Bis-Tris Gel system, following the manufacturers protocol (Thermo Scientific). Proteins were visualized by staining the gels with Coomassie Brilliant Blue G250 (Serva).

Size exclusion chromatography (SEC)

Recombinantly expressed proteins in PBS (10 mm Na_2HPO_4, 1.8 mm KH_2PO_4, 137 mm NaCl, 2.7 mm KCl, pH 7.4) were analysed on a Superose 6 Increase 3.2/300 column (Cytivia) with a flow rate of 0.05 ml/min and 0.1 ml fractions were collected. All runs were performed at 4 °C. The void volume was implemented as indicated by the manufacturer's instructions.

Adhesion assay

Confluent HEp-2 cells were grown at 37 °C and specific concentrations of soluble recombinant proteins were added to the ccm in a total volume of 250 µl. Binding was allowed for 1 h at 4° C. After extensive washing, cells were lysed in phospho-lysis buffer (1 % NP-40, 1 % Triton X-100, 20 mM Tris/HCl, 150 mM NaCl, 1 mM Na_2VO_4). The lysate was prepared for SDS/PAGE and immunoblotting using anti-His antibodies, for quantification of recombinant protein, and anti-β-actin as internal loading control.

Pulldown assays

Confluent HEp-2 cells were grown in 25 cm² flasks and 2 µM of soluble recombinant His-tagged proteins were mixed with overlaying ccm (without FCS and antibiotics) to a total volume of 3 ml. Binding was allowed for 1 h at 4° C, then cells were washed three times with HBSS and lysed with phospho-lysis buffer. Lysate was centrifuged at 1000 rpm and the soluble fraction was loaded on Ni-NTA agarose. His-tagged proteins and their bound host cell binding partners were eluted with PBS containing 500 mM

Imidazole. Enriched proteins in the elution fraction were identified by mass spectrometry analysis.

Quantitative mass-spectrometric analysis of rD72 host cell binding partners

Eluates from His-pmpD pulldown assays were prepared for mass spectrometric analysis by in-gel digestion with trypsin essentially as described earlier [67].

Briefly, eluates were shortly separated in a polyacrylamide gel, proteins reduced with dithiothreitol, alkylated with iodoacetamide and digested overnight with 0.1 µg trypsin. Peptides were extracted from the gel and subsequently purified by solid phase extraction (HLB µ-elution plate, Waters) according to the manufacturer's instructions. Finally, peptides were dried in a vacuum concentrator, resuspended in 17 µl 0.1% (v/v) trifluoroacetic acid and analyzed by liquid chromatography coupled mass spectrometry as described with modifications mentions below [68].

First, peptides were trapped on a 2 cm long precolumn and then separated by a one-hour gradient on a 25 cm long C18 analytical column using an Ultimate 3000 rapid separation liquid chromatography system (Thermo Fisher Scientific). Second, peptides were injected in an QExactive plus (Thermo Fisher Scientific) mass spectrometer online coupled by a nano-source electrospray interface. The mass spectrometer was operated in data-dependent positive mode. Survey spectra were recorded with following settings: resolution 140000, automatic gain control target 3000000, maximum ion time 50 ms, scan range 200-2000 m/z, profile mode. Up to 20 precursors were selected by the quadrupole of the instrument (4 m/z isolation window), fragmented by higher-energy collisional dissociation (normalized collision energy: 30) and fragment spectra recorded in the orbitrap analyzer: resolution 17500, automatic gain control target 100000, maximum ion time 50 ms, scan range 200-2000 m/z, centroid mode. Fragmented peptides were excluded for the next 10 second.

Peptide and protein identification was carried out with MaxQuant version 2.1.3.0 (MaxPlack Institute for Biochemistry, Planegg, Germany) with standard parameters if not stated otherwise. Proteins sequences from homo sapiens (79038 entries of UP000005640, UniProt knowledge base, downloaded on 18th January 2022) as well as one entry for PmpD were used and the match between runs function and label-free quantification (LFQ) enabled.

Identified proteins were filtered (contaminants, "identified by site", reverse hits and proteins only identified with one peptide removed) and only protein identified with at

least four valid values in one experimental group considered for statistical analysis on log_2 transformed LFQ-intensities. Missing values were imputed with values drawn from a downshifted (1.8 standard deviations (s.d.)) normal distribution (0.3 s.d.) and differentially abundant proteins between the two groups (PBS, pmpD) determined by the significance analysis of microarray method using an FDR of 5% and S_o of 0.1 [69].

Infection assay

For all infection assays, cells were seeded at sub-confluent density and grown in cell culture medium (ccm) to confluence for two days at 37 °C. For approach (i), chlamydial EBs (MOI = 10) were added to the two-day-old ccm covering the confluent cell layer and incubated for 2 h at 37 °C. For approach (ii), the confluent cell layer was washed three times with HBSS and fresh ccm, supplemented with EBs (MOI = 10) was added and incubated for 2 h at 37 °C. For approach (iii), soluble recombinant rD72 was added to the two-day-old ccm covering the confluent cell layer. After 1 h incubation at 37 °C, chlamydial EBs (MOI = 10) were added and incubated for 2 h at 37 °C. For approach (iv), the two-day-old ccm used for cell growth was isolated and sCLU was extracted via immunoprecipitation using Protein-G-agarose (Merck) and an anti-clusterin α-chain antibody, following the manufacturers protocol. The flow-through depleted in sCLU was returned to HEp-2 cells and chlamydial EBs (MOI = 10) were added and incubated for 2 h at 37 °C.

For all four approaches, after the initial 2 h of incubation with EBs, the ccm containing unbound chlamydial EBs was removed and fresh ccm supplemented with cycloheximide (1.2 µl/ml) was added to the cells. Infection was allowed for 24 h at 37 °C, before the cells were prepared for immunofluorescence microscopy. The presences of sCLU in the ccm for the different approaches was monitored by immunoblotting using an anti-clusterin α-chain antibody.

Immunofluorescence microscopy

Infected cells were fixed with 3 % para-formaldehyde for 10 min at RT, washed three times with PBS and permeabilized with 96 % methanol (-20 °C) at room temperature. The primary antibody (anti-MOMP, 1:500) was diluted in bufferX (5 % BSA, 0.5 % Triton-X 100, 0.2 % Tween20) and incubated for 1 h at RT. Cells were washed three times with PBS and secondary antibody (anti-goat coupled to Alexa594, 1:1000) diluted in buffer X, was incubated for 60 min at RT. Cells were washed three times and

DAPI was used to visualize DNA. Microscopy was performed using a Nikon Eclipse Ti-E C2 confocal microscope (DS-Qi1MC Camera) and confocal images were generated using NIS Element software (Nikon) and quantified using ImageJ.

Statistical analysis

Graphics were created in OriginPro v.2021b (OriginLab). The data represent the mean ± s.d. For simple paired analyses between two groups, a Student´s *t* test was chosen. Images were prepared using the open-source software Inkscape (www.inkscape.org).

Author Contribution

F.K. and J.H.H. designed and performed the experiments, analysed the data and wrote the manuscript. Both authors contributed to the article and approved the submitted version.

Funding

This study was funded by a scholarship to F.K. by the Graduate School “Molecules of Infection IV (MOI IV)” founded by the Jürgen Manchot Foundation. We acknowledge grant support from the DFG to J.H.H. (Project-ID 267205415) of CRC 1208.

Conflict of interest

The authors declare no conflict of interest.

Acknowledgments

We thank J. Reiners for the help with SEC analysis. We thank BMFZ HHU, specifically Dr. Poschmann and Prof. Dr. Stühler for processing the mass-spectrometry analysis of the rD72 pulldown experiments.

Reference

1. Rodrigues R, Sousa C, Vale N. Chlamydia trachomatis as a Current Health Problem: Challenges and Opportunities. Diagnostics (Basel). 2022;12(8).
2. Malecela MN, Ducker C. A road map for neglected tropical diseases 2021-2030. Trans R Soc Trop Med Hyg. 2021;115(2):121-3.
3. Elwell C, Mirrashidi K, Engel J. Chlamydia cell biology and pathogenesis. Nat Rev Microbiol. 2016;14(6):385-400.
4. Kalman S, Mitchell W, Marathe R, Lammel C, Fan J, Hyman RW, et al. Comparative genomes of Chlamydia pneumoniae and C. trachomatis. Nat Genet. 1999;21(4):385-9.
5. Murray SM, McKay PF. Chlamydia trachomatis: Cell biology, immunology and vaccination. Vaccine. 2021;39(22):2965-75.
6. de Vrieze NH, de Vries HJ. Lymphogranuloma venereum among men who have sex with men. An epidemiological and clinical review. Expert Rev Anti Infect Ther. 2014;12(6):697-704.
7. Moulder JW. Interaction of chlamydiae and host cells in vitro. Microbiol Rev. 1991;55(1):143-90.
8. Christensen S, McMahon RM, Martin JL, Huston WM. Life inside and out: making and breaking protein disulfide bonds in Chlamydia. Crit Rev Microbiol. 2019;45(1):33-50.
9. Abdelrahman YM, Belland RJ. The chlamydial developmental cycle. FEMS Microbiol Rev. 2005;29(5):949-59.
10. Hegemann JH, Moelleken K. Chlamydial adhesion and adhesins. In: Tan M, Bavoil, P., editor. Intracellular Pathogens I: Chlamydiales Washington, DC: ASM Press; 2012.
11. Stallmann S, Hegemann JH. The Chlamydia trachomatis Ctad1 invasin exploits the human integrin beta1 receptor for host cell entry. Cell Microbiol. 2016;18(5):761-75.
12. Mölleken K, Hegemann JH. The Chlamydia outer membrane protein OmcB is required for adhesion and exhibits biovar-specific differences in glycosaminoglycan binding. Mol Microbiol. 2008;67(2):403-19.
13. Becker E, Hegemann JH. All subtypes of the Pmp adhesin family are implicated in chlamydial virulence and show species-specific function. Microbiologyopen. 2014;3(4):544-56.
14. Stephens RS, Koshiyama K, Lewis E, Kubo A. Heparin-binding outer membrane protein of chlamydiae. Mol Microbiol. 2001;40(3):691-9.
15. Fechtner T, Stallmann S, Moelleken K, Meyer KL, Hegemann JH. Characterization of the interaction between the chlamydial adhesin OmcB and the human host cell. J Bacteriol. 2013;195(23):5323-33.
16. Wuppermann FN, Mölleken K, Julien M, Jantos CA, Hegemann JH. Chlamydia pneumoniae GroEL1 protein is cell surface associated and required for infection of HEp-2 cells. J Bacteriol. 2008;190(10):3757-67.
17. Grimwood J, Stephens RS. Computational analysis of the polymorphic membrane protein superfamily of Chlamydia trachomatis and Chlamydia pneumoniae. Microb Comp Genomics. 1999;4(3):187-201.
18. Henderson IR, Lam AC. Polymorphic proteins of Chlamydia spp.--autotransporters beyond the Proteobacteria. Trends Microbiol. 2001;9(12):573-8.

19. Henderson IR, Navarro-Garcia F, Desvaux M, Fernandez RC, Ala'Aldeen D. Type V protein secretion pathway: the autotransporter story. Microbiol Mol Biol Rev. 2004;68(4):692-744.
20. Swanson KA, Taylor LD, Frank SD, Sturdevant GL, Fischer ER, Carlson JH, et al. Chlamydia trachomatis polymorphic membrane protein D is an oligomeric autotransporter with a higher-order structure. Infect Immun. 2009;77(1):508-16.
21. Kiselev AO, Stamm WE, Yates JR, Lampe MF. Expression, processing, and localization of PmpD of Chlamydia trachomatis serovar L2 during the chlamydial developmental cycle. PLoS ONE. 2007;2(6):e568.
22. Wehrl W, Brinkmann V, Jungblut PR, Meyer TF, Szczepek AJ. From the inside out--processing of the Chlamydial autotransporter PmpD and its role in bacterial adhesion and activation of human host cells. Mol Microbiol. 2004;51(2):319-34.
23. Mölleken K, Schmidt E, Hegemann JH. Members of the Pmp protein family of Chlamydia pneumoniae mediate adhesion to human cells via short repetitive peptide motifs. Mol Microbiol. 2010;78(4):1004-17.
24. Kiselev AO, Skinner MC, Lampe MF. Analysis of pmpD expression and PmpD post-translational processing during the life cycle of Chlamydia trachomatis serovars A, D, and L2. PLoS One. 2009;4(4):e5191.
25. Favaroni A, Hegemann JH. Chlamydia trachomatis Polymorphic Membrane Proteins (Pmps) Form Functional Homomeric and Heteromeric Oligomers. Front Microbiol. 2021;12:709724.
26. Cervantes PW, Segelke BW, Lau EY, Robinson BV, Abisoye-Ogunniyan A, Pal S, et al. Sequence, structure prediction, and epitope analysis of the polymorphic membrane protein family in Chlamydia trachomatis. PLoS One. 2024;19(6):e0304525.
27. Paes W, Dowle A, Coldwell J, Leech A, Ganderton T, Brzozowski A. The Chlamydia trachomatis PmpD adhesin forms higher order structures through disulphide-mediated covalent interactions. PLoS One. 2018;13(6):e0198662.
28. Gu L, Guo Z. Alzheimer's Abeta42 and Abeta40 peptides form interlaced amyloid fibrils. J Neurochem. 2013;126(3):305-11.
29. Paes W, Brown N, Brzozowski AM, Coler R, Reed S, Carter D, et al. Recombinant polymorphic membrane protein D in combination with a novel, second-generation lipid adjuvant protects against intra-vaginal Chlamydia trachomatis infection in mice. Vaccine. 2016;34(35):4123-31.
30. Crane DD, Carlson JH, Fischer ER, Bavoil P, Hsia RC, Tan C, et al. Chlamydia trachomatis polymorphic membrane protein D is a species-common pan-neutralizing antigen. Proc Natl Acad Sci U S A. 2006;103(6):1894-9.
31. Kari L, Southern TR, Downey CJ, Watkins HS, Randall LB, Taylor LD, et al. Chlamydia trachomatis polymorphic membrane protein D is a virulence factor involved in early host-cell interactions. Infect Immun. 2014;82(7):2756-62.
32. Wang Y, LaBrie SD, Carrell SJ, Suchland RJ, Dimond ZE, Kwong F, et al. Development of Transposon Mutagenesis for Chlamydia muridarum. J Bacteriol. 2019;201(23).
33. Mölleken K, Becker E, Hegemann JH. The Chlamydia pneumoniae invasin protein Pmp21 recruits the EGF receptor for host cell entry. PLoS Pathog. 2013;9(4):e1003325.

34. Luczak SE, Smits SH, Decker C, Nagel-Steger L, Schmitt L, Hegemann JH. The Chlamydia pneumoniae Adhesin Pmp21 Forms Oligomers with Adhesive Properties. J Biol Chem. 2016;291(43):22806-18.
35. Li X, Zuo Z, Wang Y, Hegemann JH, He C. Polymorphic Membrane Protein 17G of Chlamydia psittaci Mediated the Binding and Invasion of Bacteria to Host Cells by Interacting and Activating EGFR of the Host. Front Immunol. 2021;12:818487.
36. Romero MD, Moelleken K, Hegemann JH, Carabeo RA. Chlamydia Adhesion and Invasion. Chlamydia Biology: From Genome to Disease. 2020:59-84.
37. Choi NH, Mazda T, Tomita M. A serum protein SP40,40 modulates the formation of membrane attack complex of complement on erythrocytes. Mol Immunol. 1989;26(9):835-40.
38. Takada Y, Ye X, Simon S. The integrins. Genome Biol. 2007;8(5):215.
39. Ruoslahti E. RGD and other recognition sequences for integrins. Annu Rev Cell Dev Biol. 1996;12:697-715.
40. Debrine AM, Karplus PA, Rockey DD. A structural foundation for studying chlamydial polymorphic membrane proteins. Microbiol Spectr. 2023;11(6):e0324223.
41. Bettens K, Vermeulen S, Van Cauwenberghe C, Heeman B, Asselbergh B, Robberecht C, et al. Reduced secreted clusterin as a mechanism for Alzheimer-associated CLU mutations. Mol Neurodegener. 2015;10:30.
42. Poon S, Easterbrook-Smith SB, Rybchyn MS, Carver JA, Wilson MR. Clusterin is an ATP-independent chaperone with very broad substrate specificity that stabilizes stressed proteins in a folding-competent state. Biochemistry. 2000;39(51):15953-60.
43. Hatters DM, Lindner RA, Carver JA, Howlett GJ. The molecular chaperone, alpha-crystallin, inhibits amyloid formation by apolipoprotein C-II. J Biol Chem. 2001;276(36):33755-61.
44. Gross C, Guerin LP, Socol BG, Germain L, Guerin SL. The Ins and Outs of Clusterin: Its Role in Cancer, Eye Diseases and Wound Healing. Int J Mol Sci. 2023;24(17).
45. Burkey BF, deSilva HV, Harmony JA. Intracellular processing of apolipoprotein J precursor to the mature heterodimer. J Lipid Res. 1991;32(6):1039-48.
46. de Silva HV, Harmony JA, Stuart WD, Gil CM, Robbins J. Apolipoprotein J: structure and tissue distribution. Biochemistry. 1990;29(22):5380-9.
47. Vasilevsky S, Stojanov M, Greub G, Baud D. Chlamydial polymorphic membrane proteins: regulation, function and potential vaccine candidates. Virulence. 2016;7(1):11-22.
48. Nizard P, Tetley S, Le Drean Y, Watrin T, Le Goff P, Wilson MR, et al. Stress-induced retrotranslocation of clusterin/ApoJ into the cytosol. Traffic. 2007;8(5):554-65.
49. Wilson MR, Easterbrook-Smith SB. Clusterin is a secreted mammalian chaperone. Trends Biochem Sci. 2000;25(3):95-8.
50. Humphreys DT, Carver JA, Easterbrook-Smith SB, Wilson MR. Clusterin has chaperone-like activity similar to that of small heat shock proteins. J Biol Chem. 1999;274(11):6875-81.
51. Satapathy S, Wilson MR. The Dual Roles of Clusterin in Extracellular and Intracellular Proteostasis. Trends Biochem Sci. 2021;46(8):652-60.
52. Madadi S, Schwarzenbach H, Saidijam M, Mahjub R, Soleimani M. Potential microRNA-related targets in clearance pathways of amyloid-beta: novel

therapeutic approach for the treatment of Alzheimer's disease. Cell Biosci. 2019;9:91.
53. Howlett DR, Hortobagyi T, Francis PT. Clusterin associates specifically with Abeta40 in Alzheimer's disease brain tissue. Brain Pathol. 2013;23(6):623-32.
54. Itakura E, Chiba M, Murata T, Matsuura A. Heparan sulfate is a clearance receptor for aberrant extracellular proteins. J Cell Biol. 2020;219(3).
55. Pillay S, Meyer NL, Puschnik AS, Davulcu O, Diep J, Ishikawa Y, et al. An essential receptor for adeno-associated virus infection. Nature. 2016;530(7588):108-12.
56. Yayon A, Klagsbrun M, Esko JD, Leder P, Ornitz DM. Cell surface, heparin-like molecules are required for binding of basic fibroblast growth factor to its high affinity receptor. Cell. 1991;64(4):841-8.
57. Liu J, Thorp SC. Cell surface heparan sulfate and its roles in assisting viral infections. Med Res Rev. 2002;22(1):1-25.
58. Kounnas MZ, Loukinova EB, Stefansson S, Harmony JA, Brewer BH, Strickland DK, et al. Identification of glycoprotein 330 as an endocytic receptor for apolipoprotein J/clusterin. J Biol Chem. 1995;270(22):13070-5.
59. Mölleken K, Hegemann JH. Acquisition of Rab11 and Rab11-Fip2-A novel strategy for Chlamydia pneumoniae early survival. PLoS Pathog. 2017;13(8):e1006556.
60. Hallstrom T, Uhde M, Singh B, Skerka C, Riesbeck K, Zipfel PF. Pseudomonas aeruginosa Uses Dihydrolipoamide Dehydrogenase (Lpd) to Bind to the Human Terminal Pathway Regulators Vitronectin and Clusterin to Inhibit Terminal Pathway Complement Attack. PLoS One. 2015;10(9):e0137630.
61. Partridge SR, Baker MS, Walker MJ, Wilson MR. Clusterin, a putative complement regulator, binds to the cell surface of Staphylococcus aureus clinical isolates. Infect Immun. 1996;64(10):4324-9.
62. Fox CR, Parks GD. Complement Inhibitors Vitronectin and Clusterin Are Recruited from Human Serum to the Surface of Coronavirus OC43-Infected Lung Cells through Antibody-Dependent Mechanisms. Viruses. 2021;14(1).
63. RStudio Team (2020). RStudio: Integrated Development Environment for R. RStudio, Boston, MA. Available from: http://www.rstudio.com/
64. R Core Team (2024). R: A Language and Environment for Statistical Computing. Vienna, Austria. Available from: https://www.R-project.org/
65. Jantos CA, Heck S, Roggendorf R, Sen-Gupta M, Hegemann JH. Antigenic and molecular analyses of different Chlamydia pneumoniae strains. J Clin Microbiol. 1997;35:620-3.
66. Sambrook J, Maniatis T, Fritsch E. Molecular cloning: A laboratory manual. Cold Spring Harbor, N. Y.: Cold Spring Harbor laboratory; 1989.
67. Grube L, Dellen R, Kruse F, Schwender H, Stuhler K, Poschmann G. Mining the Secretome of C2C12 Muscle Cells: Data Dependent Experimental Approach To Analyze Protein Secretion Using Label-Free Quantification and Peptide Based Analysis. J Proteome Res. 2018;17(2):879-90.
68. Prescher N, Hansch S, Knobbe-Thomsen CB, Stuhler K, Poschmann G. The migration behavior of human glioblastoma cells is influenced by the redox-sensitive human macrophage capping protein CAPG. Free Radic Biol Med. 2021;167:81-93.
69. Tusher VG, Tibshirani R, Chu G. Significance analysis of microarrays applied to the ionizing radiation response. Proc Natl Acad Sci U S A. 2001;98(9):5116-21.

Supplementary Information

Secreted host cell clusterin binds *Chlamydia trachomatis* PmpD and is essential for infection

Fabienne Kocher[1], Johannes H. Hegemann[1*]

1 Heinrich Heine University Düsseldorf, Faculty of Mathematics and Natural Sciences, Institute for Functional Microbial Genomics, Düsseldorf, Germany

*** Corresponding author: johannes.hegemann@hhu.de**

Supplementary Figures

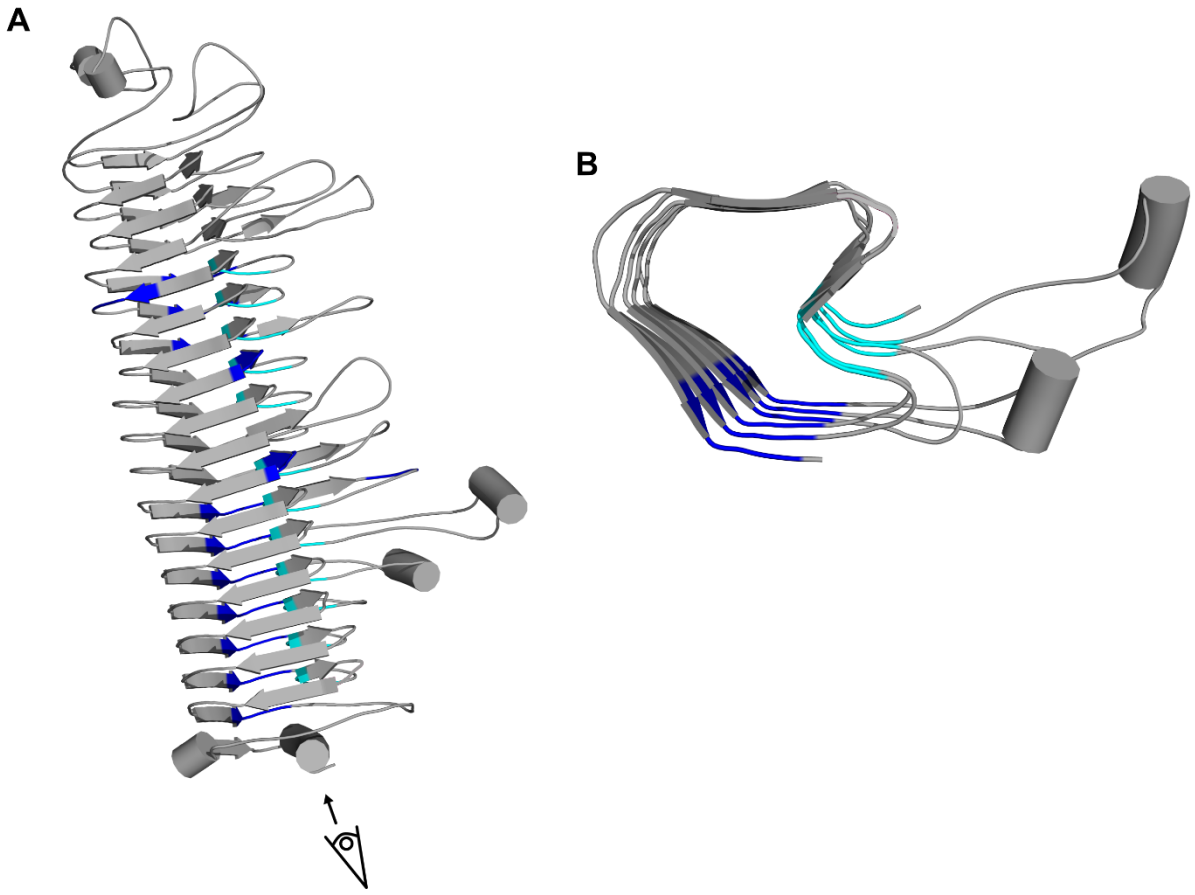

Supplementary Figure 1: Predicted 3D-model for D72 from *Ctr* PmpD.
(A) The structure prediction generated by RoseTTAFold [1] for rD72, a fragment of *Ctr* PmpD spanning residues 68-761, indicates a lengthy β-helical structure. The FxxN and GGA(I,L,V) motifs are highlighted in dark and light blue, respectively. **(B)** Bottom view of the predicted structure as indicated in **(A)**, shows the FxxN and GGA(I,L,V) motifs stacked on top of each other.

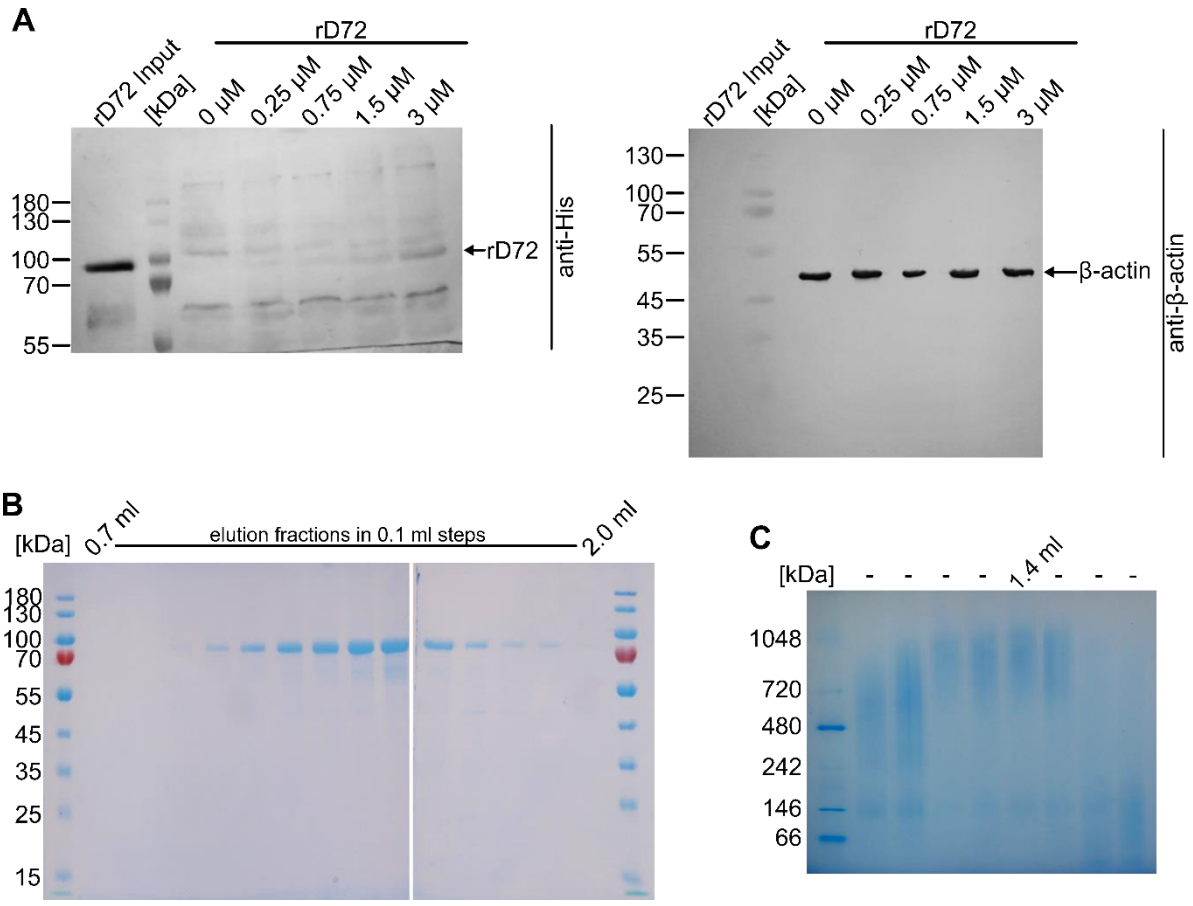

Supplementary Figure 2: Uncropped gels and blots from Figure 1.

(A) Immunoblot pictures from Fig. 1B, representing rD72 affinity to HEp-2 cells. On the left, bound rD72 is visualized using an anti-His antibodies. On the right, the internal loading control (actin) is visualized with an anti-β-actin antibody. **(B)** Uncropped SDS-PAGE gel from Fig. 1C with the individual SEC elution fractions (in 0.1 ml steps) indicated. **(C)** Uncropped Blue Native-PAGE gel from Fig. 1C with the sample from the SEC elution at 1.4 ml indicated. The residual lanes (-) contain protein samples not relevant for this study.

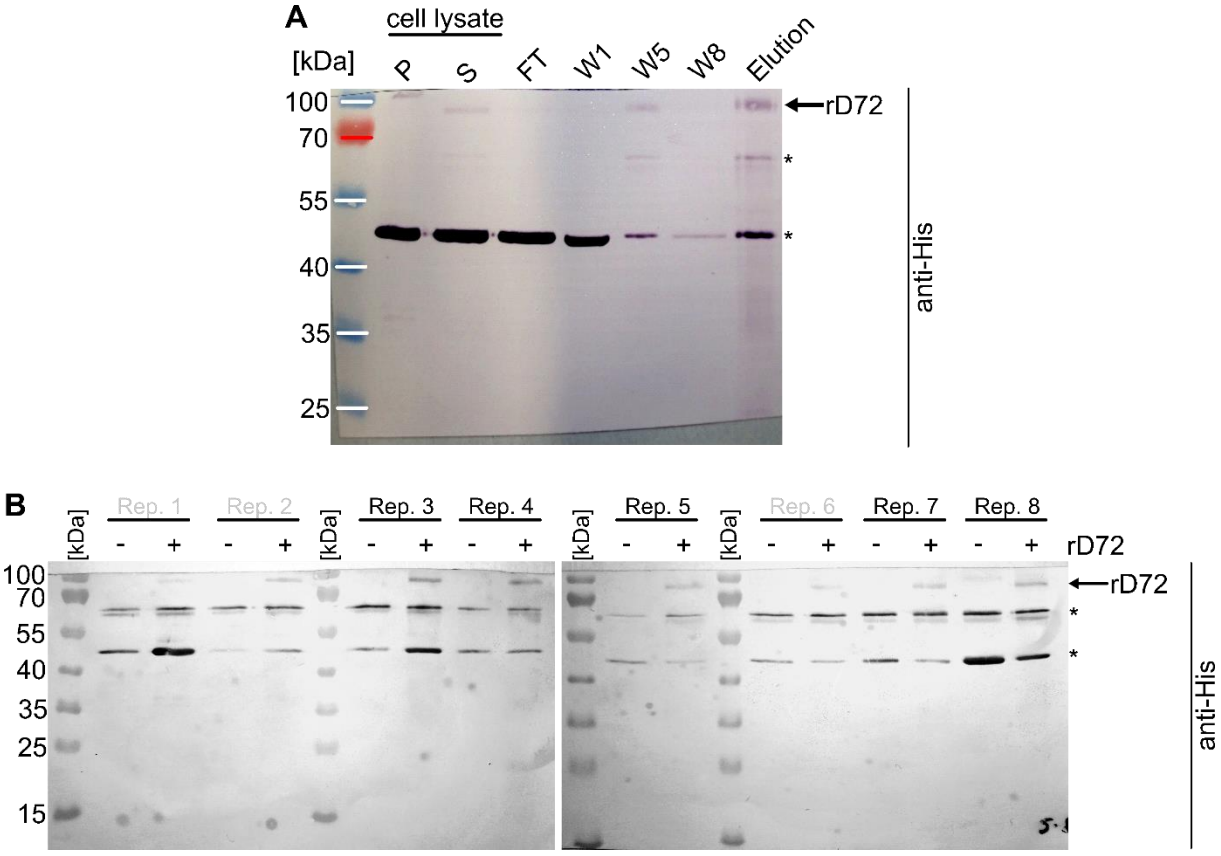

Supplementary Figure 3: Uncropped blot for Fig. 2A and biological replicates generated for mass spectrometry.

(A) Immunoblot picture from Fig. 2A monitoring the pulldown assay with rD72 as bait on epithelial cells, visualized with an anti-His antibody. Unspecific bands are indicated with an asterisk. **(B)** The pulldown elution fractions of the negative controls (-) and the test samples (+) were analysed by Western blot and probed with an anti-His antibody. Replicates used for mass spectrometry analysis are marked in black, replicates which were not processed further are marked in grey.

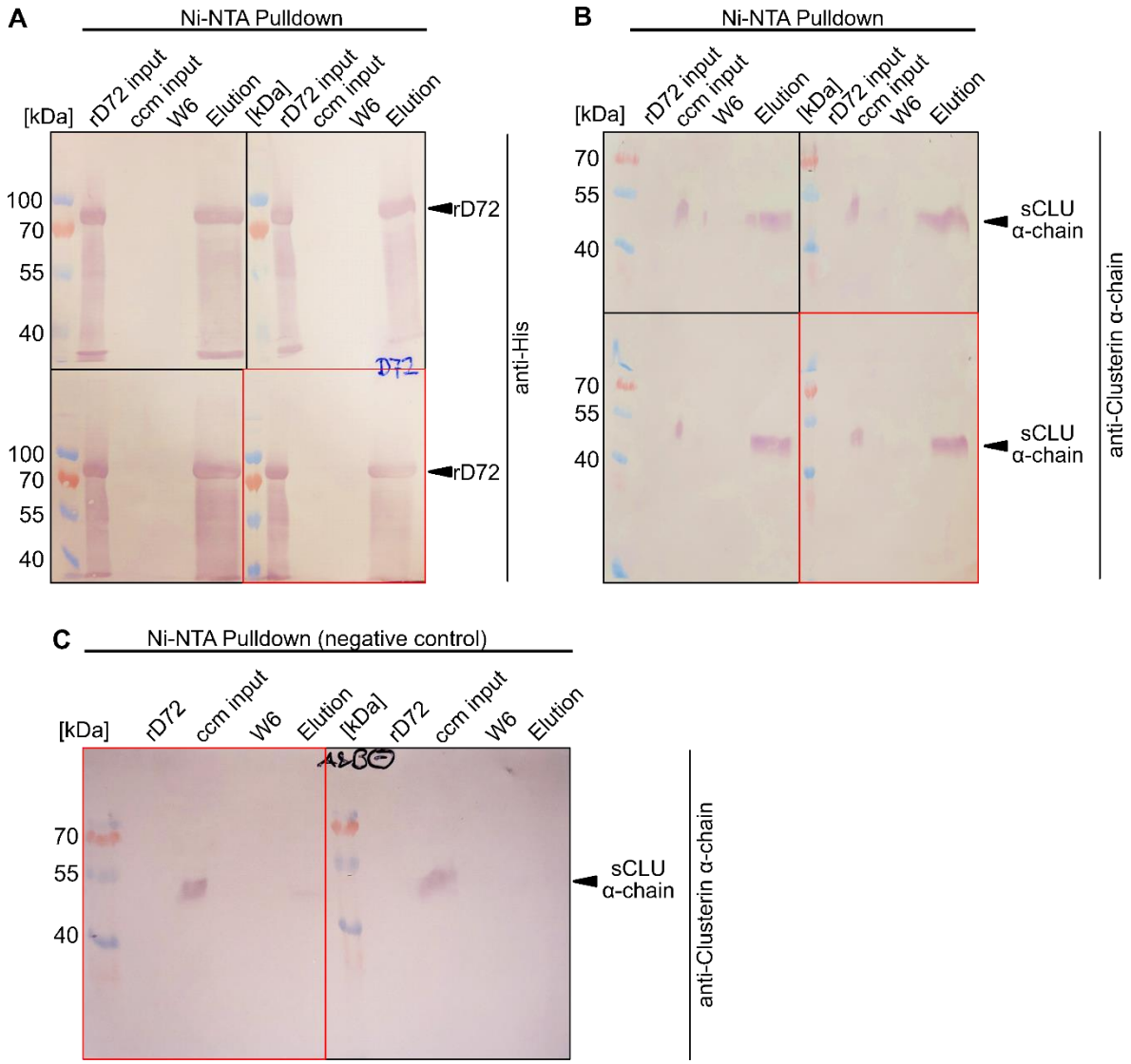

Supplementary Figure 4: Replicates and uncropped blots of the pulldown assay shown in Fig. 3.

(A) and **(B)** Ni-NTA pulldown assays where rD72 was used as bait and incubated with isolated cell culture medium (ccm) from epithelial cells grown for two days. The protein compositions of the individual fractions were analysed by immunoblotting with an anti-His antibody **(A)** or an anti-Clusterin α-chain antibody **(B)**. (W6 = wash 6). The boxes indicate the four replicates with red boxes marking the blot from Fig. 3B. **(C)** Replicates of the negative control where no rD72 was used as bait protein. The protein compositions of the individual fractions were analysed by immunoblotting with an anti-Cluster α-chain antibody. (W6 = wash 6). The boxes indicate the two replicates, with the red box showing the blot presented in Fig. 3C.

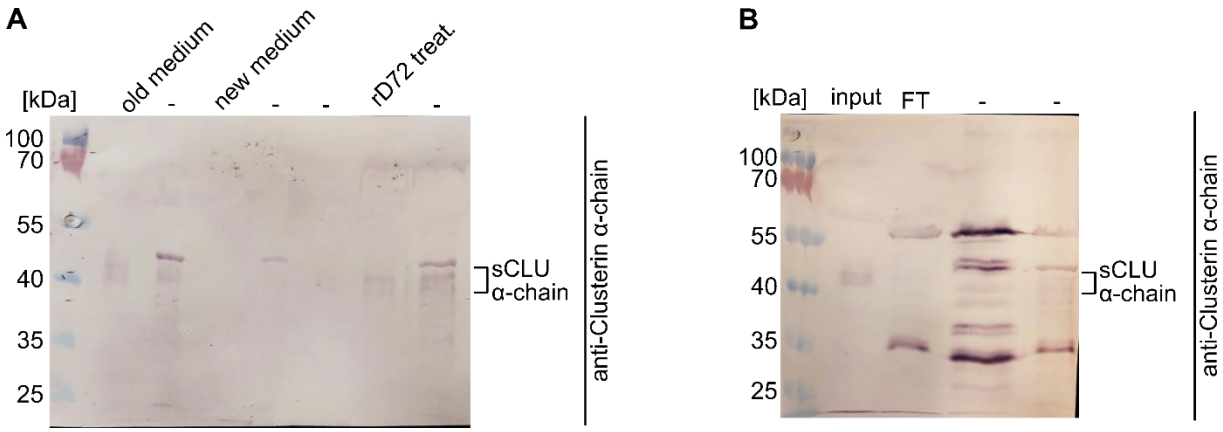

Supplementary Figure 5: Uncropped blot for Figure 4.

(A) Western blot from Fig. 4B, monitoring the sCLU abundance in the different experimental approaches (i-iii) described in Fig. 4A, using an anti-Clusterin α-chain antibody. **(B)** Western blot from Fig. 4B, monitoring the sClu abundance for approach iv, described in Fig. 4A, using an anti-Clusterin α-chain antibody. (FT = Flow Through).

Supplementary Table

Supplementary Table 1. Vectors and oligonucleotides for cloning *pmpD* fragments.

Pmp fragment	Vector	Primer sequence (5' to 3')
PmpD (D72)	pKM32 [2]	GAAATTAACTATGAGAGGATCTCACCATCACCATCACCATCA CCATCACCATGATAGTCAGGCTGAAGGACAG
		GGAGTCCAAGCTCAGCTAATTAAGCTTGGCTGCAGGTCGAC TAAGCTTGATTAGCTGCAGTAATAAAAC

Supplementary Table 2. List of significantly enriched host cell proteins found in mass spectrometry analysis.

Protein ID	Protein name	Gene name	MW [kDa]	Localization
P04792	Heat shock protein beta-1	HSPB1	23.704	cytosolic
Q9H936; Q9H1K4	Mitochondrial glutamate carrier 1 & 2	SLC25A22; SLC25A18	34.47	mitochondrial
Q9NZJ7	Mitochondrial carrier homolog 1	MTCH1	43.121	mitochondrial
P10909	Clusterin	CLU	52.494	intra- & extracellular
P05141	ADP/ATP translocase 2	SLC25A5	32.852	mitochondrial
Q9UJS0	Calcium-binding mitochondrial carrier protein Aralar2	SLC25A13	74.175	mitochondria

References

1. Baek M, DiMaio F, Anishchenko I, Dauparas J, Ovchinnikov S, Lee GR, et al. Accurate prediction of protein structures and interactions using a three-track neural network. Science. 2021;373(6557):871-6.
2. Mölleken K, Schmidt E, Hegemann JH. Members of the Pmp protein family of Chlamydia pneumoniae mediate adhesion to human cells via short repetitive peptide motifs. Mol Microbiol. 2010;78(4):1004-17.

4 Part II: Manuscript II

Title:

The *Chlamydia pneumoniae* effector SemD exploits its host's endocytic machinery by structural and functional mimicry

Authors:

Fabienne Kocher, Violetta Applegate, Jens Reiners, Astrid Port, Dominik Spona, Sebastian Hänsch, Amin Mirzaiebadizi, Mohammad Reza Ahmadian, Sander HJ Smits, Johannes H. Hegemann, Katja Mölleken

Contribution:

Fabienne Kocher (F.K.): 55 %, Violetta Applegate (V.A.): 7 %, Jens Reiners (J.R.): 7 %, Astrid Port (A.P.): 1 %, Dominik Spona (D.S.): 1 %, Sebastian Hänsch (S.H.): 3 %, Amin Mirzaiebadizi (A.M.): 3 %, Mohammad Reza Ahmadian (M.R.A.): 1 %, Sander HJ Smits (S.H.J.S.): 7 %, Johannes H. Hegemann (J.H.H.): 10 %, Katja Mölleken (K.M.): 5 %

Conceptualisation: F.K., K.M. and J.H.H., methodology F.K., K.M., M.R.A., A.M., S.H.J.S. and J.H.H.; investigation: F.K., V.A., J.R., A.P., D.S., S.H., A.M., M.R.A., S.H.J.S. and K.M., writing—original draft: F.K., K.M., S.H.J.S. and J.H.H.; writing—review & editing: F.K., K.M., S.H.J.S. and J.H.H; funding acquisition: J.H.H.

Individual contributions to the figures in the publication:

F.K. prepared all figures and prepared the proteins for Fig. 1, 2, 3, 4 (except $Cdc42_{GppNHp}$), 5 and 6. Furthermore, F.K. provided experimental data for Fig. 3c,d; 4a,b,e,f; 5b,c; 6a,b; Supplementary Fig. 1a; 2a-c; 4a-d and 5.

V.A., A.P and S.H.J.S generated and measured protein crystals for X-ray crystallography and analysed the data represented in Fig. 1b,d; 2b-c; 3a and Supplementary Fig. 8

J.R. measured the proteins and protein complexes using SAXS and analysed the data represented in Fig. 1c; 5d,e; 6c; Supplementary Fig. 1c-h; 3; 6 and 7

S.H. wrote and provided the custom code for Fiji 1.54f used for the GUV analyses in Fig. 3c,d and 5b,c

A.M. prepared $Cdc42_{(m)GppNHp}$ and provided experimental data for Fig. 4c,d

K.M. had a supporting function in protein preparation

Published in:

Nature Communications, August 2024

DOI: https://doi.org/10.1038/s41467-024-51681-3

2-year Impact factor: 14.7
5-year Impact factor: 16.1

I hereby confirm that this information is correct.

Düsseldorf, 22 October 2024

Fabienne Kocher

nature communications

Article

https://doi.org/10.1038/s41467-024-51681-3

The *Chlamydia pneumoniae* effector SemD exploits its host's endocytic machinery by structural and functional mimicry

Received: 12 February 2024

Accepted: 15 August 2024

Published online: 24 August 2024

Check for updates

Fabienne Kocher[1], Violetta Applegate[2], Jens Reiners[2], Astrid Port[2], Dominik Spona[1], Sebastian Hänsch[3], Amin Mirzaiebadizi[4], Mohammad Reza Ahmadian[4], Sander H. J. Smits[2,5], Johannes H. Hegemann[1,6] ✉ & Katja Mölleken[1,6]

To enter epithelial cells, the obligate intracellular pathogen *Chlamydia pneumoniae* secretes early effector proteins, which bind to and modulate the host-cell's plasma membrane and recruit several pivotal endocytic host proteins. Here, we present the high-resolution structure of an entry-related chlamydial effector protein, SemD. Co-crystallisation of SemD with its host binding partners demonstrates that SemD co-opts the Cdc42 binding site to activate the actin cytoskeleton regulator N-WASP, making active, GTP-bound Cdc42 superfluous. While SemD binds N-WASP much more strongly than Cdc42 does, it does not bind the Cdc42 effector protein FMNL2, indicating effector protein specificity. Furthermore, by identifying flexible and structured domains, we show that SemD can simultaneously interact with the membrane, the endocytic protein SNX9, and N-WASP. Here, we show at the structural level how a single effector protein can hijack central components of the host's endocytic system for efficient internalization.

The obligate intracellular bacterial pathogen *Chlamydia pneumoniae* (*Cpn*) causes infections of the upper and lower respiratory tract[1,2]. A certain proportion of these can result in severe respiratory illnesses, such as pneumonia, asthma and chronic bronchitis, as well as multiple sclerosis, inflammatory arthritis, lung cancer and Alzheimer's disease[2–6].

Cpn's developmental cycle begins with the adhesion of the infectious elementary body (EB) to the host-cell's plasma membrane (PM), and its internalisation into a membrane-enclosed "inclusion". The initial, transient contact between EB and host cell enables chlamydial surface proteins, such as Pmp proteins and LipP, to stably bind and activate host-cell receptors that trigger receptor-mediated internalisation[7–9]. However, engulfment of the EB requires a membrane vesicle that is three to four times larger in diameter than a classical endocytotic vesicle[10]. *Cpn* solves this problem by secreting several entry-related, early effector proteins directly into the host cell via its type-III-secretion system (T3SS). These include soluble factors, such as Cpn0572 (the homologue of *Chlamydia trachomatis (Ctr)* TarP), and proteins that bind to the host's PM, such as SemC and SemD[11–13]. By hijacking components of the host's endocytic machinery, early effectors trigger the formation of an intracellular membrane-enclosed vesicle that encompasses the EB[14–16]. The membrane-bound effectors SemC and SemD play a vital role in this process. Each possesses an amphipathic helix (APH) with high affinity for phosphatidylserine (PS),

[1]Heinrich Heine University Düsseldorf, Faculty of Mathematics and Natural Sciences, Institute for Functional Microbial Genomics, Düsseldorf, Germany. [2]Heinrich Heine University Düsseldorf, Faculty of Mathematics and Natural Sciences, Center for Structural Studies, Düsseldorf, Germany. [3]Heinrich Heine University Düsseldorf, Faculty of Mathematics and Natural Sciences, Center for Advanced Imaging, Düsseldorf, Germany. [4]Institute of Biochemistry and Molecular Biology II, Medical Faculty and University Hospital Düsseldorf, Heinrich Heine University Düsseldorf, Düsseldorf, Germany. [5]Heinrich Heine University Düsseldorf, Faculty of Mathematics and Natural Sciences, Institute of Biochemistry, Düsseldorf, Germany. [6]These authors jointly supervised this work: Johannes H. Hegemann, Katja Mölleken. ✉e-mail: johannes.hegemann@hhu.de

a specific phospholipid found in the inner leaflet of the PM[12,13]. The binding of SemC to PS induces extensive membrane curvature while SemD (382 aa) recruits and activates central endocytic host proteins[12,13].

Downstream of its N-terminal APH, SemD harbours two proline-rich domains ($PRD1_{91\text{-}100}$ and $PRD2_{117\text{-}122}$, Fig. 1a), the first of which binds to the SH3 domain of SNX9[12]. During classical endocytosis, SNX9, a BAR domain (bin-amphiphysin-rvs) protein, binds to the PM, induces membrane curvature and promotes vesicle closure[17–19]. Similarly, by recruiting SNX9 via SemD, *Cpn* amplifies membrane deformation at the site of EB entry and ensures the closure and maturation of the endocytic vesicle.

SemD also possesses two centrally located WH2 domains, which are involved in G-actin binding[12]. Furthermore, the C-terminal 165 residues (aa 218-382) of SemD are required for recruitment of N-WASP, an endocytic host protein that re-organises the actin cytoskeleton by interacting with the actin-branching complex Arp2/3[12]. N-WASP is a ubiquitously expressed member of the WASP family[20]. Signal reception and transduction of N-WASP are mediated by its basic region (BR), its GTPase-binding domain (GBD) and its verprolin-central-acidic (VCA) domain, respectively. The GBD domain consists of the Cdc42/Rac interactive domain (CRIB) and a C-sub motif (Fig. 2a)[21,22]. In resting cells, N-WASP resides in an autoinhibited cytosolic state mediated by intramolecular interactions between the GBD and VCA domains[22,23]. During endocytosis, Cdc42, a small GTPase belonging to the Rho family, is activated by guanine nucleotide exchange factors (GEFs) that catalyse the replacement of bound GDP by GTP[24]. Active, GTP-bound Cdc42 ($Cdc42_{GTP}$) binds to the BR-GBD domain of N-WASP, and

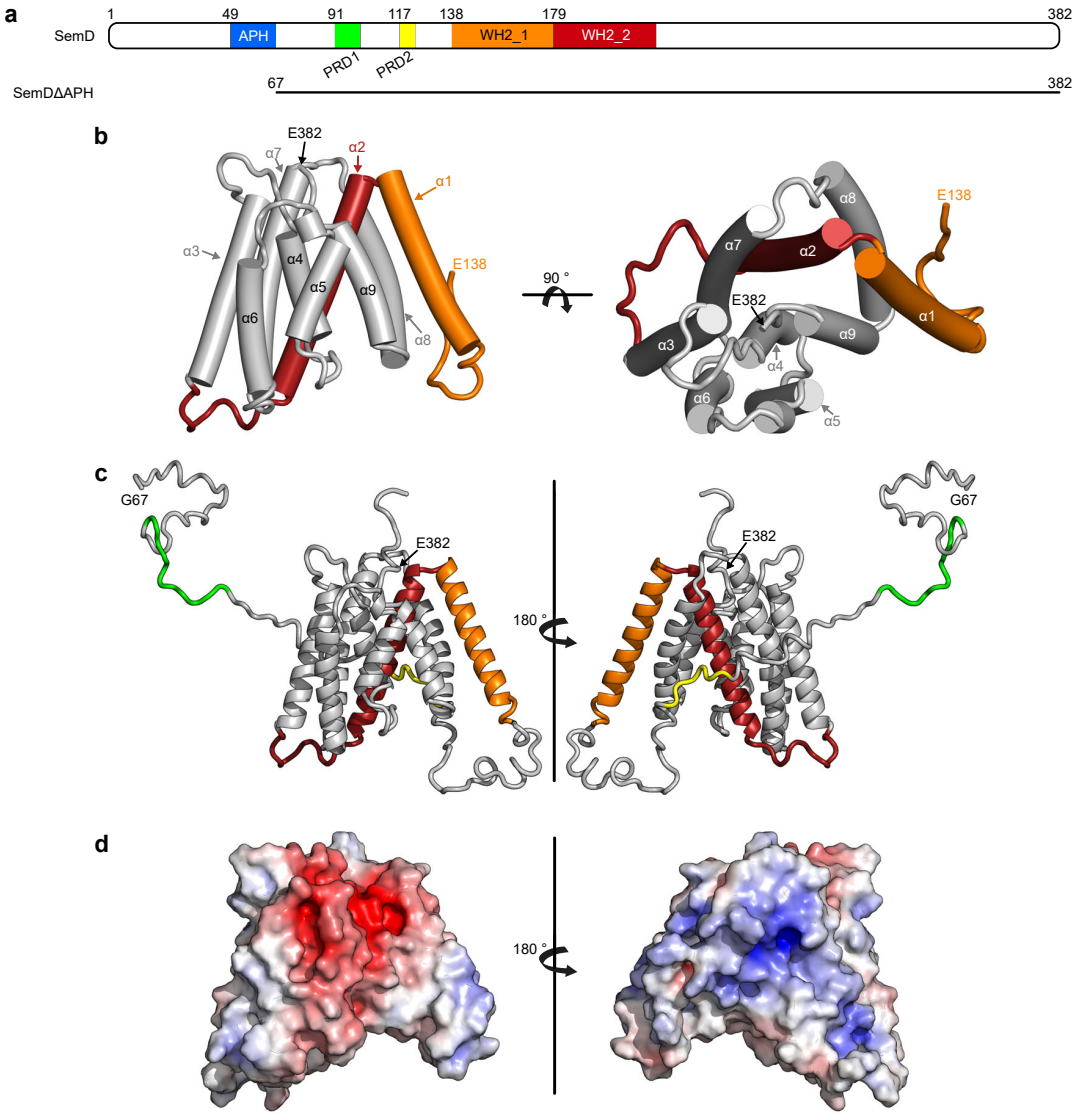

Fig. 1 | Crystal structure of SemDΔAPH. a Schematic representation of the primary structure of SemD, containing an $APH_{49\text{-}66}$, two proline-rich domains ($PRD_{191\text{-}100}$, $PRD2_{117\text{-}122}$) and two WH2 domains ($WH2\_1_{138\text{-}178}$, $WH2\_2_{179\text{-}216}$). $SemD\Delta APH_{67\text{-}382}$ is represented as a black bar. **b** The structure of SemDΔAPH as resolved by X-ray crystallography. The helices are depicted as cylinders and numbered from 1 to 9, starting at the N-terminus (α1- α9). In accordance with the colour code in **a**, the WH2_1 and WH2_2 are depicted in orange and red, respectively. The N-terminal E138 and the C-terminal E382 (both marked by black arrows) represent the first and last amino acids visible in the electron density. Right panel: 90° rotation. **c** SAXS best-fit CORAL model (χ^2 value of 1.197), based on the SemDΔAPH crystal structure, and including the added flexible tails (further models are shown in Supplementary Fig. 1h). PRD1 and PRD2 are coloured in green and yellow, respectively. Right panel: 180° rotation. G67 is the N-terminal amino acid, while E382, the last C-terminal residue of SemD, is followed by the C-terminal 10x-His-Tag. **d** Electrostatic surface representation of SemDΔAPH highlighting the negatively (red) and positively (blue) charged patches. Right panel: 180° rotation.

https://doi.org/10.1038/s41467-024-51681-3

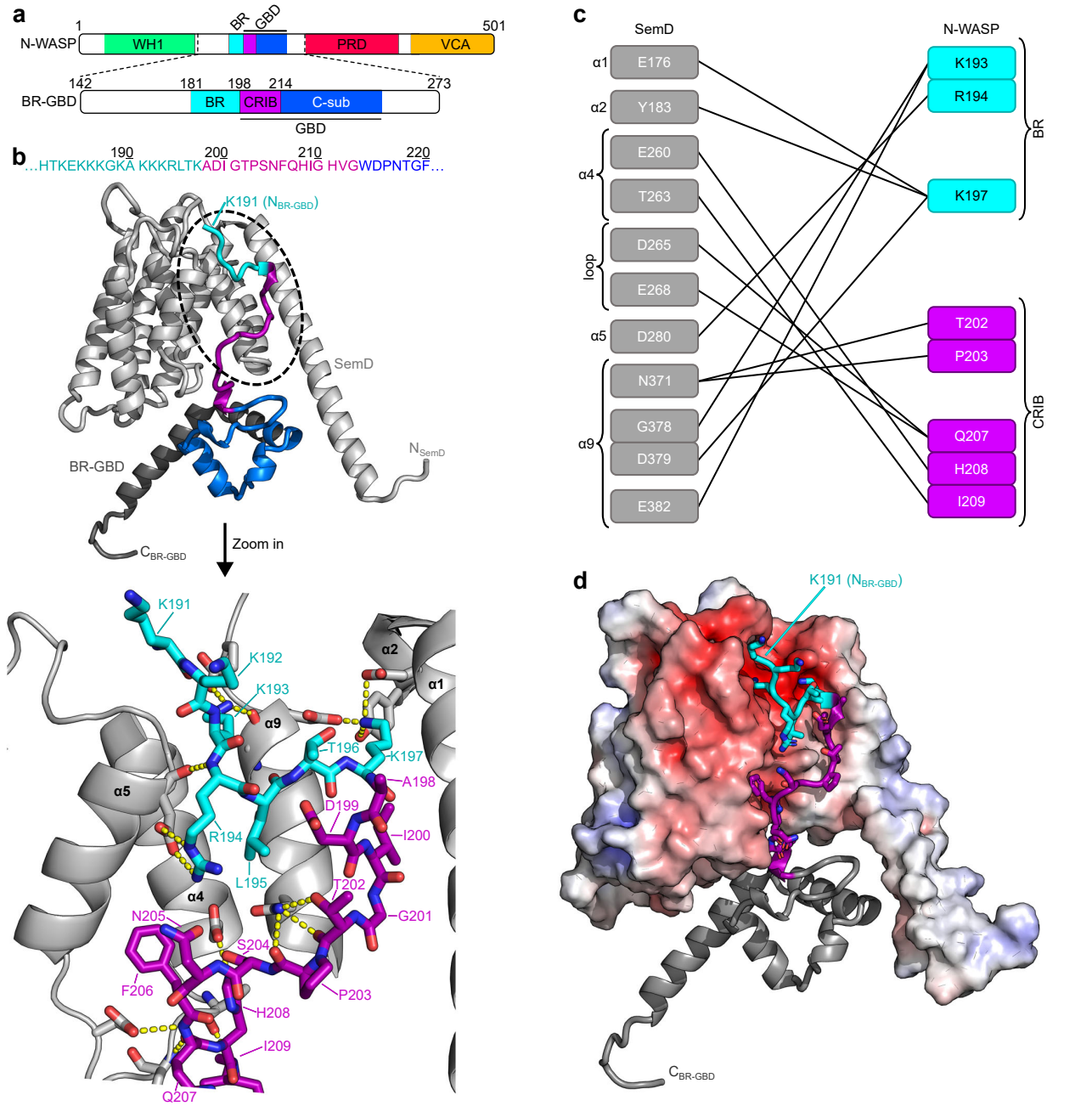

Fig. 2 | SemD engages with BR-GBD in a Cdc42$_{GTP}$-mimicking manner. **a** Schematic representation of the N-WASP primary sequence. BR-GBD$_{142-273}$ was used for complex formation with SemDΔAPH. It contains the BR$_{181-197}$ domain (basic region, cyan), the CRIB$_{198-213}$ domain (Cdc42/Rac interactive binding motif, magenta) and the C-sub$_{214-250}$ domain (blue). **b** The structure of SemDΔAPH in complex with BR-GBD as resolved by X-ray crystallography, shown in cartoon representation. SemDΔAPH is shown in light grey, BR-GBD is coloured in dark grey with the BR domain in cyan, the CRIB domain in magenta and C-sub domain in blue. The zoom in shows details of the binding of SemDΔAPH to BR-GBD. Important residues of SemDΔAPH and BR-GBD are shown in stick representation, while the rest of SemDΔAPH is shown as cartoon. Interactions (<3.5 Å) are shown by the yellow dashes. **c** Schematic representation of the detailed interactions between SemDΔAPH and BR-GBD. **d** Electrostatic representation of SemDΔAPH, highlighting the negatively charged patch in red and positively charged surface areas in blue. BR-GBD is coloured in dark grey (cartoon) with the BR domain in cyan and the CRIB domain in magenta, both depicted with stick residues.

triggers the release of the VCA domain, which in turn binds and actives the Arp2/3 complex (Supplementary Fig. 2b)[23,25]. Moreover, the BR binds to PI(4,5)P_2 in the inner leaflet of the PM, and recruits the actin polymerisation machinery to the site of endocytosis[26].

Cdc42 plays a central role in a large number of diverse biological processes such as the cell cycle, controlling gene transcription, regulating the cytoskeleton, cell movement and polarisation, hence being a target for many virulence factors secreted by bacterial pathogens[27–29]. These factors modulate the activity of Cdc42 by mimicking host regulators such as GEFs, GTPase activating proteins (GAPs) and guanine dissociation inhibitors (GDIs), or by covalently modifying Cdc42[30–34]. In addition, bacterial effector proteins can bind the autoinhibited Cdc42-binding domain of N-WASP, thereby initiating actin polymerisation[35].

During a *Cpn* infection, the C-terminus of the membrane-bound SemD interacts with the BR-GBD domain of N-WASP, thus triggering N-WASP activation and Arp2/3-mediated actin polymerisation via an unknown mechanism[12]. This ensures the provision of branched F-actin bundles required for extensive membrane deformation and maturation of the EB-containing vesicle.

In this work, we elucidate the mechanism involved by determining the three-dimensional structure of SemD, alone and in complex with its host interaction partners. We demonstrate that SemD, a protein of 382 aa, can interact simultaneously with the PM, SNX9 and N-WASP, thereby combining membrane association and deformation with modulation of the actin polymerisation machinery. Using small-angle X-ray scattering (SAXS), crystallography and mutational analysis, we show that SemD structurally and functionally mimics the activation of N-WASP by $Cdc42_{GTP}$, thus enabling *Cpn* to activate N-WASP in a $Cdc42_{GTP}$-independent manner. Further, by using pulldown assays and stopped-flow experiments, we show that SemD binds N-WASP more tightly than $Cdc42_{GTP}$, and that SemD is a specific N-WASP activator, not binding to formin like-protein L2 (FMNL2), another $Cdc42_{GTP}$-target protein. Our structural data also reveal that the N-WASP binding region of SemD is separated from its PRD1 – which is responsible for SNX9-SH3 binding – and from the membrane-binding APH domain via flexible linker regions. These features permit highly adaptable rearrangements of the individual binding sites, which reduce steric hindrance and facilitate simultaneous binding of the PM, SNX9 and N-WASP. These concurrent interactions enable *Cpn* to rapidly modulate the PM and the actin cytoskeleton, which ensures the successful formation of a large endocytic vesicle, and the rapid uptake of the EB within 15 minutes after its initial adhesion to a non-phagocytic host cell.

Results

SemD folds into a multipurpose interaction structure

To elucidate how SemD functions at the molecular level, we determined the 3D structure of the protein, N-terminally truncated up to and including the APH motif ($SemD\Delta APH_{67\text{-}382}$) at a resolution of 2.1 Å (Fig. 1a, b, Supplementary Fig. 1a, b and Supplementary Table 1). The resulting structure revealed that the C-terminal portion of SemDΔAPH (aa 138-382) folds into a rigid core, consisting of nine α-helices, which is N-terminally flanked by a long intrinsically disordered region (IDR, aa 67-137, Fig. 1b). Owing to its flexibility, the latter is not visible in the electron density. The proline-rich domains (PRD1 and PRD2) are within the IDR and provide a highly flexible interaction surface. The first and second α-helices harbour the WH2_1 and WH2_2 domains involved in G-actin binding[12] (Fig. 1b). Within the electron density, the amino acids are clearly visible, except for the connecting loop between helices 2 and 3, which is presumably flexible; here, the side-chains were not included in the final model. Although structural comparisons using EBI-fold revealed similar proteins (all with a root-mean-square deviation (RMSD) > 3.5 Å), no informative conclusions could be reached, since the only feature shared between them was a high helical content.

To clarify how SemDΔAPH behaves in solution, we performed SAXS analysis. We found that SemDΔAPH is a monomer in solution (Supplementary Table 2) and the *p(r)* function indicated a globular core – corresponding to the helical core domain revealed by the X-ray structure – and an elongated tail (Supplementary Fig. 1c–g). We calculated the theoretical scattering of the solved SemDΔAPH crystal structure and compared it with the experimental data for SemDΔAPH in solution. The resulting CRYSOL fit yielded a χ^2 value of 14.63 (an indicator on how well the model fits to the scattering curve in solution) and showed a high mismatch in the low s region (Supplementary Fig. 1c). This is not surprising, because the N-terminal residues (aa 67-137) are not solved in the crystal structure and the *p(r)* function showed an elongated tail, most probably the N-terminal region. Based on the information derived from SAXS data, we added the missing N-terminal residues (aa 67-137) to complete the SemDΔAPH structure (Fig. 1c). The resulting models showed that these N-terminal residues comprise the IDR tail (the best-fit model is shown in Fig. 1c, an overlay of independent models, showing the same tendency of the tail orientation, are shown in Supplementary Fig. 1h). This resulted in an improved χ^2 value of 1.20 (Supplementary Table 2). Furthermore, electrostatic analysis of the rigid core of SemD revealed a large, negatively charged patch on the front of the protein and a smaller positively charged patch on the back (Fig. 1d).

Taken together, the combined crystallographic and SAXS-based structure of SemDΔAPH reveals that its N-terminal segment, with which SH3 domain-containing proteins interact, is flexible. The nine α-helices that constitute the rigid core include the two WH2 domains, involved in G-actin binding, and the N-WASP interaction site[12]. Electrostatic analysis of the rigid core reveals two highly charged patches; a negative patch on the front and a positive patch on the back.

SemD structurally mimics $Cdc42_{GTP}$ for N-WASP activation

Generally, $Cdc42_{GTP}$ activates N-WASP by binding to its BR-GBD domain, which leads to the release of the VCA domain of N-WASP. The VCA domain then recruits the Arp2/3 complex, initiating actin branching and polymerisation (Supplementary Fig. 2b). However, during *Cpn* uptake, secreted SemD, whose APH domain interacts with the PM, binds to N-WASP and activates it in an as yet unknown fashion, thus initiating the formation of branched F-actin structures upon recruitment of the Arp2/3 complex[12]. Intriguingly, it has been shown that, when bound to synthetic membranes via its APH domain, SemD is capable of binding and activating N-WASP[12]. The interaction between the two proteins requires the C-terminal part of SemD (aa 218-382) and the BR-GBD segment of N-WASP (Fig. 2a)[12]. To understand the activation of N-WASP by SemD, we structurally analysed the complex formed by recombinant SemDΔAPH and the BR-GBD domain of N-WASP. To this end, we purified the recombinant proteins separately, allowed them to interact and isolated the resulting complex by size exclusion chromatography (SEC, Supplementary Fig. 2a). The elution fractions containing the complex were pooled and analysed by both crystallography and SAXS (Fig. 2b, d).

The co-crystal of SemDΔAPH in complex with BR-GBD yielded a structure with a medium resolution of 3.3 Å, which is attributable to the flexible termini of both proteins. Interestingly, the loop connecting helices 2 and 3 ($_{208}$GTSSTG$_{213}$) of SemDΔAPH is stabilised in the complex and can now be modelled. Despite the moderate resolution of the crystals containing the SemDΔAPH – BR-GBD complex, the interaction surface between the two proteins is well resolved. Comparison of the structures of SemDΔAPH alone and in complex with BR-GBD revealed virtually identical conformations of the SemD core regions, as indicated by a low RMSD of 0.7 Å. Next, we identified intermolecular contact sites between SemDΔAPH and BR-GBD by identifying the amino acids that were closer than 3.5 Å to each other[36]. We found three positively charged residues within the BR domain of N-WASP (K193, R194 and K197) that interact directly with the negatively charged area found on the front of SemD, formed by helices α1, α2, α5 and α9 (Fig. 2b–d). Additionally, five residues of the N-WASP CRIB domain engage with residues in the SemD binding groove, mainly formed by helix α4, the adjacent loop and helix α9 (Fig. 2b, c). The N-WASP C-sub domain is located underneath the helical arrangement of SemDΔAPH, flanked by its extended helix α1 (Fig. 2b, d). Owing to the flexibility of the N-terminal domains of SemDΔAPH and BR-GBD, these regions are not resolved in the crystal structure of the complex.

Using SAXS, we validated the results obtained by crystallography. Analysis of BR-GBD alone showed that, in solution, it forms a monomer with a globular central region, flanked by a highly flexible N-terminal domain (Supplementary Fig. 3a–d, Supplementary Table 2). SAXS analysis of the SemDΔAPH – BR-GBD complex confirmed 1:1 stoichiometry in solution (Supplementary Table 2), in accordance with the

crystal structure. Analysis of the *p(r)* function and the dimensionless Kratky plot showed, that, upon formation of the complex, the unstructured segment of the BR-GBD does not adopt a specific secondary structure, but must take on a more constrained posture to bind to the core region of SemDΔAPH (Supplementary Fig. 3e–j), while the other domains retain their flexible characteristics. To confirm the position of the globular C-sub domain of N-WASP, we used the ensemble optimization method (EOM). Here, the interaction surface between SemDΔAPH and the N-WASP BR and CRIB segments found in the crystal structure is fixed, and the C-sub domain is allowed to vary freely in 3D space. Under these conditions, the conformation of the C-sub domain is the same as that seen in the crystal structure. Moreover, the final EOM models of the complex formed by SemDΔAPH and BR-GBD revealed, that an elongated complex conformation is preferred, which is attributable to the flexible N-termini of SemDΔAPH and BR-GBD (Supplementary Fig. 3k).

Taken together, our structural data show that the interaction of SemD with N-WASP requires the CRIB domain, together with the five C-terminal BR residues (aa 193-197) three of which are positively charged. Three of the five amino acids interact with the negatively charged patch on SemD, while the CRIB domain is embedded in the binding groove provided by SemD (Fig. 2).

SemD binds the N-WASP BR-GBD in a bipartite fashion

As described above, SemD binds to N-WASP by interacting with positively charged residues of the BR and with the CRIB domain. Moreover, structurally speaking, this mechanism is very similar to the interaction of WASP with $Cdc42_{GTP}$[37]. WASP and N-WASP belong to the same protein family, share 56% identity and 74% similarity, and have strikingly similar domain architectures and regulatory mechanisms[23]; however, the structure of the N-WASP – $Cdc42_{GTP}$ complex is not available thus far. Both proteins are crucial for transducing cell surface signals to the actin cytoskeleton, but while N-WASP is expressed ubiquitously, WASP is only present in non-erythroid hematopoietic cells[38]. To activate WASP (and N-WASP), $Cdc42_{GTP}$ interacts with the C-terminal residues of the BR domain – starting at the $KKK_{230\text{-}232}$ motif (corresponding to $KKR_{192\text{-}194}$ in N-WASP) – and with the CRIB domain (Fig. 3a)[23]. Mutational analysis indicated that the binding is strongly impeded when the $KKK_{230\text{-}232}$ motif in WASP is replaced by either uncharged or negatively charged amino acids[23,39]. Interestingly, with the C-terminal BR residues engaged in $Cdc42_{GTP}$ binding, the N-terminal BR residues can simultaneously bind to membranes containing $PI(4,5)P_2$, its preferred lipid[23].

Given the high structural similarity between the modes of interaction used by SemD and $Cdc42_{GTP}$ to bind and activate N-WASP, we tested for functional mimicry. To do so, we constructed deletion variants of the N-WASP BR-GBD domain lacking either the BR (BR-GBDΔ) or both the BR and the CRIB domain (BR-GBDΔΔ) (Fig. 3b). We also investigated whether or not the N-terminal BR residues mediate binding to $PI(4,5)P_2$ when SemD occupies the C-terminal BR residues. As an experimental setup, we chose to use giant unilamellar vesicles (GUVs) as a synthetic membrane model of the PM.

To test for recruitment of the individual BR-GBD variants by SemD, we used PS-containing GUVs, which mimic the lipid preferentially bound by SemD. For quantification, we calculated the fluorescence intensity ratio by measuring the maximal intensity at the perimeter of the GUV and setting it in relation to the average background intensity outside the GUV. In our control experiments, GFP alone showed no unspecific binding to GUV-bound SemD labelled with rhodamine ($SemD^{Rhod}$), and BR-GBD fused to GFP ($BR\text{-}GBD_{GFP}$) showed no binding to GUVs (Fig. 3c). Upon incubating $BR\text{-}GBD_{GFP}$ with $SemD^{Rhod}$ and GUVs, immediate colocalization of both proteins at the perimeter of the GUV was observed, indicating rapid and direct binding of $BR\text{-}GBD_{GFP}$ to GUV-bound $SemD^{Rhod}$ (Fig. 3c). Quantification revealed that binding persisted over a period of 20 min, and that fluorescence intensity at the GUV perimeter is 44.5 ± 15.3-fold higher than the average background fluorescence outside the GUV (Fig. 3d). Interestingly, upon incubation of $BR\text{-}GBD\Delta_{GFP}$ (lacking the BR domain) with $SemD^{Rhod}$ and GUVs, weak binding was visible after 5 min, which significantly increased over the next 15 min. However, even after 20 min, the fluorescence intensity ratio was more than 18-fold lower than the signal obtained for $BR\text{-}GBD_{GFP}$ (Fig. 3c, d). Finally, we also examined the binding of $BR\text{-}GBD\Delta\Delta_{GFP}$ (lacking both BR and CRIB) to $SemD^{Rhod}$. Quantification revealed a low fluorescence intensity ratio of 1.1 ± 0.2, which did not change over the next 20 min. Comparison of the data for $BR\text{-}GBD\Delta\Delta_{GFP}$ with the negative control GFP revealed no significant difference in fluorescence intensity ratio, at 1.1 ± 0.4. We therefore concluded that BR-GBDΔΔ, which lacks both BR and the CRIB domain, shows no recruitment to GUV-bound $SemD^{Rhod}$.

Next, we tested for simultaneous binding of $BR\text{-}GBD_{GFP}$ to $PI(4,5)P_2$ and $SemD^{Rhod}$ by using $PI(4,5)P_2$-containing GUVs. Indeed, $BR\text{-}GBD_{GFP}$ alone bound to $PI(4,5)P_2$-containing GUVs while $SemD^{Rhod}$ alone showed only a very weak colocalization to $PI(4,5)P_2$-containing GUVs (Supplementary Fig. 2c). When $SemD^{Rhod}$ was incubated with $PI(4,5)P_2$-bound $BR\text{-}GBD_{GFP}$, immediate colocalization of both proteins was observed at the perimeter of the GUV, suggesting that BR-GBD can indeed interact with both, lipids and SemD, simultaneously, in a manner similar to that of the N-WASP BR segment upon its interaction with $Cdc42_{GTP}$.

Taken together, these data imply that SemD not only structurally but also functionally mimics $Cdc42_{GTP}$ to recruit, bind and activate the central endocytic host protein N-WASP. Thereby, SemD binds to the BR-GBD via a bipartite interaction, which involves (i) the binding of positively charged amino acids located in the C-terminal BR domain to the negatively charged patch on SemD and (ii) the insertion of the CRIB domain into the binding groove provided by SemD. Thus, during *Cpn* uptake, the secreted and PM-bound SemD recruits N-WASP and abrogates its intramolecular autoinhibition by mimicking the $Cdc42_{GTP}$ activity in structure and function, leading to VCA release and finally to Arp2/3-mediated F-actin branching.

SemDΔAPH outcompetes $Cdc42_{GppNHp}$ for binding to N-WASP

So far, we have shown that SemD structurally and functionally mimics $Cdc42_{GTP}$ to bind and activate N-WASP. During a *Cpn* infection, PM-bound SemD redirects N-WASP function to the bacterial entry site thus mimicking $Cdc42_{GTP}$ for N-WASP binding. To compare N-WASP binding to SemD and $Cdc42_{GTP}$, respectively, we performed in vitro GFP-Trap® pulldown assays, using $BR\text{-}GBD_{GFP\text{-}His}$ as bait. $BR\text{-}GBD_{GFP\text{-}His}$ was incubated with $SemD\Delta APH_{His}$, or with Cdc42 bound to a non-hydrolysable GTP analogue ($Cdc42_{GppNHp}$)[23,40], or with equimolar amounts of $SemD\Delta APH_{His}$ and $Cdc42_{GppNHp}$. Following pulldown, we probed the composition of the flow through (FT) and elution fractions using immunodetection (Fig. 4a) and assessed the binding efficiency to $BR\text{-}GBD_{GFP\text{-}His}$, by correlating the band intensity of the elution to that of the FT (Elution:FT ratio, Fig. 4b). The negative control GFP indicated no unspecific binding to neither $SemD\Delta APH_{His}$ nor $Cdc42_{GppNHp}$ (Supplementary Fig. 4b). Conversely, the positive controls indicated evident binding of $SemD\Delta APH_{His}$ and $Cdc42_{GppNHp}$ respectively, to $BR\text{-}GBD_{GFP\text{-}His}$, with a quantified Elution:FT ratio of ~ 100% for each (Fig. 4a, b). Moreover, when equimolar ratios of $SemD\Delta APH_{His}$ and $Cdc42_{GppNHp}$ were added simultaneously to $BR\text{-}GBD_{GFP\text{-}His}$, $SemD\Delta APH_{His}$ showed an Elution:FT ratio of ~ 100 %, comparable to the positive control, while $Cdc42_{GppNHp}$ was now detected only in the FT (Fig. 4a, b). This experiment indicates that BR-GBD preferentially binds SemDΔAPH in the presence of active Cdc42. This result was confirmed and extended by stopped-flow measurements, in which addition of $SemD\Delta APH_{His}$ to a preformed $BR\text{-}GBD_{His}$ – $Cdc42_{GppNHp}$ complex led to dissociation of the latter (Fig. 4d), while $Cdc42_{GppNHp}$ in the absence of SemDΔAPH binds to $BR\text{-}GBD_{His}$ on a millisecond

https://doi.org/10.1038/s41467-024-51681-3

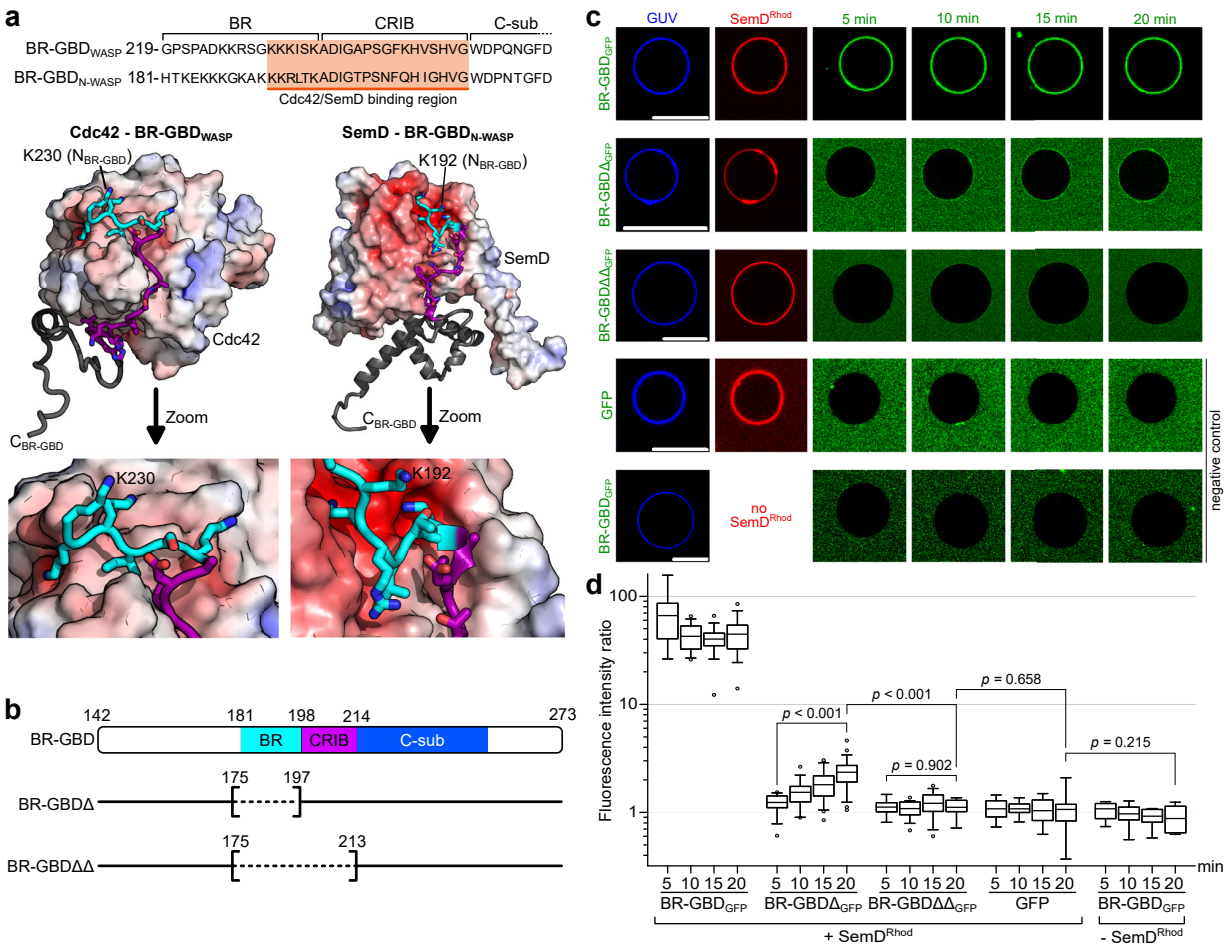

Fig. 3 | SemD recruits the BR-GBD region of N-WASP to membrane vesicles. **a** Amino acid sequence of WASP$_{219-259}$ (*human*) and N-WASP$_{181-221}$ (*Rattus norvegicus*) (of which the latter is identical to N-WASP$_{184-224}$ from *human*) (*top*). The orange box shows the sequence involved in binding to Cdc42$_{GTP}$ and SemD, respectively. The lower panel shows the structures of Cdc42$_{GTP}$ in complex with BR-GBD$_{WASP}$ (PDB: 1CEE[37]) and SemDΔAPH bound to BR-GBD$_{N-WASP}$. Cdc42$_{GTP}$ binds to the positively charged C-terminal KKK$_{230-232}$ motif of the BR from WASP and embeds the CRIB domain in the less charged binding groove. The same binding mechanism is observed for SemD, in which a negatively charged patch engages with the positively charged KKR$_{192-194}$ motif within the N-WASP BR domain and inserts the subsequent N-WASP CRIB domain into the SemD binding groove. **b** Schematic representation of BR-GBD and the deletion variants BR-GBDΔ (lacking the BR$_{175-197}$ domain) and BR-GBDΔΔ (lacking the BR$_{175-197}$ and the CRIB$_{198-213}$ domains). Dashed lines in square brackets mark the deleted protein regions. The first and last deleted amino acids are indicated. **c** Confocal images of PS-containing GUVs with rhodamine-labelled SemD (SemD^{Rhod}) and BR-GBD variants fused to GFP (BR-GBD$_{GFP}$). (scale bars 10 μm). **d** Quantification of bound protein to the GUV membrane based on the ratio of the maximal fluorescence at the perimeter of the GUV to the average background fluorescence outside the GUV. For each variant and time point, the fluorescence intensity ratio was calculated for up to 22 independent GUVs. The data are represented as boxplots with whiskers. The boxes are limited by the 25th and 75th percentile, including 50% of the data. The centre line shows the mean score. Whiskers denote 5–95% of all data and outliers are shown as grey dots. For comparing two groups, an unpaired, two-sided Student's *t* test was used. The data are representative for two independent data sets, both yielding similar results. Source data of both data sets are provided as Source Data file.

timescale (Fig. 4c). Collectively, these data show that SemD has a stronger binding capacity for N-WASP than active Cdc42$_{GTP}$, and is able to displace Cdc42$_{GTP}$ from the Cdc42$_{GTP}$ – N-WASP complex. Thus, during a *Cpn* infection, the locally secreted and PM-bound SemD underneath the invading EB most probably binds and activates cytosolic as well as Cdc42$_{GTP}$-bound N-WASP to initiate the branched F-actin mesh required for EB internalisation.

The preference of SemD for N-WASP over the physiological N-WASP activator Cdc42$_{GTP}$ raises the question of whether SemD is a specific activator of N-WASP or can also activate other Cdc42 target effectors. Cdc42 has been implicated as a key regulator of F-actin reorganisation, e.g. via activation of WASP/N-WASP to generate branched F-actin structures, as well as Formins, which play a critical role in nucleating actin filaments and promoting their elongation, thus influencing a large number of major cellular processes, involving actin dynamics such as cell motility, cell division and intracellular transport[41]. Formins are autoinhibited and require binding of active Cdc42$_{GTP}$ to the Formin GTPase binding domain for activation[42]. In in vitro pulldown assays, we tested whether SemD interacts with the mammalian FMNL2. We used recombinant FMNL2$_{GST}$ as bait and tested the binding of SemDΔAPH$_{His}$ and Cdc42$_{GppNHp}$ to it by analysing the FT and elution fractions (Fig. 4e). As expected, Cdc42$_{GppNHp}$ binds to FMNL2$_{GST}$, reaching an Elution:FT ratio significantly higher than the negative control with GST only (Fig. 4f). Interestingly, incubation of SemDΔAPH with GST or FMNL2$_{GST}$ showed no significant difference (Fig. 4e, f and Supplementary Fig. 4c, d). Thus, SemDΔAPH does not bind to FMNL2$_{GST}$, indicating that SemD specifically activates N-WASP and is not a general activator of Cdc42$_{GTP}$-dependent effector proteins, such as FMNL2.

Taken together, these data show that SemD copies Cdc42$_{GTP}$ at the EB entry side for N-WASP recruitment and activation.

https://doi.org/10.1038/s41467-024-51681-3

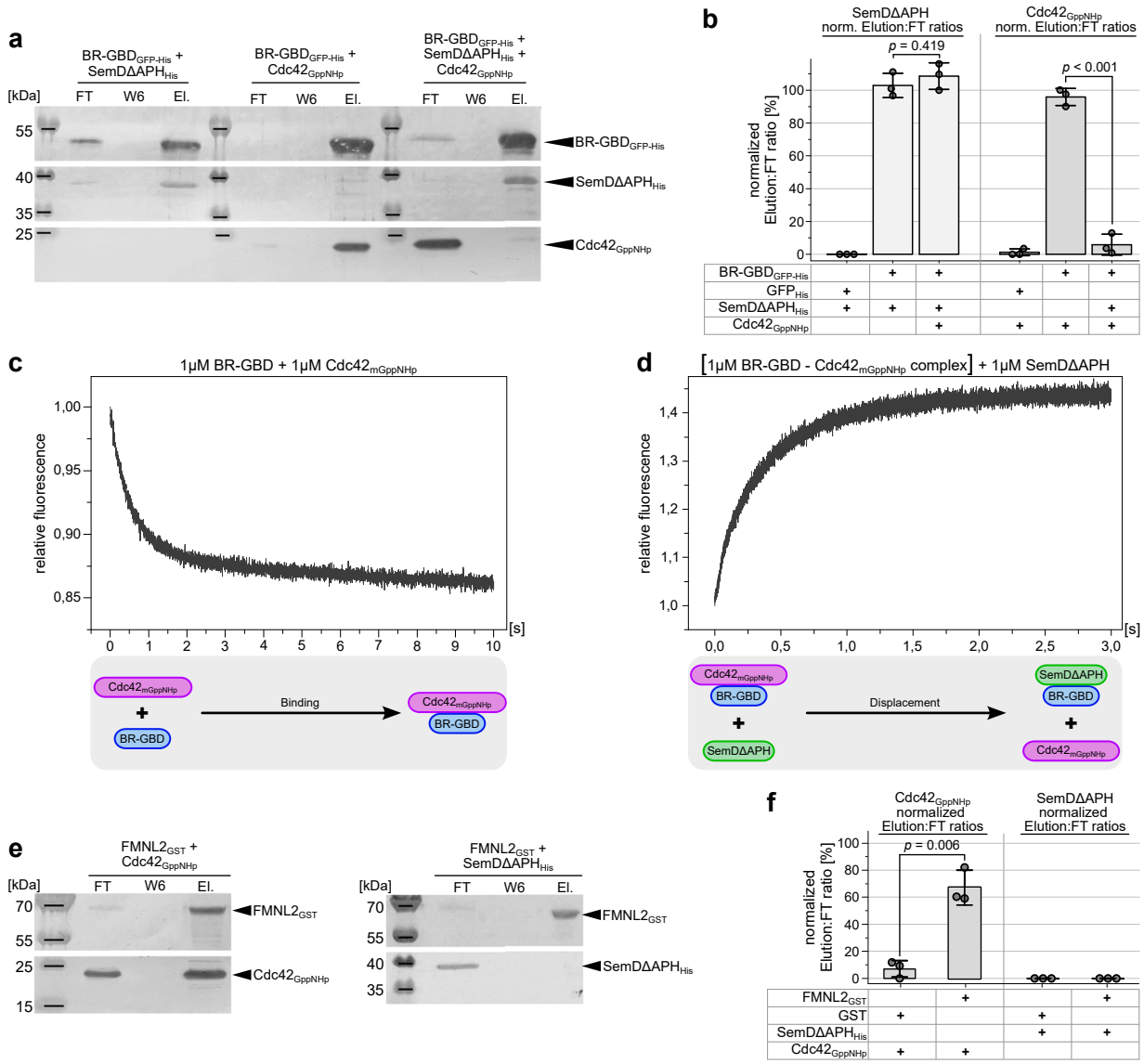

Fig. 4 | Relative to Cdc42$_{GppNHp}$, SemDΔAPH displays enhanced and specific binding to N-WASP. a GFP Trap® Pulldown experiments using equimolar ratios of purified recombinant SemDΔAPH$_{His}$, and active Cdc42 bound to the non-hydrolysable GTP analogue (Cdc42$_{GppNHp}$), were used to test their respective binding to BR-GBD$_{GFP-His}$. Complex formation between BR-GBD$_{GFP-His}$ and SemDΔAPH$_{His}$ or Cdc42$_{GppNHp}$ served as positive controls. Flow through (FT), wash 6 (W6) and elution (El.) fractions were analysed by SDS/PAGE and probed with anti-His (SemDΔAPH$_{His}$ and BR-GBD$_{GFP-His}$) and anti-Cdc42 (Cdc42) antibodies. Pull-down experiments were repeated three times with similar results. Replicates and negative controls are provided in Supplementary Fig. 4a and as Source Data to Fig. 4. **b** Quantification of western blotting in **a** is described in methods. Normalised (norm.) data are displayed as mean ± s.d. ($n = 3$ biologically independent experiments). Unpaired, two-sided Student's t-test was used to compare two groups. **c**, **d** Stopped-Flow experiments used to test the binding of equimolar ratios of BR-GBD$_{His}$ and Cdc42$_{mGppNHp}$ (**c**), as well as the displacement of Cdc42$_{mGppNHp}$ from BR-GBD$_{His}$ by the addition of an equimolar amount of SemDΔAPH$_{His}$ (**d**). The lower panels schematically indicate the relevant interactions. **e** GST-Agarose pulldown experiments used to probe the interactions of Formin L2$_{GST}$ (FMNL2$_{GST}$) with Cdc42$_{GppNHp}$ and SemDΔAPH$_{His}$ with Cdc42$_{GppNHp}$. Complex formation between Cdc42$_{GppNHp}$ and FMNL2$_{GST}$ served as a positive control. Flow through (FT), wash 6 (W6) and elution (El.) fractions were analysed by SDS/PAGE and probed with anti-His (SemDΔAPH$_{His}$), anti-GST (FMNL2$_{GST}$) and anti-Cdc42 (Cdc42) antibodies. Pulldown experiments were repeated three times with similar results. Replicates and negative controls are provided in Supplementary Fig. 4b, c and as Source Data to Fig. 4. **f** Quantification of western blotting in **e** is described in methods. Normalised (norm.) data are displayed as mean ± s.d. ($n = 3$ biologically independent experiments). Unpaired, two-sided Student's t test was used to compare two groups.

The SH3 domain of SNX9 stabilises the PRD1 in SemD

The SemD – N-WASP structure also revealed that the PRD1 and PRD2 domains of SemD, which are required for binding of the SH3 domain of Pacsin 2/3 or SNX9, are located on the flexible N-terminus of SemD, and not in its core region. To ascertain whether the interaction of SemD with SNX9 affects the structure of SemD and whether simultaneous binding of SNX9 and N-WASP to SemD is structurally feasible, we first examined the interaction between SemD and SNX9.

For this purpose, SemD, and a point mutated version ($_{mut}$SemD), in which the 12 proline and arginine residues in the PRD1 and PRD2 motifs were replaced by valine and alanine residues, respectively, were tested for interaction with the SH3 domain of SNX9 (Fig. 5a). Using PS-containing GUVs, that mimic the inner leaflet of the PM, we analysed

https://doi.org/10.1038/s41467-024-51681-3

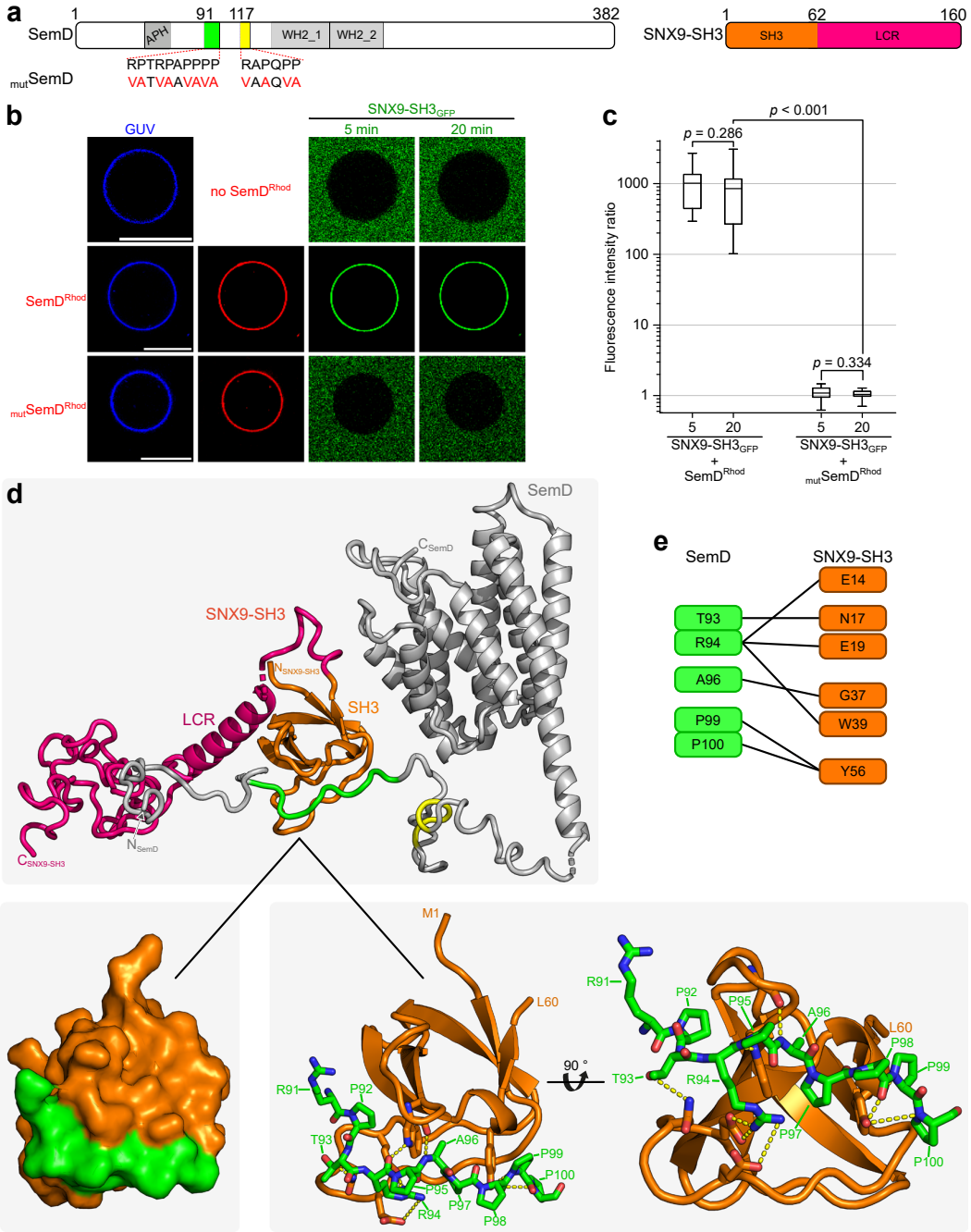

Fig. 5 | SemD binds to SNX9-SH3 PRD1. a (left) Schematic representation of SemD with PRD1 and PRD2 in green and yellow, respectively. Mutations for $SemD_{mut}$ are indicated by the amino acids in red. (right) Schematic representation of SNX9-SH3 with the SH3 in orange and the low complexity region (LCR) in pink. **b** Confocal images of PS-containing GUVs with labelled SemD or $SemD_{mut}$ and $SNX9\text{-}SH3_{GFP}$. (scale bars 10 μm). **c** Quantification of bound protein to the GUV membrane based on the ratio of the maximal fluorescence at the perimeter of the GUV to the average background fluorescence outside the GUV. For each variant and time point, the fluorescence intensity ratio was calculated for up to four independent GUVs. The data are represented as boxplots with whiskers. The boxes are limited by the 25th and 75th percentile, including 50 % of the data. The centre line shows the mean score. Whiskers denote 5–95% of all data and outliers are shown as grey dots. For comparing two groups, an unpaired, two-sided Student's *t* test was used. The data are representative for three independent data sets, all yielding similar results. Source data of all data sets are provided as Source Data file. **d** Cartoon model of SemDΔAPH (grey) with SNX9-SH3 (SH3 in orange) as determined by SAXS using the programme CORAL. SNX9-SH3 (orange) binds to PRD1 (green) of SemDΔAPH. (zoom in) The interactions between the two domains are displayed. **e** Proposed details of the interactions between the two domains, based on the model shown in **d**.

the ability of membrane-bound $SemD^{Rhod}$ and $_{mut}SemD^{Rhod}$ to recruit $SNX9\text{-}SH3_{GFP}$ (Fig. 5b). $SemD^{Rhod}$ immediately bound to PS-GUVs and rapidly recruited $SNX9\text{-}SH3_{GFP}$ (which does not bind to GUVs on its own), thus confirming published data[12] (Fig. 5b, c). Quantification revealed essentially immediate saturation of $SNX9\text{-}SH3_{GFP}$ binding to membrane-bound $SemD^{Rhod}$ with no further increase over the next 20 min. Strikingly, $_{mut}SemD^{Rhod}$ was unable to recruit $SNX9\text{-}SH3_{GFP}$ to GUVs at all (Fig. 5b, c). This complete loss of the ability of $_{mut}SemD^{Rhod}$

to recruit SNX9-SH3$_{GFP}$ clearly indicates that the PRD1 and/or PRD2 domain(s) are responsible for SNX9-SH3 binding. To analyse the effect of binding on the SemD structure, we set out to characterise the interaction on a structural level. Thus, we expressed and purified recombinant SemDΔAPH and SNX9-SH3, allowed for complex formation and purified the resulting complex via SEC (Supplementary Fig. 5). The isolated complex was then analysed by SAXS (Fig. 5d).

SAXS analysis of SNX9-SH3 apo indicated that the protein is found as a monomer in solution with a structured core, and a flexible region indicated via the Kratky plot (Supplementary Fig. 6 and Supplementary Table 2). We initially modelled the SemDΔAPH – SNX9-SH3 complex with AlphaFold2[43] to get information about the binding interface. It is predicted that the SH3 domain of SNX9 interacts with the PRD1 in SemD (Fig. 5d and Supplementary Fig. 7, Supplementary Table 2). The N-terminal part of the SemDΔAPH AlphaFold2 prediction showed very low values of the predicted local distance difference test (pLDDT <30), in line with our conclusion of the flexibility. The only exceptions are the amino acids responsible for the interaction with the SH3 domain from SNX9-SH3 (pLDDT values ~ 80). The SNX9-SH3 prediction showed only for the N-terminal part including the SH3 domain high pLDDT values (between 60–80) and the remaining C-terminal part remains unclear (pLDDT values < 30, Supplementary Fig. 7b). To prove the resulting AlphaFold2 complex model, we calculated the theoretical scattering pattern of this model and compared it with the experimental scattering data of the SemDΔAPH – SNX9-SH3 complex in solution. The resulting CRYSOL fit offered a χ^2 value of 8.49 and showed a high mismatch in the low s region (Supplementary Fig. 7c). This indicates that even the modelled complex contains all residues, and that the orientation of the domains/tails are not in line with the in-solution behaviour. The SAXS analysis of the SemDΔAPH – SNX9-SH3 complex confirmed a stoichiometry of 1:1, based on the molecular weight (Supplementary Table 2). We used the SemDΔAPH crystal structure and the binding interface of SH3 with PRD1 in SemD predicted by the AlphaFold2 model as a starting point for our modelling. The remaining flexible extensions were then remodelled with CORAL to better describe the in-solution behaviour of the SemDΔAPH – SNX9-SH3 complex (Supplementary Table 2). The resulting best-fit model of the remodelled SemDΔAPH – SNX9-SH3 complex is shown in Fig. 5d (an overlay of independent CORAL models is shown in Supplementary Fig. 7h). Based on our modelling, six residues of the SH3 domain bind to five specific residues of SemD PRD1 (Fig. 5d, e). Thus, PRD2 is not involved in direct contact with the SH3 of SNX9, in agreement with previous results obtained by Spona et al.[12], in which pulldown of SemD lacking the PRD1 showed no binding to SNX9.

Furthermore, structural analysis of the modelled complex showed that SH3 binding to PRD1 does not disrupt the conformation of the SemD core region, and therefore does not affect its ability to bind N-WASP. Indeed, the binding sites for host proteins on SemD are separated by flexible linkers, which minimise steric hindrance and allow the individual domains to be separately targeted in the 3D space.

SemD binds simultaneously to several host partners

Our findings thus far indicate that SemD contains spatially separated binding sites that are connected by highly flexible linker regions, which sterically allow simultaneous interactions with the PM, N-WASP and SNX9. To assess the potential concurrent binding of these interaction partners, we mixed and incubated recombinantly expressed SemDΔAPH, SNX9-SH3 and BR-GBD, and analysed the composition of the complex in the sample using SEC. Indeed, the resulting chromatogram showed one main peak, eluting at 9.9 ml, that contained all three proteins, as evidenced by SDS/PAGE analysis (Fig. 6a).

To set these findings in context with membrane-bound SemD, we used our GUV model system to ascertain whether such a complex is formed under these conditions. After allowing SemD^{Rhod} to bind to PS-containing GUVs, we added a three-fold molar excess (relative to SemD) of either DyLight 650 labelled SNX9-SH3 (SNX9-SH3$^{DyLight\ 650}$) or BR-GBD$_{GFP}$, to fully saturate SemD^{Rhod}, which forms a 1:1 complex with SNX9-SH3 and with BR-GBD, respectively. We then added the second binding partner in an equimolar ratio to SemD^{Rhod}. As expected, even after the initial saturation of SemD^{Rhod} with one of the binding partners, the second partner was immediately recruited by SemD^{Rhod} (Fig. 6b). This effect does not depend on either the sequence of addition or the quantity of the introduced binding partner, indicating that a stable complex with both partners can be consistently assembled on the target membrane.

By combining our X-ray crystallographic and SAXS data for SemDΔAPH – BR-GBD and SemDΔAPH – SNX9-SH3, we were able to develop a potential 3D model for the complex that includes all three interaction partners (Fig. 6c), which confirmed that simultaneous interactions with SNX9-SH3 and BR-GBD are sterically possible. However, the exact arrangement of the individual binding sites remains elusive owing to the flexibility of the linker regions connecting the individual binding sites in SemD. Hence, our data indicate that PM-bound SemD can simultaneously recruit the host endocytic proteins SNX9 and N-WASP using spatially separated binding domains.

Discussion

As an obligate intracellular pathogen, *Chlamydia pneumoniae* interacts with host-cell proteins that ensure its survival and propagation. Perhaps the most critical stage in its replication cycle is its entry into a host cell.

For internalisation, the infectious EB (diameter 300-400 nm) requires co-option of the host's endocytic machinery to form a membrane-enclosed vesicle that is some 60 times larger in volume and 16 times larger in surface area than a classical endocytic vesicle (diameter 100 nm)[10]. This requires extensive remodelling of the PM and diversion of the host's actin cytoskeleton to enable growth, maturation and closure of the vesicle. Effector proteins translocated into the host cell play a vital role in these processes. The early secreted *Cpn* effector protein SemD binds to the inner leaflet of the PM below the invading EB and directly recruits G-actin and the essential endocytic proteins SNX9 and N-WASP[12].

Our structural study reveals that SemD interacts with host proteins via binding domains that are connected by intrinsically disordered linker sequences. This highly flexible arrangement facilitates simultaneous binding of several host endocytic proteins and modulation of the host's PM (Fig. 7). The precise contribution of these complexes to infection in vivo remains to be established, further complicated by the absence of a method for generating genetically manipulated *Cpn* strains.

We have shown in this study that SemD uses its C-terminal rigid core to bind and activate the actin nucleation- and branching-promoting factor N-WASP by structurally and functionally mimicking the normal role of the endogenous N-WASP activator Cdc42$_{GTP}$. Our structural and biochemical data further reveal that SemD provides the negatively charged patch and the binding groove required for selective binding of the positively charged C-terminal part of the BR and the CRIB domains of N-WASP, respectively, thus mimicking Cdc42$_{GTP}$-mediated N-WASP activation (Figs. 3a and 7). These interactions release the VCA domain of the autoinhibited N-WASP, which stimulates the Arp2/3 complex, thus promoting actin nucleation and branching. Intriguingly, the $K_{193}R_{194}K_{197}$ (KRK) motif in the C-terminal part of the BR region is responsible for both of these contacts with SemD (Fig. 2) and for binding to Cdc42$_{GTP}$, since a 9 aa deletion within the BR, that leaves the KRK motif intact, does not affect binding of the N-WASP mutant to Cdc42$_{GTP}$[25]. Mimicking of the endogenous Cdc42$_{GTP}$ protein, which is involved in many different cellular processes, requires specific activation of N-WASP by SemD. Based on our structural analysis, this occurs via the interaction of the KRK motif within the C-terminal BR region of N-WASP with a negatively charged patch on

https://doi.org/10.1038/s41467-024-51681-3

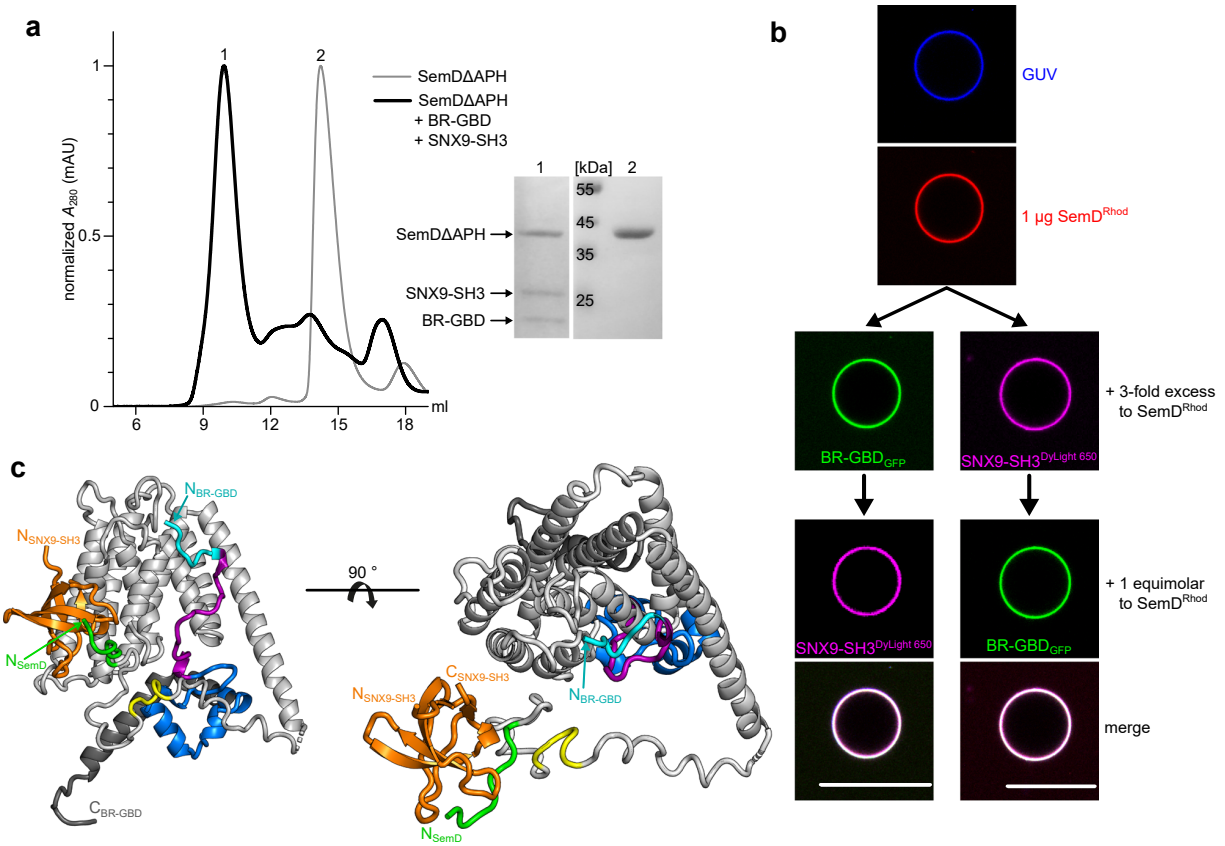

Fig. 6 | SemD simultaneously interacts with various binding partners. a SEC chromatograms of the complex composed of SemDΔAPH, BR-GBD and SNX9-SH3 (black), or SemDΔAPH alone (grey). The absorbance at 280 nm was normalised for the maximal absolute absorbance of the individual sample. The chromatogram of the complex revealed a major peak eluting at 9.9 ml (peak 1), while SemDΔAPH alone elutes at 14.2 ml (peak 2). The protein compositions of peaks 1 and 2 were analysed on an SDS gel (right) after staining with Coomassie brilliant blue. Lanes 1 and 2 were loaded with samples of the indicated peaks ($n = 1$). **b** Confocal images of PS-containing GUVs incubated with SemD^{Rhod}. A three-fold excess of either BR-GBD$_{GFP}$ ($n = 4$) or labelled SNX9-SH3 (SNX9-SH3$^{DyLight\ 650}$) ($n = 6$) was added, before the third binding partner was added in an equimolar ratio to SemD (scale bars 10 µm). **c** The structures of SNX9-SH3 and BR-GBD obtained by SAXS overlaid on SemDΔAPH. The nine core helices of SemDΔAPH are depicted in grey and the PRD1 and PRD2 in green and yellow, respectively. BR-GBD is depicted in cyan, magenta and blue, in accordance with the colour scheme in Fig. 2, and the depiction of the SNX9-SH3 domain in orange follows the colour scheme used in Fig. 5. Note that the three-dimensional orientation of the bound SH3 domain towards the nine-helix core might be different, owing to the presence of the flexible linker in between the two. Right panel: 90° rotation.

SemD, which is much larger than that found on Cdc42 (Fig. 3a) and involves negatively charged amino acids on four different helices (α1, α2, α5 and α9) of the SemD's rigid core (Fig. 2c). Indeed, membrane-bound SemD recruits the BR-GBD segment more than 18-fold more efficiently than the BR-GBDΔ mutant, which lacks residues 181 to 197 including the KRK motif (Fig. 3). Comparison of the rigid core structure of SemD alone and when bound to the BR-GBD fragment reveals almost identical conformations, suggesting that SemD serves as a stable platform for BR-GBD, thus maximising the chances for fast recruitment via electrostatic interactions. Our pulldown and stopped-flow experiments indicate that SemD binds N-WASP much more tightly than active Cdc42$_{GTP}$ does, and indeed SemD can displace Cdc42$_{GTP}$ from the Cdc42$_{GTP}$ – N-WASP complex (Fig. 4a–d). Thus, during a *Cpn* infection, SemD is secreted via the T3SS by the adhering EB, interacts with the cytosolic leaflet of the PM and recruits and activates cytosolic, autoinhibited N-WASP, but might also dislodge N-WASP from Cdc42$_{GTP}$ – N-WASP complexes. The strong binding of SemD to N-WASP probably accounts for the efficiency with which the locally PM-bound SemD recruits N-WASP to establish the branched F-actin mesh required for EB internalisation. Moreover, *Cpn* has maximised this actin-branching process by evolving a SemD protein, which according to our data does not bind to FMNL2, which is also activated by Cdc42$_{GTP}$ (Fig. 4e–f) and nucleates and elongates unbranched actin filaments at the barbed end[41]. Comparison of Cdc42$_{GTP}$ – N-WASP and SemD – N-WASP (Fig. 3a) with the Cdc42$_{GTP}$ – FMNL2 structure[44] reveals remarkable differences. N-WASP strongly interacts via its positively charged residues in the BR and the CRIB with the negatively charged patch on the front of Cdc42$_{GTP}$ and SemD, respectively. Conversely, FMNL2 interacts with Cdc42$_{GTP}$ via multiple hydrophobic and polar contacts formed between all five armadillo repeats of FMNL2 and the two switch regions of Cdc42. These differences probably account for the inability of SemD to bind FMNL2[44].

Thus, SemD is not only a very efficient activator of N-WASP, but is likely to be restricted in its activity to that protein. This would ensure that the limited numbers of SemD molecules secreted by the invading *Cpn* are fully available for this process. For actin nucleation and elongation of unbranched actin filaments *Cpn* secretes within the first 15 min of infection the soluble effector protein CPn0572, which belongs to the TarP protein family[45].

The SemD-mediated local reorganisation of the actin network is probably transient and short-lived, until bacterial entry has succeeded. In *Salmonella*, following host-cell entry, the architecture of the cytoskeleton is restored by, for example, the bacterial GTPase-activating protein SptP, which reverses the activation of Rac1

https://doi.org/10.1038/s41467-024-51681-3

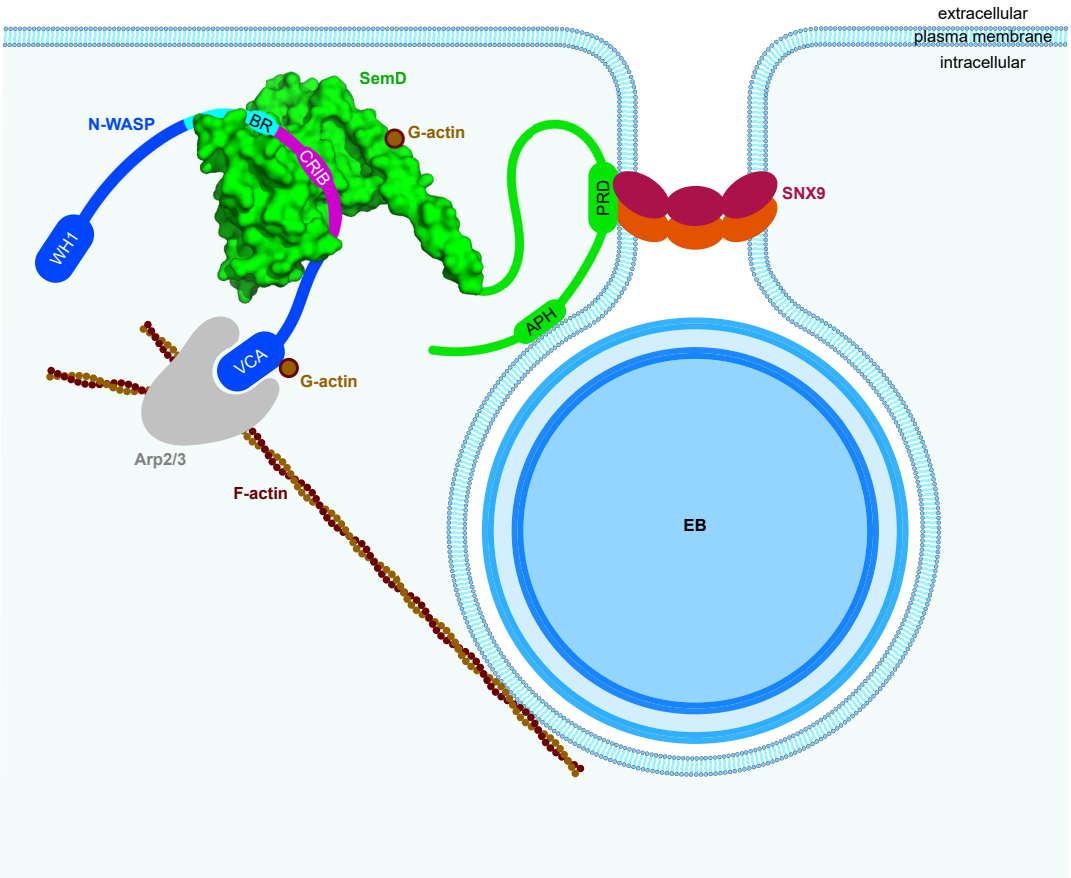

Fig. 7 | A chlamydial effector exploits structural and functional mimicry to manipulate the host endocytic machinery. The *Cpn* elementary body (EB) secrets SemD into the host cell, which binds to the inner leaflet of the plasma membrane. There, SemD recruits, binds and activates N-WASP by structurally and functionally mimicking the $Cdc42_{GTP}$ activation mechanism. SemD interacts with the C-terminal, positively charged amino acids of the N-WASP BR domain and further, the CRIB domain binds into the SemD binding groove. This then leads to the release of N-WASP from its auto-inhibited state. SemD also binds to the SNX9-SH3 domain, which brings the SNX9-BAR domain closer to the membrane. This in turn induces membrane deformation and eventually leads to closure of the matured endocytic vesicle. Due to the arrangement of the individual binding domains, which are connected by flexible linker regions, the binding sites can be freely oriented in 3D space, thus minimising steric hindrance. This can explain why SemD is postulated to be capable of binding simultaneously to the PM, SNX9 and N-WASP in vivo and hijacking their functions to promote the growth and maturation of the endocytic vesicle.

and Cdc42[46]. It will be interesting to ascertain how this is achieved by *Chlamydiae*.

The SemD-mediated activation of N-WASP differs fundamentally from that triggered by other pathogens, which evolved effector proteins mimicking modulators of Cdc42 activity, such as GAPs, GEFs and GDIs, or utilise covalent modification of the Rho GTPase (see introduction). The SemD activity is also completely different from the function of the effector $EspF_U$ secreted by enterohaemorrhagic *Escherichia coli* (EHEC). NMR data have revealed that $EspF_U$ binds the GBD domain via a C-like motif (similar to that found within the VCA domain) that releases the endogenous VCA domain in autoinhibited N-WASP[35,47]. Interestingly, initial data suggest that the *Ctr* effector TmeA might activate N-WASP like $EspF_U$ does which would imply that *Cpn* has evolved a completely different mechanism for F-actin polymerisation and branching, possibly as an adaptation to the different target tissues involved (*Cpn*: lung epithelia; *Ctr*: eye + urogenital tract epithelia)[48,49].

SemD also binds the BAR-containing protein SNX9, which is required for membrane deformation and recruitment of dynamin, and eventually leads to the scission of the matured vesicle[50]. Our model analysis suggests that, in the flexible N-terminal half of SemD, which is separated by a linker sequence from the rigid core that mediates N-WASP interaction, five residues in the PRD1 domain interact with six residues in the β-sheet structure of the SNX9-SH3 domain (Figs. 5 and 7). This binding mechanism is typical for proline-rich peptides that interact with SH3 domains, as has been shown for several other interaction partners (PDB: 1QWE, 2JMA, 2DRK, 2KXC). The predicted PRD2 domain is not involved in SH3 binding, as previously suggested by Spona et al.[12]. Thus, the amino acid sequences N- and C-terminal to PRD1 remain unstructured and may act as linkers that separate the PRD1 – SNX9-SH3 complex from the N-terminal membrane-binding domain APH and the C-terminal SemD core domain, which is involved in N-WASP binding (Figs. 6 and 7). Our structural model, based on the individual conformations of each protein pair (SemD + SNX9-SH3; SemD + $N\text{-}WASP_{BR\text{-}GBD}$), reveals that all protein interactions can occur simultaneously (Fig. 6c), and we have verified this by biochemical and membrane binding experiments that confirm concurrent recruitment of SNX9-SH3 and BR-GBD to GUV-bound SemD (Fig. 6b).

Helices α1 and α2 of SemD's rigid core carry the two predicted WH2 sequences essential for G-actin binding[12]. However, the stoichiometry of this interaction is not clear. Our SemD structure implies that WH2_1 on α-helix 1 is largely available for interaction with G-actin, while WH2_2 on α-helix 2 is not fully accessible (Fig. 1b, c), suggesting that WH2_1 might constitute the G-actin binding domain. Recruitment of G-actin by SemD increases the local G-actin concentration, which should promote formation of F-actin branches via the N-WASP-Arp2/3 pathway.

During evolution, *Cpn* has undergone a dramatic reduction in genome size to about 1 million bp in total. Consequently, many proteins must perform more than one task and our structural analysis reveals that this holds for SemD, an effector protein that is involved in the reshaping of membrane structure and actin cytoskeletal organisation during chlamydial endocytosis. Our data support a model in which a single PM-bound chlamydial effector protein, SemD, can simultaneously interact with several host proteins by separating the SemD binding domains with unstructured linker regions. Hence, the ability of SemD to mimic $Cdc42_{GTP}$ permits recruitment, binding and activation of the endocytic host protein N-WASP.

Methods

Antibodies and reagents

All lipids used in this study were obtained from Avanti Lipids and NHS-Rhodamine and DyLight650-NHS were sourced from Thermo Scientific. The primary antibody anti-penta-His (#34660, 1:2500) was purchased from Qiagen, anti-Cdc42 (#610929, 1:1000) was obtained from BD Transduction Laboratories and anti-GST (sc-374171, 1:500) was obtained from Santa Cruz Biotechnology. The secondary anti-mouse antibody coupled to alkaline phosphatase (#A3562, 1:30000) was purchased from Sigma-Aldrich.

Cloning, protein expression and purification

Cloning steps were carried out by in vivo homologous recombination in *Saccharomyces cerevisiae*. *semD* constructs used in this study were amplified from synthetic *semD* DNA purchased from GenScript, which was codon optimised for *Escherichia coli (E. coli)* expression. The *SNX9-SH3* sequence was amplified from a sequence encoding mCherry-SNX9[13], the *BR-GBD* fragments were amplified from a sequence encoding GFP-N-WASP (Addgene, #47406, *Rattus norvegicus*; The N-WASP BR-GBD protein fragment from *R. norvegicus* and *human* differ by 3 amino acids located N-terminal to the BR domain outside of our co-crystal structure). The fragments were integrated either into pSL4 (generating C-terminal 10xHis fusions) or into pDS94 (generating C-terminal GFP-10xHis fusions) (Plasmid list in Supplementary Table 4). The plasmid encoding FMNL2 (S171DD) fused to GST has been published previously[44]. Expression of the His-tagged proteins was carried out in *E. coli* BL21 (DE3, Invitrogen), and expression of GST-tagged FMNL2 was carried out in *E. coli* Rosetta. His-tagged proteins were purified using Ni-NTA Agarose (Cube Biotech) and dialysed in phosphate-buffered saline (PBS) (10 mM Na_2HPO_4, 1.8 mM KH_2PO_4, 137 mM NaCl, 2.7 mM KCl, pH 8.5), apart from SemDΔAPH for which a pH of 6.0 was used. GST-tagged FMNL2 was purified using Glutathione Agarose (Thermo Scientific) and dialysed in buffer containing 10 mM Tris-HCl, 150 mM NaCl, pH 8.5.

The preparation of Cdc42 in complex with guanosine 5′-(βγ-imino)-triphosphate (GppNHp) and N-methyl-anthraniloyl-labelled GppNHp (mGppNHp) was carried out as described by Eberth and Ahmadian[51]. In brief, human *CDC42* was integrated into pGEX-4T-1 (generating a GST-fusion)[23] and expressed in *E. coli* Rosetta. GDP-bound GST-Cdc42 was purified using a Glutathione sepharose column (Pharmacia, Uppsala, Sweden) and the GST-tags were cleaved with thrombin at 4 °C overnight. Proteins were reapplied to Glutathione Sepharose and cleaved Cdc42 was collected in the flow through. Protein quality and concentration were assessed by SDS-PAGE and high-performance liquid chromatography (HPLC), utilising a Beckman Gold HPLC system with a reversed-phase C18 column. GDP-bound Cdc42 proteins were incubated with a 1.5-fold excess of GppNHp/mGppNHp, non-hydrolysable GTP analogues, and agarose bead-coupled alkaline phosphatase (0.1–1 U per mg of Cdc42) to degrade GDP to GMP and Pi, thus facilitating the replacement of GDP with GppNHp/mGppNHp. The course of the reaction was monitored via HPLC using a buffer containing 100 mM potassium phosphate (pH 6.5), 10 mM tetrabutylammonium bromide, and 7.5–25% acetonitrile. Upon complete degradation of GDP, the samples were applied to prepacked NAP-5 columns to exchange the buffer for a fresh one devoid of free nucleotides. The concentration of nucleotide-bound Cdc42 was checked using the Bradford assay and HPLC to calculate the amount of active GppNHp-bound Cdc42. The proteins were then snap-frozen and stored at −80 °C for downstream analysis. Preparatory steps of $Cdc42_{GppNHp}$ are provided in Source Data.

Size exclusion chromatography

SEC was performed on an ÄKTA™ pure 25 L (Cytiva). For purified proteins, a pre-equilibrated HiLoad 16/600 Superdex 200 pg column was used with a flow-rate of 0.8 ml/min, for pre-formed complexes, a pre-equilibrated Superdex 200 increase 10/300 GL column (Cytiva) was used with a flow rate of 0.5 ml/min. All runs were performed at 4 °C.

Pulldown assays

Recombinant BR-GBD fused to GFP, or GFP alone, was mixed with an equimolar ratio of the test protein(s) and incubated for 5 min at RT. GFP Trap® agarose, preincubated in 3 % BSA, was added to the mixture, and binding was allowed to proceed for 30 min at 4 °C. After collection of the flow through, agarose was washed 6x with wash buffer (10 mM Tris-HCl, 200 mM NaCl, pH 8.5) and bound proteins were eluted by boiling the agarose in SDS sample buffer.

Recombinant FMNL2 fused to GST, or GST alone, was mixed with an equimolar ratio of the test protein(s) and incubated for 5 min at RT. Glutathione agarose was added to the mixture and binding was allowed for 30 min at 4 °C. After collecting the flow through, agarose was washed 6x with wash buffer (50 mM Tris-HCl, 150 mM NaCl, pH 8.5) and bound proteins were eluted by boiling the agarose in SDS sample buffer.

Individual steps were monitored by SDS/PAGE and immunoblot analysis, using specific primary and secondary antibodies.

Western blot quantification

Band intensities of the Flow Through (FT) and elution (El.) fractions were determined using the software GelAnalyzer 23.1.1. Bands were semi-automatically defined. The Elution:FT ratio [%] was calculated by dividing the intensity of the eluate by the total intensity, i.e. FT plus eluate. The ratio was normalised to the Elution:FT ratio [%] of the bait protein used. Individual band intensities and uncropped western blots are displayed in Source Data.

$$\text{Elution : FT ratio}[\%] = \frac{\text{Elution}}{\text{Elution} + \text{FT}} \tag{1}$$

$$\text{normalized elution : FT ratio}[\%] = \text{Elution : FT ratio} * \frac{1}{(\text{Elution : FT ratio})_{\text{bait}}} \tag{2}$$

Fluorescence stopped-flow spectrometry

Rapid fluorescence measurements were performed using a Hi-Tech Scientific stopped-flow spectrophotometer (Applied Photophysics SX20), as described by Hemsath et al.[23]. An excitation wavelength of 360 nm was used for N-methylanthraniloyl (m) derivatives of guanosine nucleotides in the stopped-flow analysis. Fluorescence detection was facilitated by a photomultiplier equipped with a cut-off filter to detect wavelengths above 408 nm. The association of N-WASP BR-GBD with mGppNHp-bound Cdc42 was measured using a buffer containing 30 mM Tris-HCl, 10 mM K_2HPO_4/KH_2PO_4 (pH 8.5), 5 mM $MgCl_2$ and 3 mM DTT at 25 °C. The experiment setup involved equimolar ratios of the proteins. The contents of one syringe containing 1 μM of mGppNHp-bound Cdc42 and a second syringe containing 1 μM N-WASP BR-GBD were rapidly mixed, and the change of relative

fluorescence was monitored in real-time. In a subsequent experiment, competition between SemDΔAPH and mGppNHp-bound Cdc42 was evaluated by rapidly mixing 1 μM of the pre-prepared complex of mGppNHp-bound Cdc42 and N-WASP BR-GBD with 1 μM of SemDΔAPH. The change in relative fluorescence was monitored in real-time.

Preparation of giant unilamellar vesicles

GUVs were prepared as described previously[52]. Briefly, PS-containing GUVs were prepared by mixing 9.75 mol% DOPC, 25 mol% cholesterol, 0.25 mol% Marina Blue™ DHPE and 25 mol% DOPS. Lipid mixtures were prepared and added to a chamber built of ITO-coated slides (Präzisions Glas & Optik) which were glued together with Vitrex (Vitrex Medical). The resulting cavity was filled with 10 % sucrose solution and sealed with Vitrex. The slides were connected via clamps to a frequency generator and an alternating voltage of 2.0 Vp-p was applied at a frequency of 11 Hz. The GUVs were grown in the dark at room temperature for 2–3 h.

Protein binding studies on giant unilamellar vesicles

For microscopic analyses, Angiogenesis μ-slides (Ibidi) were coated for 5–10 min at RT with 2 mg/ml β-casein (Merck) and washed three times with PBS. Then NHS-rhodamine-labelled recombinant SemD (1 μg) was mixed with 15 μl PBS and recombinant binding partner fused to GFP (1 μg) was added, together with 5 μl GUVs. For binding studies with three proteins, NHS-rhodamine-labelled recombinant SemD (1 μg) was mixed with recombinant BR-GBD fused to GFP (1-3 μg) and NHS-650–labelled recombinant SNX9-SH3 (1-3 μg) and 5 μl GUVs were added. The GUVs were allowed to settle down for 5 min at room temperature and then imaged for further 15 min at room temperature.

Microscopy

General imaging was performed using an inverse Nikon TiE Live Cell Confocal C2plus equipped with a 100x TIRF objective and a C2 SH C2 Scanner. All images were generated with Nikon NIS Elements software and quantified using ImageJ.

Fluorescence intensity ratio analysis

Acquired confocal GUV data were semi-automatically analysed using a self-written *fiji* macro to estimate signal accumulation at the perimeter of the GUV in relation to the surrounding medium. Multiple line selections were orthogonally placed at the GUV membrane, with the membrane placed in the middle. First, the macro plots a line-intensity profile for each selection with a given predefined linewidth (here: 5) in order to extract intensity data for the relevant signal channel and to store it in an array. The intensity of the signal surrounding the GUV is calculated as the mean intensity (I_{out}) of a predefined width (here: 1/5 of total profile length) at the front end of the line profile. Second, signal intensity peaks of the profile are identified by applying the built-in "array.findMaxima"-function with a given tolerance (here: 450), that returns peaks by default in descending significance order. The peak positions are checked, if they are located within a predefined width around the centre of the line profile (here: same as background width) and the intensity of the first, most significant peak (I_{peak}) within the limits, it is used for the following ratio calculation. Finally, the intensity ratio (r_{int}) is calculated as the quotient of signal intensity at the peak position (I_{peak}) divided by the mean signal intensity in the surrounding medium (I_{out}).

$$R_{int} = \frac{I_{peak}}{I_{out}} \quad (3)$$

Statistical analysis and data representation

Graphs were prepared using OriginPro v.2021b (OriginLab). For the comparison of two groups, an unpaired, two-sided Student's *t*-test was used. A *p*-value of less than 0.01 was considered as statistically significant. Images were prepared using the open-source software Inkscape (www.inkscape.org).

Structure determination via crystallisation

SemDΔAPH, either alone or in a complex with BR-GBD, was crystallised by sitting-drop vapour-diffusion in PBS at pH 6 (SemDΔAPH) or pH 8.5 (SemDΔAPH + BR-GBD) at 12 °C and at concentrations of 24 and 10 mg/ml, respectively. 0.1 μl were mixed with 0.1 μl of reservoir solution consisting of 0.1 M Citric acid (pH 2.5), 20% (w/v) PEG 6000 (pH 4) for SemDΔAPH and 0.1 M ammonium formate, 0.1 M MES (pH 6.2), 25% v/v PEG 400 for SemDΔAPH + BR-GBD. Crystals formed after 12-24 h (SemDΔAPH) or 5 d (SemDΔAPH + BR-GBD) were harvested and cryoprotected with mineral oil followed by flash-freezing in liquid nitrogen. Diffraction data were collected at −173 °C (100 K) at beamline P13 (DESY, Hamburg, Germany) using a 0.9763 Å wavelength for SemDΔAPH or at beamline ID30A-3 (ESRF, Grenoble, France) using a 0.9677 Å wavelength for SemDΔAPH + BR-GBD. Data reduction was performed using XDS[53] and Aimless[54] from the CCP4 Suite[55]. The structure was solved via molecular replacement with Phaser[56] using an AlphaFold[57] model (SemDΔAPH) or the apo structure (SemDΔAPH + BR-GBD) as search model. The initial model was refined alternating cycles of manual model building in COOT[58,59] and automatic refinement using Phenix[60] v.1.19.2. Data collection and refinement statistics are reported in Supplementary Table 1. In the SemDΔAPH + BR-GBD structure one amino acid, Glu207, was found not to obey the Ramachandran rule, and is positioned in the disallowed region. This residue is involved in a crystal contact.

SAXS measurement

SEC-SAXS data were collected on the P12 beamline (PETRA III, DESY Hamburg[61]). The sample-to-detector distance of the P12 beamline was 3.00 m, resulting in an achievable q-range of 0.03-0.07 nm-1. The measurements were performed at 20 °C with a protein concentration of 8 mg/ml for SemDΔAPH, 10 mg/ml for BR-GBD, 8 mg/ml for SemDΔAPH + BR-GBD and 3.3 mg/l for SemDΔAPH + SNX9-SH3. The SEC-SAXS runs were performed on a Superdex200 increase 10/300 GL column (100 μl injection volume, buffer: PBS pH 8.5 + 3 % glycerol) with a flow rate of 0.6 ml/min. 2400 frames were collected for each protein sample with an exposure time of 0.995 sec/frame. Data were collected on relative scale or absolute intensity against water.

All programmes used for data processing were part of the ATSAS Software package (Version 3.0.5)[62]. Primary data reduction was performed with the programmes CHROMIXS[63] and PRIMUS[64]. With the Guinier approximation[65], the forward scattering *I(0)* and the radius of gyration (R_g) were determined. The programme GNOM[66] was used to estimate the maximum particle dimension (D_{max}) with the pair-distribution function *p(r)*. The rigid body results from the crystal structure were used as a starting template to complete the structures of SemDΔAPH and BR-GBD (flexible N- and C-terminal parts were remodelled) with the programme CORAL[67]. The flexibility ensemble analysis of the SemDΔAPH + BR-GBD complex was done with EOM[68,69], based on the solved crystal structure and completed with the missing amino acids. The SemDΔAPH + SNX9-SH3 complex docking was done with CORAL[67], based on the solved SemDΔAPH structure and an AlphaFold2[43,57] prediction of the interaction site from the SH3 domain with the flexible SemDΔAPH tail.

Reporting summary

Further information on research design is available in the Nature Portfolio Reporting Summary linked to this article.

Data availability

We uploaded the SAXS data to the Small-Angle X-ray Scattering Biological Data Bank (SASBDB)[70], with the following accession codes: SASDTQ5 (SemDΔAPH), SASDTR5 (BR-GBD), SASDTS5 (SNX9-SH3),

SASDTT5 (SemDΔAPH + SNX9-SH3) and SASDTU5 (SemDΔAPH + BR-GBD). The crystal structures were deposited in the Protein Data Bank (PDB) with the accession codes 8S5R (SemDΔAPH) and 8S5T (SemDΔAPH+ BR-GBD). Further, the cited structures in this paper can be found with the following accession codes: 1QWE (C-SRC SH3 + APP12). 2JMA (R21A Spc-SH3:P41 complex). 2DRK (SH3 + Acan125). 2KXC (IRTKS-SH3 + ExpFu-R47). 1CEE (Cdc42 + WASP). The authors declare that the data supporting the findings of this study are available within the paper and its extended data files. Data underlying Figs. 3d, 4a, b, e, f, 5c and 6a and Supp. Figs. 2a, 4a, b, c, d and 5a are provided as Source Data files. All other data are available from the corresponding author upon request. Source data are provided with this paper.

Code availability

A custom code for Fiji 1.54 f used for the analysis of GUVs is available on https://github.com/SHaensch/2023_GUVQuant or https://doi.org/10.5281/zenodo.13165623.

References

1. Kuo, C. C. et al. Chlamydia pneumoniae (TWAR) in coronary arteries of young adults (15-34 years old). *Proc. Natl Acad. Sci. USA* **92**, 6911–6914 (1995).
2. Hahn, D. L. Chlamydia pneumoniae and chronic asthma: updated systematic review and meta-analysis of population attributable risk. *PLoS ONE* **16**, e0250034 (2021).
3. Balin, B. J. et al. Chlamydia pneumoniae: an etiologic agent for late-onset dementia. *Front. Aging Neurosci.* **10**, 302 (2018).
4. Beagley, K. W., Huston, W. M., Hansbro, P. M. & Timms, P. Chlamydial infection of immune cells: altered function and implications for disease. *Crit. Rev. Immunol.* **29**, 275–305 (2009).
5. Gerard, H. C. et al. Chlamydophila (Chlamydia) pneumoniae in the Alzheimer's brain. *FEMS Immunol. Med. Microbiol.* **48**, 355–366 (2006).
6. Porritt, R. A. & Crother, T. R. Chlamydia pneumoniae infection and inflammatory diseases. *Immunopathol. Dis. Ther.* **7**, 237–254 (2016).
7. Moelleken, K. & Hegemann, J. H. The Chlamydia outer membrane protein OmcB is required for adhesion and exhibits biovar-specific differences in glycosaminoglycan binding. *Mol. Microbiol.* **67**, 403–419 (2008).
8. Mölleken, K., Becker, E. & Hegemann, J. H. The Chlamydia pneumoniae invasin protein Pmp21 recruits the EGF receptor for host cell entry. *PLoS Pathog.* **9**, e1003325 (2013).
9. Galle, J. N., Fechtner, T., Eierhoff, T., Römer, W. & Hegemann, J. H. A Chlamydia pneumoniae adhesin induces phosphatidylserine exposure on host cells. *Nat. Commun.* **10**, 4644 (2019).
10. Rennick, J. J., Johnston, A. P. R. & Parton, R. G. Key principles and methods for studying the endocytosis of biological and nanoparticle therapeutics. *Nat. Nanotechnol.* **16**, 266–276 (2021).
11. Braun, C. et al. CPn0572, the C. pneumoniae ortholog of TarP, reorganizes the actin cytoskeleton via a newly identified F-actin binding domain and recruitment of vinculin. *PLoS ONE* **14**, e0210403 (2018).
12. Spona, D., Hanisch, P. T., Hegemann, J. H. & Mölleken, K. A single chlamydial protein reshapes the plasma membrane and serves as recruiting platform for central endocytic effector proteins. *Commun. Biol.* **6**, 520 (2023).
13. Hänsch, S. et al. Chlamydia-induced curvature of the host-cell plasma membrane is required for infection. *Proc. Natl Acad. Sci. USA* **117**, 2634–2644 (2020).
14. Cossart, P. & Sansonetti, P. J. Bacterial invasion: the paradigms of enteroinvasive pathogens. *Science* **304**, 242–248 (2004).
15. Cossart, P. & Helenius, A. Endocytosis of viruses and bacteria. *Cold Spring Harb Perspect Biol* **6**, a016972 (2014).
16. Colonne, P. M., Winchell, C. G. & Voth, D. E. Hijacking host cell highways: manipulation of the host actin cytoskeleton by obligate intracellular bacterial pathogens. *Front. Cell Infect. Microbiol.* **6**, 107 (2016).
17. Simunovic, M., Voth, G. A., Callan-Jones, A. & Bassereau, P. When physics takes over: BAR proteins and membrane curvature. *Trends Cell Biol.* **25**, 780–792 (2015).
18. Lundmark, R. & Carlsson, S. R. SNX9 - a prelude to vesicle release. *J. Cell Sci.* **122**, 5–11 (2009).
19. Lundmark, R. & Carlsson, S. R. Regulated membrane recruitment of dynamin-2 mediated by sorting nexin 9. *J. Biol. Chem.* **279**, 42694–42702 (2004).
20. Kramer, D. A., Piper, H. K. & Chen, B. WASP family proteins: Molecular mechanisms and implications in human disease. *Eur. J. Cell Biol.* **101**, 151244 (2022).
21. Machesky, L. M. & Insall, R. H. Scar1 and the related Wiskott-Aldrich syndrome protein, WASP, regulate the actin cytoskeleton through the Arp2/3 complex. *Curr. Biol.* **8**, 1347–1356 (1998).
22. Kim, A. S., Kakalis, L. T., Abdul-Manan, N., Liu, G. A. & Rosen, M. K. Autoinhibition and activation mechanisms of the Wiskott-Aldrich syndrome protein. *Nature* **404**, 151–158 (2000).
23. Hemsath, L., Dvorsky, R., Fiegen, D., Carlier, M. F. & Ahmadian, M. R. An electrostatic steering mechanism of Cdc42 recognition by Wiskott-Aldrich syndrome proteins. *Mol. Cell* **20**, 313–324 (2005).
24. Melendez, J., Grogg, M. & Zheng, Y. Signaling role of Cdc42 in regulating mammalian physiology. *J. Biol. Chem.* **286**, 2375–2381 (2011).
25. Rohatgi, R. et al. The interaction between N-WASP and the Arp2/3 complex links Cdc42-dependent signals to actin assembly. *Cell* **97**, 221–231 (1999).
26. Padrick, S. B. & Rosen, M. K. Physical mechanisms of signal integration by WASP family proteins. *Annu. Rev. Biochem.* **79**, 707–735 (2010).
27. Bustelo, X. R., Sauzeau, V. & Berenjeno, I. M. GTP-binding proteins of the Rho/Rac family: regulation, effectors and functions in vivo. *Bioessays* **29**, 356–370 (2007).
28. Fu, J. et al. The role of cell division control protein 42 in tumor and non-tumor diseases: a systematic review. *J. Cancer* **13**, 800–814 (2022).
29. Boquet, P. Small GTP binding proteins and bacterial virulence. *Microbes Infect.* **2**, 837–843 (2000).
30. Alto, N. M. et al. Identification of a bacterial type III effector family with G protein mimicry functions. *Cell* **124**, 133–145 (2006).
31. Huang, Z. et al. Structural insights into host GTPase isoform selection by a family of bacterial GEF mimics. *Nat. Struct. Mol. Biol.* **16**, 853–860 (2009).
32. Burkinshaw, B., Prehna, G., Worrall, L. & Strynadka, N. Structure of salmonella effector protein SopB N-terminal domain in complex with host Rho GTPase Cdc42. *J. Biol. Chem.* **287**, 13348–13355 (2012).
33. Schmidt, G. et al. Gln 63 of Rho is deamidated by Escherichia coli cytotoxic necrotizing factor-1. *Nature* **387**, 725–729 (1997).
34. Mosaddeghzadeh, N. & Ahmadian, M. R. The RHO family GTPases: mechanisms of regulation and signaling. *Cells* **10**, 1831 (2021).
35. Sallee, N. A. et al. The pathogen protein EspF(U) hijacks actin polymerization using mimicry and multivalency. *Nature* **454**, 1005–1008 (2008).
36. Tsai, C.-J., Lin, S. L., Wolfson, H. J. & Nussinov, R. Protein-protein interfaces: architectures and interactions in protein-protein interfaces and in protein cores. their similarities and differences. *Crit. Rev. Biochem. Mol. Biol.* **31**, 127–152 (1996).
37. Abdul-Manan, N. et al. Structure of Cdc42 in complex with the GTPase-binding domain of the 'Wiskott-Aldrich syndrome' protein. *Nature* **399**, 379–383 (1999).

38. Takenawa, T. & Suetsugu, S. The WASP-WAVE protein network: connecting the membrane to the cytoskeleton. *Nat. Rev. Mol. Cell Biol.* **8**, 37–48 (2007).
39. Wu, D. & Zhou, H. X. Designed mutations alter the binding pathways of an intrinsically disordered protein. *Sci. Rep.* **9**, 6172 (2019).
40. Ahmadian, M. R., Wittinghofer, A. & Herrmann, C. Fluorescence methods in the study of small GTP-binding proteins. *Methods Mol. Biol.* **189**, 45–63 (2002).
41. Schonichen, A. & Geyer, M. Fifteen formins for an actin filament: a molecular view on the regulation of human formins. *Biochim. Biophys. Acta* **1803**, 152–163 (2010).
42. Peng, J., Wallar, B. J., Flanders, A., Swiatek, P. J. & Alberts, A. S. Disruption of the Diaphanous-related formin Drf1 gene encoding mDia1 reveals a role for Drf3 as an effector for Cdc42. *Curr. Biol.* **13**, 534–545 (2003).
43. Mirdita, M. et al. ColabFold: making protein folding accessible to all. *Nat. Methods* **19**, 679–682 (2022).
44. Kuhn, S. et al. The structure of FMNL2-Cdc42 yields insights into the mechanism of lamellipodia and filopodia formation. *Nat. Commun.* **6**, 7088 (2015).
45. Zrieq, R., Braun, C. & Hegemann, J. H. The chlamydia pneumoniae tarp ortholog CPn0572 stabilizes host F-actin by displacement of cofilin. *Front. Cell Infect. Microbiol.* **7**, 511 (2017).
46. Fu, Y. & Galan, J. E. A salmonella protein antagonizes Rac-1 and Cdc42 to mediate host-cell recovery after bacterial invasion. *Nature* **401**, 293–297 (1999).
47. Cheng, H. C., Skehan, B. M., Campellone, K. G., Leong, J. M. & Rosen, M. K. Structural mechanism of WASP activation by the enterohaemorrhagic E. coli effector EspF(U). *Nature* **454**, 1009–1013 (2008).
48. Keb, G., Ferrell, J., Scanlon, K. R., Jewett, T. J. & Fields, K. A. Chlamydia trachomatis TmeA directly activates N-WASP to promote actin polymerization and functions synergistically with TarP during invasion. *mBio* **12**, e02861-20 (2021).
49. Faris, R., McCullough, A., Andersen, S. E., Moninger, T. O. & Weber, M. M. The Chlamydia trachomatis secreted effector TmeA hijacks the N-WASP-ARP2/3 actin remodeling axis to facilitate cellular invasion. *PLoS Pathog.* **16**, e1008878 (2020).
50. Carlton, J., Bujny, M., Rutherford, A. & Cullen, P. Sorting nexins-unifying trends and new perspectives. *Traffic* **6**, 75–82 (2005).
51. Eberth, A. & Ahmadian, M. R. In vitro GEF and GAP assays. *Curr. Protoc. Cell Biol.* **Chapter 14**, 19 (2009).
52. Mathivet, L., Cribier, S. & Devaux, P. F. Shape change and physical properties of giant phospholipid vesicles prepared in the presence of an AC electric field. *Biophys. J.* **70**, 1112–1121 (1996).
53. Kabsch, W. Xds. *Acta Crystallogr. D Biol. Crystallogr.* **66**, 125–132 (2010).
54. Evans, P. R. & Murshudov, G. N. How good are my data and what is the resolution? *Acta Crystallogr. D Biol. Crystallogr.* **69**, 1204–1214 (2013).
55. Winn, M. D. et al. Overview of the CCP4 suite and current developments. *Acta Crystallogr. D Biol. Crystallogr.* **67**, 235–242 (2011).
56. McCoy, A. J. et al. Phaser crystallographic software. *J. Appl. Crystallogr.* **40**, 658–674 (2007).
57. Jumper, J. et al. Highly accurate protein structure prediction with AlphaFold. *Nature* **596**, 583–589 (2021).
58. Emsley, P. & Cowtan, K. Coot: model-building tools for molecular graphics. *Acta Crystallogr. D Biol. Crystallogr.* **60**, 2126–2132 (2004).
59. Emsley, P., Lohkamp, B., Scott, W. G. & Cowtan, K. Features and development of Coot. *Acta Crystallogr. D Biol. Crystallogr.* **66**, 486–501 (2010).
60. Liebschner, D. et al. Macromolecular structure determination using X-rays, neutrons and electrons: recent developments in Phenix. *Acta Crystallogr. D Struct. Biol.* **75**, 861–877 (2019).
61. Blanchet, C. E. et al. Versatile sample environments and automation for biological solution X-ray scattering experiments at the P12 beamline (PETRA III, DESY). *J. Appl. Crystallogr* **48**, 431–443 (2015).
62. Manalastas-Cantos, K. et al. ATSAS 3.0: expanded functionality and new tools for small-angle scattering data analysis. *J. Appl. Crystallogr.* **54**, 343–355 (2021).
63. Panjkovich, A. & Svergun, D. I. CHROMIXS: automatic and interactive analysis of chromatography-coupled small-angle X-ray scattering data. *Bioinformatics* **34**, 1944–1946 (2018).
64. Konarev, P. V., Volkov, V. V., Sokolova, A. V., Koch, M. H. J. & Svergun, D. I. PRIMUS: a Windows PC-based system for small-angle scattering data analysis. *J. Appl. Crystallogr.* **36**, 1277–1282 (2003).
65. Guinier, A. Small-angle X-ray diffraction: application to the study of ultramicroscopic phenomena. *Ann. Phys.* **11**, 161–237 (1939).
66. Svergun, D. Determination of the regularization parameter in indirect-transform methods using perceptual criteria. *J. Appl. Crystallogr.* **25**, 495–503 (1992).
67. Petoukhov, M. V. et al. New developments in the ATSAS program package for small-angle scattering data analysis. *J. Appl. Crystallogr.* **45**, 342–350 (2012).
68. Bernado, P., Mylonas, E., Petoukhov, M. V., Blackledge, M. & Svergun, D. I. Structural characterization of flexible proteins using small-angle X-ray scattering. *J. Am. Chem. Soc.* **129**, 5656–5664 (2007).
69. Tria, G., Mertens, H. D., Kachala, M. & Svergun, D. I. Advanced ensemble modelling of flexible macromolecules using X-ray solution scattering. *IUCrJ* **2**, 207–217 (2015).
70. Kikhney, A. G., Borges, C. R., Molodenskiy, D. S., Jeffries, C. M. & Svergun, D. I. SASBDB: Towards an automatically curated and validated repository for biological scattering data. *Protein Sci.* **29**, 66–75 (2020).

Acknowledgements

We acknowledge DESY (Hamburg, Germany), a member of the Helmholtz Association HGF, for the provision of experimental facilities. Parts of this research were carried out at PETRA III and we would like to thank Haydyn Mertens and Dmytro Soloviov (EMBL Hamburg) for their assistance in using beamline P12. We also acknowledge the European Synchrotron Radiation Facility (ESRF) for the provision of synchrotron radiation facilities and we would like to thank Petra Pernot, for assistance in using beamline BM29. The crystal datasets were collected at the P13 beamline at DESY Hamburg and ID30A-3 at the ESRF Grenoble. Here, we would like to thank Selina Storm and Igor Melnikov for their excellent support during data collection. We thank our reviewers for the constructive comments. F.K. was a scholarship holder of the Graduate School "Molecules of Infection IV (MOI IV)" funded by the Jürgen Manchot Foundation. The Center for Structural Studies is funded by the DFG (Grant Nos. 417919780, INST 208/761-1 FUGG, INST 208/868-1 FUGG and INST 208/740-1 FUGG to S.H.J.S.). We acknowledge grant support from the DFG to A.M. and M.R.A. (grant number: AH 92/8-3) and to J.H.H. (Project-ID 267205415) of CRC 1208.

Author contributions

Conceptualisation: F.K., K.M. and J.H.H.; methodology F.K., K.M., M.R.A., A.M., S.H.J.S. and J.H.H.; investigation: F.K., V.A., J.R., A.P., D.S., S.H., A.M., M.R.A., S.H.J.S. and K.M., writing—original draft: F.K., K.M., S.H.J.S. and J.H.H.; writing—review & editing: F.K., K.M., S.H.J.S. and J.H.H; funding acquisition: J.H.H. and S.H.J.S.

Funding

Open Access funding enabled and organized by Projekt DEAL.

Competing interests

The authors declare no competing interests.

Additional information

Supplementary information The online version contains supplementary material available at https://doi.org/10.1038/s41467-024-51681-3.

Correspondence and requests for materials should be addressed to Johannes H. Hegemann.

Peer review information *Nature Communications* thanks Matthias Geyer, Laurent Terradot and the other, anonymous, reviewer for their contribution to the peer review of this work. A peer review file is available.

Supplementary Information

The C*hlamydia pneumoniae* effector SemD exploits its host's endocytic machinery by structural and functional mimicry

Kocher et al.

Supplementary Content

Supplementary Figures 2
Supplementary Tables 13
Supplementary References 19
Uncropped Scans of gels and blots 20

Supplementary Figures

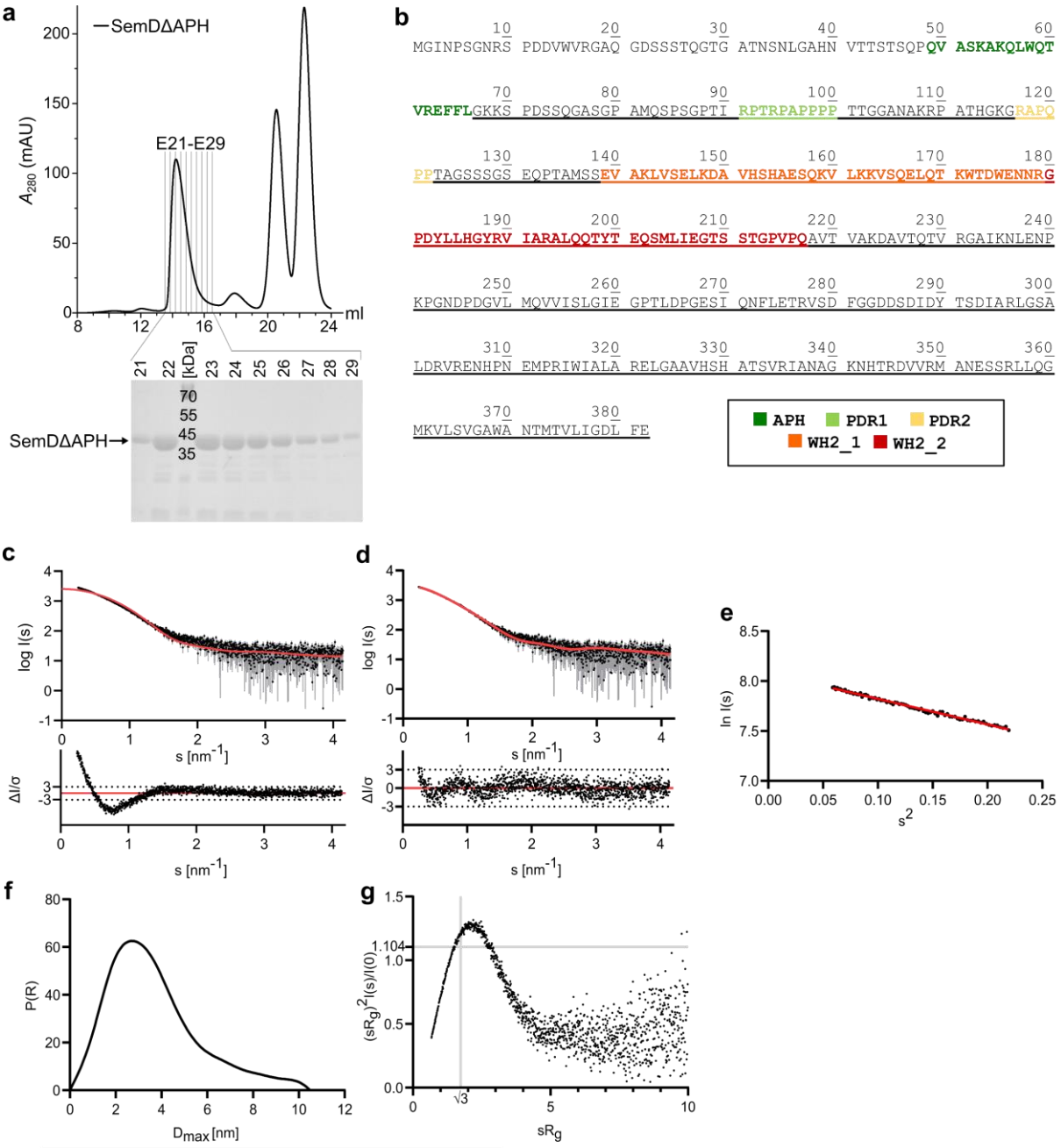

Supplementary Figure 1 | SemDΔAPH purification and SAXS analysis. a SEC of SemDΔAPH (*top*) in PBS, separated on a HiLoad 16/600 Superdex 200 pg column. From elution fractions 21-29, SDS samples were prepared and loaded on an SDS gel, stained with Coomassie brilliant blue (*bottom*). **b** Amino acid sequence of full length SemD (residues 1-382). The underlined fragment corresponds to SemDΔAPH (residues 67-382). Individual domains are marked: amphipathic helix (APH, darkgreen), proline-rich domains (PRD1: bright green, PRD2: yellow), WH2_1 (orange) and WH2_2 (red). **c** Theoretical scattering data of the SemDΔAPH crystal structure. Experimental data are shown in black dots, with grey error bars. The theoretical scattering fit (χ^2 value of 14.63) created with CRYSOL, is shown as red line and below is the residual plot of the data. **d** Scattering data of SemDΔAPH. Experimental data are shown in black dots, with grey error bars. The best CORAL model fit (χ^2 value of 1.197) is shown as red line and below is the residual plot of the data. **e** The Guinier plot of SemDΔAPH showed a stable Guinier region with a R_g of 2.78 nm. **f** The *p(r)* function of SemDΔAPH showed a globular molecule with an elongated part and a D_{max} value of 10.49 nm. **g** Dimensionless Kratky plot of SemDΔAPH showed an elongated particle. Source data for **c-g** are provided as Source Data file. **h** Overlay of ten independent CORAL models with a χ^2 value ranging from 1.197 – 2.098. The SemDΔAPH crystal structure shown in cartoon representation was used as template and the missing residues were modelled with CORAL and shown as loops. The grey model (χ^2 value of 1.197) is shown in detail in Fig. 1c.

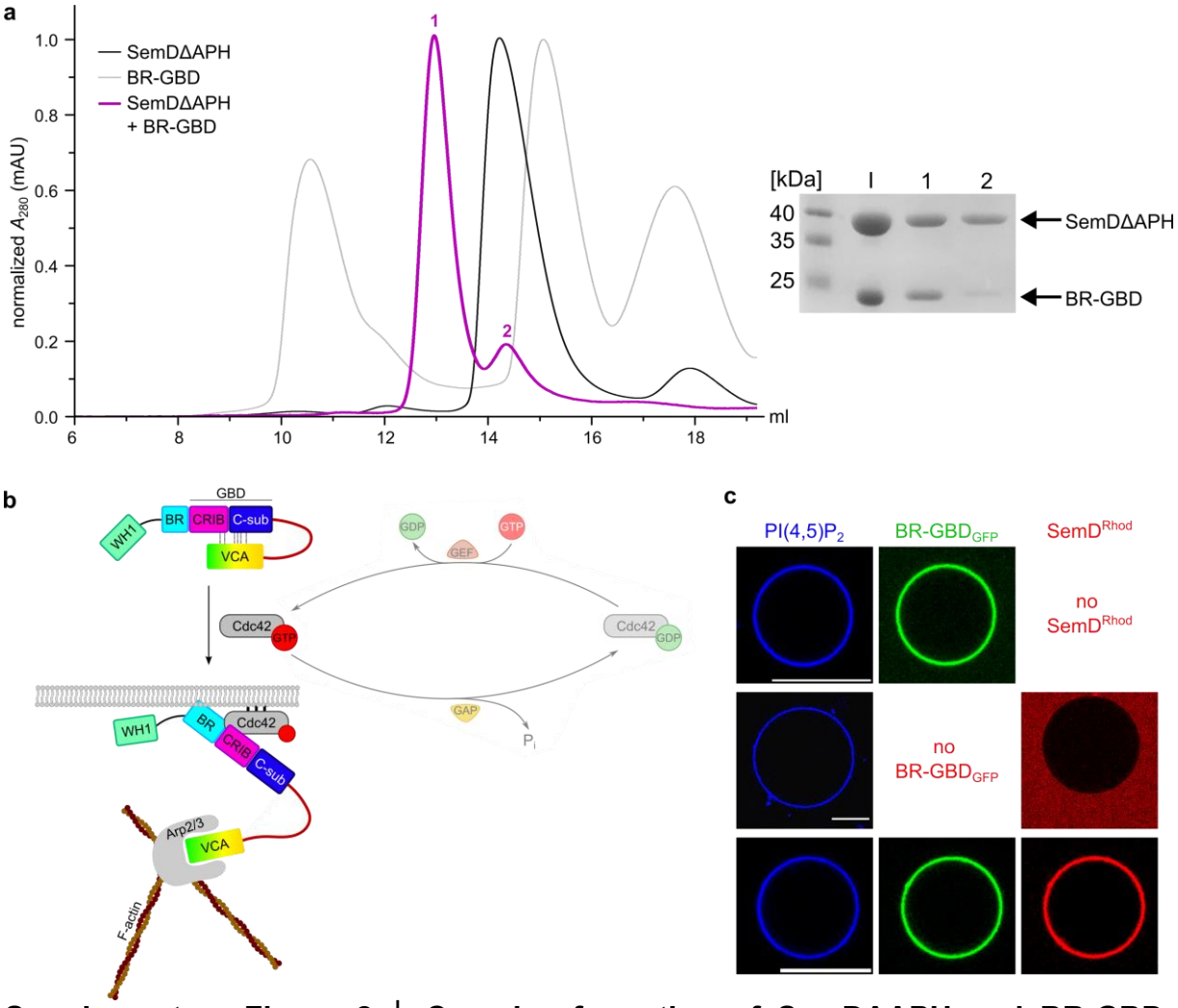

Supplementary Figure 2 | Complex formation of SemDΔAPH and BR-GBD. **a** SEC (*left*) for SemDΔAPH (black), BR-GBD (grey) and SemDΔAPH + BR-GBD (magenta). Protein composition of peak 1 and 2 were analysed on an SDS gel (*right*), stained with Coomassie brilliant blue. The gel was loaded from left to right with the SEC-input sample (I), Peak 1 (1) and Peak 2 (2). **b** Schematic representation of N-WASP activation by $Cdc42_{GTP}$. **c** Confocal images of PI(4,5)P_2-GUVs with rhodamine-labelled SemD ($SemD^{Rhod}$) and $BR\text{-}GBD_{GFP}$. (Scale bars 10 µm).

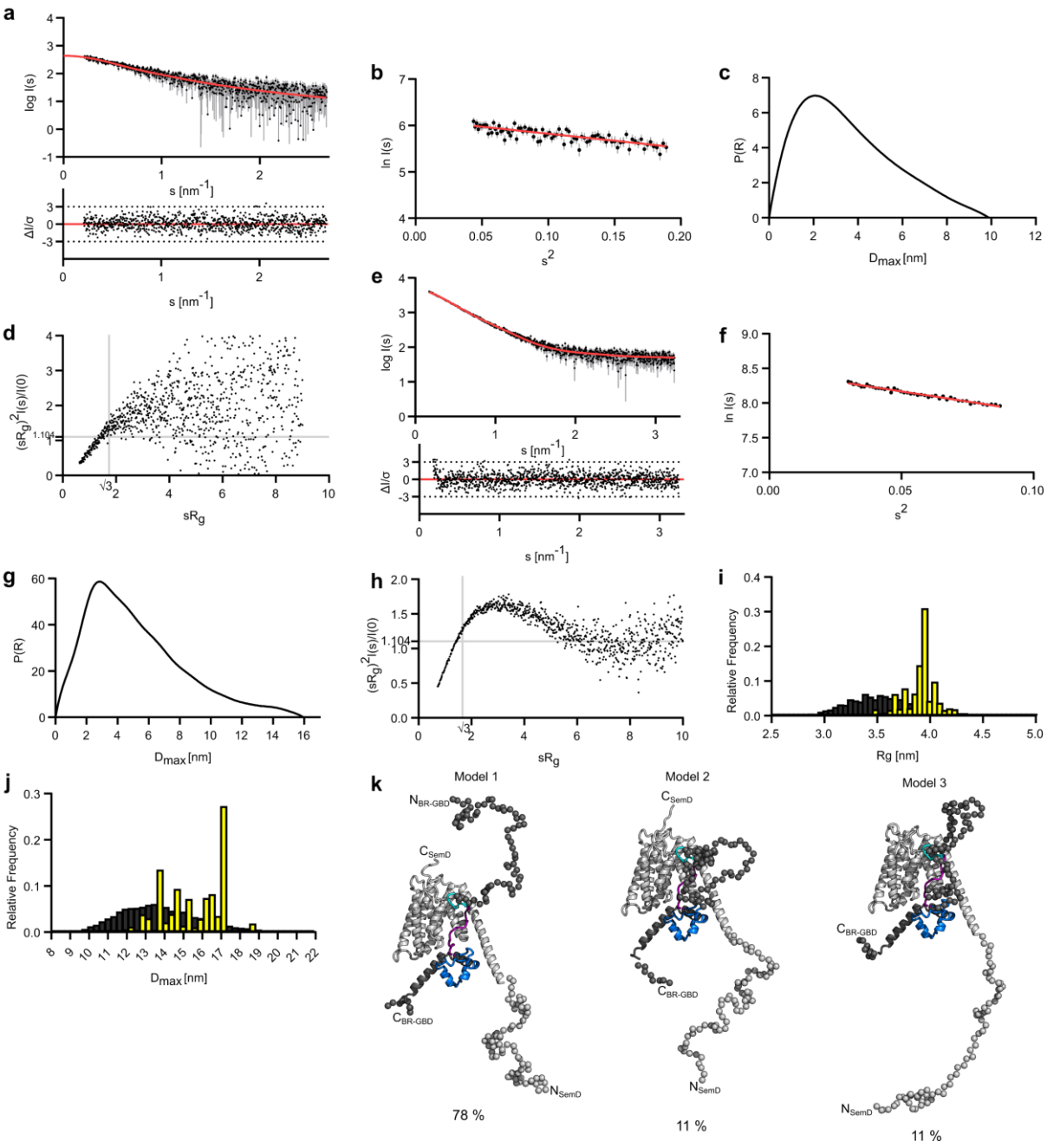

Supplementary Figure 3 | Small-angle X-ray scattering data from BR-GBD alone and SemDΔAPH in complex with BR-GBD. a Scattering data of BR-GBD. Experimental data are shown in black dots, with grey error bars. The GNOM fit is shown as red line and below is the residual plot of the data. **b** The Guinier plot of BR-GBD showed a stable Guinier region with a R_g of 3.01 nm. **c** The *p(r)* function of BR-GBD showed a globular molecule with an elongated part and a D_{max} value of 9.90 nm.

d The Dimensionless Kratky plot showed a high degree of flexibility for BR-GBD apo. **e** Scattering data of SemDΔAPH in complex with BR-GBD. Experimental data are shown in black dots, with grey error bars. The EOM ensemble model fit is shown as red line and below is the residual plot of the data. **f** The Guinier plot of SemDΔAPH in complex with BR-GBD showed a stable Guinier region with a R_g of 4.19 nm. **g** The *p(r)* function of SemDΔAPH in complex with BR-GBD showed an elongated particle with a D_{max} value of 15.94 nm. **h** The Dimensionless Kratky plot of SemDΔAPH in complex with BR-GBD showed an elongated particle with a high degree of flexibility. **i&j** R_g and D_{max} distribution of SemDΔAPH in complex with BR-GBD. Ensemble pool is shown in grey, selected EOM models are shown in yellow. The EOM analysis showed that the assembled complex (in blue) favoured a more extended conformation in comparison to the random pool (in grey). Source data for **a-j** are provided as Source Data File. **k** Selected EOM models from SemDΔAPH in complex with N-WASP. The used parts from the crystal structure of SemDΔAPH in complex with N-WASP are shown in cartoon representation and the missing termini parts in spheres. On the left site Model 1 with a volume fraction of 78 % is shown, in the middle and on the right are Model 2 and 3 with a volume fraction of 11 % each.

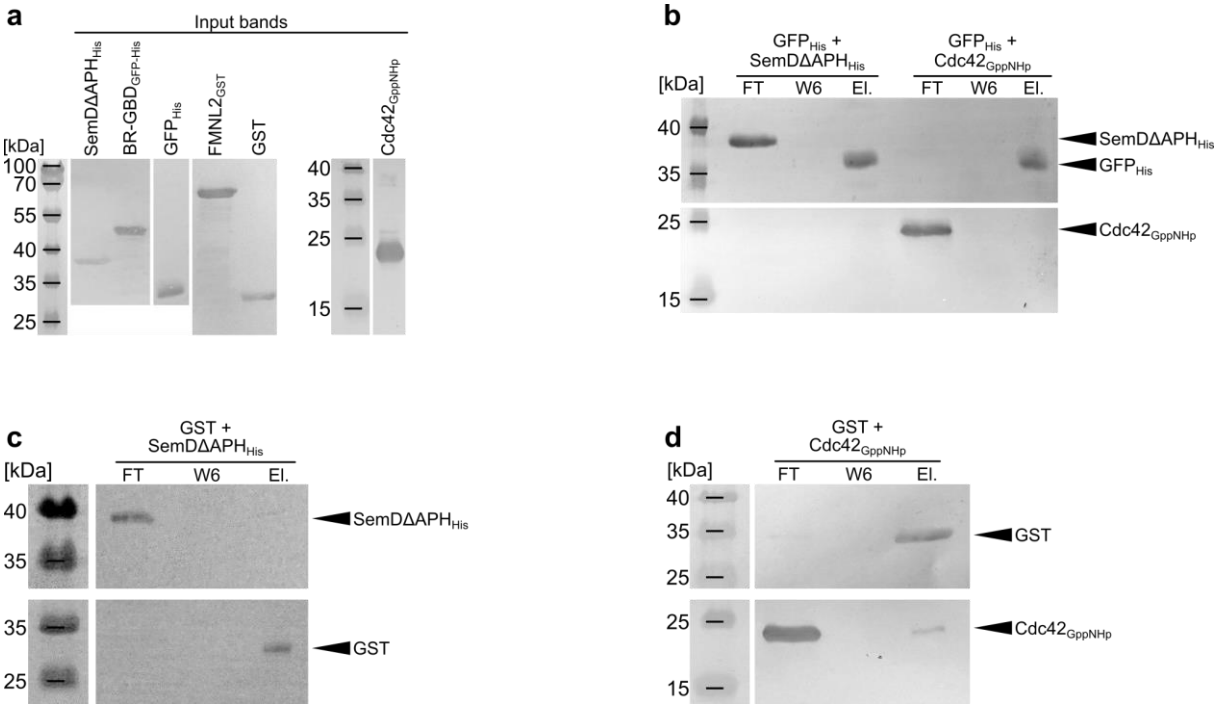

Supplementary Figure 4 | Negative controls for pulldown assays from Figure 4. **a** Input bands for the recombinant and tagged proteins used for pulldown experiments from Fig. 4. **b** Negative control for GFP-Trap® pulldown experiments from Fig. 4a. SemDΔAPH$_{His}$ and Cdc42$_{GppNHp}$ were tested against GFP$_{His}$. flow-through (FT), W6 and Elution (El) were fractionated by SDS/PAGE and probed with anti-His for GFP$_{His}$ and SemDΔAPH$_{His}$ and anti-Cdc42 antibodies for Cdc42$_{GppNHp}$. **c,d** Negative control for GST-pulldown from Fig. 4e. SemDΔAPH$_{His}$ and Cdc42$_{GppNHp}$ were tested against GST. flow-through (FT), W6 and Elution (El) were fractionated by SDS/PAGE and probed with anti-GST for GST, anti-His for SemDΔAPH$_{His}$ and anti-Cdc42 antibodies for Cdc42$_{GppNHp}$. Uncropped blots are provided as Source Data file.

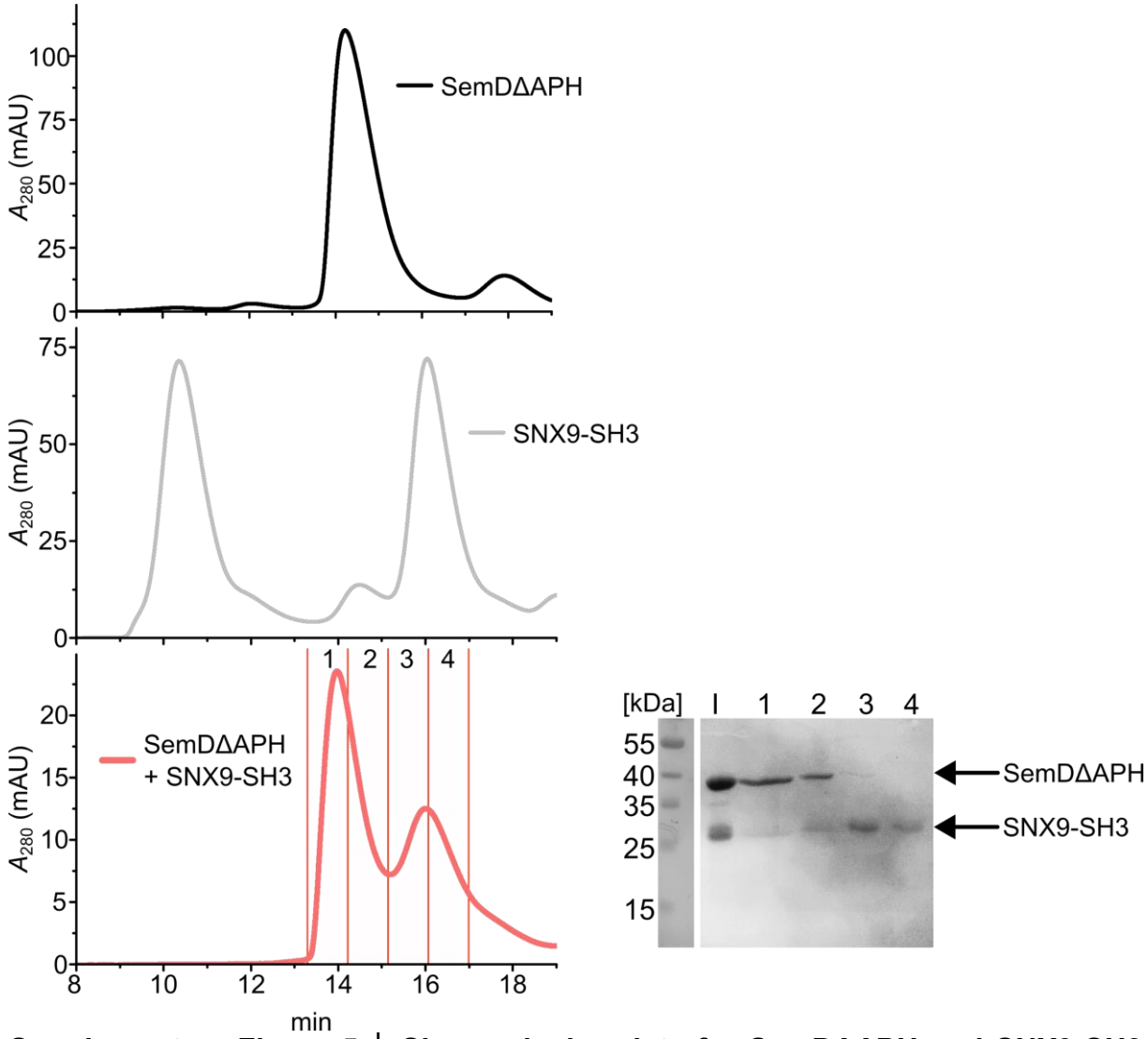

Supplementary Figure 5 | Size exclusion data for SemDΔAPH and SNX9-SH3 complex purification. SEC for SemDΔAPH (top, black), SNX9-SH3 (middle, grey) and SemDΔAPH + SNX9-SH3 (bottom, red). For the elution fractions 1 to 4, SDS samples were prepared and the protein composition was analysed on an SDS gel (right), stained with Coomassie brilliant blue. The gel was loaded from left to right with the SEC-input sample (I) and elutions 1-4.

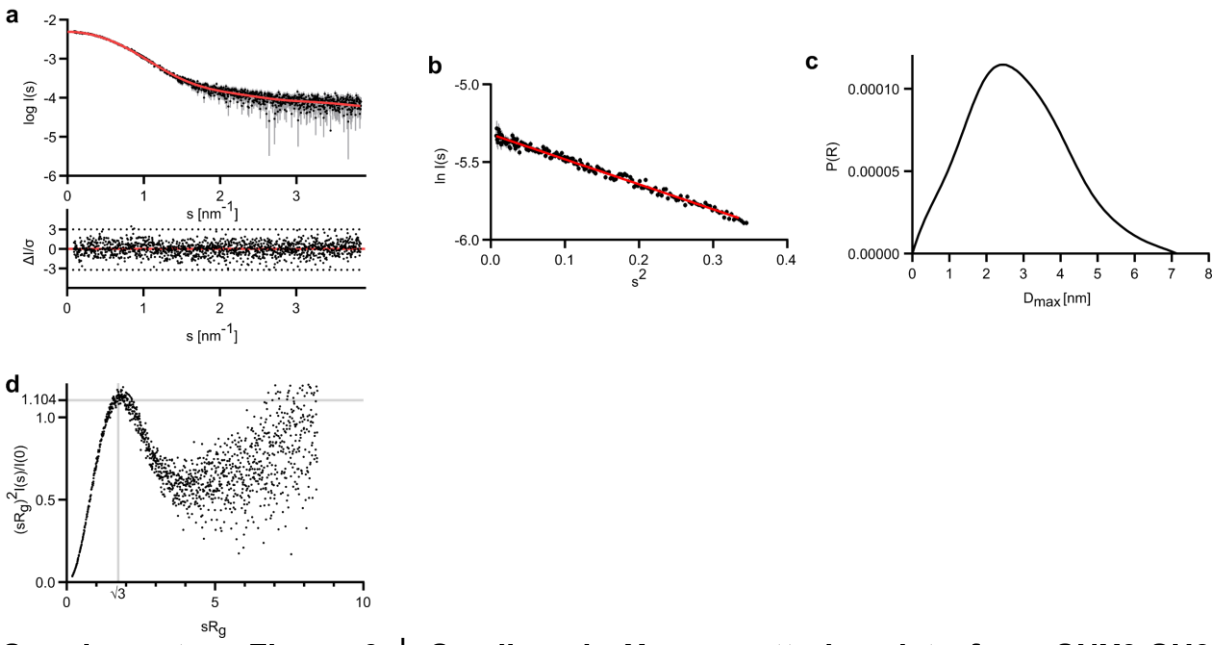

Supplementary Figure 6 | Small-angle X-ray scattering data from SNX9-SH3 alone. a Scattering data of SNX9-SH3 alone. Experimental data are shown in black dots, with grey error bars. The GNOM fit is shown as red line and below is the residual plot of the data. **b** The Guinier plot of SNX9-SH3 showed a stable Guinier region with a R_g of 2.20 nm. **c** The *p(r)* function of SNX9-SH3 apo showed a globular molecule with an elongated part and a D_{max} value of 7.14 nm. **d** The Dimensionless Kratky plot of SNX9-SH3 showed a compact globular molecule containing flexible parts. Source data for **a-d** are provided as Source Data file.

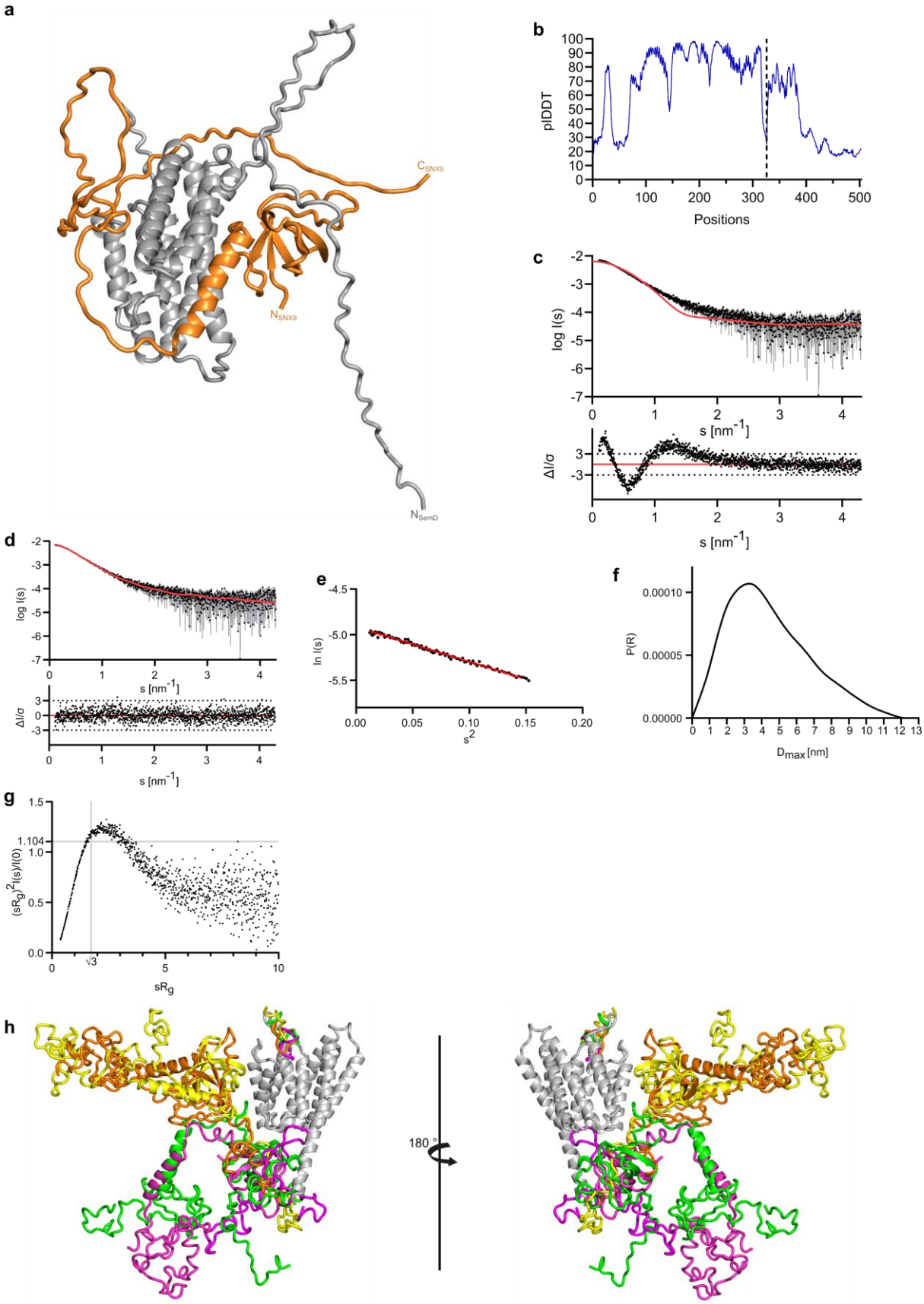
a
C_{SNX9}
N_{SNX9}
N_{SemD}
b
pIDDT
Positions
c
log I(s)
s [nm^{-1}]
ΔI/σ
d
e
ln I(s)
s^2
f
P(R)
D_{max} [nm]
g
$(sR_g)^2I(s)/I(0)$
1.104
√3
sR_g
h
180 °

Supplementary Figure 7 | Small-angle X-ray scattering data from SemDΔAPH in complex with SNX9-SH3. **a** An AlphaFold2 prediction of SemDΔAPH (grey) in complex with SNX9-SH3 (orange). **b** pLDDT score from the AlphaFold2 prediction. The left part corresponds to SemDΔAPH and the right part to SNX9-SH3. **c** Theoretical scattering of the SemDΔAPH in complex with SNX9-SH3 from AlpfaFold2 prediction. Experimental data are shown in black dots, with grey error bars. The theoretical scattering fit (χ^2 value of 8.49) created with CRYSOL, is shown as red line and below is the residual plot of the data. **d** The experimental Scattering data of SemDΔAPH in complex with SNX9-SH3 are shown in black dots, with grey error bars. The best CORAL model fit (χ2 value of 1.018) is shown as red line and below is the residual plot of the data. **e** The Guinier plot of SemDΔAPH in complex with SNX9-SH3 showed a stable Guinier region with a *Rg* of 3.39 nm. **f** The *p(r)* function of SemDΔAPH in complex with SNX9-SH3 showed an elongated molecule and a D_{max} value of 12.16 nm. **g** The Dimensionless Kratky plot of SemDΔAPH in complex with SNX9-SH3 apo showed a compact globular molecule still containing flexible elements. Source data for **a-g** are provided as Source Data file. **h** Overlay of 4 independent CORAL models with a χ^2 value ranging from 1.018 – 1.092. The SemDΔAPH crystal structure (shown in grey) and the AlphaFold2 docking interface from SNX9-SH3 with the N-terminal part of SemDΔAPH, shown in cartoon representation were used as templates and the missing residues as well as the orientation were modelled with CORAL. The orange model (χ2 value of 1.018) is shown in detail in Fig. 5d.

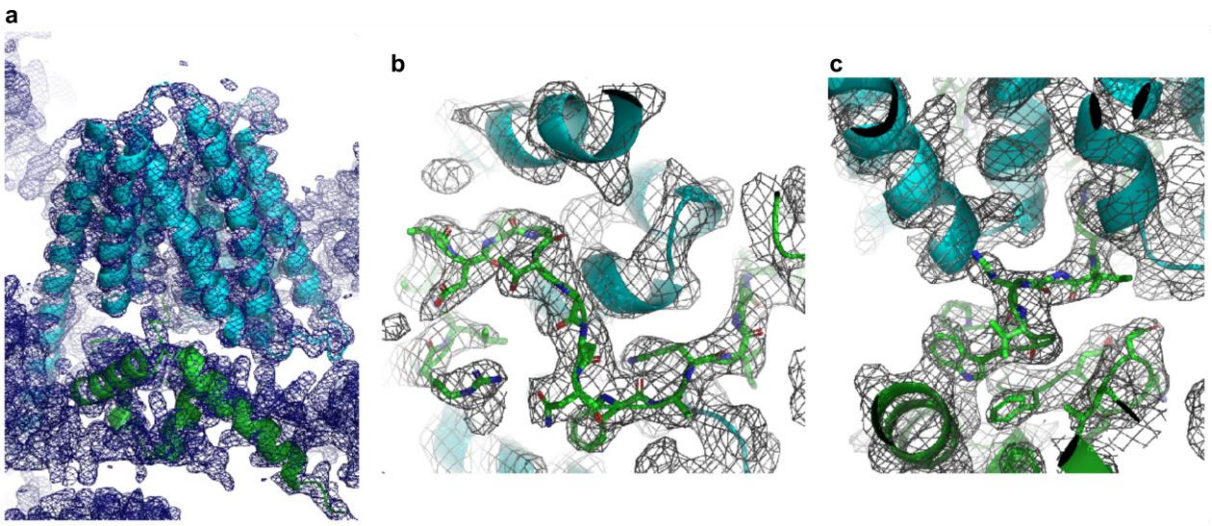

Supplementary Figure 8 | Electron density of the SemD – BR-GBD interface. a Shown is the electron density of the overall structure of SemD (highlighted as blue cartoon) and BR-GBD (highlighted as green cartoon). **b,c** Zoom in on the interaction interface. For clarity reasons the SemD structure is shown as cartoon, whereas the BR-GBD protein is shown as sticks. The electron density (2F0-Fc) is shown as grey mesh, contoured at 1.0 sigma. Although the structure is of medium resolution, the side chains of BR-GBD are clearly visible in the electron density.

Supplementary Tables

Supplementary Table 1. Data collection and refinement statistics of the crystal structure of SemDΔAPH and SemDΔAPH - BR-GBD complex

	SemDΔAPH	**SemDΔAPH + BR-GBD**
Data collection		
Space group	P1	P 31 2 1
Cell dimensions		
a, *b*, *c* (Å)	46.99 51.95 58.62	120.22 120.22 65.24
α, β, γ (°)	88.33 105.89 117.43	90.0 90.0 120.0
Resolution (Å)	45.82 - 2.1 (2.175 - 2.1)*	52.06 - 3.3 (3.418 - 3.3) *
R_{sym} or R_{merge}	0.07588 (0.5214)	0.1328 (0.8603)
$I / \sigma I$	10.61 (2.56)	17.63 (3.40)
Completeness (%)	97.65 (97.52)	99.66 (99.65)
Redundancy	3.5 (3.6)	20.7 (21.8)
Refinement		
Resolution (Å)	45.82 - 2.1 (2.175 - 2.1)*	52.06 - 3.3 (3.418 - 3.3) *
No. reflections	26816 (2675)	8408 (852)
R_{work} / R_{free}	0.2195 /0.2745	0.2277 /0.2439
No. atoms		
Protein	3560	2617
Ligand/ion	0	0
Water	216	0
B-factors	(Ask for input)	
Protein	38.76	92.85
Ligand/ion	-	-
Water	40.8	-
R.m.s. deviations		
Bond lengths (Å)	0.011	0.012
Bond angles (°)	1.19	1.68

*Data collection resulted in both dataset from a single crystal. *Values in parentheses are for highest-resolution shell.

Supplementary Table 2. Overall SAXS Data of SemDΔAPH, BR-GBD, SNX9-SH3 and the corresponding complexes

Data collection parameters					
SAXS Device	P12, PETRA III, DESY Hamburg[1]				
Detector	PILATUS 6 M (423.6 x 434.6 mm^2)				
Detector distance (m)	3.0				
Beam size	120 µm x 200 µm				
Wavelength (nm)	0.124				
Sample environment	Quartz glass capillary, 1 mm ø				
Absolute scaling method	Comparison with scattering from pure H_2O				
Normalization	To transmitted intensity by beam-stop counter				
Scattering intensity scale	Absolute scale or relative scale, cm^{-1}				
s range (nm^{-1})‡	0.03 – 7.0				
Sample	**SemDΔAPH apo**	**BR-GBD apo**	**SemDΔAPH + BR-GBD**	**SNX9-SH3 apo**	**SemDΔAPH + SNX9 SH3**
Organism	*Chlamydia pneumoniae GiD*[2]				
UniProt ID (range)	Q9Z7M7 (67-382)	O08816 (142-273)		Q9Y5X1 (1-160)	
Mode of measurement	Online SEC-SAXS				
SEC-Column	Superdex200 increase 10/300 GL				
Flowrate (ml/min)	0.6				
Injection volume (µl)	100				
Temperature (°C)	20				
Exposure time (# frames)	0.995 s (2400)				
# frames used for averaging	19	22	17	46	63
Protein buffer	PBS (137 mM NaCl, 2.7 mM KCl, 10 mM Na_2HPO_4, 1.8 mM KH_2PO_4), pH 8.5, 3% Glycerol				
Protein concentration (mg/ml)	8	10	8	3.3	3.3

Structural parameters					
Guinier Analysis (PRIMUS)					
$I(0) \pm \sigma$ (cm^{-1})	3224.17 ± 9.92	456.12 ± 13.03	4722.19 ± 35.06	0.0049 ± 0.000014	0.0073 ± 0.00002
$R_g \pm \sigma$ (nm)	2.78 ± 0.01	3.01 ± 0.13	4.19 ± 0.04	2.20 ± 0.01	3.39 ± 0.02
s-range (nm^{-1})	0.243 – 0.468	0.209 – 0.432	0.173 – 0.295	0.087 – 0.579	0.110 – 0.382
min < sRg < max limit	0.67 – 1.30	0.63 – 1.30	0.74 – 1.24	0.19 – 1.27	0.37 – 1.29
Data point range	1 - 82	1 - 81	1 - 45	1 - 170	1 - 95
Linear fit assessment (R^2)	0.99	0.64	0.98	0.98	0.99
PDDF/P(r) Analysis (GNOM)					
$I(0) \pm \sigma$ (cm^{-1})	3279.00 ± 9.82	434.70 ± 8.56	4667.00 ± 34.88	0.0049 ± 0.000012	0.0074 ± 0.00003
$R_g \pm \sigma$ (nm)	2.95 ± 0.01	2.91 ± 0.06	4.29 ± 0.05	2.23 ± 0.007	3.53 ± 0.02
D_{max} (nm)	10.49	9.90	15.94	7.14	12.16
Porod volume (nm^3)	67.39	19.49	102.29	41.60	93.81
s-range (nm^{-1})	0.243 – 4.142	0.212 – 2.682	0.173 – 3.236	0.087 – 3.845	0.110 – 4.30
χ2 / CorMap P-value	0.925 / 0.081	1.013 / 0.579	1.070 / 0.234	0.972 / 0.076	0.977 / 0.759
Molecular mass (kDa)					
From $I(0)$	n.d.	n.d.	n.d.	n.d.	n.d.
From Qp^3	38.03	15.69	60.09	16.44	52.51
From MoW2[4]	37.53	18.91	48.24	16.79	46.93
From Vc[5]	37.22	16.79	43.03	21.95	49.44
Bayesian Inference[6]	36.90	18.05	45.68	18.68	49.78
From sequence	35.13	19.74	54.87	18.80	53.90

Rigid body modeling					
CORAL					
Symmetry	P1				P1
s-range for fit (nm^{-1})	0.243 – 4.142				0.110 – 4.30
χ^2, CorMap *P*-value	1.197 / 0.005				1.018 / 0.507
EOM					
Symmetry			P1		
s-range for fit (nm^{-1})			0.173 – 3.236		
χ^2, CorMap *P*-value			1.107 / 0.033		
SASBDB accession codes[7]	SASDTQ5	SASDTR5	SASDTU5	SASDTS5	SASDTT5
Software					
ATSAS Software Version[8]			3.0.5		
Primary data reduction			CHROMIXS[9] / PRIMUS[10]		
Data processing			GNOM[11]		
Rigid body modelling			CORAL[12]		
Flexibility ensemble modelling			EOM[13,14]		
Structure validation			CRYSOL[15]		
Statistic goodness-of-fit test			χ^2, CorMap[16]		
Model visualization			PyMOL[17]		

‡s = 4πsin(θ)/λ, 2θ – scattering angle, n.d. not determined

Supplementary Table 3. PCR Primers

Internal number	Name	Sequence (5' -3')
C-4130	Flag-BR_CRIB-TEV Hin	TAGAAATAATTTTGTTTAACTTTAAGAAGGAGATATACATATGGATTACA AAGACGATGACGATAAGGATTACAAAGACGATGACGATAAGTCTGAAA AAAGACGAGATGCTC
C-4131	Flag-BR_CRIB-TEV Her	CTCAATGGTGATGGTGATGATGGTGGTGATGGTGCTCGAGTCCTTGA AAATACAAGTTTTCTGCTTGCCTTCGGAGTTCAT
C-4214	CPn0677_co 67-382 in pSL4 hin	AAATAATTTTGTTTAACTTTAAGAAGGAGATATACATATGGGTAAGAAA AGCCCGGATAG
C-4215	CPn0677_co 67-382 in pSL4 her	CCGGATCTCAATGGTGATGGTGATGATGGTGGTGATGGTGTTCGAAC AGATCACCAATCAG
C-4364	SNX9_SH3 in pSL4 hin	AAATAATTTTGTTTAACTTTAAGAAGGAGATATACATATGGCCACCAAG GCTCGGGT
C-4365	SNX9_SH3 in pSL4 her	GATGATGGTGGTGATGGTGCTCGAGTGCGGCCGCAAGCTTACCAGTT GCTGGTCCTTGGTA
C-4428	P1 Dead her	CGTGGGTCGCCGGACGCTTCGCGTTCGCGCCACCGGTGGTCGCAAC CGCAACAGCCGCAACGGTCGCAACAATGGTCGCGCCGCTCGGGCTT TGCATC
C-4429	P2 Dead hin	CGGTGGCGCGAACGCGAAGCGTCCGGCGACCCACGGTAAGGGTGTT GCGGCGCAGGTTGCGACCGCGGGTAGCAGCAG
C-4430	677co in pSL4 hin	AAATAATTTTGTTTAACTTTAAGAAGGAGATATACATATGGGTATCAAC CCGAGCGGCA
C-4483	pSL4 CRIB short For	TCCAGAAATCACAACAAACAGGTTTTATAGTTCACAAGTCGCAGATATT GGAACACCAAGTA
C-4484	pSL4 CRIB short Rev	GTCCAATGTGCTGGAAATTACTTGGTGTTCCAATATCTGCGACTTGTG AACTATAAAACCTG
C-4489	pKM431/436 sirGFP hin	CCTCTAGAAATAATTTTGTTTAACTTTAAGAAGGAGATATATGTCTGAA AAAAGACGAGATGC
C-4490	pKM431/436 sirGFP her	GCACCACCCCGGTGAACAGCTCCTCGCCCTTGCTCACCATTGAACTA CCACTTGATCCCTCGAGTGCGGCCGCAAGCT
C-4581	SH3 in pDS94 hin	CTAGAAATAATTTTGTTTAACTTTAAGAAGGAGATATACCATGGCCACC AAGGCTCGGGT
C-4582	SH3 in pDS94 her	ACCCCGGTGAACAGCTCCTCGCCCTTGCTCACCATTGAACTACCACTT GATCCAAGCTTACCAGTTGCTGGTCC
C-4565	pFK31_BR-Crib siGFP in pDS94 rvs	GCACCACCCCGGTGAACAGCTCCTCGCCCTTGCTCACCATTGAACTA CCACTTGATCCTGCTTGCCTTCGGAGTTC

Supplementary Table 4. Plasmids

Name	Reference
pSL4	Luczak S. Dissertation[18]
pDS94	This plasmid is based on: pET His6 GFP TEV LIC cloning vector (1GFP), gifted from Scott Gradia (Addgene plasmid # 29663; http://n2t.net/addgene:29663; RRID:Addgene_29663) and was equipped with a 10x C-terminal His-tag and a CEN/ARS/TRP cassette

Supplementary References

1 Blanchet, C. E. *et al.* Versatile sample environments and automation for biological solution X-ray scattering experiments at the P12 beamline (PETRA III, DESY). *J Appl Crystallogr* **48**, 431-443 (2015).

2 Jantos, C. A., Heck, S., Roggendorf, R., Sen-Gupta, M. & Hegemann, J. H. Antigenic and molecular analyses of different Chlamydia pneumoniae strains. *J. Clin. Microbiol.* **35**, 620-623 (1997).

3 Porod, G. Die Röntgenkleinwinkelstreuung Von Dichtgepackten Kolloiden Systemen - 1 Teil. *Kolloid-Zeitschrift and Zeitschrift Fur Polymere* **124**, 83-114 (1951).

4 Fischer, H., de Oliveira Neto, M., Napolitano, H. B., Polikarpov, I. & Craievich, A. F. Determination of the molecular weight of proteins in solution from a single small-angle X-ray scattering measurement on a relative scale. *Journal of Applied Crystallography* **43**, 101-109 (2010).

5 Rambo, R. P. & Tainer, J. A. Accurate assessment of mass, models and resolution by small-angle scattering. *Nature* **496**, 477-481 (2013).

6 Hajizadeh, N. R., Franke, D., Jeffries, C. M. & Svergun, D. I. Consensus Bayesian assessment of protein molecular mass from solution X-ray scattering data. *Scientific Reports* **8**, 7204 (2018).

7 Kikhney, A. G., Borges, C. R., Molodenskiy, D. S., Jeffries, C. M. & Svergun, D. I. SASBDB: Towards an automatically curated and validated repository for biological scattering data. *Protein Sci* **29**, 66-75 (2020).

8 Manalastas-Cantos, K. *et al.* ATSAS 3.0: expanded functionality and new tools for small-angle scattering data analysis. *J Appl Crystallogr* **54**, 343-355 (2021).

9 Panjkovich, A. & Svergun, D. I. CHROMIXS: automatic and interactive analysis of chromatography-coupled small angle X-ray scattering data. *Bioinformatics* (2017).

10 Konarev, P. V., Volkov, V. V., Sokolova, A. V., Koch, M. H. J. & Svergun, D. I. PRIMUS: a Windows PC-based system for small-angle scattering data analysis. *Journal of Applied Crystallography* **36**, 1277-1282 (2003).

11 Svergun, D. I. Determination of the Regularization Parameter in Indirect-Transform Methods Using Perceptual Criteria. *Journal of Applied Crystallography* **25**, 495-503 (1992).

12 Petoukhov, M. V. *et al.* New developments in the ATSAS program package for small-angle scattering data analysis. *J Appl Crystallogr* **45**, 342-350 (2012).

13 Bernado, P., Mylonas, E., Petoukhov, M. V., Blackledge, M. & Svergun, D. I. Structural characterization of flexible proteins using small-angle X-ray scattering. *J Am Chem Soc* **129**, 5656-5664 (2007).

14 Tria, G., Mertens, H. D., Kachala, M. & Svergun, D. I. Advanced ensemble modelling of flexible macromolecules using X-ray solution scattering. *IUCrJ* **2**, 207-217 (2015).

15 Svergun, D., Barberato, C. & Koch, M. H. J. CRYSOL– a Program to Evaluate X-ray Solution Scattering of Biological Macromolecules from Atomic Coordinates. *Journal of Applied Crystallography* **28**, 768-773 (1995).

16 Franke, D., Jeffries, C. M. & Svergun, D. I. Correlation Map, a goodness-of-fit test for one-dimensional X-ray scattering spectra. *Nat Methods* **12**, 419-422 (2015).

17 PyMOL. The PyMOL Molecular Graphics System, Version 2.0 Schrödinger, LLC. (2015).

18 Luczak, S. *Biochemical and Biophysical Characterization of the Adhesin and Invasin Pmp21 from Chlamydia pneumoniae* PhD thesis, Heinrich Heine University, Düsseldorf, (2017).

Uncropped Scans of gels and blots

Uncropped gel to Supplementary Figure 1a

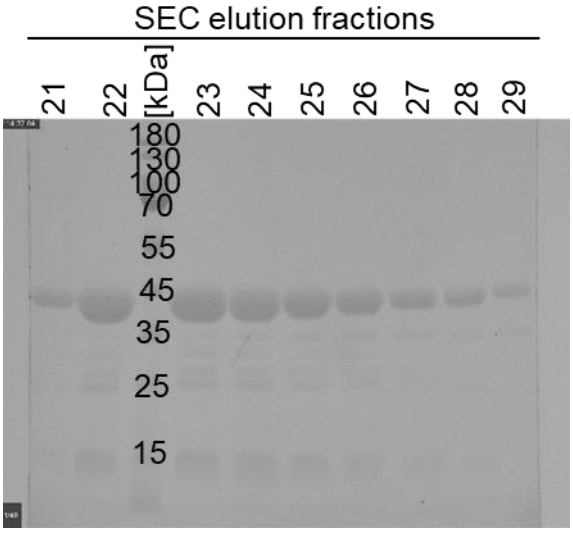

Uncropped gel to Supplementary Figure 2a

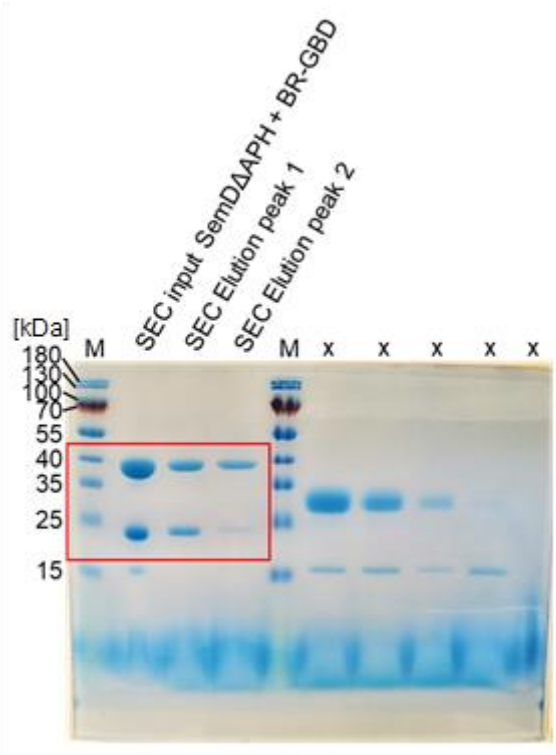

Uncropped gel to Supplementary Figure 5

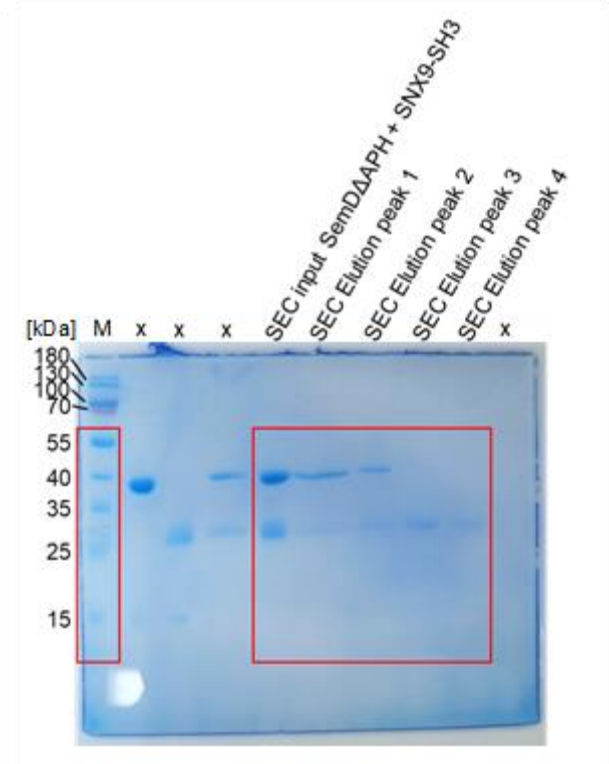

5 Part III: Further Results

5.1 Introduction and Summary of previous results

Previous studies have shown that all nine *Ctr* Pmps mediate adhesion to epithelial cells [93]. However, the adhesion capacity of *Ctr* PmpG to epithelial cells remains controversial, as different assays using different *Ctr* PmpG fragments have led to inconsistent results [93, 96, 236]. Nevertheless, PmpG is believed to play a specific role in chlamydial infections, as it belongs to a species-specifically expanded subgroup, making it a particularly interesting Pmp. Furthermore, for none of the nine *Ctr* Pmps, the host cell binding partner was identified so far, and the epidermal growth factor receptor (EGFR), the host cell binding partner for *Cpn* Pmp21, the homologue of *Ctr* PmpD, could also not be verified for *Ctr* PmpD [93].

Hence, the aim was to identify a host cell binding partner for *Ctr* PmpD. Doing so, in Manuscript I (section 3), pulldown assays using PmpD as bait on epithelial cells, combined with biochemical assays identified secreted clusterin (sCLU) as a host cell binding partner for *Ctr* PmpD. sCLU is a secreted host cell protein which has a chaperone-like activity in the extracellular space by binding to aggregated proteins, such as those with amyloid-like structures, and facilitating their cellular uptake for degradation [237]. Additionally, sCLU inhibits the terminal complement pathway by interfering with the membrane attack complex (MAC), which may help *Ctr* to evade the immune system [238]. Infection assays, manipulating sCLU abundancies during the early stages of infection in HEp-2 cells showed that the absence of sCLU significantly reduced the *Ctr* infection rate. This indicated the crucial role of sCLU in the early stages of a *Ctr* infection.

5.2 Objectives

One aim is to assess and characterize the adhesion capacity of PmpG to epithelial cells. A soluble fragment, G72, which is known to be proteolytically processed *in vivo,* will be used. Recombinant G72 (rG72) is added to cell culture medium and incubated with confluent epithelial cells to evaluate its adhesion capacity. Investigating the

adhesion of PmpG to epithelial cells should help develop a standardized protocol that can then be further developed for identifying host cell binding partners for *Ctr* PmpG. The second aim focuses on *Ctr* PmpD. In parallel with the pulldown approach presented in Manuscript I (section 3), a second approach is conducted. *Ctr* is transformed with a construct encoding the PmpD passenger domain ($PmpD_{PD}$) genetically fused to APEX2. Transformed EBs are used for infection assays on epithelial cells. During early infection, when EBs adhere to host cells, APEX2 biotinylation is initiated and proteins in close proximity (1 – 10 nm) to APEX2-$PmpD_{PD}$ are biotinylated and subsequently identified via mass spectrometry.

5.3 Material

5.3.1 Chemicals and reagents

Chemical and reagents	Source
4′,6-diamidin-2-phenylindol (DAPI)	Sigma
5-bromo-4-chloro-3-indolyl-phosphat (BCIP)	Sigma
Acetic acid	Roth
Acrylamide (Rotiphorese® Gel 30 (37.5:1))	Roth
Adenine	Sigma
Agar	BD
Agarose	Biozym
Alanine	Merck
Ammonium persulfate (APS)	Merck
Amphotericin B	Life technologies
Ampicillin	Sigma
Arginine	Fluka
Asparagine	Merck
Aspartic acid	Merck
Bovine serum albumin (BSA)	Serva
Bradford reagent	Bio-Rad
Calcium chloride ($CaCl_2$)	Riedel-de Haën
Carrier-DNA	Sigma
Casein peptone	BD
Chloramphenicol	Merck
Cycloheximide	Sigma
Cysteine	Merck

D(+)-Galactose	AppliChem
D(+)-Glucose	Roth
D(+)-Raffinose	Sigma
Deoxynucleoside-5'-Triphosphate (dNTPs)	Fermentas
Dimethylformamide (DMF)	Roth
Dimethyl sulfoxide (DMSO)	Sigma
Dithiothreitol (DTT)	Sigma
DMEM GlutaMAX™	Gibco
Ethanol (96 %)	VWR
Ethidium bromide solution (10 mg/ml)	Roth
Fetal bovine serum (FKS)	Gibco
Gentamycin	Invitrogen
Glutamic acid	Sigma
Glutamine	Merck
Glycerin	AppliChem
Hanks buffered salt solution (HBSS)	Gibco
Hydrogen chloride (HCl)	Roth
Histidine	Roth
Imidazole	Sigma
Isoleucine	Roth
Isopropanol	Roth
Isopropyl β-D-1-thiogalactopyranoside (IPTG)	Roth
Leucine	Roth
Lithium acetate	Roth
Magnesium chloride	Roth
Methionine	Merck
Milk powder	Roth
Ni-NTA Agarose	Cube Biotech
Nitro Blue Tetrazolium (NBT)	Sigma
Non-essential amino acids (MEM)	Gibco
Peptone	Bacto
Phenylalanine	Acros Organics
Polyethylene glycol (PEG)	Roth
Ponceau S	Sigma
Proline	Merck
Protease-Inhibitor-Cocktail (EDTA free)	Roche
Serine	Roth
Sodium chloride	VWR
Sodium dihydrogen phosphate (NaH_2PO_4)	Roth

Sodium dodecyl sulfate (SDS)	Roth
Sodium hydroxide (NaOH)	Roth
Sodium lauroyl sarcosinate (Sarcosyl)	Sigma
Sodium phosphate dibasic (Na_2HPO_4)	Roth
Streptavidin agarose	Thermo
Sucrose	Roth
Tetramethylethylenediamine (TEMED)	Roth
Threonine	Merck
Tris(hydroxymethyl)aminomethane (Tris)	Roth
Triton X-100	Sigma
Tryptone	Difco
Tryptophane	AppliChem
Tween 20	Merck
Tyrosine	AppliChem
Uracil	Sigma
Urea	Sigma
Valine	AppliChem
Vitamine solution (MEM)	Invitrogen
Vectashield	Liniaris
Yeast extract	Bacto
Yeast nitrogen base (YNB)	Difco

5.3.2 Material, machines and devices

Materials	Source
Amicon Ultra centrifugal filter units (various sizes)	Merck milipore
Cell scraper	Nunc
Cell culture flasks (25 cm² and 75 cm²)	Thermo Scientific
Cell culture plates (6-wells and 24-wells)	Thermo Scientific
Cryo tubes (1.8 ml)	Nunc
Cuvettes (disposable)	Sarstedt
Dialysis clips	Pierce
Dialysis tubes (12-15 kDa cut-off)	Serva
Electroporation cuvettes	Bio-Rad
Falcons (15 ml and 50 ml)	Sarstedt
Fernbach flask (1 L)	Duran
Glass beads	Braun
Glass coverslips	Thermo
Glass flasks (50-2000 ml)	Schott
glass test tubes	Duran/Schott

Nitrile gloves	VWR
PCR reaction tubes	Sarstedt
PDVF transfer membrane	Millipore
Petri dishes	Sarstedt
Pipette tips (2 µl, 20 µl, 200 µl, 1000 µl)	Sarstedt
Protein purification manual columns	Thermo
Reaction tubes (1,5 and 2 ml)	Sarstedt
Reaction tubes screw lid (2 ml)	Sarstedt
Round Bottom centrifuge tubes (12 ml)	Greiner
Ultracentrifugation tubes	Beckman Coulter
Whatman blotting paper	VWR

Machines and devices	Source
- 80°C freezer Modell TwinCool	Haier Biomedical
Analytic balance	Sartorius
BioPhotometer Plus	Eppendorf
Centrifuge Avanti J-25 (Rotors: JLA10.500, JA25-50)	Beckmann Coulter
Centrifuge Beckmann J2-21 (Rotors: JA10, JA20)	Beckmann Coulter
Centrifuge Biofuge pico	Heraeus
Centrifuge Biofuge Primo R	Heraeus
Centrifuge Megafuge 1.0R	Heraeus
Centrifuge Multifuge 3SR+	Heraeus
Centrifuge Rotanta 460R	Hettich
Electrophoresis Power Supply EPS 301 and EPS 601	Amersham Bioscience
Electroporation system GenePulser	Bio-Rad
Gel documentation system	Bio-Rad
Gilson Pipetman micropipettes - P2 (0.2-2 µl) - P20 (2-20 µl) - P200 (20-200 µl) - P1000(100-1000 µl)	Gilson
Homogenizer Precellys 24	Bertin Technologies
Incubator HEPA class 100	Thermo
Incubator Memmert BE Modell 600	Heraeus
Incubator Multitron	Infors
Magnetic stirrer	IKA
Microwave	Bosch
NanoDrop 2000C	Peqlab
PCR Thermocycler PTC-200	MJ Research
pH-Meter pH720	inoLab

Pierce G2 Fast Blotter (Western blot apparatus)	Pierce
Safety bench Hera safe	Heraeus
SDS-electrophoresis apparatus SE-260	Hoefer
Shakers	Infors
SpeedVac vacuum concentrator SC110	Savant
Thermoblock	West Instruments
Ultrasonic bath	Bandelin
Ultrasonic Homogenizer Sonopuls HD2200	Bandelin
Vortex Genie 2	Scientific Industries

5.3.3 Solutions and buffers

Solutions and buffers	Compositions
4x Running gel buffer	1.5 M Tris/HCl 0.4 % SDS pH 8,8
4x Stacking gel buffer	0.5 M Tris/HCl 0.4 % SDS pH 6,8
4x SDS Protein blue marker buffer	200 mM Tris/HCl (pH 6,9) 8 % SDS 0.2 % Bromophenol blue 20 % Glycerin
5-Bromo-4-chloro-3-indolyl phosphate (BCIP) solution	5% (w/v) BCIP in 10 ml Dimethylformamide (DMF)
Blocking solution	5 g milk powder 100 ml PBS pH 7,4 0.05 % Tween 20
Buffer B (Denaturing lysis buffer)	8 M Urea 0.1 M NaH_2PO_4 10 mM Tris pH 8.0
Buffer C (Denaturing protein purification buffer)	8 M Urea 0.1 M NaH_2PO_4 10 mM Tris pH 6.3
Buffer P1	50 mM Tris/HCl pH 8,0 10 mM EDTA pH 8,0 100 µg/ml RNase in ddH_2O

Buffer P2	200 mM NaOH 1 %SDS in ddH_2O
Buffer P3	2.55 M KOAc in ddH_2O
$CaCl_2$ buffer	10 mM Tris/HCl 50 mM $CaCl_2$ pH 7.4
Detection buffer (Western Blot)	0.1 M Tris/HCl pH9,5 0.1 M NaCl 50 mM MgCl2 in ddH_2O
Lithium acetate buffer	1 M Lithium acetate, pH 8.4 – 8.9 in ddH_2O
Nitro blue tetrazolium (NBT) solution	5 % NBT in 70 % DMF
Polyethylenglykol (PEG)	50 % (w/v) PEG in ddH_2O
Phosphate buffered saline (PBS), 1x	137 mM NaCl 2.7 mM KCl 10 mM Na_2HPO_4 1.8 mM KH_2PO_4 in ddH_2O
PBS ++ buffer	PBS buffer 0.5 mM $MgCl_2$ 1 mM $CaCl_2$
Quenching solution	PBS++ 10 mM Trolox 20 mM Sodium ascorbate 20 mM Sodium azid
RIPA buffer	25 mM Tris/HCl (pH 7.6) 1% NP-40 1 % Sodium Deoxycholate 0.1 % SDS 150 mM NaCl in ddH_2O
SDS-PAGE running buffer	50 mM Tris 0.2 mM Glycine 0.1 % SDS pH 8.3
SPG buffer	75 g Sucrose 0.52 g KH_2PO_4 1.53 g Na_2HPO_4 0.72 g Glutamic acid in 1 L ddH_2O, pH 7.5

Transfer buffer (Western Blot)	25 mM Tris 150 mM Glycine 10 % Methanol 0.05 % SDS in ddH_2O

5.3.4 Enzymes

The used restriction enzymes were applied as described by the manufacturer for linearization or restriction analysis of plasmids.

Enzyme	Source
ALLin™ HiFi DNA-Polymerase, 2 U/µl	HighQu
DNAse	Sigma
Lysozym	Sigma
ProteinaseK	Roche
Restriction enzymes (*Sma*I, *Dpn*I, *Nde*I, *Nco*I)	Thermo Fisher
Trypsin	Invitrogen

5.3.5 Antibodies

5.3.5.1 Primary antibodies

Antibody	Reactivity	Origin	Dilution	Source
α-Penta-His	10x Histidine Tag	mouse	1:2500 (WB)	Qiagen
α-FLAG-HRP	FLAG-tag	mouse	1:1000 (WB)	Merck
α-MOMP	*Ctr* MOMP	goat	1:500 (IF)	BioRad
α-tubulin	human tubulin	rat	1:1000 (WB)	SantaCruz
α-actin	human actin	mouse	1:2000 (WB)	Sigma

WB = Western blot, IF = Immunofluorescence

5.3.5.2 Secondary antibodies

Antibody	Reactivity	Origin	Dilution	Source
α-mouse-AP	mouse	rabbit	1:30000 (WB)	Sigma
α-rat-AP	rat	rabbit	1:30000 (WB)	Sigma
α-goat Alexa Fluor™ 594	goat	donkey	1:200 (IF)	Thermo Fisher

WB = Western blot, IF = Immunofluorescence

5.3.6 Kits

Kit	Source
Plasmid Midi Kit	Qiagen

5.3.7 Plasmids and oligonucleotides

5.3.7.1 Oligonucleotides for cloning and sequencing

Oligonucleotides were designed for cloning via homologous recombination in *S. cerevisiae* and have a length of roughly 60 nucleotides in total, from which 40 nucleotides are homolog to the vector and 20 nucleotides are homolog to the gene. If required, the oligonucleotide was extended to insert a sequence coding for a tag or spacer region. Oligonucleotides for sequencing have a length of ~ 20 nucleotides.

	Number	Name	Sequence (5'-3')
C	C-4543	PmpD pKM32 fwd (pFK14)	GAAATTAACTATGAGAGGATCTCACCATCACCATCACCATCACCATCACCATGATAGTCAGGCTGAAGGACAG
C	C-4544	PmpD pKM32 rvs (pFK14)	GTCCAAGCTCAGCTAATTAAGCTTGGCTGCAGGTCGACTAACGTAAGCAAGAAATAGCACC
C	C-4540	PmpG pKM32 fwd (pFK15)	GAAATTAACTATGAGAGGATCTCACCATCACCATCACCATCACCATGCAGCAGAAATCATGATTCCT
C	C-4542	PmpG pKM32 rvs (pFK15)	GGAGTCCAAGCTCAGCTAATTAAGCTTGGCTGCAGGTCGACTATGGAACCAAAGAAGCTACTCG
C	C-4514	1_incDprom(40)+PmpISS(20) fwd	GAGAAATGAGATCTGGCTAAAATCTGTCGAAGTGAGGTTTATGCGACCTGATCATATGAAC
C	C-4515	2_BB(40)+NcoI+APEX2(20) rvs	CCAAAGAGTGTTCGCAACGAGTGTAGATTGACGTTCTGGATGCCATGGGACGGCATCAGCAAACCCAAG
C	C-4516	3_APEX2(40)+NcoI+BB(20) fwd	GCTCACCAAAAGCTTTCCGAGCTTGGGTTTGCTGATGCCGTCCCATGGCATCCAGAACGTCAATCTACAC
C	C-4517	4_BB(20)+incD term.(40)	GTCTCCCTCCTCTTTTTCCTACGCGAATCACATGTCATCCCTAGAACCTGTAAGTGGTCCC
C	C-4518	5_APEX-PmpD32_fwd (pFK27)	GCTCACCAAAAGCTTTCCGAGCTTGGGTTTGCTGATGCCGTCTGCGTAGATCTTCATGCTGG

C	C-4519	6_PmpD1207-PmpIBB_rvs (pFK27)	CCAAAGAGTGTTCGCAACGAGTGTAGATTGACGTTCTGGATGAGGATCTAATCGATATCCAGTAGG
S	C-3571	pDMs2-8 for	TTAGATTCTTCAAAGCTCAGCGAG
S	C-3573	pDMs5-9 in myc Rev	TTTCCTACGCGAATCACATGTC
S	C-4534	PmpD middle	CGGGTTCGTATTGTAGATAAC
S	C-4535	PmpD middle rev	CATTCAGGGCTGTAATATGCG
S	C-4536	Seq_PmpG start_fwd	CGAACTCAATATCTCTATCCG
S	C-4537	Seq_PmpG start_rvs	GTCCGTATGTTCTCGAAAGTC
S	C-4538	Seq_PmpG middle_fwd	GCAGTTACGAATCCTCCTAC
S	C-4539	Seq_PmpG middle_rvs	CGTATATCTAAAATGGATCCC
S	C-4507	D68-699 middle	GCTAATGGAGGAGCGATTG
S	C-4508	D68-1232 middle	CCACTCTCTTCAGGATATTC

C = Oligonucleotide for cloning, S = Oligonucleotide for sequencing

5.3.7.2 Plasmids

The plasmid numbers correspond to an internal plasmid collection.

Number	Name	Construct
1941	pKM32	Expression vector with an N-terminal His-tag and with integrated CEN-ARS-URA3 from pAC2 (Mölleken et al. [94])
2991	pKM280	pKM213 (Braun et al. [239]) with the complete *pgp1* ORF
4264	pSW24	Chlamydial expression vector with 3x FLAG-tag and APEX2 (Wintgens [236])
4261	pFK19	Expression vector pKM32 with *pmpD* fragment (residues 68-698) integrated with an N-terminal 10xHis-tag
4252	pFK15	Expression vector pKM32 with *pmpG* fragment (residues 27-710) integrated with an N-terminal 10xHis-tag

4253	pFK26	Expression vector pKM280 with *pmpI* SS, 3x Flag-tag, APEX2 and *pmpI* β-barrel
4254	pFK27	Expression vector pFK26 with *pmpI* SS, 3x Flag-tag, APEX2, *pmpD* fragment (32-1207) and *pmpI* β-barrel

5.3.8 Cells and cell lines

	Name	Feature
Prokaryotic cells and cell lines	*Escherichia coli* Origami (DE3)	*Δ(ara-leu)7697 ΔlacX74 ΔphoA Pvu*II *phoR araD139 ahpC galE galK rpsL* F'[*lac*$^+$ *lacI*^{q} *pro*] (DE3) *gor522*::Tn*10 trxB* (Str^R, Tet^R) (Novagen)
	Escherichia coli XL1-blue	recA1 endA1 gyrA96 thi-1 hsdR17 supE44 relA1 lac [F proAB lacIqZΔM15 Tn10 (Tetr)], (Stratagene)
	Escherichia coli GM48	F– thr leu thi lacY galK galT ara fhuA tsx dam dcm glnV44
	Chlamydia trachomatis serovar L2/434/Bu	ATCC No. VR-902B
Eukaryotic cells and cell lines	*Saccharomyces cerevisiae* CEN.PK2-1C	*MATα ura3-52; trp1-289: leu2-3, 11; his3-Δ1[240]*
	HEp-2 cell line	Epithelial laryngeal carcinoma cell line, human origin, HeLa morphology (ATTC-No.: CCL-23)

5.3.9 DNA and Protein size standards

Ladder	Standard size	Source
PageRuler^{TM} Prestained	180, 130, 100, 70, 55, 40, 35, 25, 15, 10 [kDa]	Thermo Fisher
PageRuler^{TM} Prestained Plus	250, 130, 100, 70, 55, 35, 25, 15, 10 [kDa]	Thermo Fisher
1 kb DNA-Ladder Mix	10000, 8000, 6000, 5000, 4000, 3500, 3000, 2500, 2000, 1500, 1200, 1000, 900, 800, 700, 600, 500, 400, 300, 200, 100 [bp]	Thermo Fisher

5.3.10 Media

Medium	Composition
Cell culture medium	500 ml DMEM GlutaMAX™ 50 ml FKS 5 ml MEM non-essential amino acids (100 X) 5 ml MEM vitamins (100 X) 5 ml Amphotericin B (250 µg/ml) 500 µl Gentamycin (50 mg/ml)
Chlamydia cultivation medium	Cell culture medium + 12 µl/ml Cycloheximide
LB medium (*E. coli*)	10 g Bacto Tryptone 5 g Yeast extract 5 g NaCl For plates: 13.5 g Agar The components are mixed, dissolved in 1 L diH_2O and autoclaved. After cooling down to at least 50 °C and shortly before usage, required antibiotics are supplemented (Ampicillin: 50 µg/ml, Kanamycin: 10 µg/ml and 15 µg/ml for liquid and solid medium, respectively)
YPD$^+$ medium (*S. cerevisiae*)	20 g Glucose 10 g Yeast extract 20 g Casein Peptone 2 ml Adenine stock solution (2 mg/ml) 4 ml Tryptophan stock solution (5 mg/ml) For plates: 13.5 g Agar Components are mixed, dissolved in 1 L diH_2O and autoclaved.
SD-minimal medium (*S. cerevisiae*)	20 g Glucose 1.7 g Yeast Nitrogen Base 5 g Ammonium sulfate 2 g Amino acid mix For plates: 15 g Agar Components are mixed, dissolved in 1 L diH_2O and the pH is adjusted to 6.0. Afterwards, the medium is autoclaved. For selection medium, the corresponding amino acid(s) or nucleobase is not added.

Amino acid mix	0.5 g	Adenine	10 g	Leucine
	2 g	Alanine	2 g	Lysine
	2 g	Arginine	2 g	Methionine
	2 g	Asparagine	2 g	PABA
	2 g	Aspartic acid	2 g	Phenylalanine
	2 g	Cysteine	2 g	Proline
	2 g	Glutamine	2 g	Serine
	2 g	Glutamic acid	2 g	Threonine
	2 g	Glycine	2 g	Tryptophan
	2 g	Histidine	2 g	Tyrosine
	2 g	Inositol	2 g	Uracil
	2 g	Isoleucine	2 g	Valine

5.4 Methods

5.4.1 Cultivation of different organisms

5.4.1.1 Cultivation of Saccharomyces cerevisiae

Cultivation of *S. cerevisiae* CEN.PK2 was performed at 30 °C in YPD^{+}-Medium and shaking. Transformed *S. cerevisiae* CEN.PK2 was cultivated at 30 °C and shaking in SD-medium, lacking the marker amino acid which is present in plasmid-expressing cells.

5.4.1.2 Cultivation of E. coli

E. coli strains Origami (DE3), XL1-Blue and GM48 are cultivated under aerobic conditions at 37 °C in LB-Medium and shaking. For the selection of transformed *E. coli*, the LB-medium was supplemented with Ampicillin (50 µg/ml).

5.4.1.3 Cultivation of epithelial HEp-2 cells

Eukaryotic HEp-2 cells were cultivated in cell culture medium at 37 °C and 6 % CO_2.

5.4.1.3.1 Trypsinization and passaging of adherent HEp-2 cells

Prior to passaging, the adherent HEp-2 cells are detached from the cell culture flask by trypsin. Trypsin is a sequence specific protease which cleaves the extracellular matrix as well as cell contacts. Thereby, the cells are detached form the cell culture flask and further they are partially separated.

- Cell culture medium is carefully removed from HEp-2 cells grown in 75 cm² flaks
- Cells are carefully washed three times with 10 ml HBSS

- Cells layer is covered with 5 ml trypsin solution and incubated at 37 °C until cells detach
- Trypsin solution is neutralized by the addition of 5 ml cell culture medium
- Cell solution is transferred into a 12 ml round-bottom centrifuge tube and cells are pelleted for 10 min at 500 rpm (Rotanta 460R)
- Supernatant is discarded and the cell pellet is resolved in 5ml of fresh cell culture medium
- For passaging of cells in according flasks, cell solution is diluted as follows:
    - 75 cm² flask: 1 ml of trypsinized cells in 15 ml cell culture medium
    - 25 cm² flask: 0.5 ml of trypsinized cells in 5 ml cell culture medium
    - 6- /24-well plates: trypsinized cells are diluted 1:10-1:30 with cell culture medium and wells are filled with 1 ml of diluted cell suspension
- Cells were incubated for 2-3 days at 37 °C, 6 % CO_2

5.4.1.4 Cultivation of Chlamydia

Chlamydia trachomatis (Ctr) and *Chlamydia pneumoniae (Cpn)* are obligate intracellular pathogens and hence need a host cell for successful division and replication. Therefore, monolayers of HEp-2 cells are used for cultivating chlamydia. The cell culture medium is supplemented with 12 µl/ml Cycloheximide (100 mg/ml), inhibiting human cell replication. Propagated *Chlamydia* can be stored in SPG buffer at -80 °C.

For the cultivation of *Chlamydia*, confluent 25 cm² flaks are used.

- 1 ml of *Chlamydia* (~ 10^7 IFU/ml) in SPG is thawed and filled to 5 ml with cell culture medium
- *Chlamydia* suspension is added to confluently grown HEp-2 cells in a 25 cm² flak
- To facilitate the attachment and uptake of *Chlamydia* to and into HEp-2 cells, flasks are centrifuged at 1560 x g and 30 °C for 60 min (Rotana 460R)
- Cells are incubated for 1h at 37 °C and 6 % CO_2
- Cell culture medium is replaced with 5 ml of fresh cell culture medium supplemented with Cycloheximide (12 µl/ml)
- Infected cells are incubated at 37 °C and 6 % CO2 for 2 days (*Ctr*) or 3 days (*Cpn*)

- Cells are detached form the flask using a sterile cell scraper and cell suspension is collected in a 50 ml centrifuge tube
- Cell suspension is sonicated for 45 sec with 40 % power to disrupt cells and centrifuged for 10 min at 2670 rpm (Rotana 460R)
- Supernatant is collected in a new tube and centrifuged again for 10 min at 2670 x g (Rotana 460R)
- The supernatant can be further processed as follows:
    - Infection of a new confluent 25 cm² flask (dilution 1.2 - 1:4)
    - Frozen in SPG at -80 °C (dilution 1:1)
    - Concentration of the chlamydial suspension
        - Chlamydial suspension is centrifuged for 30 min at 4 °C and 15000 rpm (Biofuge Primo R, Heraeus)
            - Supernatant is discarded and pellet is resuspended in minimal amounts of SPG buffer, using an ultrasound bath, and frozen at -80 °C
            - Or
            - Pellet is processed for extraction of genomic chlamydial DNA (see section 5.4.1.5)

5.4.1.5 Extraction of chlamydial DNA

- Chlamydial pellet (see section 5.4.1.4) is two times washed in 1 ml H_2O and centrifuged for 30 min at 4 °C and 15000 rpm (Biofuge Primo R, Heraeus)
- Washed chlamydial pellet is resuspended in 100 µl H_2O with 10 µl of Proteinase K (40 mg/ml) and incubated for 2 h at 55 °C
- Proteinase K is inactivated by incubation at 100 °C for 10 min
- 140 µl H_2O and 250 µl Phenol-Chloroform are added to the mixture and the suspension is centrifuged at 13000 rpm for 10 min at RT (Biofuge Primo R, Heraeus)
- The upper 200 µl of the suspension are transferred to a new centrifugation tube and 200 µl isopropanol and 20 µl sodium acetate are added
- The suspension is frozen for 30 min at -80 °C
- After the suspension was thaw on ice, it is centrifuged for 30 min at 4 °C, 15000 rpm (Biofuge Primo R, Heraeus)

- The supernatant is discarded and the pellet is washed with 500 µl 70 % ethanol
- DNA is pelleted again by centrifugation for 30 min at 4 °C, 15000 rpm (Biofuge Primo R, Heraeus)
- The supernatant is discarded and the DNA pellet is dried before resuspension in 50 µl H_2O

5.4.2 Biomolecular methods

5.4.2.1 Transformation and homologous recombination in S. cerevisiae

Integration of a gene of interest into a linearized target vector is performed using the model organism *S. cerevisiae*. The linearized vectors as well as the amplified gene of interest, carrying homology overhang regions to the linearized vector, are transformed into S. cerevisiae, using the lithium acetate (LiAc) method [241]. The gene of interest is integrated into the vector by homologous recombination.

- 5 ml of liquid YPD^+-medium is inoculated with a swap of CEN.PK2 and incubated overnight at 30 °C while shaking (140 rpm)
- A fraction of the overnight culture is diluted in 50 ml YPD^+-medium, reaching a final OD_{600} of 0.1
- The main culture is incubated at 30 °C for 4-5 h until an OD_{600} is reached, corresponding to 2 x 10^7 cells/ml
- The culture is harvest by centrifugation for 5 min at 3500 rpm, 30 °C (Megafuge 1.0 R)
- The supernatant is discarded and the pellet is washed in 25 ml ddH_2O
- Yeast cells are centrifuged again (5 min, 3500 rpm, 30 °C (Megafuge 1.0 R)) and the pellet is resuspended in 1 ml of 100 mM LiAc (pH 8.4 – 8.9)
- The suspension is transferred to a 1.5 ml centrifuge tube and yeast cells are sedimented again for 5 seconds at 13000 rpm (Heraeus Biofuge pico)
- The supernatant is discarded and the sedimented cells are resuspended in 500 µl 100 mM LiAc (pH 8.4 – 8.9), reaching a concentration of 2 x 10^9 cells/ml
    - Yeast cells can be stored under the given conditions at 4 °C for up to one week
- For each transformation, 50 µl from the stock are transferred into a separate 1.5 ml centrifuge tube and pelleted again for 15 seconds, 13000 rpm, RT

- Supernatant is carefully removed and discarded
- The transformation mix is added to the aliquoted yeast cells in the following order:
    - 240 µl sterile PEG (50% w/v)
    - 36 µl of 1 M LiAc
    - 50 µl of ss-DNA (2 mg/ml)
        - Previously denatured at 100 °C (5 min) and quickly cooled on ice
    - x µl (0.1-10 µg) linearized vector + DNA fragment (1:3 ratio)
        - negative control: linearized vector only
        - positive control: plasmid DNA
    - 34 – x µl ddH_2O
- Transformation mix is vortexed and incubated for 30 min at 30 °C and then for 30 min at 42 °C
- Transformation mix is centrifuged for 5 sec at 13000 rpm
- Supernatant is discarded and cell pellet is resolved in 200 µl ddH_2O
- From the suspension 80 % and 20 % are platted on two separate SD-Agar plates and colonies are grown for 2-3 days at 30 °C

5.4.2.2 DNA isolation from S. cerevisiae

Plasmids generated by homolog recombination in *S. cerevisiae* need to be isolated for plasmid amplification.

- 5 ml liquid SD medium is inoculated with a single yeast colony carrying the desired plasmid (prepared in section 5.4.2.1)
- Culture is grown over night at 30 °C and 140 rpm
- From the 5 ml overnight culture, 2 ml are taken and transferred into a 2 ml reaction tube
- Yeast cells are centrifuged for 5 sec at 13000 rpm (Biofuge Pico)
- The supernatant is discarded and the cell pellet is washed in 1 ml ddH_2O and pelleted again by centrifugation (5 sec, 13000 rpm)
- The supernatant is discarded and the pellet is resuspended in 300 µl P1 buffer
- To the suspension, 300 µl P2 buffer and 1/3 of the volume of sterilized glass beads are added

- The reaction tube is placed in the Precellys24 and yeast cells are disrupted by vibrating twice for 30 seconds
- Suspension is sedimented for 2 min at 2000 rpm and the supernatant is carefully collected in a new 2 ml reaction tube
- 500 µl P3 buffer is added to the transferred supernatant, the suspension is gently mixed by inverting the reaction tube and then incubated on ice for 10 min
- The suspension is centrifuged for 10 min at 13000 rpm and 750 µl of the suspension are transferred in a new reaction tube
- The transferred suspension is topped with 750 µl ice cold isopropanol, vortexed and centrifuged for 30 min at 13000 rpm
- The supernatant is discarded and the pellet is overlaid with 500 µl 70 % EtOH
    - Pellet is not to be resuspended in ethanol
- Reaction tube is centrifuged for 10 min at 13000 rpm and supernatant is removed
- The pellet is dried and resuspended in 20 µl ddH_2O

5.4.2.3 Transformation in E. coli *using electroporation*

For the transformation of plasmid DNA into *E. coli* using electroporation, electrocompetent *E. coli* cells are exposed to electric voltage. Thereby, the cell membrane temporarily becomes permeable which enables DNA uptake.

- Electrocompetent *E. coli* cells, stored at -80 °C are thaw on ice
- 5-10 µl DNA is topped to 300 µl with ddH_2O and transferred into the precooled electroporation cuvette
- 10 µl electrocompetent *E. coli* cells are added and mixed by pipetting up and down
- Electroporation is performed (Gene Pulser) at 2.1 V, 100 Ohm and 25 µF
- Immediately, 1 ml LB is added to the electroporated cells and suspension is transferred into a sterile reaction tube
- Cells are incubated for 30 – 60 min at 140 rpm and 37 °C
- Cells are pelleted via centrifugation for 5 sec at 13000 rpm
- Supernatant is removed down to 100 µl
- Cells are resuspended in the residual supernatant and platted on LB agar plates, supplemented with the appropriate antibiotics

- Transformed *E. coli* are grown over night at 37 °C

5.4.2.4 Transformation of Chlamydia trachomatis *L2*

- *Ctr* L2 is aliquoted to 250 µl ant 100 µl in separate reaction tubes and EBs are pelleted by centrifugation for 20 min at 15000 rpm, 4 °C
- Supernatant is discarded and each pellet is resuspended in 100 µl $CaCl_2$ buffer, using an ultrasound bath
- 2 µg of plasmid DNA is added to resuspended EBs and incubated for 20 min at RT
- HEp-2 cells from a 75 cm² flask are trypsinated and pelleted for 10 min at 500 rpm (Rotanta 460R)
- Pellet is resuspended in 250 µl $CaCl_2$ buffer
- Each EB aliquot (incubated with DNA) is mixed with 125 µl HEp-2 cells and topped to 2 ml with cell culture medium supplemented with Cycloheximide (12 µl/ml) and transferred in a well of a 6-well plate
- Plate is centrifuged for 60 min at 1200 rpm and 37 °C and infection is allowed at 37 °C and 6 % CO_2
- After 12-18 h, the medium is exchanged with fresh cell culture medium supplemented with Cycloheximide (12 µl/ml) and PenG (1 µg/ml)
- 48 h after centrifugation, cells are scraped with a cell scraper and transferred into a 50 ml Falcon
- Suspension is sonicated for 45 sec with 40 % power to disrupt cells and centrifuged for 15 min at 2800 rpm (Rotana 460R)
- Supernatant is retained, diluted and put on confluently grown HEp-2 cells in a 6 well plate as follows:
    - Well 1: 1.25 ml cell suspension + 0.75 ml cell culture medium
    - Well 2: 0.5 ml cell suspension + 1.5 ml cell culture medium
    - Well 3: 0.25 ml cell suspension + 1.75 ml cell culture medium
- After the plate is centrifuged for 60 min at 1200 rpm and 37 °C, the medium is exchanged with fresh cell culture medium supplemented with Cycloheximide (12 µl/ml) and PenG (1 µg/ml)
- Infection is allowed at 37 °C and 6 % CO_2 for 48 h

- **Harvest**: Cells from wells with visible inclusions are scraped and combined in a single 50 ml Falcon
- **Disruption**: Suspension is sonicated for 45 sec with 40 % power to disrupt cells and centrifuged for 15 min at 2800 rpm (Rotana 460R)
- **Centrifugation**: Supernatant is transferred to new reaction tubes as 2 ml aliquots and pelleted by centrifugation at 15000 rpm and 4 °C for 20 min
- **Infection**: Pellet is resuspended in SPG buffer, topped to 5 ml with cell culture medium, added to confluently grown HEp-2 cells in a 24 cm² flask, centrifuged (60 min, 1200 rpm, 37 °C) and medium is exchanged with fresh cell culture medium supplemented with Cycloheximide (12 µl/ml) and PenG (1 µg/ml)
    - Alternatively, in SPG, suspension can be stored at -80 °C
- Infection is allowed at 37 °C and 6 % CO_2 for 48 h
- Cells are processed as described (Harvest, Disruption and Centrifugation)
    - For cells with inclusions, pellet is resuspended in SPG buffer and diluted 1:5 – 1:10 for reinfection, the rest is stored at -80 °C
    - For cells without (or only with few) inclusions: pellet is resuspended in SPG buffer and diluted 1:1 for a reinfection
- Harvest, Disruption, Centrifugation and Infection are repeated until EBs are propagated and purified sufficiently
    - Pellet after Centrifugation can always be resuspended in SPG buffer and stored at -80 °C

5.4.2.5 Plasmid isolation from E. coli mini-preparation

- A single E. coli colony carrying the desired plasmid is inoculated overnight at 37 °C and 140 rpm in 2 ml LB medium supplemented with the required antibiotics
- 2 ml from the overnight culture are transferred into a sterile reaction tube and centrifuged at 13000 rpm for 5 sec
- Supernatant is discarded and pellet is resuspended in 100 µl buffer P1
- 100 µl buffer P2 is added and mixed by cautiously inverting the reaction tube
- 100 µl buffer P3 is added and mixed by cautiously inverting the reaction tube
- Suspension is centrifuged for 10 min at 13000 rpm
- In a new reaction tube, supernatant is mixed with 1 ml isopropanol by vortexing

- Suspension is centrifuged at 13000 rpm for 20 min
- Supernatant is discarded and 500 µl EtOH (70 %) is added to the pellet
    - Pellet is not dissolved in EtOH
- Suspension is centrifuged at 13000 rpm for 5 min and supernatant is discarded
- DNA pellet is dried using the SpeedVac
- Dried DNA is resuspended in 50 µl ddH_2O
    - Can be used for further processing or stored at -20 °C

5.4.2.6 Plasmid isolation from E. coli *midi-preparation*

Isolation of larger and purer plasmid DNA from *E. coli* is performed by inoculating a single *E. coli* colony carrying the desired plasmid in 25 – 100 ml LB medium supplemented with the required antibiotics overnight at 37 °C while shaking (140 rpm). The DNA from the overnight culture is isolated using the plasmid midi kit from Qiagen, according to the manufacturers protocol [242].

5.4.2.7 Agarose gel electrophoresis

Using an 0.7-1% agarose gel, linearized DNA fragments are compared and analysed. Circular plasmids are digested with restriction endonucleases at 30 – 37 °C for at least 2 h, as specified by the manufacturers protocol.

- 0.7-1 % agarose (w/v) is dissolved in H_2O by heating to 100 °C
- Agarose is cooled down to ~ 50 °C, 1 µg/ml ethidium bromide is added and mixed
- Agarose is solidified by cooling down to RT
- DNA samples are prepared by mixing ~100 ng DNA with DNA blue marker and H_2O to a total volume of 15 µl
- DNA ladder (1 kb DNA-Ladder Mix) and DNA samples are separated at 140 V (20 – 80 min)
- DNA is visualized under UV light

5.4.3 Biochemical methods

5.4.3.1 Induction of gene expression in E. coli

Vectors transformed into *E. coli* for heterologous gene expression are under control of a lac-Operator. Through addition of Isopropyl-β-D-thiogalactopyranosid (IPTG), a mimic of allolactose which binds to a repressor at the operator region, the gene expression is induced.

- Transformed *E. coli* cells are incubated overnight at 37 °C, shaking, in 50 ml LB medium supplemented with the required antibiotics
- OD_{600} of the overnight culture is determined photometrically
- 1 L LB medium supplemented with the required antibiotics is inoculated to a final OD_{600} of 0.1 with the overnight culture
- Culture is grown at 37 °C and 140 rpm for 4-5 h until it reaches an OD_{600} of 0.6-0.8
- The addition of 1 mM IPTG induces gene expression, which is then allowed overnight at 20 °C and 140 rpm
- *E. coli* cells are pelleted by centrifugation at 5000 rpm for 10 min (Beckmann J2-21)
- Supernatant is discarded and pellet is resuspended in 20 ml PBS per L culture
- *E. coli* cells are pelleted at 4600 rpm for 15 min
    - Pellet is resuspended in 2 ml PBS per L culture and frozen at -20 °C

      or
    - Pellet is lysed and further processed as described in section 5.4.3.2

5.4.3.2 E. Coli *cell lysis under denaturing conditions*

For successful protein purification, the proteins of interest need to be released and transferred into the supernatant of *E. coli* cells. Hence, cells are lysed under denaturing conditions (for rG72), using 8 M urea and 1 % Triton X-100.

- Cell pellet of a 1 L culture is resuspended in 20 ml denaturing lysis buffer supplemented with 1 % Triton X-100
- Suspension is incubated overnight at 4 °C on the wheel
- Suspension is sonicated 3 times for 20 sec on ice

    - Between the sonification steps, suspension is cooled down again and mixed by inversion
- Cell lysate is centrifuged for 60 min at 24000 rpm (Avanti J-25) to pellet insoluble cell debris
- Supernatant is transferred into a sterile reaction tube and pellet is discarded

5.4.3.3 Purification of proteins fused to a 10xHis-tag under denaturing conditions using manual columns

- The lysate from section 5.4.3.2, containing the protein of interest, is incubated with 1 ml of equilibrated Ni-NTA agarose per liter of culture
- Imidazole is added to a final concentration of 10 mM
- Agarose and lysate are incubated for 2 h at 4 °C on the wheel
- Mixture is filled into a manual protein purification column with a filter and a sample from the flow through is collected for SDS-PAGE analysis
- The agarose with the bound proteins is washed two times with 15 ml buffer B supplemented with 40 mM Imidazole
    - From each washing step, a sample is taken for SDS-PAGE analysis
- The agarose with the bound proteins is washed two times with 15 ml buffer C supplemented with 80 mM Imidazole
    - From each washing step, a sample is taken for SDS-PAGE analysis
- Manual protein purification column is sealed and 2 ml buffer C supplemented with 500 mM Imidazole is incubated for 5 min with the agarose
    - Elution fraction is collected and protein concentration is measured via Bradford
    - This step is repeated until no more protein is detected in the elution

5.4.3.4 Determination of protein concentration using Bradford

Measuring protein concentrations using the Bradford assay is based on the binding of Coomassie Brilliant Blue G-250 dye, which is a component of the Bradford reagent, to proteins. The dye binds preferentially to basic and aromatic residues and upon binding, its absorption maximum is transferred from λ=470 nm to λ=595 nm. This leads to a change of colour from red to blue. The intensity of the blue colour, which is proportional to the protein concentration, is measured by using a spectrophotometer.

- 790 µl ddH_2O is mixed with 10 µl recombinant protein and 200 µl Bradford reagent
    - For blank, 10 µl recombinant protein are substituted by plain protein buffer
- Mixture is incubated at RT for 10 min and the absorption at λ=595 nm is determined with a spectrophotometer (BioPhotometer plus)
- Protein concentration (µg/ml) is calculated by:
  Concentration = ($absorption_{595nm}$*1000)/(Bradford factor*sample volume)
    - The Bradford factor is determined by a calibration curve using 0.5-10 µg BSA

5.4.3.5 Refolding proteins by dialysis and buffer exchange

- Collected elution fractions are combined as needed
    - For rG72. a final concentration of ~1 mg/ml is targeted
- The length of the dialysis tube (12-15 kDa cut-off) is cut accordingly and boiled in water for 10 min
    - For a 2 ml elution. the dialysis tube should be ~6 cm in length
- Tube is cooled in ice-cold. ddH_2O
- The dialysis tube is sealed on one end with a clip and recombinant protein pipetted into the tube
- The dialysis tube is sealed at the other end as well and incubated for 2 nights in precooled 2 L PBS (pH 7.4), at 4 °C
    - The next morning and the evening after, the buffer is renewed
- The refolded proteins are transferred into a sterile reaction tube and centrifuged for 10 min at 4 °C and 13000 rpm to remove precipitate
- Protein purity can be analysed via SDS-PAGE analysis
- For short-term storage, proteins are kept at 4 °C, for long-term storage, proteins are flash frozen in liquid nitrogen and stored at -80 °C

5.4.3.6 Protein separation via SDS-PAGE

In polyacrylamide gel, denatured proteins are separated according to their molecular weight. Therefore, the proteins are cooked in SDS protein blue marker buffer, containing SDS, which binds to proteins, denatures them and gives them a negative

charge proportional to its length. Additionally, DTT is added to the samples, which breaks disulfide bonds. The protein sample is loaded on a polyacrylamide gel and by applying an electric field, the negatively charged proteins migrate through the gel towards the anode. Thereby, the gel functions as a molecular filter where large proteins migrate slower than small proteins.
A polyacrylamide gel consists of two components; a stacking gel at the top and a running gel at the bottom. The stacking gel concentrates the proteins in a thin band before they then enter the running gel and are separated by their molecular weight.

5.4.3.6.1 Preparation of samples for SDS-PAGE

- Protein is diluted in a reaction tube with ddH_2O to the desired concentration in a volume of 32.5 µl
- 12.5 µl protein blue marker and 5 µl DTT (1M) is added
- Sample is boiled for 10 -15 min at 100 °C
- The sample is cooled down and centrifuged for 5 sec at 13000 rpm
    - The sample can be loaded directly on a gel or can be stored at -20 °C

5.4.3.6.2 Preparation of SDS-Polyacrylamide gel

- A glass plate and a teflon-sheet are pinched in a casting chamber with a spacer in between
- Running gel is mixed and TEMED is added shortly before it is poured between the glass and teflon sheet
- The running gel is covered with isopropanol until it is polymerised
- Isopropanol is removed and gel is washed thoroughly with H_2O
- The stacking gel is mixed and poured on top of the running gel, immediately after a comb is inserted into the stacking gel buffer
- Stacking gel is left until it is polymerized
- Gel is removed from the casting chamber and can immediately be used or stored in wet paper towels at 4 °C for up to 10 days

Reagent	Running gel (for 4 gels)		stacking gel (for 4 gels)
	10 %	**15 %**	
ddH_2O	8.4 ml	5 ml	6 ml
4x running / stacking buffer	5 ml	5 ml	2.5 ml
30 % Acrylamide (37.5:1)	6.7 ml	10 ml	1.5 ml
10 % APS	200 µl	200 µl	200 µl
TEMED	50-100 µl	50-100 µl	50 µl

5.4.3.6.3 SDS gel electrophoresis

- The wells of the gel are marked and the comb is carefully removed
- The gel is clamped in an electrophoresis chamber
- The chamber is filled with 1x running buffer, filling the well with buffer as well
- Per well up to 25 µl of sample can be loaded, one well is loaded with 7 µl protein ladder
- Lid is placed on top and electrophoresis takes place at 200 V for 60-90 min until the ladder is separated nicely

5.4.3.7 Staining of SDS-PAGE gels

To visualize proteins separated by SDS-PAGE, the gels need to be stained with Coomassie brilliant blue G-250 dye. As already described in section 5.4.3.4, Coomassie binds to basic and aromatic amino acids of proteins and absorbs light at 595 nm, appearing blue.

- After electrophoresis, the glass and teflon sheets are carefully disassembled and the stacking gel is removed and discarded
- The running gel is cautiously removed from the plate and washed three times for 10 min each with H_2O, heated to 100 °C in the microwave
    - The washing removes residual SDS and salts form the buffer which would increase the background
- After the third washing step, H_2O is removed and Coomassie solution is added
- The solution with the immersed gel is heated in the microwave at 600 W for 10 sec and then incubated on the shaker (40 rpm) at RT until protein bands appear
- Coomassie solution is collected in a flask (can be reused) and gel is destained in H_2O to remove the staining background

5.4.3.8 Western Blot analysis

The proteins separated by SDS-PAGE can be transferred to a polyvinylidenfluorid (PDVF) membrane. Thereby, the proteins are immobilized on the membrane and can be specifically stained by immunodetection using antibodies.

5.4.3.8.1 Protein transfer to a PVDF membrane

- One PVDF membrane (7 x 9 cm) and two Whatman filter papers (7 x 10 cm) are prepared
- The PVDF membrane is activated in MeOH for 10 min at RT and then equilibrated in transfer buffer
- Whatman papers are directly equilibrated in transfer buffer
- Transfer-sandwich is prepared between the metal plate and the lid of a Pierce G2 Fast Blotter in a distinct order:
  metal plate – Whatman paper – PVDF membrane – gel – Whatman paper – lid
- Proteins are transferred at 25 V, 1A for 20 – 30 min
- PVDF membrane is carefully removed and blocked in blocking solution for 10 min at RT, shaking (40 rpm)

5.4.3.8.2 Protein immunodetection

- PVDF membrane is removed from blocking solution and incubated for 1 h at RT with the primary antibody diluted in blocking solution
  - Alternatively, this step can be done at 4 °C for over night
- PVDF membrane is washed three times in PBS at 40 rpm for 10 min each
  - Removes unspecifically bound primary antibody
- PVDF membrane is incubated with the secondary antibody diluted in blocking solution for 1 h at RT
  - Alternatively, this step can be done at 4 °C for over night
- PVDF membrane is washed three times in PBS as 40 rpm for 10 min each
- PVDF is stained by incubation in the dark in 20 ml detection buffer with 33 µl BCIP and NBT solution each
- The reaction is stopped when bands appear by washing the PVDF membrane in H_2O
- Membrane is air-dried and stored under light-free conditions

5.4.3.9 Detergent extraction assay

- Pooled EBs from infected cells confluently grown in a 24 cm² flask were aliquoted in three reaction tubes and pelleted at 13000 rpm and 4 °C for 30 min
- The pellets were resuspended and incubated for 1 h at 37 °C in
    - 50 µl PBS
    - 50 µl PBS + 1 % Triton X-100
    - 50 µl PBS + 2 % Sarcosyl
- Mixture is ultracentrifuged at 100'000 x g for 1 h at 4 °C
- The supernatant was transferred to a new reaction tube and mixed with SDS sample buffer
- The pellet was resuspended in SDS sample buffer

5.4.3.10 APEX2 biotinylation assay

5.4.3.10.1 Biotinylation of chlamydial surface interaction partners

- Pooled EBs from infected HEp-2 cells confluently grown in a 24 cm² flask are pelleted at 15000 rpm for 20 min
- EBs are washed in 1 ml PBS (pH 7.4) and centrifuged at 15000 rpm for 20 min
- Pellet is resuspended in 200 µl PBS++
- 2.5 mM biotin phenol is added and EBs are incubated for 10 min at 37 °C
- 1 mM H_2O_2 is added and incubated for 1 min sharp
- 200 µl Quenching solution is added and EBs are centrifuged for 20 min at 15000 rpm
- Pellet is washed twice Quenching solution
- EBs are lysed for 30 min on ice with RIPA buffer + 5 mM Trolox + 10 mM Sodium ascorbate + 10 mM Sodium azid
- 100 µl preequilibrated streptavidin agarose is added and incubated overnight at 4 °C, shaking (120 rpm)
- Streptavidin pulldown is performed according to manufacturer's protocol

5.4.3.10.2 Biotinylation of host cell interaction partners

- EBs (MOI = 5) are added to HEp-2 cells in 0.75 ml serum free cell culture medium supplemented with 2.5 mM biotin phenol in a well of a six-well plate

    - HEp-2 cells are preequilibrated in serum free cell culture medium 12 h prior to infection
- EBs and HEp-2 cells are incubated for 20 min rotating (2800 rpm)
- 1 mM H_2O_2 in serum free medium is added for 1 min sharp
- Medium is removed and quenching solution is added immediately
- Cells are washed 3x with quenching solution
- RIPA buffer + 5 mM Trolox + 10 mM Sodium ascorbate + 10 mM Sodium azid is incubated with cells for 30 min on ice
- Cells are scraped, lysate is transferred to a sterile reaction tube and centrifuged at 15000 rpm for 30 min
- Pellet is discarded and 100 µl preequilibrated streptavidin agarose is added to the supernatant and incubated overnight at 4 °C, shaking (120 rpm)
- Streptavidin pulldown is performed according to manufacturer's protocol

5.4.4 Cell biological methods

5.4.4.1 Adhesion assay with soluble recombinant protein

- HEp-2 cells are confluently grown in a 24-well plate (1 * 10^6 cells/well)
- Cells are washed three times with cold HBSS
- Recombinant protein diluted in cell culture medium is incubated on HEp-2 cells at 4 °C
    - Incubation time and protein concentration are adjusted as needed
- Cell culture medium is removed and cells are washed three times with HBSS
- Phospho-lysis buffer is added to each well and incubated for 30 min at 4 °C
- Lysate is collected in a sterile reaction tube and prepared for immunoblotting
    - Lysate is mixed with protein blue marker and boiled for 10 min at 100 °C

5.4.4.2 Immunodetection of Chlamydia using fluorescence microscopy

5.4.4.2.1 Fixation and permeabilization of HEp-2 cells infected with wild type and transformed *Ctr* L2

- HEp-2 cells grown on glass coverslips in a 24-well plate are infected with wild type and transformed *Ctr* L2

- 42 hours after infection, cell culture medium is removed and cells are washed with HBSS
- Cells are fixed and permeabilized by incubation with ice cold methanol for 10 min
- Cells are washed three times with PBS + 0.1 % Saponin
    - Cells can be stored on PBS + 0.1 % Saponin at 4 °C

5.4.4.2.2 Indirect immunofluorescence

- Stored cells from 5.4.4.2.1 are incubated with the primary antibody diluted in 30 µl PBS for 1 h at RT
- Primary antibody is removed and cells are washed three times with PBS
- Fluorescent-labeled secondary antibody is diluted in 30 µl PBS and incubated with cells for 1 h at RT
- Cells are washed three times with PBS
- Dapi (1µg/ml) is diluted in PBS and incubated with cells for 10 min at RT (stains DNA)
- Cells are washed three times with PBS
- A small droplet (2-3 µl) of Vectashield is placed on a microscopy slide
- Dried cells on glass coverslip are placed on the Vectashield drop with the cells facing down
- The edges are sealed with nail polish and can be analysed by fluorescence microscopy or stored at 4 °C for 3-4 days

5.4.5 Bioinformatic programs

To quantify and analyse the results, various bioinformatic tools were utilised.

Tool	Application	Source link
R version 4.4.1 and R Studio	motif search and schematic representation of Pmps	https://cran.r-project.org/bin/windows/base/ https://posit.co/download/rstudio-desktop/
InkScape	preparation of figures	https://inkscape.org/
AlphaFold	Protein structure prediction	https://alphafold.ebi.ac.uk/
Fiji (ImageJ)	Preparation of microscopic images	https://imagej.net/software/fiji/

5.5 Further Results

5.5.1 Adhesion of *Ctr* PmpG to epithelial cells

Ctr PmpG is considered a significant component during the early stages of a chlamydial infection, indicated by several reasons. While *Ctr* possesses only a single PmpG, in other chlamydial species the PmpG subfamily is highly expanded (*Cpn*: 13 members, *Cps*: 14 members, *C. abortus*: 11 members [243]). Additionally, for Pmp17G, a member of the *Cps* PmpG subfamily, the adhesive function was demonstrated and furthermore, its host cell receptor was suggested being the epidermal growth factor receptor (EGFR) [110]. However, for *Ctr* PmpG, no host cell receptor has been proposed and its role as adhesin has not yet been fully elucidated. Becker et al. [93] tested the adhesive function of Pmp passenger domains (PD) to epithelial cells by fusing it with the yeast surface protein Aga2. By quantifying yeast cells bound to epithelial cells, they confirmed that all nine *Ctr* Pmp PDs, including the tested $PmpG_{PD}$ fragment (Fig. 10), mediate similar affinity to epithelial cells [93]. They confirmed these results by showing the adhesion of latex beads coated with $PmpG_{PD}$ to epithelial cells. Moreover, they showed that preincubation of epithelial cells with soluble recombinant $PmpG_{PD}$ could partially neutralize a following *Ctr* infection [93]. Interestingly, Favaroni and Hegemann [96], who used a different PmpG fragment, which spanned only the C-terminal half of the PD (Fig. 10), suggested that this

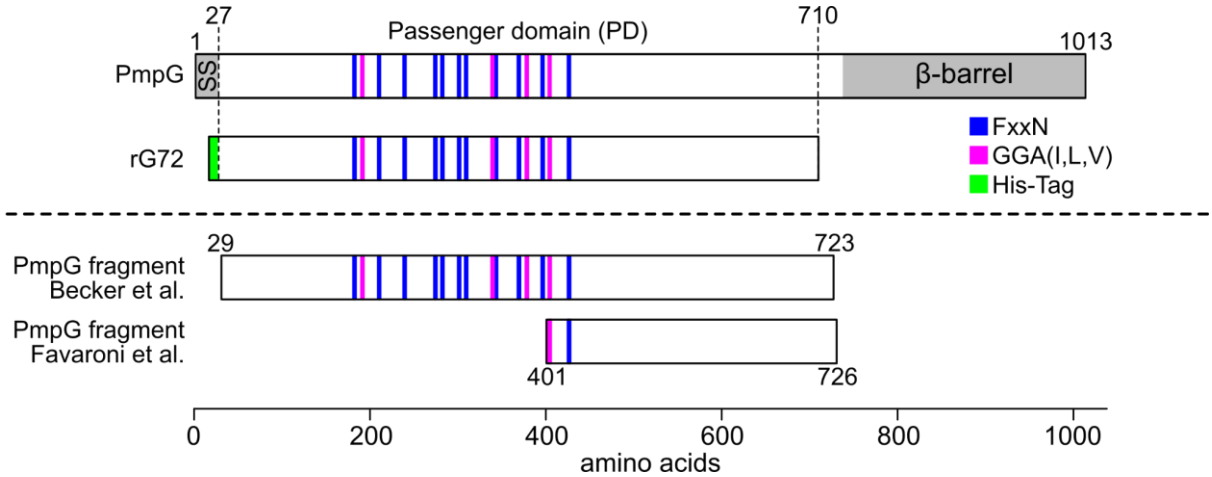

Figure 10: Schematic representation of PmpG from *Ctr* serovar E, DK20

The signal sequence (SS) and β-barrel of the full-length PmpG are indicated by grey boxes. The central passenger domain (in white) contains 11 FxxN (blue) and 4 GGA(I,L,V) (magenta) repeats. rG72 spans residues 27-710 of the full-length PmpG. The genetically fused His-tag is shown in green. The fragments used by Becker et al. [93] and Favaroni and Hegemann [96] are depicted with their respective first and last amino acids indicated.

fragment lacks adhesive capacity to epithelial cells. However, it is important to note that these results are not only based on a different PmpG fragment compared to Becker et al. [93], but also on a different experimental approach for testing PmpG adhesion. Instead of immobilizing the tested PmpG fragment on a surface, they incubated soluble recombinant PmpG with epithelial cells and tested the binding by immunoblot analysis (Fig. 11).

Before identifying a potential host cell binding partner for *Ctr* PmpG, its adhesion capacity to epithelial cells must be clarified. In this work, the adhesion of a fragment similar to the one used by Becker et al. [93] was tested by following an adhesion assay protocol proposed by Favaroni and Hegemann [96] (Fig. 10&11). Specifically, a naturally processed fragment of PmpG (aa 27-710, G72), suggested to be present in the EB outer membrane complex, was identified from literature [92, 244] and genetically fused to an N-terminal 10xHis-tag (Fig. 10). Unlike the PmpG fragment used by Favaroni and Hegemann [96], which contained only one FxxN and one GGA(I,L,V) motif, G72 encompasses all 11 FxxN and 4 GGA(I,L,V) motifs from the full-length PmpG, just like the fragment used by Becker et al. [93] (Fig. 10). Recombinant G72 (rG72) was incubated with epithelial cells, and bound protein was identified by immunoblot analysis (Fig. 11). To assess the rG72 adhesion capacity, either the protein concentration or the incubation time were varied.

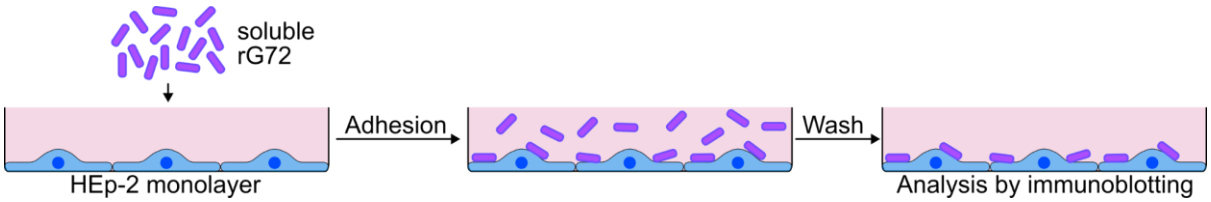

Figure 11: Schematic representation of the performed adhesion assays using soluble rG72
Soluble rG72 was incubated with confluently grown HEp-2 cells. Either the incubation time or the rG72 concentration was varied to assess the adhesion capacity of rG72. After allowing rG72 to adhere to HEp-2 cells, the supernatant was aspirated and unbound protein was removed by washing the cells three times with HBSS. HEp-2 cells were lysed and binding of rG72 was analysed by immunoblotting using an anti-His antibody.

5.5.1.1 rG72 exhibits concentration- and time-dependent binding to HEp-2 cells

In the first adhesion assay, different rG72 concentrations were tested for their adhesion to HEp-2 cells. The incubation time was set to 1 h, while the temperature was kept constant at 4 °C to prevent potential internalization processes. As a negative control, epithelial cells were incubated with plain cell culture medium (Fig. 12b).

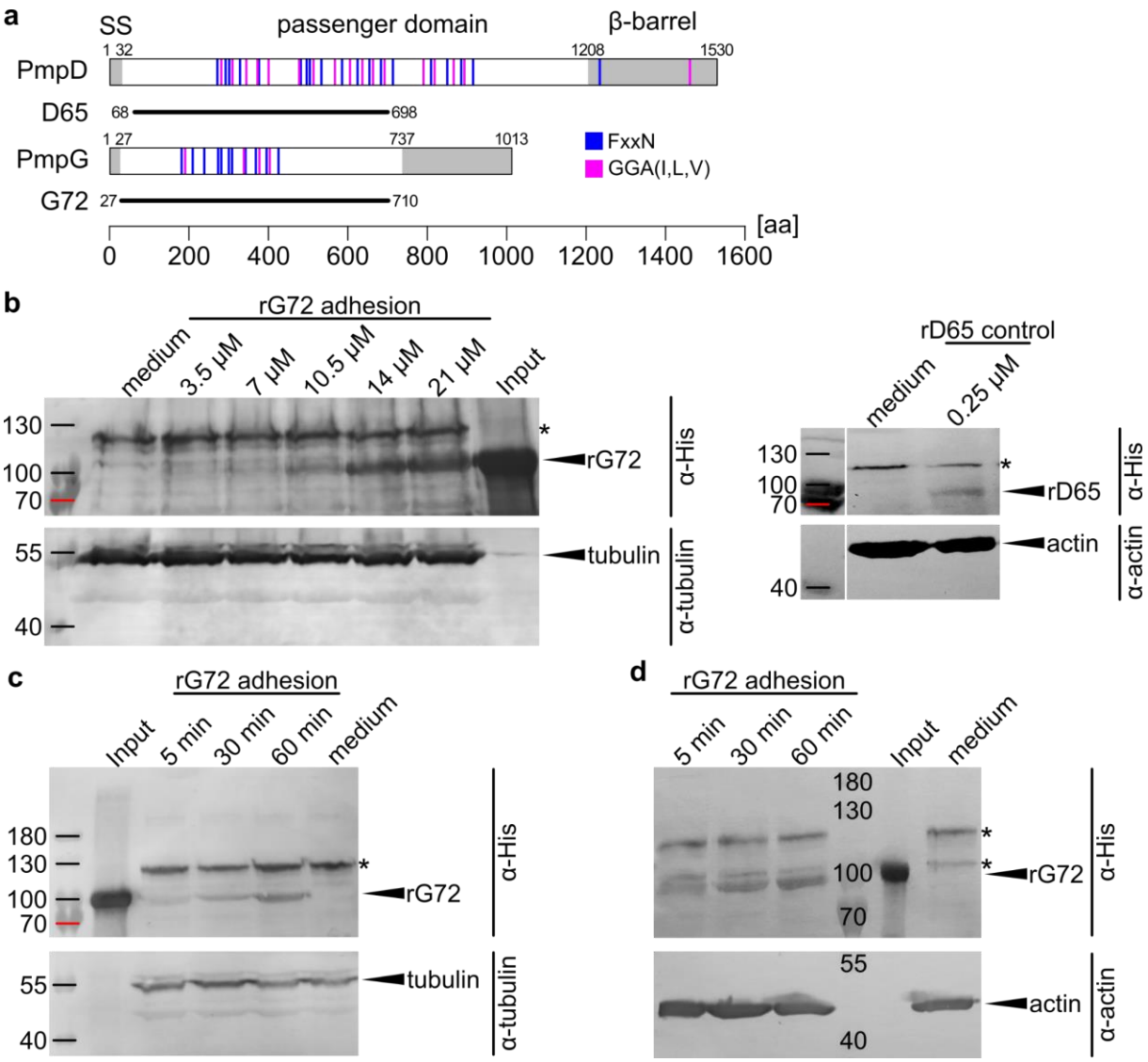

Figure 12: rG72 shows concentration and time dependent adhesion to epithelial HEp-2 cells

a Schematic representation of the PmpG (G72) and PmpD (D65) fragments used in the adhesion assays. **b** The concentration dependent adhesion capacity was tested by incubating 3.5 - 21 µM of rG72 on HEp-2 cells for 1h at 4 °C. Cells grown in plain cell culture medium served as negative control, while soluble rG72 was used as input sample. Additionally, the adhesion capacity of rD65 is shown by incubating 0.25 µM of soluble protein with HEp-2 cells. As internal loading control, verifying a constant amount of HEp-2 cells, tubulin or actin levels were monitored using anti-tubulin or anti-actin antibodies, respectively. rG72 and rD65 were detected using an anti-His antibody. Unspecific bands are marked with asterisks (*). **c** The time dependence of rG72 binding to HEp-2 cells was tested by incubating 10 µM rG72 for 5 - 60 min on HEp-2 cells at 4 °C. Cells grown in plain cell culture medium served as negative control, soluble rG72 was used as input sample. As internal loading control, verifying a constant amount of HEp-2 cells, tubulin level was monitored using an anti-tubulin antibody. Unspecific bands are marked with asterisks (*). **d** Biological replicate of **c**, where actin levels were monitored as internal loading control, using an anti-actin antibody.

Under these experimental conditions, rG72 concentrations higher than 10 µM were needed to detect adhesion to HEp-2 cells by immunoblotting and with increasing concentrations, increasing signal intensities were observed (Fig. 12b). To evaluate the adhesion capacity, rD65, a recombinant *Ctr* PmpD fragment comparable to rG72 (Fig. 12a), was simultaneously tested under the same experimental conditions. Adhesion of rD65, which possesses a genetically fused N-terminal 10xHis-tag, was detectable by immunoblotting at concentrations as low as 0.25 µM (Fig. 12b). This indicates that rG72 mediates relatively weak adhesion to HEp-2 cells compared to rD65, as concentrations of rG72 need to be 40 times higher than those of rD65 for detection by immunoblotting.

To assess changes in adhesion over time, the binding of rG72 to HEp-2 cells was monitored at specific time points between 5 – 60 min at 4 °C, with a constant rG72 concentration of 10 µM (Fig. 12c,d). Bound rG72 was detectable after 5 min of incubation with an increase of bound protein for longer incubation periods (Fig. 12c,d). In summary, these data demonstrate that the PmpG fragment rG72 acts as an adhesin on epithelial cells, as previously suggested by Becker et al. [93]. However, adhesion is indicated to be substantially weaker than, for example, the *Ctr* PmpD fragment, rD65, as 40 times higher concentrations are needed for the detection of bound protein by immunoblotting. Additionally, rG72 binding to HEp-2 cells is detectable after 5 min of incubation, with a significant increase in bound protein over time.

5.5.2 Identification of *Ctr* PmpD binding partners using APEX2 proximity labelling

In previous studies, the formation of homo- and heterooligomeric complexes formed by Pmp passenger domains was demonstrated *in vitro* [96, 245]. Later, Wintgens showed that these oligomers are also conceivable *in vivo*, located on the chlamydial surface [236]. To demonstrate this, he transformed *Ctr* L2 with a plasmid encoding a fusion protein containing the PmpI SS at the N-terminus, followed by a 3x FLAG-tag (for protein detection), APEX2, the PmpI$_{PD}$ and, at the C-terminus, the PmpI β-barrel (Fig. 13b). The peroxidase APEX2 biotinylates proteins within close proximity (1-10 nm) when hydrogen peroxide (H_2O_2) and biotin-phenol are added [236, 246]. The constitutive incD promoter was used for gene expression. With this arrangement, the APEX2-PmpI$_{PD}$ domain was expected to localize on the chlamydial surface, as it is generally proposed for the PD of Pmps. Upon initiation of APEX2 activity, proximal

proteins to APEX2-PmpIPD were biotinylated, which were then separated from non-biotinylated proteins via a streptavidin pulldown. The elution fraction was analysed by mass spectrometry [236]. Under these conditions, initial results indicated that PmpB, PmpG, PmpF and especially PmpD were in close proximity to PmpIPD [236].

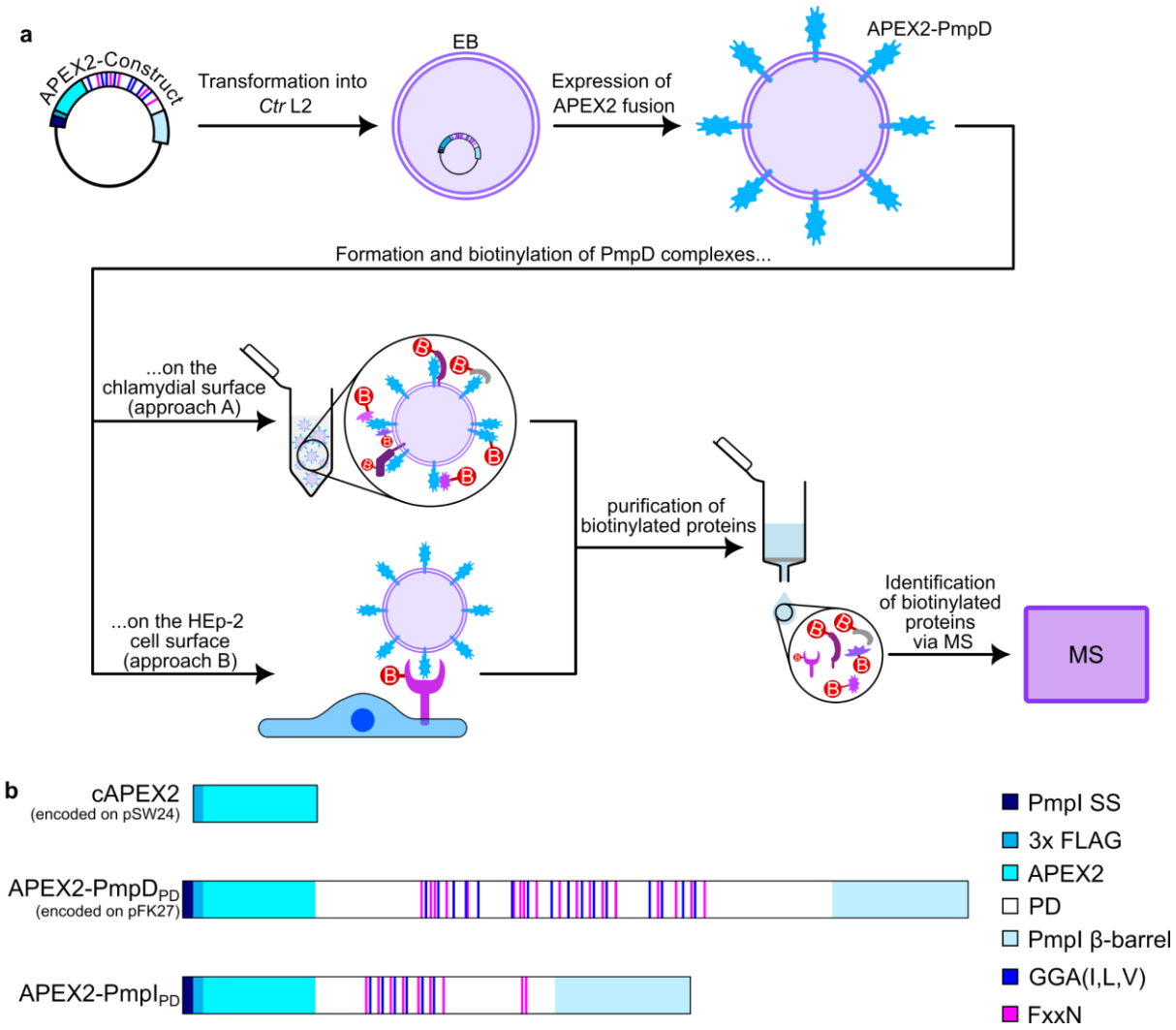

Figure 13: Schematic overview of the experimental procedure and the fusion proteins used

a Schematic overview of the experimental procedure. The plasmid carrying the APEX2 fusion construct is transformed into *Ctr* serovar L2 where the protein is ectopically expressed. Transformed EBs are selected and proteins on the chlamydial surface or on the HEp-2 cell surface forming complexes with the APEX2 fusions are biotinylated. The biotinylated peptides are purified using streptavidin agarose and the enriched proteins in the eluate are analysed by Western blot and identified via mass spectrometry (MS). **b** Schematic overview of the used fusion proteins. cAPEX2 consists of a 3xFLAG-tag and the APEX2 peroxidase, serving as negative control. APEX2-PmpDPD has the PmpI signal sequence (PmpI SS), a 3x FLAG-tag, the APEX2 peroxidase, the PmpD passenger domain with GGA(I,L,V) and FxxN motives and the PmpI β-barrel. APEX2-PmpDPD has the same architecture as APEX2-PmpIPD which was designed and used by Wintgens [236].

In this work, the aim was to identify a host cell binding partner for *Ctr* PmpD. Hence, the methodological approach established by Wintgens [236] was adopted but the plasmid sequence encoding PmpI$_{PD}$ was substituted with that of PmpD$_{PD}$ (residues 32-1207, Fig. 12a), generating a plasmid encoding a fusion protein containing the PmpI SS, a 3x FLAG-tag, APEX2, the PmpD$_{PD}$ and the PmpI β-barrel, under the control of the constitutive incD promoter (pFK27, Fig. 13b). *Ctr* L2 EBs transformed with this plasmid were used for biotinylation of proximal proteins on the chlamydial surface (approach A) or for biotinylation of proteins proximal to APEX2-PmpD$_{PD}$ when the EBs have bound to epithelial cells, identifying a potential *Ctr* PmpD host cell binding partner (Fig. 13a). As negative control, *Ctr* L2 EBs transformed with a plasmid encoding a 3xFLAG-tag genetically fused to APEX2 (pSW24) were used, which protein product was expected to be localized in the chlamydial cytosol (Fig. 13b).

5.5.2.1 APEX2-PmpD$_{PD}$ ectopically expressed in Ctr *L2 localizes in the outer membrane*

Ctr serovar L2 was transformed with pFK27 (APEX2-PmpD$_{PD}$), as described in section 5.4.2.4. To ensure the retention of the plasmid DNA, which encodes ampicillin resistance (Fig. S2), transformed chlamydial EBs were propagated in HEp-2 cells grown in cell culture medium supplemented with penicillin G (which belongs to the same class of antibiotics like ampicillin) (Fig. 14a). DNA from pooled EBs was extracted and PCR on the extracted DNA confirmed the presence of the plasmid (Fig. 14b, section 5.4.1.5). EBs transformed with pSW24, the plasmid encoding cytosolic APEX2 (cAPEX2), were kindly provided by S. Wintgens.

After verifying successful transformation, ectopic protein expression was confirmed by lysing pooled EBs and analyse the lysed fraction via immunoblotting using an anti-FLAG antibody. As negative control, wild-type (wt) *Ctr* L2 EBs were lysed, indicating no unspecific background signal (Fig. 14c). For APEX2-PmpD$_{PD}$ (186.7 kDa), as well as for cAPEX2 (30.3 kDa), bands at approximately the expected molecular weights were detected (Fig. 14c).

To evaluate whether cAPEX2 or APEX2-PmpD$_{PD}$ are membrane-bound or cytosolically located, a detergent extraction assay was performed (Fig. 14d). Pooled EBs from each transformation were aliquoted into two separate reaction tubes and treated with either 1 % Triton X-100, which permeabilizes membranes, or 2 % Sarcosyl, which permeabilizes and solubilises membranes. PBS treatment was used

as negative control, leaving chlamydial EBs intact. The treated EBs were ultracentrifuged to separate insoluble cell debris (pellet fraction) from soluble proteins (supernatant fraction). Both fractions were analysed by immunoblotting using an anti-FLAG antibody for protein detection (Fig. 14d). For both constructs, cAPEX2 and APEX2-PmpD$_{PD}$, analysis of the PBS treatment indicated that both proteins are solely present in the pellet fraction after ultracentrifugation, attributed to intact and pelleted

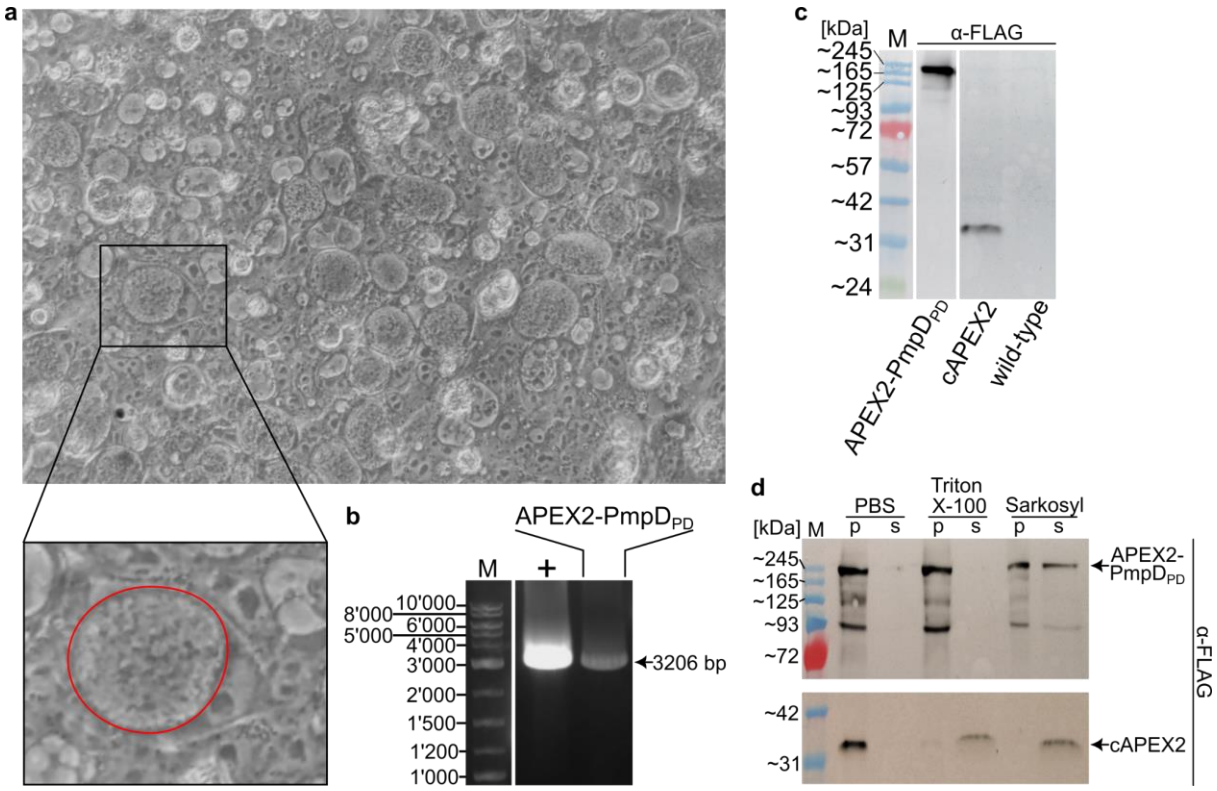

Figure 14: Control experiments for the verification of plasmid transformation and fusion protein expression

a Microscopic picture of HEp-2 cells infected with APEX2-PmpD$_{PD}$ transformed *Ctr* L2, grown for 42 h in cell culture medium supplemented with Penicillin G. The red circle in the zoom shows an inclusion filled with *Ctr* L2. **b** Agarose gel for the analysis of PCR-amplified DNA from *Ctr* L2 transformed with the plasmid carrying the APEX2-PmpD$_{PD}$ fusion construct. Primers aligned in the *apex2* gene (forward primer) and in the *pmpD* gene (reverse primer), leading to a PCR product of 3206 bp. As a positive control (+), the same primers were used for DNA amplification using untransformed plasmid DNA as template. **c** Protein expression in transformed *Ctr* L2 was analysed by the lysis of pooled EBs and analysis of the lysate by immunoblotting, using an anti-FLAG antibody. Untransformed wild-type *Ctr* L2 served as negative control (wild-type). EBs transformed with the plasmid encoding for APEX2-PmpD$_{PD}$ and cAPEX2 showed a band at the expected molecular weight of approximately 200 and 31 kDa, respectively. **d** Pooled EBs ectopically expressing cAPEX2 or APEX2-PmpD$_{PD}$ were treated with PBS, 1 % Triton X-100 and 2 % Sarcosyl and cell debris were separated from soluble proteins by ultracentrifugation. Samples from the pellet (p) and supernatant (s) fractions were analysed by immunoblotting, using an anti-FLAG antibody.

EBs. For detergent-treated samples, immunoblot analysis indicated that cAPEX2 is localised in the chlamydial cytosol. It appeared in the supernatant fraction already with mild detergent treatment, such as 1 % Triton X-100, which permeabilizes the membrane but does not solubilise it, thereby releasing soluble, cytosolic proteins into the supernatant. Conversely, upon treatment with 1% Triton X-100, APEX2-PmpD$_{PD}$ was still exclusively found in the pellet fraction, but for EBs treatment with harsh detergent, such as 2 % Sarcosyl, APEX2-PmpD$_{PD}$ appeared in both the pellet and supernatant fraction (Fig. 14d). Sarcosyl solubilises the membrane, leaving only large membrane debris intact, and thereby transfers most membrane-bound proteins into the supernatant. In conclusion, these results indicate a cytosolic localisation of cAPEX2 and a membrane-bound localization for APEX2-PmpD$_{PD}$.

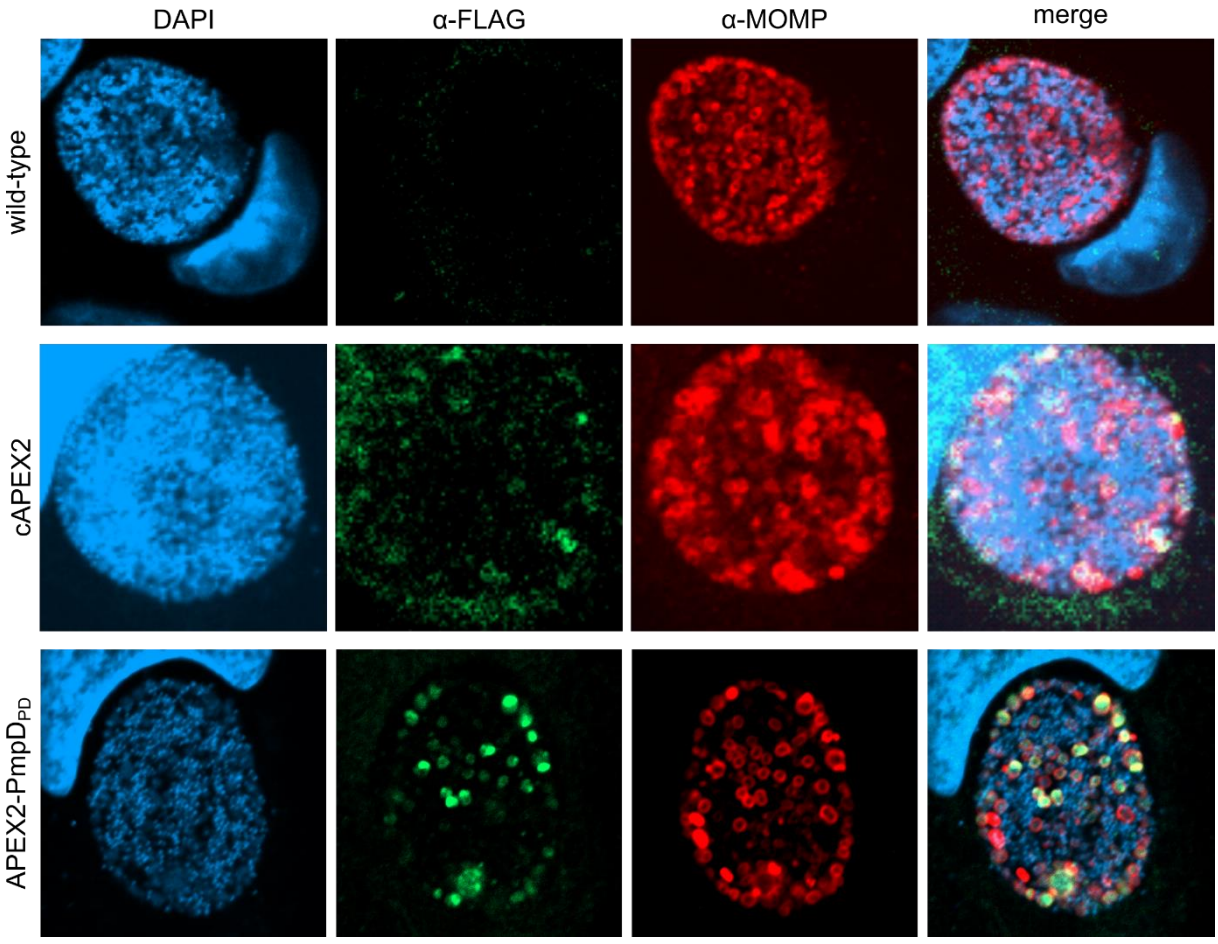

Figure 15: Fluorescence microscopy of wild-type or transformed *Ctr* L2

a Fluorescence microscopy of inclusions from HEp-2 cells infected with wild type or transformed *Ctr* L2 at 42 hpi. Cells were fixed with MeOH and immunostained with a FITC-labelled anti-FLAG antibody and an anti-MOMP antibody. DNA was stained with DAPI. Images are from individual focal planes. (Due to technical concerns, scalebars are missing).

Next, the expression and localization of the fusion proteins during a *Ctr* L2 infection were analysed. HEp-2 cells were infected with *Ctr* L2 transformed with either pSW24 (encoding cAPEX2) or pFK27 (encoding APEX2-PmpD$_{PD}$), or with wild-type *Ctr* L2 as negative control. At 42 hours post-infection (hpi), when most RBs transitioned back into EBs, cells were fixed and permeabilised using methanol. APEX2-fusion proteins were visualized by immunofluorescence, using a FITC-labelled anti-FLAG antibody. The negative control, cells infected with wild-type *Ctr* L2, showed no cross-reactivity with the anti-FLAG antibody (Fig. 15). DNA was visualized using DAPI and an anti-MOMP antibody was used to stain *Chlamydia* (Fig. 15). In all three samples, the MOMP signal exhibited strong outer membrane staining, shown by a distinct ring-like immunofluorescence pattern, consistent with the known localization of MOMP on the chlamydial outer membrane. In cells infected with *Ctr* L2 transformed with pSW24, the immunofluorescence signal appeared diffuse and did not colocalize with MOMP signal, suggesting a cytosolic localization of cAPEX2. However, FLAG-signal was also observed outside the inclusion and considering that the negative control ruled out antibody cross-reactivity, these would suggest the presence of cAPEX2 in the cell cytosol. Hence, these results should be interpreted with caution and further experiments are needed to clarify the source of the anti-FLAG signal outside the chlamydial inclusion. For *Ctr* L2 transformed with pFK27, the immunofluorescence signal for APEX2-PmpD$_{PD}$ exhibited ring-like patterns, which were highly similar to and colocalize with the MOMP signal. This indicates that APEX2-PmpD$_{PD}$ is anchored in the outer chlamydial membrane (Fig. 15).

5.5.2.2 APEX2 proximity labelling of PmpD$_{PD}$ interaction partners suggests involvement of IGF2R

After verifying the expression and localization of the APEX2-fusion proteins in transformed *Ctr* L2, EBs were collected and the APEX2 biotinylation reaction was initiated either in solution, to identify chlamydial PmpD binding partners (Fig. 13a, approach A), or early in infection, when EBs have attached to HEp-2 cells, to identify PmpD host cell receptors (Fig. 13a, approach B). Biotinylated proteins were purified via streptavidin pulldown and the elution fraction was analysed by immunoblotting and mass spectrometry (Fig. 13a).

For approach A, EBs from infected, confluent HEp-2 cells in a 24 cm² flask were collected and the APEX2-PmpD$_{PD}$ biotinylation reaction was initiated by adding biotin phenol and H_2O_2. As negative controls, wild-type EBs and EBs transformed with pSW24 were used. After the biotinylation reaction, the pelleted EBs were lysed and biotinylated proteins were purified using streptavidin agarose. The elution fractions were analysed by immunoblotting with streptavidin detection (Fig. 16a,b). In the first assay, for wild-type EBs, only faint bands were detected while for EBs expressing cAPEX2, distinct bands of different molecular weights were observed, confirming that cAPEX2 was functional and biotinylated proximal proteins (Fig. 16a). Intriguingly, for EBs expressing APEX2-PmpD$_{PD}$, only faint bands were detected in the elution fraction by immunoblotting, comparable to the wild-type negative control (Fig. 16a). Thus, the assay was repeated with double the amount of EBs but similar results to the first assay were obtained (Fig. 16b). Biotinylated protein levels were significantly lower in the APEX2-PmpD$_{PD}$ samples compared to the cAPEX2 samples. This suggests a potential failure of APEX2 fused to PmpD$_{PD}$ to biotinylate nearby proteins. A reason for this might be the unintentional inactivation of APEX2 upon fusion to PmpD$_{PD}$ or unsuccessful export of the fusion protein, which could occur if it is trapped in the

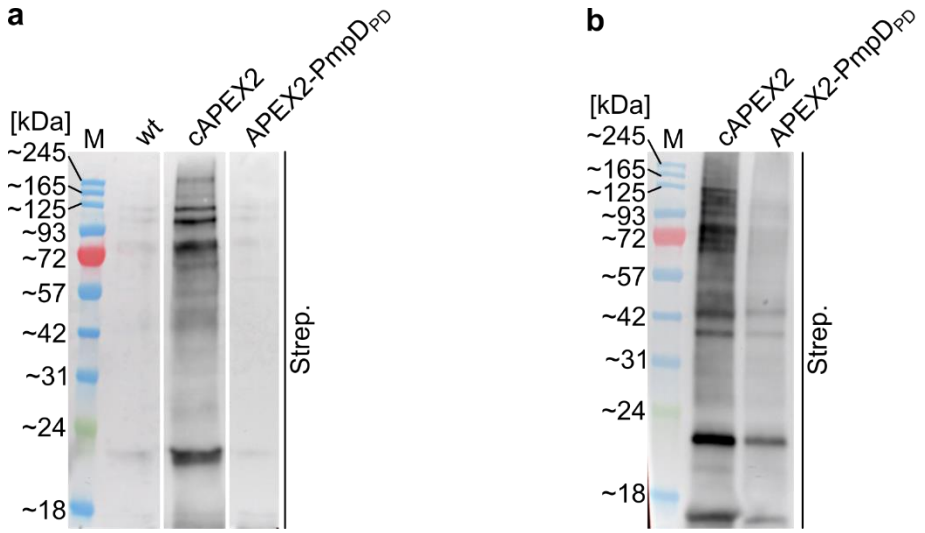

Figure 16: Proximity labelling assay on the chlamydial EB cell surface

a *Ctr* L2 wild-type (wt) or transformed EBs ectopically expressing cAPEX2 or APEX2-PmpD$_{PD}$ from infected HEp-2 cells, confluently grown in a 24 cm² flask, were pooled. The biotinylation reaction was initiated according to the protocol described in section 5.4.3.10.1. EBs were lysed and biotinylated proteins were purified using streptavidin agarose. Elution fractions were analysed by immunoblotting using streptavidin for detection. **b** Replication of **a** for EBs transformed with cAPEX2 and APEX2-PmpD$_{PD}$. EBs from HEp-2 cells confluently grown in two 24 cm² flasks were pooled and used for the biotinylation reaction.

translocation domain formed by the PmpI β-barrel. Hence, before analysis of the elution fractions by mass spectrometry, the protocol first needs to be refined and successful surface localization of APEX2-PmpD$_{PD}$ needs to be confirmed. Due to time constraints these experiments were not completed and the samples were not analysed by mass spectrometry.

For approach B, pooled EBs transformed with pFK27, expressing APEX2-PmpD$_{PD}$, were incubated with HEp-2 cells and the biotinylation reaction was initiated after 15 min, the time point at which most EBs have interacted with their host cell receptors. The cells were lysed and biotinylated proteins were purified via streptavidin pulldown and analysed by mass spectrometry (Fig. 13a). As negative control, HEp-2 cells were infected with wild-type EBs, to determine the level of endogenously biotinylated host cell proteins.

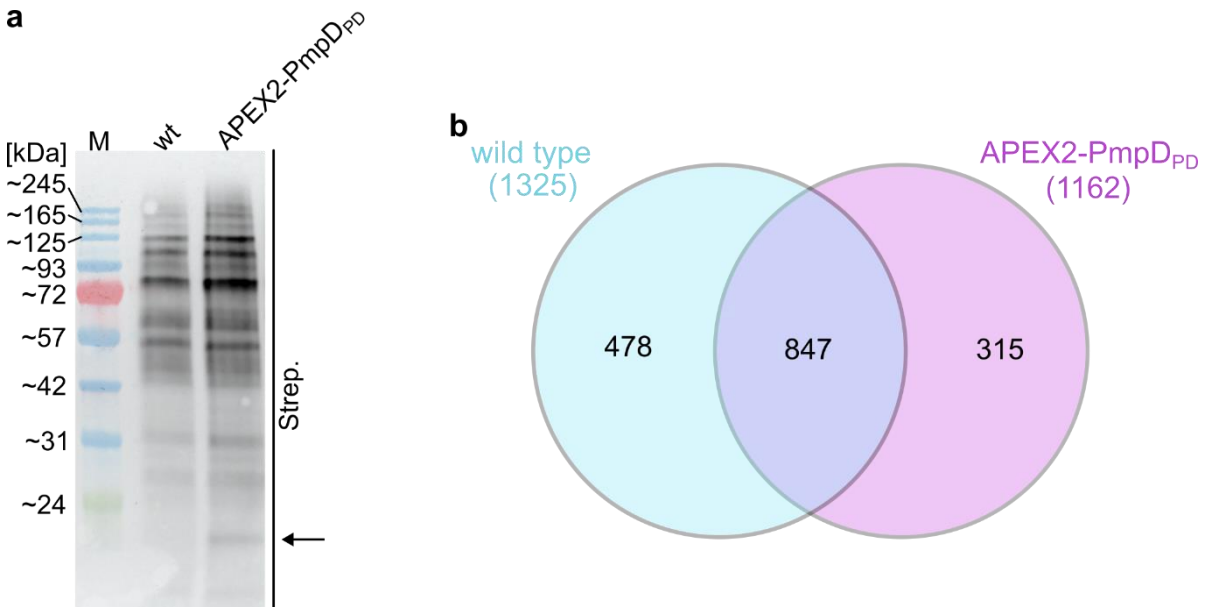

Figure 17: Proximity labelling epithelial cell surface proteins via adhesion of *Ctr* L2 EBs ectopically expressing APEX2-PmpD$_{PD}$

a HEp-2 cells were infected with *Ctr* L2 EBs ectopically expressing APEX2-PmpD$_{PD}$. As negative control, cells were infected with wild-type *Ctr* L2. Biotinylation reaction was initiated after 15 min of incubating EBs with HEp-2 cells at RT. Cells were lysed and biotinylated proteins were purified using streptavidin agarose. Elution fractions were analysed via Western blot and mass spectrometry. **b** Venn diagram for the peptides found in the mass spectrometry analysis for the wild type negative control (blue) and the APEX2-PmpD$_{PD}$ sample (purple). The wild-type sample contained peptides from 1325 different proteins while the APEX2-PmpD$_{PD}$ sample contained peptides for 1162 different proteins. Mass spectrometry analysis revealed that 847 proteins were shared in both samples, while 478 and 315 proteins were exclusively present in the wild-type sample and the APEX2-PmpD$_{PD}$ sample, respectively.

Immunoblot analysis indicated a higher abundance of biotinylated proteins where cells were infected with EBs expressing APEX2-PmpD$_{PD}$, compared to the negative control, cells infected with wild-type EBs (Fig. 17a). Additionally, unique bands were distinguished in the APEX2-PmpD$_{PD}$ sample, for instance the band below 24 kDa (Fig. 17a, arrow). Mass spectrometry analysis of biotinylated proteins identified 1640 different proteins in both samples combined, with 478 unique to the wild-type negative control and 315 unique to pFK27 transformed EBs. Albeit with different intensities, 847 proteins were shared in both samples (Fig. 17b). Due to time limitations, no biological replicates were prepared and a preliminary data analysis was performed by focusing on the unique proteins identified exclusively in the APEX2-PmpD$_{PD}$ sample. Among the top 100 hits, 21 were indicated to have a cell surface or secreted isoform, while the remaining 79 were suggested to be intracellular (Table 1). As an overall top hit, the insulin-like growth factor 2 receptor (IGF2R) was identified, which possesses an extracellular domain and is anchored in the PM [247, 248].

Taken together, these results provide preliminary evidences of potential host cell interaction partners for PmpD. However, to confirm these findings, biological replicates are indispensable, and the potential interaction partners need to be verified by further biological and biochemical assays.

Table 1: List of unique proteins found exclusively for APEX2-PmpD$_{PD}$. From the 315 uniquely identified proteins in the APEX2-PmpD$_{PD}$ sample, the top 100 are listed, sorted by the number of assigned spectra (fragmentation spectra resulting from mass spectrometry are assigned to trypsin fragments of proteins from a database).

	Accession ID	alternative ID	# of assigned spectra	Localisation [249]
1	P11717	IGF2R	13	plasma membrane
2	Q9Y4W6	AFG3L2	8	intracellular
3	P49792	RANBP2	8	intracellular
4	Q02218	OGDH	7	intracellular
5	Q4LDE5	SVEP1	7	intracellular and extracellular
6	P17066	HSPA6	6	intracellular and extracellular
7	O15230	LAMA5	6	extracellular
8	Q96AQ6	PBXIP1	6	intracellular
9	Q9UHN6	CEMIP2	6	plasma membrane
10	Q9NTJ3	SMC4	6	intracellular
11	Q9BSJ8	ESYT1	6	plasma membrane
12	P42224	STAT1	6	intracellular
13	Q7L0Y3	TRMT10C	6	intracellular

14	P50213	IDH3A	6	intracellular
15	Q6UB35	MTHFD1L	6	intracellular
16	O60313	OPA1	6	intracellular
17	Q9P0L0	VAPA	6	plasma membrane
18	P11388	TOP2A	5	intracellular
19	P27635	RPL10	5	intracellular
20	Q93063	EXT2	5	secreted
21	Q9P2K2	TXNDC16	5	secreted
22	Q9NZB2	FAM120A	5	plasma membrane
23	Q96KA5	CLPTM1L	5	intracellular
24	O75787	ATP6AP2	5	intracellular
25	P28331	NDUFS1	5	intracellular
26	Q8NAT1	POMGNT2	5	intracellular
27	O95573	ACSL3	5	intracellular
28	Q9BXW7	HDHD5	5	intracellular
29	O95672	ECEL1	5	intracellular
30	Q14573	ITPR3	5	intracellular
31	Q92621	NUP205	5	intracellular
32	Q10713	PMPCA	5	intracellular
33	Q9Y4P3	TBL2	5	intracellular
34	Q9UHD8	SEPTIN9	5	intracellular
35	Q9Y2G8	DNAJC16	5	intracellular
36	Q9NZJ5	EIF2AK3	5	intracellular
37	Q6DD88	ATL3	5	intracellular
38	Q04721	NOTCH2	5	plasma membrane
39	P35658	NUP214	5	intracellular
40	P30519	HMOX2	5	intracellular
41	P61026	RAB10	4	intracellular
42	P50993	ATP1A2	4	plasma membrane
43	Q15418	RPS6KA1	4	intracellular
44	P34955	SERPINA1	4	secreted
45	Q3ZCQ8	TIMM50	4	intracellular
46	Q9Y305	ACOT9	4	intracellular
47	P38435	GGCX	4	intracellular
48	P28288	ABCD3	4	intracellular
49	P52948	NUP98	4	intracellular
50	Q8NEW0	SLC30A7	4	intracellular
51	Q9Y2H6	FNDC3A	4	intracellular
52	Q6ZXV5	TMTC3	4	intracellular
53	Q9NVP1	DDX18	4	intracellular
54	Q96N66	MBOAT7	4	intracellular
55	Q8IY81	FTSJ3	4	intracellular

56	P23142	FBLN1	4	secreted
57	Q14669	TRIP12	4	intracellular
58	Q6NVY1	HIBCH	4	intracellular
59	Q96IR7	HPDL	4	intracellular
60	Q9NZI8	IGF2BP1	4	intracellular
61	P52564	MAP2K6	4	intracellular
62	Q8TBM8	DNAJB14	4	intracellular
63	P84095	RHOG	4	intracellular
64	P29122	PCSK6	4	secreted
65	Q9H6E4	CCDC134	4	secreted
66	Q9BTX1	NDC1	4	intracellular
67	Q9UNF1	MAGED2	4	secreted
68	Q14839	CHD4	4	intracellular
69	P15151	PVR	4	secreted
70	Q14739	LBR	4	intracellular
71	Q6PKC3	TXNDC11	4	intracellular
72	P24539	ATP5PB	4	intracellular
73	P61254	RPL26	4	intracellular
74	Q04917	YWHAH	4	intracellular
75	P18077	RPL35A	4	intracellular
76	Q92930	RAB8B	3	intracellular
77	P51812	RPS6KA3	3	intracellular
78	P42677	RPS27	3	intracellular
79	Q71UM5	RPS27L	3	intracellular
80	O94973	AP2A2	3	intracellular
81	Q13492	PICALM	3	plasma membrane
82	Q96CS3	FAF2	3	intracellular
83	P52701	MSH6	3	intracellular
84	Q14494	NFE2L1	3	intracellular
85	Q8TCS8	PNPT1	3	intracellular
86	O75396	SEC22B	3	intracellular
87	P57088	TMEM33	3	intracellular
88	Q9HC38	GLOD4	3	intracellular
89	Q9UH99	SUN2	3	intracellular
90	P10586	PTPRF	3	intracellular
91	P35555	FBN1	3	secreted
92	Q15397	PUM3	3	intracellular
93	Q03519	TAP2	3	intracellular
94	Q8IZ52	CHPF	3	intracellular
95	Q13185	CBX3	3	intracellular
96	Q6PI48	DARS2	3	intracellular
97	Q13443	ADAM9	3	secreted

98	Q969P0	IGSF8	3	plasma membrane
99	Q9ULW0	TPX2	3	intracellular
100	Q99714	HSD17B10	3	intracellular

5.6 Discussion

5.6.1 Soluble recombinant PmpG mediates adhesion to epithelial cells

Becker et al. [93] demonstrated that all nine *Ctr* Pmps, including PmpG, function as adhesins for epithelial and endothelial cells. In their study, the tested PmpG fragment spanned almost the entire PD (Fig. 10) and therefore contained all 11 FxxN and 4 GGA(I,L,V) motifs [93]. Later, Favaroni and Hegemann [96] conducted an extensive study analysing the adhesion properties of different *Ctr* Pmp fragments that varied in total length and the number of FxxN and GGA(I,L,V) repeats. They focused on the C-terminal half of the PmpG PD (Fig. 10), for which they suggested to be adhesive incompetent in the tested concentration range. However, they also showed that the tested PmpG fragment is involved in the formation of protofibril-like structures, which were longer in heteromeric oligomers compared to the homomeric variants [96].

In this work, the experimental approach of Favaroni and Hegemann [96] was adopted to test the adhesion of rG72 to HEp-2 cells. rG72 is a fragment of the *Ctr* PmpG PD which was suggested to be proteolytically processed *in vivo* [92, 244]. Further, it closely resembles the PmpG PD fragment used by Becker et al. [93] (Fig. 10). Results indicated that rG72 shows limited adhesion to epithelial cells. To detect bound rG72 on HEp-2 cells by immunoblotting, a minimum protein concentration of 10 µM was required in the cell culture medium, which is 40 times higher than the concentration needed for rD65, a soluble *Ctr* PmpD fragment similar to rG72 (Fig. 12). Furthermore, these findings align with adhesion assays performed by Wintgens [236], in which a similar fragment of PmpG (aa 29-673), containing all naturally occurring FxxN and GGA(I,L,V) repeats, was tested for its adhesive capacity on HEp-2 cells. Wintgens concluded that at a concentration of 3 µM, the fragment showed no binding to epithelial cells using immunoblot analysis [236]. Interestingly, Becker et al. [93] used an almost identical PmpG fragment as rG72, for which they evidently demonstrated binding to epithelial cells. However, the experimental techniques differed significantly. Becker et al. [93] used surface immobilized PmpG fragments by either expressing them as a fusion construct with Aga2 on the yeast cell surface or by coating fluorescent latex

beads. The yeast cells and latex beads were then used to test adhesion to epithelial cells. However, immobilizing proteins on a surface leads to a locally increased protein concentration, which, in the case of Pmps, might be further elevated due to their tendency to form large oligomers [96]. Contrary, for adhesion assays performed in this work and in the work of Favaroni and Hegemann [96], soluble PmpG was incubated in solution, allowing tightly controlled protein concentrations that were evenly distributed in solution. Hence, under consideration of the different experimental conditions, both approaches demonstrate the adhesive property of PmpG (Fig. 12), which is however much weaker than compared to rD65.

Based on the adhesion assays presented here, it appears highly likely that *Ctr* PmpG is not a component which establishes tight binding to the target cell, nevertheless it adheres to it and is hence classified as adhesin. Taking into consideration that the unique *Ctr* PmpG belongs to a subtype which is species-specifically highly expanded (*Cpn*: 13 members, *Cps*: 14 members, *C. abortus*: 11 members [243]), it is plausible that PmpG has a crucial function in the chlamydial infection cycle. This could either be due to specific interaction with a host cell component or tissue tropism. Alternatively, PmpG might also serve as structural unit to drive homo- and heterooligomerisation of Pmps. Previous studies have shown that PmpG is involved in the formation of long, protofibril-like heterooligomers with other Pmps, that mediate stable attachment to epithelial cells [96, 236]. Therefore, further experiments are necessary to fully elucidate the role of PmpG in the early stages of a chlamydial infection. One key aim would be, to identify the host cell binding partner for *Ctr* PmpG.

5.6.2 Preliminary data suggest the interaction of *Ctr* PmpD with IGF2R

Pmps are essential adhesins that play a pivotal role during the initial stages of a chlamydial infection [85, 108]. They mediate adhesion to host cells through complex protein-protein interactions, influenced by the oligomeric state of Pmps [93, 95, 96]. Wintgens provided first evidences, that Pmp homo- and heterooligomers are present on the chlamydial surface *in vivo* [236]. By fusing APEX2 to the N-terminus of the surface-exposed $PmpI_{PD}$, Wintgens [236] mapped the native spatial environment of the chlamydial surface, revealing that among the different Pmp subtypes, PmpD was preferentially recruited by PmpI.

In this study, host cell binding partners were identified for *Ctr* PmpD. Doing so, two separate approaches were used and while the first approach, performing a pulldown

assay with a soluble recombinant PmpD fragment suggested the direct interaction with sCLU, the second approach, discussed here, was designated to provide the spatial environment of EB surface localized $PmpD_{PD}$. Therefore, the experimental approach described by Wintgens [236] was modified, by fusing the $PmpD_{PD}$ (instead of $PmpI_{PD}$) to APEX2 and by presenting EBs expressing the fusion construct (APEX2-$PmpD_{PD}$) to epithelial host cells.

As a control, prior to the presentation of EBs to HEp-2 cells, the expression and localization of APEX2-$PmpD_{PD}$ (encoded on pFK27, Fig. 13b) and cAPEX (negative control, encoded on pSW24, Fig. 13b) were analysed. Immunoblots of lysed transformed and untransformed EBs confirmed successful expression of both fusion proteins and detergent extraction assays suggested that cAPEX2 is localized in the chlamydial cytosol, while APEX2-$PmpD_{PD}$ appeared to be membrane-anchored (Fig. 14 c,d). Further, immunofluorescence of HEp-2 cells infected with *Ctr* L2 transformed with pFK27 (APEX2-$PmpD_{PD}$) indicated colocalization of APEX2-$PmpD_{PD}$ with MOMP, a known chlamydial outer membrane protein, suggesting the transport of APEX2-$PmpD_{PD}$ across the inner chlamydial membrane, presumably mediated by the PmpI signal sequence. However, it remains unclear whether the APEX2-$PmpD_{PD}$ domain is fully exported across the outer membrane or if it is trapped in the PmpI β-barrel or even the periplasmic space. Since $PmpD_{PD}$ is considerably longer than the $PmpI_{PD}$, this could lead to complications during the export process (Fig. 18). Immunofluorescence of HEp-2 cells infected with *Ctr* L2 transformed with pSW24, used as negative control, showed a diffuse signal for cAPEX2, indicating cytosolic localization, which is consistent with the results obtained from the detergent extraction assay. However, signal was unexpectedly observed in the host cell cytosol as well. Cross-reactivity of the antibody was ruled out (no FLAG-signal in cells infected with wild-type *Ctr* L2, Fig. 15), suggesting that cAPEX2 may be transported from the chlamydial cytosol into the host cell cytosol. However, this is highly unlikely since cAPEX2 lacks a signal sequence for transportation across membranes. Thus, further experiments are indispensable to determine the source of the cAPEX2 signal outside the inclusion and the present results should be interpreted with caution.

In proximity labelling assays with pooled EBs, immunoblot analysis indicated low levels of biotinylated proteins for EBs expressing APEX2-$PmpD_{PD}$, comparable to those

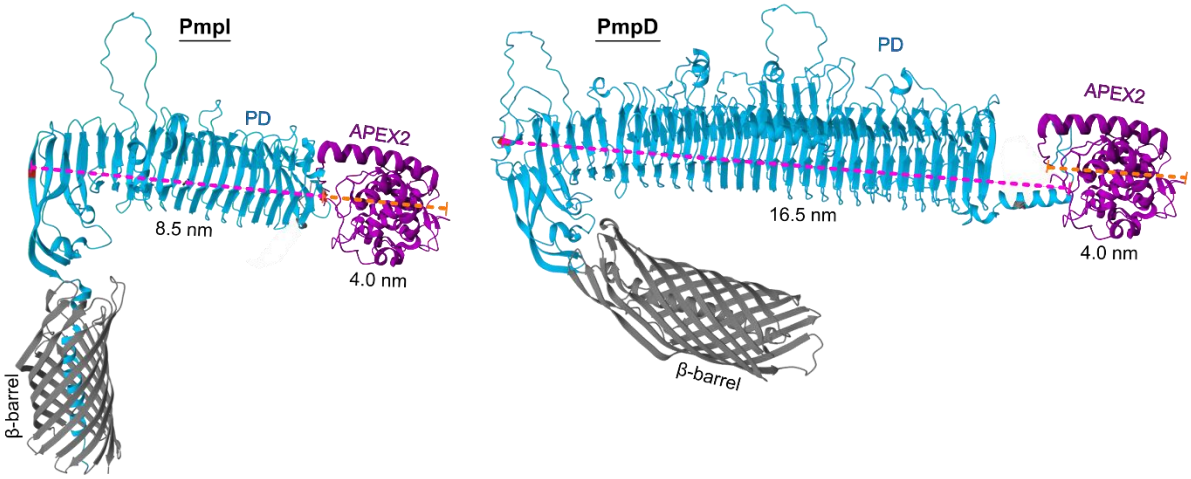

Figure 18: RoseTTAFold predicted structures of PmpI and PmpD fused to APEX2

For PmpI the PD is suggested to be 8.5 nm in length, for PmpD the PD is suggested to be 16.5 mm in length [250-253]. The C-terminal β-barrel and the N-terminal signal sequence are indicated in grey, the passenger domain is indicated in blue. At the N-terminus, the APEX2 fusion site is displayed. APEX2 has a suggested length of approximately 4 nm.

detected for the negative control (wild-type *Ctr* L2 EBs), while for cAPEX2 higher protein levels were observed (Fig. 16). Since it was shown in previous studies, that PmpD$_{PD}$ is not spatially separated from other proteins on the chlamydial surface, this indicates that biotinylation by APEX2 may have failed [236]. Possible explanations include that APEX2 is either non-functional, for example due to its fusion with PmpD, or the fusion protein is trapped (e.g. in the β-barrel), preventing proximity to other proteins. Both hypotheses could explain the low protein levels observed in immunoblot analysis, indicating complications with using the PmpI β-barrel to export APEX2 fused to PmpD$_{PD}$. Hence, additional control experiments are needed to test the APEX2 function when fused to PmpD$_{PD}$ and to determine whether the fusion construct is localized on the chlamydial surface.

Despite these challenges, EBs expressing APEX2-PmpD$_{PD}$ were used in proximity labelling experiments on HEp-2 cells to identify potential host cell receptors for PmpD$_{PD}$. Immunoblot analysis indicated clear differences between the negative control (wild-type *Ctr* L2 EBs) and EBs transformed with pFK27 (APEX2-PmpD$_{PD}$). Mass spectrometry analysis of the elution fraction revealed several potential PmpD interaction partners, though, most of them being localized intracellularly, which cannot be bound by PmpD as it is expected to adhere to the extracellular side of the host cell. However, the insulin-like growth factor 2 receptor (IGF2R), a transmembrane

glycoprotein, emerged as a top candidate (Table 1). IGF2R has a large extracellular N-terminal region, responsible for ligand binding, as for example IGF2 or ligands with a mannose 6-phosphate (M6P) residue [254]. At the C-terminus, IGF2R possess a short transmembrane domain and an intracellular tail for downstream signalling [255]. Upon IGF2 binding, endocytosis is initiated, leading to IGF2 uptake and degradation [248, 256, 257]. Since IGF2R is proposed as PmpD interaction partner, this receptor-mediated internalization pathway might be hijacked, facilitating the entry of the chlamydial EB into a non-phagocytic cell.

Interestingly, previous research on chlamydial adhesion and internalization mechanisms has already proposed the involvement of IGF2R, suggesting to enhance a chlamydial infection on endothelial cells [67, 258]. However, these findings were indicated to be true only for *Cpn* and not *Ctr*. In experiments where endothelial cells were pre-treated with M6P prior to a chlamydial infection, a significant decrease in *Cpn* infectivity was observed, while *Ctr* infectivity remained unaffected [67]. For *Ctr*, the mannose receptor was suggested to be involved, which could however not be identified in the proximity labelling assay in this work (section 5.5.2) [259]. Hence, further experiments are indispensable, in which first of all the direct interaction of *Ctr* PmpD and IGF2R needs to be verified.

Clusterin (CLU), which was identified as a direct binding partner of the N-terminal fragment of *Ctr* PmpD (D72, section 3), was not detected in the proximity labelling assay. In this assay, HEp-2 cells were grown to confluence in cell culture medium (abundant in sCLU after cell growth), which was then aspirated and the cells were washed before being incubated with fresh medium (devoid of sCLU), supplemented with APEX2-PmpD$_{PD}$ producing EBs. Consequently, at the time of APEX2 mediated biotinylation, the system contained little (or no) sCLU, which may have been insufficient for the sensitivity of the labelling system and subsequent mass spectrometry analysis. It is important to note, that since both approaches, the pulldown assay using soluble rD72 as bait and the proximity labelling assay with APEX2-PmpD$_{PD}$, were prepared in parallel, the influence of components in the cell culture medium after cell growth was not known at that time. For future replication of the proximity labelling experiment, it is critical to modify the protocol such that the cell culture medium is retained and sCLU is present during the biotinylation reaction for adequate labelling and detection.

In summary, while these findings provide preliminary evidence of potential $PmpD_{PD}$ – host-receptor interactions, further validation is required. Control experiments, replicates and follow-up studies are essential to clarify the role of IGF2R in *Ctr* entry and its interplay with sCLU. Furthermore, once the proximity labelling protocol for the identification of PmpD binding partners is well established, the $PmpD_{PD}$ in the fusion construct with APEX2 could be substituted with the PD of PmpG or any of the other seven Pmps, thereby helping to find host cell binding partners for those as well.

6 Part IV: Final Discussion and Outlook

Obligate intracellular pathogens such as *Chlamydia* depend on invading a host cell for the production of progeny. Especially the adhesion to the host cell and the subsequent internalization into it are essential steps in the chlamydial developmental cycle and research in recent years has strongly focused on elucidating the molecular mechanisms involved in these processes. Even though these mechanisms are not fully resolved by now, several important key proteins were identified, among them the polymorphic membrane proteins (Pmps), which are crucial for chlamydial attachment to a host cell and early secreted effectors, which modulate key components of the host endocytic machinery for enhancing engulfment of the attached chlamydial EB. The aim of this work was to identify host cell binding partner(s) for the *Ctr* adhesin PmpD, to investigate the adhesion capacity of *Ctr* PmpG, and to reveal the molecular mechanisms involved in the binding of SemD, a *Cpn* early effector, to key components of the host endocytic machinery and the subsequent activation of N-WASP.

6.1 *Ctr* PmpD directly binds to secreted clusterin for facilitated host cell entry and likely uses IGF2R as co-receptor

Previous research has extensively highlighted the importance of Pmps during the early stages of a chlamydial infection. *Ctr* PmpD is suggested to play a particular role in the chlamydial pathogenesis, indicated by its high conservation across species and its steady expression profile, even when under stress conditions induced by for example penicillin [78]. While the host cell receptor for PmpD remains unidentified, *Cpn* Pmp21, the homologue to *Ctr* PmpD, is known to bind to and activate the epidermal growth factor receptor (EGFR). However, an interaction of EGFR with *Ctr* PmpD could not be confirmed [86].

In the pulldown assay (section 3) and the proximity labelling assay (section 5.5.2), potential host cell binding partners for *Ctr* PmpD were identified, suggested to be the secreted host cell chaperone clusterin (CLU) and the insulin-like growth factor 2 receptor (IGF2R), also known as cation-independent mannose 6-phosphate receptor (CI-M6PR).

CLU is present in most human tissues and body fluids and exists in multiple isoforms [260]. The secreted isoform (sCLU), found in the extracellular space, has a chaperone-like activity by stabilizing and clearing misfolded or aggregated proteins. Additionally, by binding to them, sCLU mediates endocytotic uptake into the cell, typically followed by lysosomal degradation. Even though the exact mechanisms for initiating endocytosis remain elusive, in recent studies it was shown that sCLU interacts with the heparan sulfate (HS) receptor on the cell surface [260, 261]. Further, sCLU is involved in various proteinopathic diseases, including Alzheimer's disease (AD), where it binds to oligomeric Aβ, the precursor to Aβ protofibrils (the hallmark of AD), and helps transport it across the blood-brain barrier [262, 263]. Moreover, sCLU has been shown to inhibit the host immune response by blocking the formation of the membrane attack complex (MAC, a complex which binds to the pathogen's surface and forms pores leading to osmotic lysis of the pathogen) and thereby inhibiting the terminal complement pathway [238, 264].

Based on the present results, we would like to suggest that EBs, with surface-exposed PmpD, are bound by sCLU, which is also present in the extracellular space of cells. This interaction likely occurs through structural recognition, since Pmps, including PmpD, have been shown to form homo- and heterooligomers with a high propensity for β-sheet structures, similar to the protofibril filaments formed by Aβ [95, 96, 101, 236]. SEC and Blue Native-PAGE analysis of rD72 further supported this, indicating the formation of high molecular weight oligomers (section 3). Binding of sCLU to the EB surface via PmpD, and likely all other Pmps, may help the EB to evade the host immune response by hijacking the inhibitory effect of sCLU on the terminal complement pathway. This inhibition blocks the assembly of the membrane attack complex (MAC), which might otherwise form a pore in the chlamydial membrane and lead to its lysis [238]. A similar mechanism has been observed for other intracellular pathogens, such as *Pseudomonas aeruginosa* and *Staphylococcus aureus*, which bind to sCLU and deploy its function as a terminal complement pathway inhibitor by preventing the assembly of the pore-forming MAC in the pathogen's membrane [265, 266]. Further, sCLU, which binds to HS on the host cell surface, may enhance EB attachment and position it close to other receptors that might serve as co-receptors for cell entry. The use of co-receptors when interacting with host cell HS has been demonstrated for other growth factors and viruses, making a similar mechanism for *Ctr* conceivable [267-269].

Considering the proximity labelling data (section 5.5.2) one such co-receptor suggested for PmpD is the IGF2R. IGF2R is expressed in most mammalian tissues where it functions among others as endocytotic receptor for regulating extracellular insulin-like growth factor 2 (IGF2) levels, designated for degradation in lysosomes [254]. Further, cell surface IGF2R is involved in the uptake of ligands with mannose 6-phosphate residue(s) [254]. Previous studies already suggested the involvement of IGF2R for chlamydial uptake into a target cell, however it has been proposed to be relevant only for *Cpn*, and not for *Ctr* [67, 258]. Also, the interaction was hypothesized to be mediated via chlamydial MOMP, as it possesses high-mannose oligosaccharides, via which the interaction with IGF2R might be mediated [67, 270]. Hence, these experiments need to be repeated to verify the direct interaction of *Ctr* PmpD and IGF2R and further to test if other Pmps might bind to IGF2R as well. In addition, based on previous studies, it is possible that additional host co-receptors are involved, as many host cell receptors have been shown to play a role in the uptake mechanism, including the ephrin A2 receptor and the fibroblast growth factor receptor [61]. However, the chlamydial interaction partners for these receptors have not yet been identified [61].

In summary, these results shed light on how *Ctr* PmpD may mediate adhesion and uptake by engaging sCLU to facilitate host cell attachment, evade the host immune response, and interact with IGF2R, which may mediate receptor-mediated uptake and intracellular survival.

However, future investigation is necessary to fully understand the underlying mechanisms. For instance, while the direct interaction between sCLU and *Ctr* PmpD has been shown, its *in vivo* effects remain largely unknown and can only be hypothesized. Additional experiments are needed to determine, whether the inhibition of the terminal complement pathway by sCLU significantly impacts the *Ctr* infectivity or if the reduced infectivity observed in the absence of sCLU is due to reduced host cell adhesion and internalization. Further, since all Pmps are predicted to form high molecular weight oligomers, a future aim would be to identify if sCLU generally interacts with Pmp oligomers, also of other chlamydial species than *Ctr*, or if its binding is specific to *Ctr* PmpD. Another goal is to resolve the contradicting data regarding IGF2R involvement in *Ctr* infectivity. While Puolakkainen et al. [67] suggested that IGF2R is not involved in *Ctr* infectivity, the current results indicate the opposite.

However, it is important to note that the proximity labelling assay (section 5.5.2) was based on a single replicate and the precise localization and function of the APEX2-PmpD$_{PD}$ fusion protein in *Ctr* were not fully verified. Further, the experimental protocol did not allow for the detection of sCLU as an APEX2-PmpD$_{PD}$ interaction partner, as the cell culture medium used during infection was depleted of sCLU. Thus, it is important to repeat and perform additional control experiments to verify the functionality and localization of the APEX2-PmpD$_{PD}$ construct and to modify the protocol to retain cell culture medium rich in sCLU during infection.

6.2 PmpG is a weak adhesin on epithelial host cells

Even though PmpD is the best studied Pmp in *Ctr*, PmpG has also been suggested to play a key role in infectivity. The unique *Ctr* PmpG is part of a subgroup that is highly expanded in other chlamydial species (*Cpn*: 13 members, *Cps*: 14 members, *C. abortus*: 11 members [243]), suggesting possible species- and tissue-specific functions. Hence, identification of the host cell binding partner of *Ctr* PmpG would help to understand its role in infectivity. Becker et al. [93] showed that selected fragments of all nine *Ctr* Pmps, including PmpG, bind to epithelial cells when expressed as Aga2 fusion proteins on the yeast cell surface [93]. This was further supported by experiments using latex beads coated, among others, with recombinant PmpG passenger domains incubated with epithelial cells [93]. Contradicting this, Favaroni and Hegemann [96], as well as Wintgens [236], suggested that PmpG does not adhere to epithelial cells. However, they tested this using soluble PmpG fragments for adhesion assays while Becker et al. [93] used surface-immobilized PmpG fragments.
In this study (section 5.5.1), PmpG adhesion to epithelial cells was further investigated to potentially develop an adhesion assay protocol specifically for PmpG, which could later be expanded into a pulldown assay to identify PmpG host cell binding partners. To do so, different concentrations of a soluble recombinant PmpG fragment, rG72, which closely resembled the one from Becker et al. [93], were incubated with epithelial cells and binding was detected by immunoblot analysis (Fig. 12). The results confirmed that rG72 binds to epithelial cells, supporting Becker's [93] findings. However, while Becker et al. [93] proposed a similar binding capacity for all *Ctr* Pmps, the binding of rG72 in this study was significantly weaker than that of rD65, a *Ctr* PmpD fragment

similar to rG72 which was used as positive control, as 40 times higher concentrations of rG72 were required to detect adhesion on epithelial cells (Fig. 12). Becker's [93] observation that PmpD and PmpG bind to a similar extent to target cells might be due to immobilization of the proteins on a surface, leading to artificially high local Pmp concentrations, mediating better adhesion capacity.

Thus, while PmpG may indeed enhance attachment of the EB to epithelial cells during the early stages of a chlamydial infection, its weak adhesion suggests it might have another role, such as promoting Pmp oligomerization, as indicated by Favaroni and Hegemann [96], or tissue specificity. However, PmpG does bind to the target cell surface and to determine the PmpG function during the early infection, it would be important to identify the host cell components it binds to. Therefore, the adhesion assay from section 5.5.1 could serve as a basis for future pulldown assays. When establishing such a pulldown protocol, modified for PmpG, the high concentrations of PmpG required need to be considered, and it is also important to take into account that soluble components of the cell culture medium, which was used for epithelial cell growth, might be essential as well, as it was seen with sCLU and PmpD (section 3). Finally, future experiments should investigate, whether sCLU binds to *Ctr* PmpG as well.

6.3 SemD modulates the host actin cytoskeleton by structurally and functionally mimicking host cell Cdc42

Besides attachment to a host cell, chlamydial replication is highly dependent on the ability to invade host cells. During attachment, chlamydial adhesins bind to host cell surface receptors and trigger endocytic signalling. However, this alone is insufficient for successful uptake of the EB, which has a diameter that is 3 – 4 times larger than that of a typical endocytic vesicle [156]. To overcome this, *Chlamydia* manipulate the host endocytic machinery to generate a vesicle large enough for EB entry. This requires extensive remodelling of both the host plasma membrane (PM) and the actin cytoskeleton, mediated by type-III-secreted early effector proteins, including in *Cpn* the soluble CPn0572 and the membrane-bound effectors SemC and SemD [191, 231, 234]. SemD, located on a syntenic locus with *Ctr* TmeA, binds to the inner leaflet of the PM, showing high affinity for phosphatidylserine (PS), and recruits key endocytic

components, including SNX9, Pacsin 2/3, G-actin and N-WASP [191]. Further, it has been shown that SemD alone is sufficient for N-WASP binding and activation, which typically resides in an autoinhibited state (section 1.3.3.2), thereby bypassing its endogenous activator Cdc42, leading to Arp2/3-mediated actin polymerization and branching.

Crystallization studies on SemD revealed that its host protein binding sites are separated by intrinsically disordered linker regions, allowing flexible arrangement and enabling binding to multiple endocytic components simultaneously. This was shown in GUV experiments, where membrane-bound SemD recruited both SNX9 and N-WASP to the perimeter of the GUV (Manuscript II, section 4). Like all chlamydial species, C*pn* has a highly reduced genome, which is why many proteins must fulfil more than one single role [16]. Through this multifunctional performance, SemD might maximize the efficiency for fast EB uptake, which needs to be mediated within 15 – 30 min after initial host contact.

Co-crystallisation studies of N-WASP and SemD (Manuscript II, section 4) demonstrated that SemD structurally mimics Cdc42 in its active form ($Cdc42_{GTP}$), allowing it to bind and activate N-WASP. Additionally, biochemical assays indicated that SemD has an enhanced N-WASP binding site compared to $Cdc42_{GTP}$, enabling stronger binding and allowing even displacing $Cdc42_{GTP}$ from an already formed complex with N-WASP.

This type of molecular mimicry differs from all other known pathogens which hijack N-WASP function, as they typically manipulate upstream regulators of $Cdc42_{GTP}$, such as GTPase activating proteins (GAPs) or GTPase exchange factors (GEFs) [271-273]. In contrast, SemD bypasses these upstream regulators and instead targets N-WASP by mimicking $Cdc42_{GTP}$ for modulating the actin cytoskeleton, which likely allows it to drive a much faster and more efficient manipulation of the F-actin network around the growing vesicle. Interestingly, the mechanism also differs from that of *Ctr* TmeA [274]. Bioinformatic analysis combined with *in vitro* and *in vivo* assays indicated, that TmeA activates N-WASP by mimicking its VCA domain, displacing, and thus releasing, the native VCA for Arp2/3-mediated actin polymerization and branching [274]. This same mechanism is also used by EspFu from enterohemorrhagic *E. coli* (EHEC) and provides a more direct activation mechanism than SemD, since they mimic an actual N-WASP domain for activation instead of mimicking an N-WASP regulator [275].

Even though the particular molecular reason(s) for the different activation strategies for N-WASP are difficult to reveal, a hypothesize might be that it is linked to tissue tropism. *Ctr*, which infects epithelial cells in the eyes and urogenital tract, might benefit with its effector TmeA from a more direct N-WASP activation, bypassing $Cdc42_{GTP}$ completely. *Cpn*, which infects epithelial cells from the respiratory tract, may require a more subtle approach by mimicking $Cdc42_{GTP}$ to blend into host signalling pathways.
Notably, neither SemD nor TmeA directly recruit the Arp2/3 complex, despite this being an even more direct way to control actin dynamics. This suggests that activated N-WASP might serve a broader role than just controlling actin dynamics, likely including its endogenous functions of recruiting SH3-domain-containing proteins like SNX9 and Pacsin 2/3, as well as binding G-actin for F-actin formation (section 1.3.3.2). Even though SemD also binds to these components, N-WASP likely enhances their recruitment, justifying for targeting N-WASP instead of directly Arp2/3.
During this process, actin dynamics is further supported by soluble effector proteins secreted into the host cell cytosol like *Ctr* TarP and its *Cpn* homologue CPn0572 [230, 231]. They were demonstrated to remodel the host actin cytoskeleton, possibly supplying F-actin bundles needed for Arp2/3-mediated branching processes.
One important key difference between *Ctr* and *Cpn* is, how they regulate actin dynamics after successful scission of the vesicle form the donor membrane. In *Ctr*, TmeB, another secreted effector which is encoded on a bi-cistronic operon with TmeA, inhibits Arp2/3 and halts actin branching and polymerization [276]. This likely prevents excessive actin accumulation, which could lead to cell damage and thereby impede with the following stages of the chlamydial developmental cycle, which must continue for the next 2-3 days within an intact host cell. For *Cpn*, such a downregulation mechanism has not been identified yet. Although *Cpn* encodes CPn0676, a protein with significant sequence homology to *Ctr* TmeB (Fig. 9), no inhibitory effect on actin polymerization has been observed. Preliminary data on CPn0676, (gathered during the Masters project by Paula Ungnad, not published) did not show any interactions between CPn0676 and endocytic host proteins. However, CPn0676 might still play a regulatory role that is yet not fully understood, in which it may not directly interact with endocytic host proteins. Investigating CPn0676 and exploring the mechanisms that inactivate SemD are promising future research aims that may offer new insights into how *Cpn* modulates host cell processes during infection.

7 Supplementary material

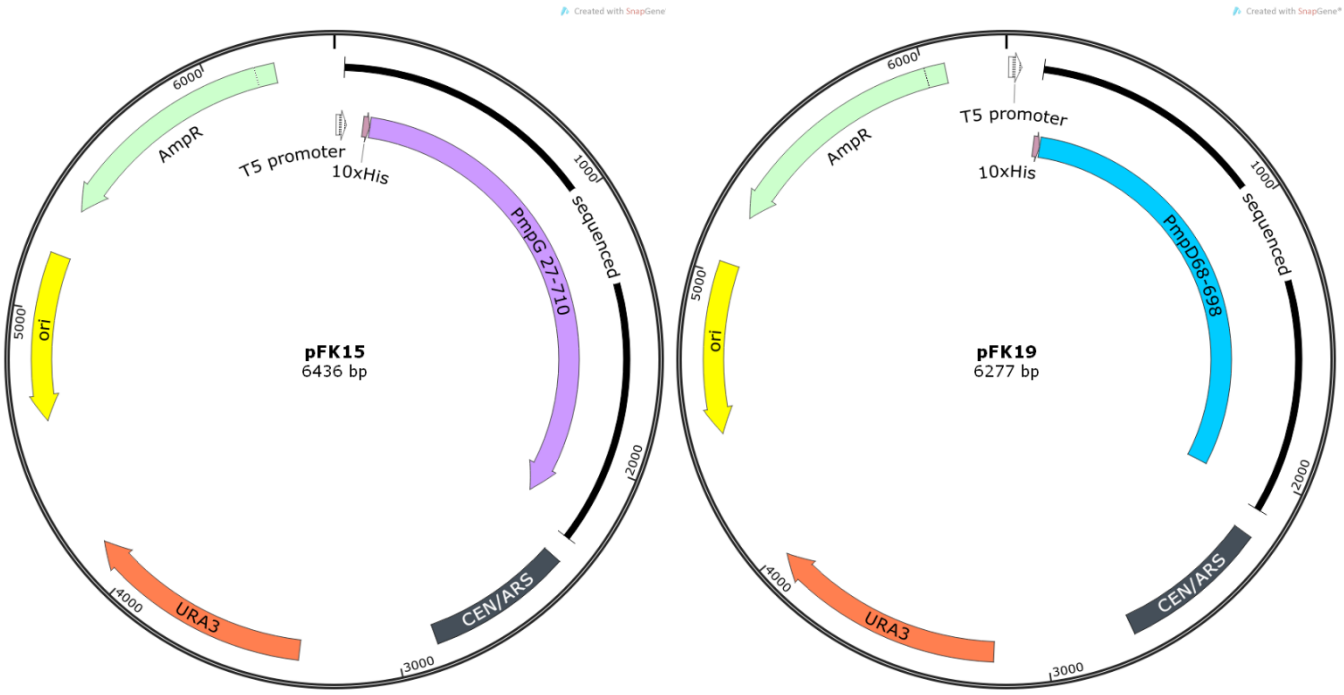

Figure S1: Designed plasmids used in PmpG adhesion studies (section 5.5.1)

Vector schematic for pFK15 and pFK19. Both plasmids are derived from pKM32. Represented are the origin of replication for propagation in yeast (*CEN/ARS*), a yeast selection marker (*URA3*), the origin of replication for bacteria (*ori*), a bacterial selection marker (*ampR*, ampicillin resistance), the T5 promoter and a 10x His-tag. Genetically fused to the His-tag is either *Ctr* serovar E PmpG (residues 27-710) in pFK15 or PmpD (residues 68-698) in pFK19. The sequenced regions are marked with a black line (sequenced).

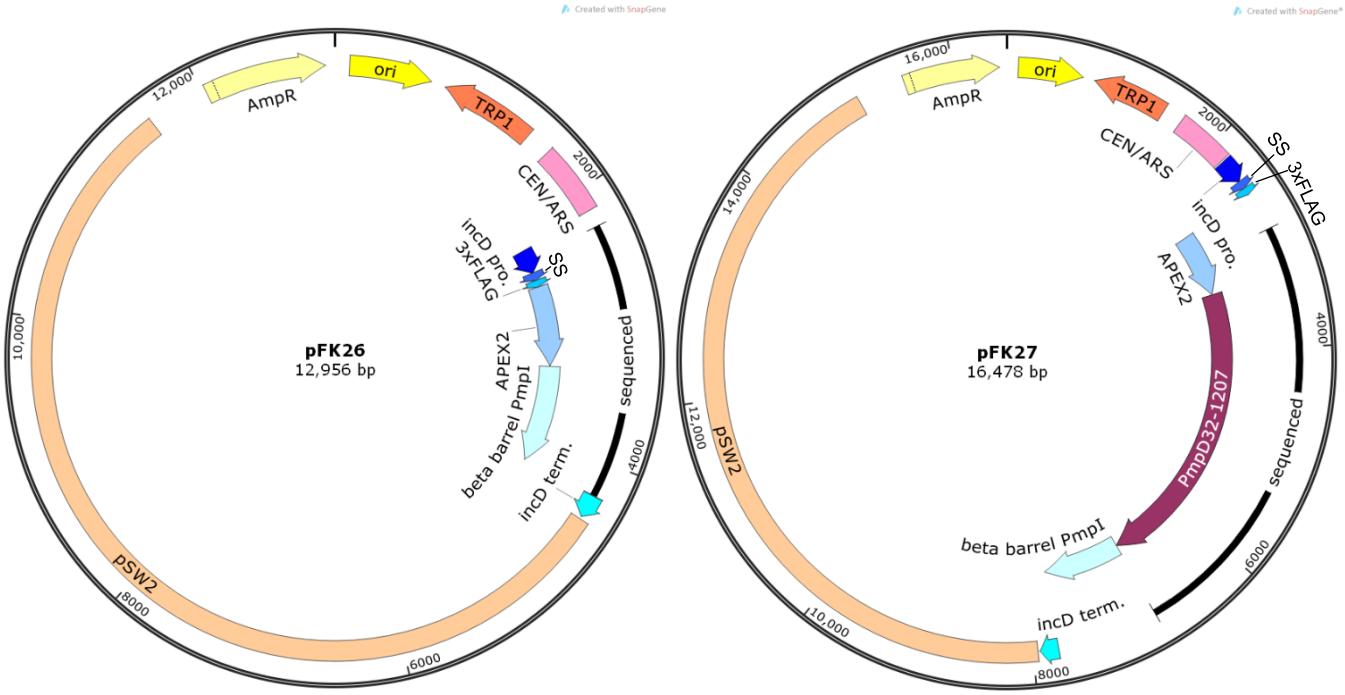

Figure S2: Designed plasmids used in APEX2 proximity labelling studies (section 5.5.2)

Vector schematic for pFK26 and pFK27. Both plasmids are derived from pKM280. Represented are the sequence of the naturally occurring plasmid from *Ctr* SW2 strain (pSW2), a bacterial selection marker (*ampR*, ampicillin resistance), the origin of replication for bacteria (*ori*), a yeast selection marker (*TRP1*), the origin of replication for propagation in yeast (*CEN/ARS*), the constitutive incD promoter (*incD pro.*), the PmpI signal sequence (*SS*), a 3xFLAG-tag (*3xFLAG*), the APEX2 sequence (*APEX2*), the PmpI β-barrel (*beta barrel PmpI*) and the incD terminator (*incD term.*). Additionally, pFK27 includes *Ctr* serovar E PmpD (residues 32-1207) fused between APEX2 and PmpI β-barrel. The sequenced regions are marked with a black line (sequenced).

8 References

1. Ouellette SP, Karimova G, Subtil A, Ladant D. Chlamydia co-opts the rod shape-determining proteins MreB and Pbp2 for cell division. Mol Microbiol. 2012;85(1):164-78.
2. Bayramova F, Jacquier N, Greub G. Insight in the biology of Chlamydia-related bacteria. Microbes Infect. 2018;20(7-8):432-40.
3. Stephens RS, Kalman S, Lammel C, Fan J, Marathe R, Aravind L, et al. Genome sequence of an obligate intracellular pathogen of humans: Chlamydia trachomatis. Science. 1998;282(5389):754-9.
4. Moulder JW. Interaction of chlamydiae and host cells in vitro. Microbiol Rev. 1991;55(1):143-90.
5. Abdelrahman YM, Belland RJ. The chlamydial developmental cycle. FEMS Microbiol Rev. 2005;29(5):949-59.
6. al-Rifai KM. Trachoma through history. Int Ophthalmol. 1988;12(1):9-14.
7. Grayston JT, Kuo CC, Campbell LA, Wang SP. Chlamydia pneumoniae sp. nov. for Chlamydia sp. Strain TWAR. Int J Syst Bacteriol. 1989;39:88-90.
8. Fukushi H, Hirai K. Proposal of Chlamydia pecorum sp. nov. for Chlamydia strains derived from ruminants. Int J Syst Bacteriol. 1992;42(2):306-8.
9. Grayston JT, Kuo CC, Wang SP, Altman J. A new Chlamydia psittaci strain, TWAR, isolated in acute respiratory tract infections. N Engl J Med. 1986;315(3):161-8.
10. Everett KD, Bush RM, Andersen AA. Emended description of the order Chlamydiales, proposal of Parachlamydiaceae fam. nov. and Simkaniaceae fam. nov., each containing one monotypic genus, revised taxonomy of the family Chlamydiaceae, including a new genus and five new species, and standards for the identification of organisms. Int J Syst Bacteriol. 1999;49 Pt 2:415-40.
11. Everett KD, Andersen AA. The ribosomal intergenic spacer and domain I of the 23S rRNA gene are phylogenetic markers for Chlamydia spp. Int J Syst Bacteriol. 1997;47(2):461-73.
12. Stephens RS, Myers G, Eppinger M, Bavoil PM. Divergence without difference: phylogenetics and taxonomy of Chlamydia resolved. FEMS Immunol Med Microbiol. 2009;55(2):115-9.
13. Greub G. International Committee on Systematics of Prokaryotes. Subcommittee on the taxonomy of the Chlamydiae: minutes of the closed meeting, 21 June 2010, Hof bei Salzburg, Austria. Int J Syst Evol Microbiol. 2010;60(Pt 11):2694.
14. Pannekoek Y, Qi-Long Q, Zhang YZ, van der Ende A. Genus delineation of Chlamydiales by analysis of the percentage of conserved proteins justifies the reunifying of the genera Chlamydia and Chlamydophila into one single genus Chlamydia. Pathog Dis. 2016;74(6).
15. Pillonel T, Bertelli C, Salamin N, Greub G. Taxogenomics of the order Chlamydiales. Int J Syst Evol Microbiol. 2015;65(Pt 4):1381-93.
16. Luu LDW, Kasimov V, Phillips S, Myers GSA, Jelocnik M. Genome organization and genomics in Chlamydia: whole genome sequencing increases understanding of chlamydial virulence, evolution, and phylogeny. Front Cell Infect Microbiol. 2023;13:1178736.
17. Voigt A, Schofl G, Saluz HP. The Chlamydia psittaci genome: a comparative analysis of intracellular pathogens. PLoS One. 2012;7(4):e35097.

18. Nunes A, Gomes JP. Evolution, phylogeny, and molecular epidemiology of Chlamydia. Infect Genet Evol. 2014;23C:49-64.
19. Moran NA. Microbial minimalism: genome reduction in bacterial pathogens. Cell. 2002;108(5):583-6.
20. Dharamshi JE, Kostlbacher S, Schon ME, Collingro A, Ettema TJG, Horn M. Gene gain facilitated endosymbiotic evolution of Chlamydiae. Nat Microbiol. 2023;8(1):40-54.
21. Collingro A, Tischler P, Weinmaier T, Penz T, Heinz E, Brunham RC, et al. Unity in variety--the pan-genome of the Chlamydiae. Mol Biol Evol. 2011;28(12):3253-70.
22. Bachmann NL, Polkinghorne A, Timms P. Chlamydia genomics: providing novel insights into chlamydial biology. Trends Microbiol. 2014;22(8):464-72.
23. Sigalova OM, Chaplin AV, Bochkareva OO, Shelyakin PV, Filaretov VA, Akkuratov EE, et al. Chlamydia pan-genomic analysis reveals balance between host adaptation and selective pressure to genome reduction. BMC Genomics. 2019;20(1):710.
24. Zhong G. Chlamydial Plasmid-Dependent Pathogenicity. Trends Microbiol. 2017;25(2):141-52.
25. Turman BJ, Darville T, O'Connell CM. Plasmid-mediated virulence in Chlamydia. Front Cell Infect Microbiol. 2023;13:1251135.
26. Valdivia RH, Bastidas RJ. The Expanding Molecular Genetics Tool Kit in Chlamydia. J Bacteriol. 2018;200(24).
27. DeMars R, Weinfurter J. Interstrain gene transfer in Chlamydia trachomatis in vitro: mechanism and significance. J Bacteriol. 2008;190(5):1605-14.
28. Richards TS, Knowlton AE, Grieshaber SS. Chlamydia trachomatis homotypic inclusion fusion is promoted by host microtubule trafficking. BMC Microbiol. 2013;13:185.
29. Wang Y, Kahane S, Cutcliffe LT, Skilton RJ, Lambden PR, Clarke IN. Development of a transformation system for Chlamydia trachomatis: restoration of glycogen biosynthesis by acquisition of a plasmid shuttle vector. PLoS Pathog. 2011;7(9):e1002258.
30. Mandel M, Higa A. Calcium-dependent bacteriophage DNA infection. J Mol Biol. 1970;53(1):159-62.
31. Mueller KE, Wolf K, Fields KA. Gene Deletion by Fluorescence-Reported Allelic Exchange Mutagenesis in Chlamydia trachomatis. mBio. 2016;7(1):e01817-15.
32. Keb G, Hayman R, Fields KA. Floxed-Cassette Allelic Exchange Mutagenesis Enables Markerless Gene Deletion in Chlamydia trachomatis and Can Reverse Cassette-Induced Polar Effects. J Bacteriol. 2018;200(24).
33. Sixt BS, Valdivia RH. Molecular Genetic Analysis of Chlamydia Species. Annu Rev Microbiol. 2016;70:179-98.
34. Wolf K, Rahnama M, Fields KA. Genetic Manipulation of Chlamydia trachomatis: Chromosomal Deletions. Methods Mol Biol. 2019;2042:151-64.
35. Mishra MK, Gerard HC, Whittum-Hudson JA, Hudson AP, Kannan RM. Dendrimer-enabled modulation of gene expression in Chlamydia trachomatis. Mol Pharm. 2012;9(3):413-21.
36. Wan W, Li D, Li D, Jiao J. Advances in genetic manipulation of Chlamydia trachomatis. Front Immunol. 2023;14:1209879.
37. Shima K, Wanker M, Skilton RJ, Cutcliffe LT, Schnee C, Kohl TA, et al. The Genetic Transformation of Chlamydia pneumoniae. mSphere. 2018;3(5).

38. Knittler MR, Sachse K. Chlamydia psittaci: update on an underestimated zoonotic agent. Pathog Dis. 2015;73(1):1-15.
39. Mohseni M, Sung S, Takov V. Chlamydia. StatPearls. Treasure Island (FL)2024.
40. Chlamydia; 2023 [Available from: https://www.who.int/news-room/fact-sheets/detail/chlamydia]
41. Elwell C, Mirrashidi K, Engel J. Chlamydia cell biology and pathogenesis. Nat Rev Microbiol. 2016;14(6):385-400.
42. Mabey D, Peeling RW. Lymphogranuloma venereum. Sex Transm Infect. 2002;78(2):90-2.
43. Stoner BP, Cohen SE. Lymphogranuloma Venereum 2015: Clinical Presentation, Diagnosis, and Treatment. Clin Infect Dis. 2015;61 Suppl 8:S865-73.
44. Kuo CC, Jackson LA, Campbell LA, Grayston JT. Chlamydia pneumoniae (TWAR). Clin Microbiol Rev. 1995;8(4):451-61.
45. Gautam J, Krawiec C. Chlamydia Pneumonia. StatPearls. Treasure Island (FL)2024.
46. Hahn DL, Azenabor AA, Beatty WL, Byrne GI. Chlamydia pneumoniae as a respiratory pathogen. Front Biosci. 2002;7:e66-76.
47. Porritt RA, Crother TR. Chlamydia pneumoniae Infection and Inflammatory Diseases. For Immunopathol Dis Therap. 2016;7(3-4):237-54.
48. Batteiger BE. Chlamydia Infection and Epidemiology. Intracellular Pathogens I2012. p. 1-26.
49. Murthy AK, Arulanandam BP, Zhong G. Chlamydia Vaccine: Progress and Challenges. Intracellular Pathogens I2012. p. 311-33.
50. Panzetta ME, Valdivia RH, Saka HA. Chlamydia Persistence: A Survival Strategy to Evade Antimicrobial Effects in-vitro and in-vivo. Front Microbiol. 2018;9:3101.
51. Matsumoto A. Fine structures of cell envelopes of Chlamydia organisms as revealed by freeze-etching and negative staining techniques. J Bacteriol. 1973;116(3):1355-63.
52. Roe SK, Zhu T, Slepenkin A, Berges A, Fairman J, de la Maza LM, et al. Structural Assessment of Chlamydia trachomatis Major Outer Membrane Protein (MOMP)-Derived Vaccine Antigens and Immunological Profiling in Mice with Different Genetic Backgrounds. Vaccines (Basel). 2024;12(7).
53. Longbottom D, Livingstone M, Aitchison KD, Imrie L, Manson E, Wheelhouse N, et al. Proteomic characterisation of the Chlamydia abortus outer membrane complex (COMC) using combined rapid monolithic column liquid chromatography and fast MS/MS scanning. PLoS One. 2019;14(10):e0224070.
54. Everett KD, Hatch TP. Architecture of the cell envelope of Chlamydia psittaci 6BC. J Bacteriol. 1995;177(4):877-82.
55. N'Gadjaga MD, Perrinet S, Connor MG, Bertolin G, Millot GA, Subtil A. Chlamydia trachomatis development requires both host glycolysis and oxidative phosphorylation but has only minor effects on these pathways. J Biol Chem. 2022;298(9):102338.
56. Hybiske K, Stephens RS. Mechanisms of host cell exit by the intracellular bacterium Chlamydia. Proc Natl Acad Sci U S A. 2007;104(27):11430-5.
57. Hammerschlag MR. The intracellular life of chlamydiae. Semin Pediatr Infect Dis. 2002;13(4):239-48.

58. Wolf K, Fischer E, Hackstadt T. Ultrastructural analysis of developmental events in Chlamydia pneumoniae-infected cells. Infect Immun. 2000;68(4):2379-85.
59. Hegemann JH, Moelleken K. Chlamydial adhesion and adhesins. In: Tan M, Bavoil, P., editor. Intracellular Pathogens I: Chlamydiales Washington, DC: ASM Press; 2012.
60. Kuo CC, Grayston T. Interaction of Chlamydia trachomatis organisms and HeLa 229 cells. Infect Immun. 1976;13(4):1103-9.
61. Romero MD, Moelleken K, Hegemann JH, Carabeo RA. Chlamydia Adhesion and Invasion. Chlamydia Biology: From Genome to Disease. 2020:59-84.
62. Su H, Raymond L, Rockey DD, Fischer E, Hackstadt T, Caldwell HD. A recombinant Chlamydia trachomatis major outer membrane protein binds to heparan sulfate receptors on epithelial cells. Proc Natl Acad Sci U S A. 1996;93(20):11143-8.
63. Stephens RS, Koshiyama K, Lewis E, Kubo A. Heparin-binding outer membrane protein of chlamydiae. Mol Microbiol. 2001;40(3):691-9.
64. Fechtner T, Stallmann S, Moelleken K, Meyer KL, Hegemann JH. Characterization of the interaction between the chlamydial adhesin OmcB and the human host cell. J Bacteriol. 2013;195(23):5323-33.
65. Wuppermann FN, Hegemann JH, Jantos CA. Heparan Sulfate-like Glycosaminoglycan Is a Cellular Receptor for Chlamydia pneumoniae. J Infect Dis. 2001;184(2):181-7.
66. Mölleken K, Hegemann JH. The Chlamydia outer membrane protein OmcB is required for adhesion and exhibits biovar-specific differences in glycosaminoglycan binding. Mol Microbiol. 2008;67(2):403-19.
67. Puolakkainen M, Kuo CC, Campbell LA. Chlamydia pneumoniae uses the mannose 6-phosphate/insulin-like growth factor 2 receptor for infection of endothelial cells. Infect Immun. 2005;73(8):4620-5.
68. Stallmann S, Hegemann JH. The Chlamydia trachomatis Ctad1 invasin exploits the human integrin beta1 receptor for host cell entry. Cell Microbiol. 2016;18(5):761-75.
69. Wuppermann FN, Mölleken K, Julien M, Jantos CA, Hegemann JH. Chlamydia pneumoniae GroEL1 protein is cell surface associated and required for infection of HEp-2 cells. J Bacteriol. 2008;190(10):3757-67.
70. Galle JN, Fechtner T, Eierhoff T, Römer W, Hegemann JH. A Chlamydia pneumoniae adhesin induces phosphatidylserine exposure on host cells. Nat Commun. 2019;10(1):4644.
71. Longbottom D, Russell M, Jones GE, Lainson FA, Herring AJ. Identification of a multigene family coding for the 90 kDa proteins of the ovine abortion subtype of Chlamydia psittaci. FEMS Microbiol Lett. 1996;142(2-3):277-81.
72. Kalman S, Mitchell W, Marathe R, Lammel C, Fan J, Hyman RW, et al. Comparative genomes of Chlamydia pneumoniae and C. trachomatis. Nat Genet. 1999;21(4):385-9.
73. Kebbi-Beghdadi C, Domrose A, Becker E, Cisse OH, Hegemann JH, Greub G. OmpA family proteins and Pmp-like autotransporter: new adhesins of Waddlia chondrophila. Pathog Dis. 2015;73(6):ftv035.
74. Rockey DD, Lenart J, Stephens RS. Genome sequencing and our understanding of chlamydiae. Infect Immun. 2000;68(10):5473-9.
75. Grimwood J, Stephens RS. Computational analysis of the polymorphic membrane protein superfamily of Chlamydia trachomatis and Chlamydia pneumoniae. Microb Comp Genomics. 1999;4(3):187-201.

76. Knudsen K, Madsen AS, Mygind P, Christiansen G, Birkelund S. Identification of two novel genes encoding 97- to 99-kilodalton outer membrane proteins of Chlamydia pneumoniae. Infect Immun. 1999;67(1):375-83.
77. Longbottom D, Russell M, Dunbar SM, Jones GE, Herring AJ. Molecular cloning and characterization of the genes coding for the highly immunogenic cluster of 90-kilodalton envelope proteins from the Chlamydia psittaci subtype that causes abortion in sheep. Infect Immun. 1998;66(4):1317-24.
78. Carrasco JA, Tan C, Rank RG, Hsia RC, Bavoil PM. Altered developmental expression of polymorphic membrane proteins in penicillin-stressed Chlamydia trachomatis. Cell Microbiol. 2011;13(7):1014-25.
79. Grimwood J, Olinger L, Stephens RS. Expression of Chlamydia pneumoniae polymorphic membrane protein family genes. Infect Immun. 2001;69(4):2383-9.
80. Vandahl BB, Birkelund S, Demol H, Hoorelbeke B, Christiansen G, Vandekerckhove J, et al. Proteome analysis of the Chlamydia pneumoniae elementary body. Electrophoresis. 2001;22(6):1204-23.
81. Tan C, Hsia RC, Shou H, Carrasco JA, Rank RG, Bavoil PM. Variable expression of surface-exposed polymorphic membrane proteins in in vitro-grown Chlamydia trachomatis. Cell Microbiol. 2010;12(2):174-87.
82. EMBL's European Bioinformatics Institute; 2023 [Available from: https://www.ebi.ac.uk/]
83. RStudio Team (2020). RStudio: Integrated Development Environment for R. RStudio, Boston, MA. Available from: http://www.rstudio.com/
84. Mirdita M, Schutze K, Moriwaki Y, Heo L, Ovchinnikov S, Steinegger M. ColabFold: making protein folding accessible to all. Nat Methods. 2022;19(6):679-82.
85. Vasilevsky S, Stojanov M, Greub G, Baud D. Chlamydial polymorphic membrane proteins: regulation, function and potential vaccine candidates. Virulence. 2016;7(1):11-22.
86. Becker E. Charakterisierung der chlamydialen Pmp Adhäsin Familie [Dissertation]2013.
87. Gomes JP, Nunes A, Bruno WJ, Borrego MJ, Florindo C, Dean D. Polymorphisms in the nine polymorphic membrane proteins of Chlamydia trachomatis across all serovars: evidence for serovar Da recombination and correlation with tissue tropism. J Bacteriol. 2006;188(1):275-86.
88. Henderson IR, Lam AC. Polymorphic proteins of Chlamydia spp.--autotransporters beyond the Proteobacteria. Trends Microbiol. 2001;9(12):573-8.
89. Vandahl BB, Pedersen AS, Gevaert K, Holm A, Vandekerckhove J, Christiansen G, et al. The expression, processing and localization of polymorphic membrane proteins in Chlamydia pneumoniae strain CWL029. BMC Microbiol. 2002;2(1):36.
90. Wehrl W, Brinkmann V, Jungblut PR, Meyer TF, Szczepek AJ. From the inside out--processing of the Chlamydial autotransporter PmpD and its role in bacterial adhesion and activation of human host cells. Mol Microbiol. 2004;51(2):319-34.
91. Kiselev AO, Stamm WE, Yates JR, Lampe MF. Expression, processing, and localization of PmpD of Chlamydia trachomatis serovar L2 during the chlamydial developmental cycle. PLoS ONE. 2007;2(6):e568.
92. Saka HA, Thompson JW, Chen YS, Kumar Y, Dubois LG, Moseley MA, et al. Quantitative proteomics reveals metabolic and pathogenic properties of

Chlamydia trachomatis developmental forms. Mol Microbiol. 2011;82(5):1185-203.
93. Becker E, Hegemann JH. All subtypes of the Pmp adhesin family are implicated in chlamydial virulence and show species-specific function. Microbiologyopen. 2014;3(4):544-56.
94. Mölleken K, Schmidt E, Hegemann JH. Members of the Pmp protein family of Chlamydia pneumoniae mediate adhesion to human cells via short repetitive peptide motifs. Mol Microbiol. 2010;78(4):1004-17.
95. Luczak SE, Smits SH, Decker C, Nagel-Steger L, Schmitt L, Hegemann JH. The Chlamydia pneumoniae Adhesin Pmp21 Forms Oligomers with Adhesive Properties. J Biol Chem. 2016;291(43):22806-18.
96. Favaroni A, Hegemann JH. Chlamydia trachomatis Polymorphic Membrane Proteins (Pmps) Form Functional Homomeric and Heteromeric Oligomers. Front Microbiol. 2021;12:709724.
97. Favaroni A, Trinks A, Weber M, Hegemann JH, Schnee C. Pmp Repertoires Influence the Different Infectious Potential of Avian and Mammalian Chlamydia psittaci Strains. Front Microbiol. 2021;12:656209.
98. Hillman RD, Jr., Baktash YM, Martinez JJ. OmpA-mediated rickettsial adherence to and invasion of human endothelial cells is dependent upon interaction with alpha2beta1 integrin. Cell Microbiol. 2013;15(5):727-41.
99. Herlyn H, Zischler H. The molecular evolution of sperm zonadhesin. Int J Dev Biol. 2008;52(5-6):781-90.
100. Thornton DJ, Rousseau K, McGuckin MA. Structure and function of the polymeric mucins in airways mucus. Annu Rev Physiol. 2008;70:459-86.
101. Paes W, Dowle A, Coldwell J, Leech A, Ganderton T, Brzozowski A. The Chlamydia trachomatis PmpD adhesin forms higher order structures through disulphide-mediated covalent interactions. PLoS One. 2018;13(6):e0198662.
102. Cervantes PW, Segelke BW, Lau EY, Robinson BV, Abisoye-Ogunniyan A, Pal S, et al. Sequence, structure prediction, and epitope analysis of the polymorphic membrane protein family in Chlamydia trachomatis. PLoS One. 2024;19(6):e0304525.
103. Debrine AM, Karplus PA, Rockey DD. A structural foundation for studying chlamydial polymorphic membrane proteins. Microbiol Spectr. 2023;11(6):e0324223.
104. Nunes A, Gomes JP, Mead S, Florindo C, Correia H, Borrego MJ, et al. Comparative expression profiling of the Chlamydia trachomatis pmp gene family for clinical and reference strains. PLoS ONE. 2007;2(9):e878.
105. Skipp P, Robinson J, O'Connor CD, Clarke IN. Shotgun proteomic analysis of Chlamydia trachomatis. Proteomics. 2005;5(6):1558-73.
106. Van Lent S, De Vos WH, Huot Creasy H, Marques PX, Ravel J, Vanrompay D, et al. Analysis of Polymorphic Membrane Protein Expression in Cultured Cells Identifies PmpA and PmpH of Chlamydia psittaci as Candidate Factors in Pathogenesis and Immunity to Infection. PLoS One. 2016;11(9):e0162392.
107. Crane DD, Carlson JH, Fischer ER, Bavoil P, Hsia RC, Tan C, et al. Chlamydia trachomatis polymorphic membrane protein D is a species-common pan-neutralizing antigen. Proc Natl Acad Sci U S A. 2006;103(6):1894-9.
108. Mölleken K, Becker E, Hegemann JH. The Chlamydia pneumoniae invasin protein Pmp21 recruits the EGF receptor for host cell entry. PLoS Pathog. 2013;9(4):e1003325.

109. Schlessinger J. Cell signaling by receptor tyrosine kinases. Cell. 2000;103(2):211-25.
110. Li X, Zuo Z, Wang Y, Hegemann JH, He C. Polymorphic Membrane Protein 17G of Chlamydia psittaci Mediated the Binding and Invasion of Bacteria to Host Cells by Interacting and Activating EGFR of the Host. Front Immunol. 2021;12:818487.
111. Kari L, Southern TR, Downey CJ, Watkins HS, Randall LB, Taylor LD, et al. Chlamydia trachomatis polymorphic membrane protein D is a virulence factor involved in early host-cell interactions. Infect Immun. 2014;82(7):2756-62.
112. Carlson JH, Porcella SF, McClarty G, Caldwell HD. Comparative genomic analysis of Chlamydia trachomatis oculotropic and genitotropic strains. Infect Immun. 2005;73(10):6407-18.
113. Swanson KA, Taylor LD, Frank SD, Sturdevant GL, Fischer ER, Carlson JH, et al. Chlamydia trachomatis polymorphic membrane protein D is an oligomeric autotransporter with a higher-order structure. Infect Immun. 2009;77(1):508-16.
114. Montigiani S, Falugi F, Scarselli M, Finco O, Petracca R, Galli G, et al. Genomic approach for analysis of surface proteins in Chlamydia pneumoniae. Infect Immun. 2002;70(1):368-79.
115. Kiselev AO, Skinner MC, Lampe MF. Analysis of pmpD expression and PmpD post-translational processing during the life cycle of Chlamydia trachomatis serovars A, D, and L2. PLoS One. 2009;4(4):e5191.
116. Wheelhouse NM, Sait M, Aitchison K, Livingstone M, Wright F, McLean K, et al. Processing of Chlamydia abortus Polymorphic Membrane Protein 18D during the Chlamydial Developmental Cycle. PLoS One. 2012;7(11):e49190.
117. Gu L, Guo Z. Alzheimer's Abeta42 and Abeta40 peptides form interlaced amyloid fibrils. J Neurochem. 2013;126(3):305-11.
118. WHO. Global health sectors strategy on sexually transmitted infections 2016-2021. 2016.
119. Baud D, Greub G. Intracellular bacteria and adverse pregnancy outcomes. Clin Microbiol Infect. 2011;17(9):1312-22.
120. Johnson RE, Newhall WJ, Papp JR, Knapp JS, Black CM, Gift TL, et al. Screening tests to detect Chlamydia trachomatis and Neisseria gonorrhoeae infections--2002. MMWR Recomm Rep. 2002;51(RR-15):1-38; quiz CE1-4.
121. Brunham RC, Rappuoli R. Chlamydia trachomatis control requires a vaccine. Vaccine. 2013;31(15):1892-7.
122. Liang S, Bulir D, Kaushic C, Mahony J. Considerations for the rational design of a Chlamydia vaccine. Hum Vaccin Immunother. 2017;13(4):831-5.
123. Phillips S, Quigley BL, Timms P. Seventy Years of Chlamydia Vaccine Research - Limitations of the Past and Directions for the Future. Front Microbiol. 2019;10:70.
124. Stephens RS, Wagar EA, Schoolnik GK. High-resolution mapping of serovar-specific and common antigenic determinants of the major outer membrane protein of Chlamydia trachomatis. J Exp Med. 1988;167(3):817-31.
125. Stephens RS, Sanchez Pescador R, Wagar EA, Inouye C, Urdea MS. Diversity of Chlamydia trachomatis major outer membrane protein genes. J Bacteriol. 1987;169(9):3879-85.
126. Pal S, Theodor I, Peterson EM, de la Maza LM. Immunization with the Chlamydia trachomatis mouse pneumonitis major outer membrane protein can elicit a protective immune response against a genital challenge. Infect Immun. 2001;69(10):6240-7.

127. Pal S, Peterson EM, Rappuoli R, Ratti G, de la Maza LM. Immunization with the Chlamydia trachomatis major outer membrane protein, using adjuvants developed for human vaccines, can induce partial protection in a mouse model against a genital challenge. Vaccine. 2006;24(6):766-75.
128. Pal S, Tifrea DF, Follmann F, Andersen P, de la Maza LM. The cationic liposomal adjuvants CAF01 and CAF09 formulated with the major outer membrane protein elicit robust protection in mice against a Chlamydia muridarum respiratory challenge. Vaccine. 2017;35(13):1705-11.
129. Pal S, Slepenkin A, Felgner J, Huw Davies D, Felgner P, de la Maza LM. Evaluation of Four Adjuvant Combinations, IVAX-1, IVAX-2, CpG-1826+Montanide ISA 720 VG and CpG-1018+Montanide ISA 720 VG, for Safety and for Their Ability to Elicit Protective Immune Responses in Mice against a Respiratory Challenge with Chlamydia muridarum. Pathogens. 2023;12(7).
130. Cheng C, Pal S, Tifrea D, Jia Z, de la Maza LM. A vaccine formulated with a combination of TLR-2 and TLR-9 adjuvants and the recombinant major outer membrane protein elicits a robust immune response and significant protection against a Chlamydia muridarum challenge. Microbes Infect. 2014;16(3):244-52.
131. Sahu R, Dixit S, Verma R, Duncan SA, Coats MT, Giambartolomei GH, et al. A nanovaccine formulation of Chlamydia recombinant MOMP encapsulated in PLGA 85:15 nanoparticles augments CD4(+) effector (CD44(high) CD62L(low)) and memory (CD44(high) CD62L(high)) T-cells in immunized mice. Nanomedicine. 2020;29:102257.
132. Sun G, Pal S, Weiland J, Peterson EM, de la Maza LM. Protection against an intranasal challenge by vaccines formulated with native and recombinant preparations of the Chlamydia trachomatis major outer membrane protein. Vaccine. 2009;27(36):5020-5.
133. Ralli-Jain P, Tifrea D, Cheng C, Pal S, de la Maza LM. Enhancement of the protective efficacy of a Chlamydia trachomatis recombinant vaccine by combining systemic and mucosal routes for immunization. Vaccine. 2010;28(48):7659-66.
134. Kari L, Whitmire WM, Crane DD, Reveneau N, Carlson JH, Goheen MM, et al. Chlamydia trachomatis native major outer membrane protein induces partial protection in nonhuman primates: implication for a trachoma transmission-blocking vaccine. J Immunol. 2009;182(12):8063-70.
135. Olsen AW, Follmann F, Erneholm K, Rosenkrands I, Andersen P. Protection Against Chlamydia trachomatis Infection and Upper Genital Tract Pathological Changes by Vaccine-Promoted Neutralizing Antibodies Directed to the VD4 of the Major Outer Membrane Protein. J Infect Dis. 2015;212(6):978-89.
136. Abraham S, Juel HB, Bang P, Cheeseman HM, Dohn RB, Cole T, et al. Safety and immunogenicity of the chlamydia vaccine candidate CTH522 adjuvanted with CAF01 liposomes or aluminium hydroxide: a first-in-human, randomised, double-blind, placebo-controlled, phase 1 trial. Lancet Infect Dis. 2019;19(10):1091-100.
137. Bunk S, Susnea I, Rupp J, Summersgill JT, Maass M, Stegmann W, et al. Immunoproteomic identification and serological responses to novel Chlamydia pneumoniae antigens that are associated with persistent C. pneumoniae infections. J Immunol. 2008;180(8):5490-8.
138. Tan C, Hsia RC, Shou H, Haggerty CL, Ness RB, Gaydos CA, et al. Chlamydia trachomatis-infected patients display variable antibody profiles against the nine-

member polymorphic membrane protein family. Infect Immun. 2009;77(8):3218-26.
139. Paes W, Brown N, Brzozowski AM, Coler R, Reed S, Carter D, et al. Recombinant polymorphic membrane protein D in combination with a novel, second-generation lipid adjuvant protects against intra-vaginal Chlamydia trachomatis infection in mice. Vaccine. 2016;34(35):4123-31.
140. Muller T, Becker E, Stallmann S, Waldhuber A, Rommler-Dreher F, Albrecht S, et al. Vaccination with the polymorphic membrane protein A reduces Chlamydia muridarum induced genital tract pathology. Vaccine. 2017;35(21):2801-10.
141. Pal S, Favaroni A, Tifrea DF, Hanisch PT, Luczak SET, Hegemann JH, et al. Comparison of the nine polymorphic membrane proteins of Chlamydia trachomatis for their ability to induce protective immune responses in mice against a C. muridarum challenge. Vaccine. 2017;35(19):2543-9.
142. Lanfermann C, Wintgens S, Ebensen T, Kohn M, Laudeley R, Schulze K, et al. Prophylactic Multi-Subunit Vaccine against Chlamydia trachomatis: In Vivo Evaluation in Mice. Vaccines (Basel). 2021;9(6).
143. Zhong G, Fan P, Ji H, Dong F, Huang Y. Identification of a chlamydial protease-like activity factor responsible for the degradation of host transcription factors. J Exp Med. 2001;193(8):935-42.
144. Chen H, Peng B, Yang C, Xie L, Zhong S, Sun Z, et al. The role of an enzymatically inactive CPAF mutant vaccination in Chlamydia muridarum genital tract infection. Microb Pathog. 2021;160:105137.
145. Murthy AK, Chambers JP, Meier PA, Zhong G, Arulanandam BP. Intranasal vaccination with a secreted chlamydial protein enhances resolution of genital Chlamydia muridarum infection, protects against oviduct pathology, and is highly dependent upon endogenous gamma interferon production. Infect Immun. 2007;75(2):666-76.
146. Penalva MA, Tilburn J, Bignell E, Arst HN, Jr. Ambient pH gene regulation in fungi: making connections. Trends Microbiol. 2008;16(6):291-300.
147. Alberts B, Heald R, Johnson A, Morgan D, Raff M, Roberts K, et al. Molecular biology of the cell. Seventh edition, international student edition ed. New York, NY: W.W. Norton & Company; 2022.
148. Kumari S, Mg S, Mayor S. Endocytosis unplugged: multiple ways to enter the cell. Cell Res. 2010;20(3):256-75.
149. Mukherjee S, Ghosh RN, Maxfield FR. Endocytosis. Physiol Rev. 1997;77(3):759-803.
150. Kaksonen M, Roux A. Mechanisms of clathrin-mediated endocytosis. Nat Rev Mol Cell Biol. 2018;19(5):313-26.
151. Maldonado-Baez L, Williamson C, Donaldson JG. Clathrin-independent endocytosis: a cargo-centric view. Exp Cell Res. 2013;319(18):2759-69.
152. Smith SM, Smith CJ. Capturing the mechanics of clathrin-mediated endocytosis. Curr Opin Struct Biol. 2022;75:102427.
153. Smith SM, Baker M, Halebian M, Smith CJ. Weak Molecular Interactions in Clathrin-Mediated Endocytosis. Front Mol Biosci. 2017;4:72.
154. Sigismund S, Argenzio E, Tosoni D, Cavallaro E, Polo S, Di Fiore PP. Clathrin-mediated internalization is essential for sustained EGFR signaling but dispensable for degradation. Dev Cell. 2008;15(2):209-19.
155. Edeling MA, Smith C, Owen D. Life of a clathrin coat: insights from clathrin and AP structures. Nat Rev Mol Cell Biol. 2006;7(1):32-44.

156. Rennick JJ, Johnston APR, Parton RG. Key principles and methods for studying the endocytosis of biological and nanoparticle therapeutics. Nat Nanotechnol. 2021;16(3):266-76.
157. Collins A, Warrington A, Taylor KA, Svitkina T. Structural organization of the actin cytoskeleton at sites of clathrin-mediated endocytosis. Curr Biol. 2011;21(14):1167-75.
158. Merrifield CJ, Qualmann B, Kessels MM, Almers W. Neural Wiskott Aldrich Syndrome Protein (N-WASP) and the Arp2/3 complex are recruited to sites of clathrin-mediated endocytosis in cultured fibroblasts. Eur J Cell Biol. 2004;83(1):13-8.
159. McMahon HT, Boucrot E. Molecular mechanism and physiological functions of clathrin-mediated endocytosis. Nat Rev Mol Cell Biol. 2011;12(8):517-33.
160. Heuser J. Three-dimensional visualization of coated vesicle formation in fibroblasts. J Cell Biol. 1980;84(3):560-83.
161. Hinshaw JE, Schmid SL. Dynamin self-assembles into rings suggesting a mechanism for coated vesicle budding. Nature. 1995;374(6518):190-2.
162. Lundmark R, Carlsson SR. SNX9 - a prelude to vesicle release. J Cell Sci. 2009;122(Pt 1):5-11.
163. Takei K, Slepnev VI, Haucke V, De Camilli P. Functional partnership between amphiphysin and dynamin in clathrin-mediated endocytosis. Nat Cell Biol. 1999;1(1):33-9.
164. El Alaoui F, Casuso I, Sanchez-Fuentes D, Arpin-Andre C, Rathar R, Baecker V, et al. Structural organization and dynamics of FCHo2 docking on membranes. Elife. 2022;11.
165. Roux A, Koster G, Lenz M, Sorre B, Manneville JB, Nassoy P, et al. Membrane curvature controls dynamin polymerization. Proc Natl Acad Sci U S A. 2010;107(9):4141-6.
166. Shin N, Ahn N, Chang-Ileto B, Park J, Takei K, Ahn SG, et al. SNX9 regulates tubular invagination of the plasma membrane through interaction with actin cytoskeleton and dynamin 2. J Cell Sci. 2008;121(Pt 8):1252-63.
167. Yarar D, Waterman-Storer CM, Schmid SL. SNX9 couples actin assembly to phosphoinositide signals and is required for membrane remodeling during endocytosis. Dev Cell. 2007;13(1):43-56.
168. Bendris N, Schmid SL. Endocytosis, Metastasis and Beyond: Multiple Facets of SNX9. Trends Cell Biol. 2017;27(3):189-200.
169. Schlossman DM, Schmid SL, Braell WA, Rothman JE. An enzyme that removes clathrin coats: purification of an uncoating ATPase. J Cell Biol. 1984;99(2):723-33.
170. Ungewickell E, Ungewickell H, Holstein SE, Lindner R, Prasad K, Barouch W, et al. Role of auxilin in uncoating clathrin-coated vesicles. Nature. 1995;378(6557):632-5.
171. Herrmann T, Leavitt L, Sharma S. Physiology, Membrane. StatPearls. Treasure Island (FL)2024.
172. McMahon HT, Boucrot E. Membrane curvature at a glance. J Cell Sci. 2015;128(6):1065-70.
173. Itoh T, Takenawa T. Regulation of endocytosis by phosphatidylinositol 4,5-bisphosphate and ENTH proteins. Curr Top Microbiol Immunol. 2004;282:31-47.

174. Kostan J, Salzer U, Orlova A, Toro I, Hodnik V, Senju Y, et al. Direct interaction of actin filaments with F-BAR protein pacsin2. EMBO Rep. 2014;15(11):1154-62.
175. Fletcher DA, Mullins RD. Cell mechanics and the cytoskeleton. Nature. 2010;463(7280):485-92.
176. Cavini IA, Leonardo DA, Rosa HVD, Castro D, D'Muniz Pereira H, Valadares NF, et al. The Structural Biology of Septins and Their Filaments: An Update. Front Cell Dev Biol. 2021;9:765085.
177. Granger E, McNee G, Allan V, Woodman P. The role of the cytoskeleton and molecular motors in endosomal dynamics. Semin Cell Dev Biol. 2014;31(100):20-9.
178. Abouelezz A, Almeida-Souza L. The mammalian endocytic cytoskeleton. Eur J Cell Biol. 2022;101(2):151222.
179. Pollard TD, Goldman RD. Overview of the Cytoskeleton from an Evolutionary Perspective. Cold Spring Harb Perspect Biol. 2018;10(7).
180. Blanchoin L, Amann KJ, Higgs HN, Marchand JB, Kaiser DA, Pollard TD. Direct observation of dendritic actin filament networks nucleated by Arp2/3 complex and WASP/Scar proteins. Nature. 2000;404(6781):1007-11.
181. Chan FY, Silva AM, Saramago J, Pereira-Sousa J, Brighton HE, Pereira M, et al. The ARP2/3 complex prevents excessive formin activity during cytokinesis. Mol Biol Cell. 2019;30(1):96-107.
182. Pollard TD. Regulation of actin filament assembly by Arp2/3 complex and formins. Annu Rev Biophys Biomol Struct. 2007;36:451-77.
183. Shin N, Lee S, Ahn N, Kim SA, Ahn SG, YongPark Z, et al. Sorting nexin 9 interacts with dynamin 1 and N-WASP and coordinates synaptic vesicle endocytosis. J Biol Chem. 2007;282(39):28939-50.
184. Takenawa T, Miki H. WASP and WAVE family proteins: key molecules for rapid rearrangement of cortical actin filaments and cell movement. J Cell Sci. 2001;114(Pt 10):1801-9.
185. Rohatgi R, Ma L, Miki H, Lopez M, Kirchhausen T, Takenawa T, et al. The interaction between N-WASP and the Arp2/3 complex links Cdc42-dependent signals to actin assembly. Cell. 1999;97(2):221-31.
186. Kaksonen M, Toret CP, Drubin DG. Harnessing actin dynamics for clathrin-mediated endocytosis. Nat Rev Mol Cell Biol. 2006;7(6):404-14.
187. Carlton J, Bujny M, Rutherford A, Cullen P. Sorting nexins--unifying trends and new perspectives. Traffic. 2005;6(2):75-82.
188. Teasdale RD, Collins BM. Insights into the PX (phox-homology) domain and SNX (sorting nexin) protein families: structures, functions and roles in disease. Biochem J. 2012;441(1):39-59.
189. Yarar D, Surka MC, Leonard MC, Schmid SL. SNX9 activities are regulated by multiple phosphoinositides through both PX and BAR domains. Traffic. 2008;9(1):133-46.
190. Feng S, Chen JK, Yu H, Simon JA, Schreiber SL. Two binding orientations for peptides to the Src SH3 domain: development of a general model for SH3-ligand interactions. Science. 1994;266(5188):1241-7.
191. Spona D, Hanisch PT, Hegemann JH, Molleken K. A single chlamydial protein reshapes the plasma membrane and serves as recruiting platform for central endocytic effector proteins. Commun Biol. 2023;6(1):520.

192. Marches O, Batchelor M, Shaw RK, Patel A, Cummings N, Nagai T, et al. EspF of enteropathogenic Escherichia coli binds sorting nexin 9. J Bacteriol. 2006;188(8):3110-5.
193. Lundmark R, Carlsson SR. The beta-appendages of the four adaptor-protein (AP) complexes: structure and binding properties, and identification of sorting nexin 9 as an accessory protein to AP-2. Biochem J. 2002;362(Pt 3):597-607.
194. Soulet F, Yarar D, Leonard M, Schmid SL. SNX9 regulates dynamin assembly and is required for efficient clathrin-mediated endocytosis. Mol Biol Cell. 2005;16(4):2058-67.
195. Kramer DA, Piper HK, Chen B. WASP family proteins: Molecular mechanisms and implications in human disease. Eur J Cell Biol. 2022;101(3):151244.
196. Stradal TE, Rottner K, Disanza A, Confalonieri S, Innocenti M, Scita G. Regulation of actin dynamics by WASP and WAVE family proteins. Trends Cell Biol. 2004;14(6):303-11.
197. Shen G, Whittington A, Wang P. Wsp1, a GBD/CRIB domain-containing WASP homolog, is required for growth, morphogenesis, and virulence of Cryptococcus neoformans. Eukaryot Cell. 2011;10(4):521-9.
198. Rohatgi R, Ho HY, Kirschner MW. Mechanism of N-WASP activation by CDC42 and phosphatidylinositol 4, 5-bisphosphate. J Cell Biol. 2000;150(6):1299-310.
199. Abdul-Manan N, Aghazadeh B, Liu GA, Majumdar A, Ouerfelli O, Siminovitch KA, et al. Structure of Cdc42 in complex with the GTPase-binding domain of the 'Wiskott-Aldrich syndrome' protein. Nature. 1999;399(6734):379-83.
200. Fukuoka M, Suetsugu S, Miki H, Fukami K, Endo T, Takenawa T. A novel neural Wiskott-Aldrich syndrome protein (N-WASP) binding protein, WISH, induces Arp2/3 complex activation independent of Cdc42. J Cell Biol. 2001;152(3):471-82.
201. Dovas A, Cox D. Regulation of WASp by phosphorylation: Activation or other functions? Commun Integr Biol. 2010;3(2):101-5.
202. Thrasher AJ, Burns SO. WASP: a key immunological multitasker. Nat Rev Immunol. 2010;10(3):182-92.
203. Pizarro-Cerda J, Cossart P. Bacterial adhesion and entry into host cells. Cell. 2006;124(4):715-27.
204. Cossart P, Helenius A. Endocytosis of viruses and bacteria. Cold Spring Harb Perspect Biol. 2014;6(8).
205. de Carvalho TM, Barrias ES, de Souza W. Macropinocytosis: a pathway to protozoan infection. Front Physiol. 2015;6:106.
206. Sieczkarski SB, Whittaker GR. Dissecting virus entry via endocytosis. J Gen Virol. 2002;83(Pt 7):1535-45.
207. Louten J. Chapter 2 - Virus Structure and Classification. In: Louten J, editor. Essential Human Virology. Boston: Academic Press; 2016. p. 19-29.
208. Pelkmans L, Helenius A. Insider information: what viruses tell us about endocytosis. Curr Opin Cell Biol. 2003;15(4):414-22.
209. Damm EM, Pelkmans L, Kartenbeck J, Mezzacasa A, Kurzchalia T, Helenius A. Clathrin- and caveolin-1-independent endocytosis: entry of simian virus 40 into cells devoid of caveolae. J Cell Biol. 2005;168(3):477-88.
210. Mercer J, Helenius A. Vaccinia virus uses macropinocytosis and apoptotic mimicry to enter host cells. Science. 2008;320(5875):531-5.
211. Finlay BB, Cossart P. Exploitation of mammalian host cell functions by bacterial pathogens [published erratum appears in Science 1997 Oct 17;278(5337):373] [see comments]. Science. 1997;276(5313):718-25.

212. Cossart P, Sansonetti PJ. Bacterial invasion: the paradigms of enteroinvasive pathogens. Science. 2004;304(5668):242-8.
213. Pizarro-Cerda J, Kuhbacher A, Cossart P. Entry of Listeria monocytogenes in mammalian epithelial cells: an updated view. Cold Spring Harb Perspect Med. 2012;2(11).
214. Hartsock A, Nelson WJ. Adherens and tight junctions: structure, function and connections to the actin cytoskeleton. Biochim Biophys Acta. 2008;1778(3):660-9.
215. Bierne H, Cossart P. InlB, a surface protein of Listeria monocytogenes that behaves as an invasin and a growth factor. J Cell Sci. 2002;115(Pt 17):3357-67.
216. Shen Y, Naujokas M, Park M, Ireton K. InlB-dependent internalization of Listeria is mediated by the Met receptor tyrosine kinase. Cell. 2000;103(3):501-10.
217. Cossart P, Roy CR. Manipulation of host membrane machinery by bacterial pathogens. Curr Opin Cell Biol. 2010;22(4):547-54.
218. Hybiske K, Stephens RS. Mechanisms of Chlamydia trachomatis Entry into Nonphagocytic Cells. Infect Immun. 2007;75(8):3925-34.
219. Majeed M, Kihlstrom E. Mobilization of F-actin and clathrin during redistribution of Chlamydia trachomatis to an intracellular site in eucaryotic cells. Infect Immun. 1991;59(12):4465-72.
220. Boleti H, Benmerah A, Ojcius DM, Cerf-Bensussan N, Dautry-Varsat A. Chlamydia infection of epithelial cells expressing dynamin and Eps15 mutants: clathrin-independent entry into cells and dynamin-dependent productive growth. J Cell Sci. 1999;112(Pt 10):1487-96.
221. Murray A, Ward ME. Control mechanisms governing the infectivity of Chlamydia trachomatis for HeLa cells: the role of calmodulin. J Gen Microbiol. 1984;130(Pt 1):193-201.
222. Hodinka RL, Davis CH, Choong J, Wyrick PB. Ultrastructural study of endocytosis of Chlamydia trachomatis by McCoy cells. Infect Immun. 1988;56(6):1456-63.
223. Wyrick PB, Choong J, Davis CH, Knight ST, Royal MO, Maslow AS, et al. Entry of genital Chlamydia trachomatis into polarized human epithelial cells. Infect Immun. 1989;57(8):2378-89.
224. Byrne GI, Moulder JW. Parasite-specified phagocytosis of Chlamydia psittaci and Chlamydia trachomatis by L and HeLa cells. Infect Immun. 1978;19(2):598-606.
225. Reynolds DJ, Pearce JH. Characterization of the cytochalasin D-resistant (pinocytic) mechanisms of endocytosis utilized by chlamydiae. Infect Immun. 1990;58(10):3208-16.
226. Subbarayal P, Karunakaran K, Winkler AC, Rother M, Gonzalez E, Meyer TF, et al. EphrinA2 receptor (EphA2) is an invasion and intracellular signaling receptor for Chlamydia trachomatis. PLoS Pathog. 2015;11(4):e1004846.
227. Nans A, Ford C, Hayward RD. Host-pathogen reorganisation during host cell entry by Chlamydia trachomatis. Microbes Infect. 2015;17(11-12):727-31.
228. Bastidas RJ, Valdivia RH. The emerging complexity of Chlamydia trachomatis interactions with host cells as revealed by molecular genetic approaches. Curr Opin Microbiol. 2023;74:102330.
229. Clifton DR, Fields KA, Grieshaber SS, Dooley CA, Fischer ER, Mead DJ, et al. A chlamydial type III translocated protein is tyrosine-phosphorylated at the site

of entry and associated with recruitment of actin. Proc Natl Acad Sci U S A. 2004;101(27):10166-71.
230. Keb G, Ferrell J, Scanlon KR, Jewett TJ, Fields KA. Chlamydia trachomatis TmeA Directly Activates N-WASP To Promote Actin Polymerization and Functions Synergistically with TarP during Invasion. mBio. 2021;12(1).
231. Braun C, Alcazar-Roman AR, Laska A, Mölleken K, Fleig U, Hegemann JH. CPn0572, the C. pneumoniae ortholog of TarP, reorganizes the actin cytoskeleton via a newly identified F-actin binding domain and recruitment of vinculin. PLoS One. 2018;14(1):e0210403.
232. Hohler M, Alcazar-Roman AR, Schenk K, Aguirre-Huamani MP, Braun C, Zrieq R, et al. Direct targeting of host microtubule and actin cytoskeletons by a chlamydial pathogenic effector protein. J Cell Sci. 2024.
233. Zrieq R, Braun C, Hegemann JH. The Chlamydia pneumoniae Tarp Ortholog CPn0572 Stabilizes Host F-Actin by Displacement of Cofilin. Front Cell Infect Microbiol. 2017;7:511.
234. Hänsch S, Spona D, Murra G, Kohrer K, Subtil A, Furtado AR, et al. Chlamydia-induced curvature of the host-cell plasma membrane is required for infection. Proc Natl Acad Sci U S A. 2020;117(5):2634-44.
235. Mojica SA, Hovis KM, Frieman MB, Tran B, Hsia RC, Ravel J, et al. SINC, a type III secreted protein of Chlamydia psittaci, targets the inner nuclear membrane of infected cells and uninfected neighbors. Mol Biol Cell. 2015;26(10):1918-34.
236. Wintgens S. Funktion oligomerer Pmp Adhäsine im Infektionsprozess von Chlamydien [Dissertation]: Institute for Functional Microbial Genomics, Heinrich Heine University Düsseldorf; 2023.
237. Satapathy S, Wilson MR. The Dual Roles of Clusterin in Extracellular and Intracellular Proteostasis. Trends Biochem Sci. 2021;46(8):652-60.
238. Tschopp J, Chonn A, Hertig S, French LE. Clusterin, the human apolipoprotein and complement inhibitor, binds to complement C7, C8 beta, and the b domain of C9. J Immunol. 1993;151(4):2159-65.
239. Braun C, Hegemann JH, Molleken K. Insights Into a Chlamydia pneumoniae-Specific Gene Cluster of Membrane Binding Proteins. Front Cell Infect Microbiol. 2020;10:565808.
240. Entian KD, Schuster T, Hegemann JH, Becher D, Feldmann H, Guldener U, et al. Functional analysis of 150 deletion mutants in Saccharomyces cerevisiae by a systematic approach. Mol Gen Genet. 1999;262(4-5):683-702.
241. Gietz RD, Schiestl RH, Willems AR, Woods RA. Studies on the transformation of intact yeast cells by the LiAc/SS-DNA/PEG procedure. Yeast. 1995;11(4):355-60.
242. Qiagen. QIAGEN® Plasmid Mini, Midi and Maxi Kits; 2016 [Available from: https://www.qiagen.com/us/resources/resourcedetail?id=c164c4ce-3d6a-4d18-91c4-f5763b6d4283&lang=en]
243. Hölzer M, Barf LM, Lamkiewicz K, Vorimore F, Lataretu M, Favaroni A, et al. Comparative Genome Analysis of 33 Chlamydia Strains Reveals Characteristic Features of Chlamydia Psittaci and Closely Related Species. Pathogens. 2020;9(11).
244. Birkelund S, Morgan-Fisher M, Timmerman E, Gevaert K, Shaw AC, Christiansen G. Analysis of proteins in Chlamydia trachomatis L2 outer membrane complex, COMC. FEMS Immunol Med Microbiol. 2009;55(2):187-95.

245. Favaroni A. Role of adhesin proteins in *Chlamydia* infection [Dissertation]: Institute for Functional Microbial Genomics, Heinrich Heine University Düsseldorf; 2017.
246. Hung V, Udeshi ND, Lam SS, Loh KH, Cox KJ, Pedram K, et al. Spatially resolved proteomic mapping in living cells with the engineered peroxidase APEX2. Nat Protoc. 2016;11(3):456-75.
247. Morgan DO, Edman JC, Standring DN, Fried VA, Smith MC, Roth RA, et al. Insulin-like growth factor II receptor as a multifunctional binding protein. Nature. 1987;329(6137):301-7.
248. Harris LK, Crocker IP, Baker PN, Aplin JD, Westwood M. IGF2 actions on trophoblast in human placenta are regulated by the insulin-like growth factor 2 receptor, which can function as both a signaling and clearance receptor. Biol Reprod. 2011;84(3):440-6.
249. UniProt C. UniProt: the Universal Protein Knowledgebase in 2023. Nucleic Acids Res. 2023;51(D1):D523-D31.
250. Probable outer membrane protein PmpI; [Available from: https://alphafold.ebi.ac.uk/entry/O84882]
251. Probable outer membrane protein PmpD; [Available from: https://alphafold.ebi.ac.uk/entry/O84818]
252. Jumper J, Evans R, Pritzel A, Green T, Figurnov M, Ronneberger O, et al. Highly accurate protein structure prediction with AlphaFold. Nature. 2021;596(7873):583-9.
253. Varadi M, Bertoni D, Magana P, Paramval U, Pidruchna I, Radhakrishnan M, et al. AlphaFold Protein Structure Database in 2024: providing structure coverage for over 214 million protein sequences. Nucleic Acids Res. 2024;52(D1):D368-D75.
254. Gauthier C, El Cheikh K, Basile I, Daurat M, Morère E, Garcia M, et al. Cation-independent mannose 6-phosphate receptor: From roles and functions to targeted therapies. Journal of Controlled Release. 2024;365:759-72.
255. Bergman D, Halje M, Nordin M, Engstrom W. Insulin-like growth factor 2 in development and disease: a mini-review. Gerontology. 2013;59(3):240-9.
256. Yu H, Rohan T. Role of the insulin-like growth factor family in cancer development and progression. J Natl Cancer Inst. 2000;92(18):1472-89.
257. Hassan AB. Keys to the hidden treasures of the mannose 6-phosphate/insulin-like growth factor 2 receptor. Am J Pathol. 2003;162(1):3-6.
258. Puolakkainen M, Lee A, Nosaka T, Fukushi H, Kuo CC, Campbell LA. Retinoic acid inhibits the infectivity and growth of Chlamydia pneumoniae in epithelial and endothelial cells through different receptors. Microb Pathog. 2008;44(5):410-6.
259. Kuo CC, Puolakkainen M, Lin TM, Witte M, Campbell LA. Mannose-receptor positive and negative mouse macrophages differ in their susceptibility to infection by Chlamydia species. Microb Pathog. 2002;32(1):43-8.
260. Sultana P, Novotny J. Clusterin: a double-edged sword in cancer and neurological disorders. EXCLI J. 2024;23:912-36.
261. Itakura E, Chiba M, Murata T, Matsuura A. Heparan sulfate is a clearance receptor for aberrant extracellular proteins. J Cell Biol. 2020;219(3).
262. Howlett DR, Hortobagyi T, Francis PT. Clusterin associates specifically with Abeta40 in Alzheimer's disease brain tissue. Brain Pathol. 2013;23(6):623-32.

263. Nelson AR, Sagare AP, Zlokovic BV. Role of clusterin in the brain vascular clearance of amyloid-β. Proceedings of the National Academy of Sciences. 2017;114(33):8681-2.
264. Xie CB, Jane-Wit D, Pober JS. Complement Membrane Attack Complex: New Roles, Mechanisms of Action, and Therapeutic Targets. Am J Pathol. 2020;190(6):1138-50.
265. Hallstrom T, Uhde M, Singh B, Skerka C, Riesbeck K, Zipfel PF. Pseudomonas aeruginosa Uses Dihydrolipoamide Dehydrogenase (Lpd) to Bind to the Human Terminal Pathway Regulators Vitronectin and Clusterin to Inhibit Terminal Pathway Complement Attack. PLoS One. 2015;10(9):e0137630.
266. Partridge SR, Baker MS, Walker MJ, Wilson MR. Clusterin, a putative complement regulator, binds to the cell surface of Staphylococcus aureus clinical isolates. Infect Immun. 1996;64(10):4324-9.
267. Pillay S, Meyer NL, Puschnik AS, Davulcu O, Diep J, Ishikawa Y, et al. An essential receptor for adeno-associated virus infection. Nature. 2016;530(7588):108-12.
268. Yayon A, Klagsbrun M, Esko JD, Leder P, Ornitz DM. Cell surface, heparin-like molecules are required for binding of basic fibroblast growth factor to its high affinity receptor. Cell. 1991;64(4):841-8.
269. Liu J, Thorp SC. Cell surface heparan sulfate and its roles in assisting viral infections. Med Res Rev. 2002;22(1):1-25.
270. Kuo CC, Takahashi N, Swanson AF, Ozeki Y, Hakomori SI. An N Linked High Mannose Type Oligosaccharide, Expressed At the Major Outer Membrane Protein of Chlamydia Trachomatis, Mediates Attachment and Infectivity of the Microorganism to Hela Cells. Journal of Clinical Investigation. 1996;98 (12):2813-8.
271. Alto NM, Shao F, Lazar CS, Brost RL, Chua G, Mattoo S, et al. Identification of a Bacterial Type III Effector Family with G Protein Mimicry Functions. Cell. 2006;124(1):133-45.
272. Burkinshaw B, Prehna G, Worrall L, Strynadka N. Structure of Salmonella Effector Protein SopB N-terminal Domain in Complex with Host Rho GTPase Cdc42. The Journal of biological chemistry. 2012;287:13348-55.
273. Schmidt G, Sehr P, Wilm M, Selzer J, Mann M, Aktories K. Gln 63 of Rho is deamidated by Escherichia coli cytotoxic necrotizing factor-1. Nature. 1997;387(6634):725-9.
274. Faris R, McCullough A, Andersen SE, Moninger TO, Weber MM. The Chlamydia trachomatis secreted effector TmeA hijacks the N-WASP-ARP2/3 actin remodeling axis to facilitate cellular invasion. PLoS Pathog. 2020;16(9):e1008878.
275. Cheng HC, Skehan BM, Campellone KG, Leong JM, Rosen MK. Structural mechanism of WASP activation by the enterohaemorrhagic E. coli effector EspF(U). Nature. 2008;454(7207):1009-13.
276. Scanlon KR, Keb G, Wolf K, Jewett TJ, Fields KA. Chlamydia trachomatis TmeB antagonizes actin polymerization via direct interference with Arp2/3 activity. Front Cell Infect Microbiol. 2023;13:1232391.

9 List of Figures

Figure 1: Chlamydial taxonomy 2
Figure 2: *Ctr* biovars and serovars 4
Figure 3: Schematic representation of the chlamydial developmental cycle 6
Figure 4: Properties and domain architecture of Pmps 9
Figure 5: Suggested processing of *Cpn* Pmp21 and *Ctr* PmpD 14
Figure 6: Schematic representation of the initial steps of clathrin-mediated endocytosis 21
Figure 7: Schematic representation of SNX9 domains and their functions 24
Figure 8: Schematic representation of N-WASP domains and their functions 26
Figure 9: Schematic representation of the operon containing *semC, semD* and *cpn0676* and the domain organisation of SemD 30
Figure 10: Schematic representation of PmpG from *Ctr* serovar E, DK20 136
Figure 11: Schematic representation of the performed adhesion assays using soluble rG72 137
Figure 12: rG72 shows concentration and time dependent adhesion to epithelial HEp-2 cells 138
Figure 13: Schematic overview of the experimental procedure and the fusion proteins used 140
Figure 14: Control experiments for the verification of plasmid transformation and fusion protein expression 142
Figure 15: Fluorescence microscopy of wild-type or transformed *Ctr* L2 143
Figure 16: Proximity labelling assay on the chlamydial EB cell surface 145
Figure 17: Proximity labelling epithelial cell surface proteins via adhesion of *Ctr* L2 EBs ectopically expressing APEX2-PmpD$_{PD}$ 146
Figure 18: RoseTTAFold predicted structures of PmpI and PmpD fused to APEX2 153

Figure S1: Designed plasmids used in PmpG adhesion studies (section 5.5.1) 163
Figure S2: Designed plasmids used in APEX2 proximity labelling studies (section 5.5.2) 164

10 Scientific record

10.1 Publications

10.1.1 Published

1. **Kocher, F**., Applegate, V., Reiners, J., Port, A., Spona, D., Hansch, S., Mirzaiebadizi, A., Ahmadian, M. R., Smits, S. H. J., Hegemann, J. H., & Molleken, K. (2024). "The *Chlamydia pneumoniae* effector SemD exploits its host's endocytic machinery by structural and functional mimicry." Nat Commun 15(1): 7294.

10.1.2 Submitted / under review

1. **Kocher, F.**, Hegemann, J. H. „Secreted host cell clusterin binds *Chlamydia trachomatis* PmpD and is essential for infection" (submitted to Frontiers in Cellular and Infection Microbiology)

2. Bugge, K., Sottini, A., Ivanović M. T., Buus, F., Saar, D., Fernandes C. B., **Kocher, F.**, Martinsen, J. H., Schuler, B., Best, R. B. & Kragelund, B. B. „Role of net charges and charge clustering in a dynamic disordered complex between an IDP and a folded protein domain". (under review in Nature Communications)

10.2 Presentations

1. **Büchler, F.**, Hegemann, J. H., "Characterization of human receptors interacting with *Chlamydia trachomatis* Pmp adhesins" MOI IV iSAB Meeting, March 15th – 17th, 2021, (online)

2. **Büchler, F.**, Hegemann, J. H., "Characterization of human receptors interacting with *Chlamydia trachomatis* Pmp adhesins" 1st MOI IV Symposium, May 24th – 26th, 2022, Bergisch Gladbach, Germany

3. **Kocher, F.**, Wintgens, S., Hegemann, J. H., "Homo- and Heterooligomerisation of *Chlamydia trachomatis* Pmps in vivo and in vitro" 19th German Chlamydia Workshop (DCW 19), March 2nd – 3rd 2023, Düsseldorf, Germany (Poster-Pitch Presentation)

4. **Kocher F**, Hegemann J.H., "SemD – a chlamydial membrane targeting effector protein acting as recruiting platform for endocytic proteins" 2nd MOI IV Symposium, April 26th – 28th, 2023, Düsseldorf, Germany

5. **Kocher, F.**, V. Applegate, J. Reiners, A. Port, D. Spona, S. Hansch, A. Mirzaiebadizi, M. R. Ahmadian, S. H. J. Smits, J. H. Hegemann and K. Molleken (2024). "The *Chlamydia pneumoniae* effector SemD exploits the host's endocytic machinery by structural and functional mimicry." 20th Chlamydia Workshop 2024, February 21st – 23rd, 2024, Ascona, Switzerland

6. **Kocher, F.**, V. Applegate, J. Reiners, A. Port, D. Spona, S. Hansch, A. Mirzaiebadizi, M. R. Ahmadian, S. H. J. Smits, J. H. Hegemann and K. Molleken (2024). "The *Chlamydia pneumoniae* effector SemD exploits the host's endocytic machinery by structural and functional mimicry." 3rd MOI IV Symposium, March 4th – 6th, 2024, Düsseldorf, Germany

7. **Kocher, F.**, V. Applegate, J. Reiners, A. Port, D. Spona, S. Hansch, A. Mirzaiebadizi, M. R. Ahmadian, S. H. J. Smits, J. H. Hegemann and K. Molleken (2024). "The *Chlamydia pneumoniae* effector SemD exploits its host's endocytic machinery by structural and functional mimicry." StructuraLink Rhein-Ruhr 2024, September 2nd – 3rd, 2024, Köln, Germany

10.3 Poster

1. **Kocher, F.**, Wintgens, S., Hegemann, J. H., "Homo- and Heterooligomerisation of *Chlamydia trachomatis* Pmps *in vivo* and *in vitro*" 19th German Chlamydia Workshop (DCW 19), March 2nd – 3rd 2023, Düsseldorf, Germany

2. **Kocher, F.**, Wintgens, S., Hegemann, J. H., "Homo- and Heterooligomerisation of *Chlamydia trachomatis* Pmps *in vivo* and *in vitro*" Chlamydia basic research society (CBRS) meeting, March 20th – 24th, 2023, Omaha, Nebraska

3. **Kocher, F.**, Hegemann J.H., „Characterization of human receptor(s) interacting with *Chlamydia trachomatis* PmpD", 2nd MOI IV Symposium, April 26th – 28th, 2023, Düsseldorf, Germany

11 Acknowledgments

On this occasion, I want to thank everyone who supported me during my PhD.

First, I want to thank Prof. Dr. Johannes H. Hegemann for giving me the opportunity to work on such an interesting project, for allowing me to work in his lab, and for his constant support during the last four years. This enabled me to grow and develop my scientific thinking.

I also want to thank Prof. Dr. Dieter Willbold, my second supervisor, for his interest in my work, his valuable input and advice.

I would like to thank and acknowledge the financial support provided by the Graduate School “Molecules of Infection IV (MOI IV)” which was funded by the Jürgen Manchot Foundation.

A special thank you goes to Dr. Katja Mölleken, you supported me in many ways with helpful comments, discussions and encouragement. And I have to admit: your Chili sin Carne is indeed better than mine!

I would also like to thank the members of the “Hegemänner” and the AG Fleig for the cheerful work environment and helpful discussions (also for the non-scientific ones) ;).

To Auntie Josi and Paula: Thank you so much for everything during the last years! It’s difficult to put into words how grateful I am. You always had my back and helped me wherever you could, representing the true spirit of “teamwork makes the dream work”. Your encouragement and support were incredibly helpful, especially during challenging times. Es war mir ein inneres Blumenpflücken!

To Mona: Thank you for allowing me to escape reality for some time, whether at the beach in the Netherlands or on long walks! Fresh air and a good chat always help! ;)

To Prof. Dr. Sander H. J. Smits, thank you for your support, especially during the last two years. I am truly grateful for your constant optimism, motivation, and great support! This made our collaboration even more valuable. :)

Connected to that I also want to thank the whole CSS, especially Jens and Violetta. Jens, thank you for your valuable time and the interesting discussions (scientific and non-scientific) whenever I decided to “shortly” pass by for a coffee break. Violetta, thank you for your great help and for accepting all the endless colour-changes I requested! ;)

Finally, I would like to thank all the other collaboration partners from our SemD-paper: Prof. Dr. Mohammad Reza Ahmadian, Astrid, Nik, Sebastian, and Amin. Thank you all for your valuable contributions and insightful discussions, which were indispensable for turning this research project into a published work!

To my Swiss friends:
Astrid and Mirjam, I just want to take a moment to say how lucky I feel to have you in my life! Thank you from the bottom of my heart for all your support, love and advice! You have no idea how grateful I am for you and I can’t wait to see what life holds next for us! Even with more than 600 km between us, you’re always there when I need you. Sooo much love and b. scoiattolo!
To Rahel, thank you for everything in the last nearly 30 years! You were literally there from day one and we’ve experienced so much and celebrated many milestones together. I truly hope there are many more things to celebrate and I’m looking forward to it!
To Isabelle, thank you so much! Ten years ago, I luckily had enough courage to ask you if the chair next to you was still free. This was the start of a wonderful journey at the UZH and you not only made studying easier but you also helped me grow and develop and for that I am endlessly grateful!

I also want to thank the record label EUROPA for the 229 episodes of “Die drei ???”, which kept me entertained during countless hours over the past four years!

The last section of my acknowledgments I dedicate to my family.
Mom, Dad, Nadine, thank you so much for giving me the freedom to find my path and for unconditionally supporting my choices! Thank you for always believing in me, even when I lost faith in myself. It's not something I take for granted, and I want you to know how proud I am of our family! Since I was little, you taught me that "morn gseht d'Welt scho wieder ganz anderst us" and "alles wird nöd ganz so heiss gässe wies kochet wird" and you were always right!

Thank you to my soon-to-be brother-in-law Maxi, my aunt and uncle Cécile and Donath, and my grandmother Gertrud for the long phone calls, your love and support.

To my in-laws, Elke, Jörg, Robin, Daniela and Lilli, thank you for welcoming me into your family, and for all the delicious breakfasts, dinners, and fun game nights!

And finally, to Niko. Thank you for your endless support and belief in me. Words cannot express my gratitude. You have been my rock during hard times, you reminded me that anything is possible when I lost hope, and you showed me a way out when I felt stuck. You stood by me through the toughest challenges and celebrated my successes with me, making each achievement even more meaningful. You have made my life what it is today and you made it possible to adopt Josie, the furriest nose of them all! You are the reason for who I am today and I'm incredibly proud of you and of us. No matter where our journey leads us, always remember: Home isn't a place, it's wherever YOU are.

12 Statutory declaration

I hereby declare that I have authored the thesis entitled

Molecular Characterization of *Chlamydia* – Host Interactions During the Early Stages of Infection

No other person's work has been used without due acknowledgment in this thesis. Where I have quoted from or adapted the work of others, the source is always given. This includes the sources of graphs and data.

Düsseldorf, 22 October 2024

Fabienne Kocher